Synthesis, Characterization and Catalytic Activity Study of Zinc Amino-bis(phenolate) Complexes Towards Ring-opening Polymerization of *rac*-Lactide

by

© Yi Liu

A Thesis submitted to the

School of Graduate Studies

in partial fulfillment of the requirements for the degree of

Master of Science (M.Sc.)

Department of Chemistry

Memorial University of Newfoundland

December 2015

St. John's Newfoundland

ABSTRACT

A series of bimetallic and trimetallic zinc complexes of amino-bis(phenolato) ligands was synthesized and characterized. Bimetallic complexes $(ZnEt)_2$**[L1]** (**1a**) and $(ZnEt)_2$**[L2]** (**1b**) (where [**L1**] = *n*-propylamine-*N*,*N*-bis(2-methylene-4,6-di-*t*-butylphenolate) and [**L2**] = *n*-propylamine-*N*,*N*-bis(2-methylene-6-*t*-butyl-4-methylphenolate) were prepared via reaction of the proligands H_2[**L1**] and H_2[**L2**] with $ZnEt_2$ in pentane. A THF adduct $(ZnEt)_2$**[L1]**·THF (**1a·THF**) was obtained by using THF as solvent. Treatment of **1a** with one or two equiv. of isopropyl alcohol gave a trimetallic zinc complex $Zn_3(i\text{-PrO})_2$**[L1]$_2$** (**2**). The catalytic activities of these complexes towards ring-opening polymerization (ROP) of *rac*-lactide were studied in the absence and presence of benzyl alcohol or isopropyl alcohol. These complexes exhibit moderate to good activity for ROP of *rac*-lactide both in the melt phase and solution. The influence of catalyst and co-initiator loading were studied and thermodynamic activation parameters were determined. Characterization of the polymers by GPC and MALDI-TOF MS showed controlled and living polymerizations for *rac*-lactide in the presence of alcohol.

ACKNOWLEDGEMENTS

I would like to thank my supervisor Professor Christopher Kozak for his kind support and invaluable time. I thank him for teaching me Organometallic Chemistry course, from which I truly understand how catalysis works in a circle and the principles guide me in my research. I thank him for giving me the opportunity to work on this interesting project, for spending time meeting with me and reviewing my posters, presentations, paper, and thesis chapters, for providing me the opportunity to attend two conferences and to communicate with other scientists and peers. I always remember in my first semester, he said to me that research is like proposing assumptions and collecting and analyzing evidence, which really helped me build a scientific mind. I like his idea that a supervisor is like a lifeguard by a swimming pool: students need to swim by themselves but the supervisor will make sure they will not drown.

I would also like to thank Professor Francesca Kerton for teaching me Green Chemistry and giving me suggestions in group meetings, from which I have not only learned chemical knowledge, but also built up strong teamwork and communication skills. I like her idea that we need to feel confortable talking about science.

I thank Professor Christopher Kozak and Francesca Kerton for arranging many group activities for us, e.g. Thanksgiving dinner, group camping, group pot-luck, etc. I thank them for building up a positive attitude in research and a friendly atmosphere in our Green Chemistry and Catalysis Group (GCCG).

I would like to thank Professor Christopher Rowley for being my committee member and teaching me in the Statistical Thermodynamics and Rate Theories course (audit). I would like to thank Professor Christina Bottaro for being my seminar examiner and Professor Michael Katz for being my seminar examiner and teaching me Crystal Structure Determination course (audit).

I am also very grateful for having a wonderful international group (GCCG). I especially would like to thank Katalin Devaine for being around and giving me help in the beginning of my research. I thank Hart Plommer for helping me with GPC. I thank all the group members for their help and for those great discussions about research or life. I thank them for the delicious food in our group pot-lucks (food from all over the world)!

I am thankful to C-CART for instrumental support. I would especially thank Dr. Celine Schneider for her advice and assistance in conducting NMR kinetic studies and thank Dr. Linda Winsor for MALDI-TOF training. Also, a thank-you to Dr. Louise Dawe who solved the crystal structures. I would also like to say a thank-you to Professor Jason Masuda (St. Mary's University) for collecting single crystal X-ray diffraction data for us.

I would like to give thanks to all the funding agencies: the Canada Foundation for Innovation (CFI), Newfoundland and Labrador Research Development Corporation, the Natural Sciences and Engineering Research Council (NSERC) of Canada and Memorial University of Newfoundland for grants to my supervisor and my financial support.

Last but not least, I thank my parents for supporting me in pursuit of my educational goals in Canada and other goals in my life. My father always believes in me and has made me strong enough to endure any hardship; my mother always inspires me to keep broadening my views and exploring my life. I would like to thank my friends in St. John's; a special thank-you to Ms Rose Reid. Because of her, I learned a lot about local culture and life and I feel at home in St. John's. I am also very thankful to my boyfriend for his understanding and support…

Table of Contents

List of Tables

List of Figures

List of Schemes

List of Symbols, Nomenclature and Abbreviations

9-AnOH: anthracenemethanol

Å: Angstrom (10^{-10} m)

ATP: attached proton test

β: stereochemical descriptor

β-BL: β-butyrolactone

BDI: β-diiminate

Bn: benzyl

BnOH: benzyl alcohol

BTP: benzotriazole-phenolate

C_6D_6: deuterated benzene

Cat: catalyst

$CDCl_3$: deuterated chloroform

cm: centimetre (10^{-2} m)

^{13}C NMR: carbon nuclear magnetic resonance

COSY: correlation spectroscopy

Conv.: conversion

δ: chemical shift (NMR spectroscopy)

$\Delta H^{\ddagger}$: enthalpy of activation

$\Delta S^{\ddagger}$: entropy of activation

D: dextrorotatory

d: doublet (spectra)

Đ: molecular weight dispersity, = M_w/M_n

DCM: dichloromethane

dd: doublet of doublets (spectra)

DHBA: 2,5-dihydroxybenzoic acid

Dipp: 2,6-diisopropylphenyl

dn/dc: differential index of refraction

DSC: differential scanning calorimetry

E_a: activation energy

ε-CL: ε-caprolactone

equiv.: equivalent

ESE: electron spin echo

ESI: electrospray ionization

Et: ethyl

etc.: and so forth

EtOH: ethanol

exptl: experimental

FTIR: Fourier transform infrared

GPC: gel permeation chromatography

$^1H\{^1H\}$ NMR: homonuclear decoupled nuclear magnetic resonance

^1H NMR: proton nuclear magnetic resonance

HPLC: high-performance liquid chromatography

HQSC: heteronuclear single quantum coherence spectroscopy

Hz: hertz

i.e.: that is

i: iso

in situ: in the reaction mixture

i-PrOH: isopropyl alcohol

J: coupling constant (NMR spectroscopy)

J: Joule

K: Kelvin

k: rate constant

kHz: kilohertz

k_{obs}: apparent first-order rate constant

L: levorotatory

LA: lactide

LDMS: laser desorption mass spectrometry

L_n: generic ligand

m.p.: melting point

m/z: mass-to-charge ratio

M: molar ($mol \cdot L^{-1}$)

mM: millimolar ($millimol \cdot L^{-1}$)

m: multiplet (spectra)

MALDI-TOF MS: matrix-assisted laser desorption ionization time-of-flight mass spectrometry

Me: methyl

MeOH: methanol

Mes: Mesityl = 2,4,6-$Me_3C_6H_2$

mg: milligram (10^{-3} g)

MHz: megahertz (10^3 Hz)

min: minute

M_n: number average molecular weight

mol: mole

MS: mass spectrometry

μL: microlitre (10^{-6} L)

M_w: weight average molecular weight

nacnac: β-diiminate

neo-PentOH: *neo*-pentanol

NHC: N-heterocyclic carbene

$^-$OAc: acetate group

ORTEP: Oak Ridge thermal ellipsoid plot

p: para

PCL: poly(caprolactone)

PDLA: poly-D-lactide

PGSE: pulsed gradient spin-echo

Ph: phenyl

PHB: poly(3-hydroxybutyrate)

$^{31}P\{^{1}H\}$ NMR: phosphorus-31 nuclear magnetic resonance (proton decoupled)

Pipp: *p*-isopropylphenyl

PLA: polylactide

PLLA: poly-L-lactide

P_m: the probability of isotactic linkages between monomer units

PMP: pentamethylpiperidine

ppm: parts per million

P_r: the probability of racemic linkages between monomer units

q: quartet (spectra)

rac: racemic

Ref: reference

ROP: ring-opening polymerization

s: singlet (spectra)

sec: secondary

θ: angle

Solv: solvent

t: tertiary

t: time

t: triplet (spectra)

t-Bu: *tert*-butyl

t-BuOH: *tert*-butyl alcohol

td: triplet of doublets (spectra)

Temp: temperature

tert: tertiary

T_g: glass transition temperature

TGA: thermal gravimetric analysis

theor: theoretical

THF: tetrahydrofuran

TMC: trimethylene carbonate

TMS: tetramethylsilane

TOF: turnover frequency

Tol.: toluene

TON: turnover number

UV-Vis: ultraviolet-visible

vs.: versus

VT ^{1}H NMR: variable temperature proton nuclear magnetic resonance

XRD: X-ray diffraction

Chapter 1 Introduction

1.1 Properties of Zinc and Organozinc Complexes

Zinc is the first row d-block element in group 12, having an electron configuration of $[Ar]3d^{10}4s^2$ and its chemistry is dominated by compounds where Zn possesses an oxidation state of +2. This provides a completely filled valence d-shell, leading to properties of both transition metals and main group metals. Indeed, some have shown preference to include group 12 metals as part of the main group.[1]

Zinc shows similar properties to magnesium, including similar structures of zinc and magnesium complexes, due to the similar radii of Zn^{2+} (0.74 Å) and Mg^{2+} (0.72 Å) ions.[2] However, zinc has higher polarizability than magnesium, which means it has a greater tendency to form covalent bonds than magnesium and thus zinc is placed on the borderline of hard and soft acid.[3]

Zinc is the 23rd most abundant element in nature, mainly present as zinc sulfide (known as zinc blende or sphalerite ores) in the crust of the earth. Zinc(II) complexes are coordinatively flexible with coordination numbers ranging from 2 to 8. Four coordinate (tetrahedral) geometries dominate the chemistry of Zn^{2+}, and five and six coordinate complexes are much less common. The coordination number and stereochemistry of zinc(II) complexes are dominated by the steric properties of the ligand and the size of the Zn^{2+} ion that has no crystal field stabilization provided by d^{10} electron configuration..

Zinc is an essential trace element in biological systems. It plays either a catalytic role such as in zinc-containing enzymes, e.g. carbonic anhydrase, or a structural role such as in so-called zinc finger motifs.[4] In some cases, zinc may exhibit both roles.

Diethylzinc, discovered by Edward Frankland in 1848, was the first main group organometallic compounds, if Zn is accepted as a main group element.[5] However, organozinc complexes such as diethyl zinc are moisture-sensitive and it was not until modern air-free handling techniques came into use that research into organozinc complexes began to thrive. The versatility and functional group tolerance of organozinc complexes makes them good nucleophiles for organic synthesis and catalysis. For example, organozinc complexes have been demonstrated to have catalytic activity for the polymerization of esters[6-13] and the copolymerization of epoxides and carbon dioxide.[14-21]

Zinc alkyls, e.g. $ZnEt_2$; zinc amides, e.g. $Zn[N(SiMe_3)_2]_2$; and zinc chloride are the most common metallating agents for exploration of new organozinc complexes. Zinc ethyl complexes can be synthesized by reaction of $ZnEt_2$ with ligands via ethane elimination and $Zn[N(SiMe_3)_2]_2$ is used as a zinc source for synthesis of zinc complexes via amine elimination reactions. Organozinc chloride complexes can be synthesized using anhydrous zinc chloride.

1.2 Lactide

Lactide (LA), namely the cyclic dimer of lactic acid condensation, has three stereoisomers, i.e. L-lactide, D-lactide and *meso*-lactide. L-lactide can be produced from renewable resources, which starts from converting starch or sugars to D-glucose,

followed by fermentation via bacteria, such as *Lactobacillus*, to give L-lactic acid, which then undergoes condensation to give low molecular weight poly(L-lactide). Depolymerization provides the monomers.[22, 23] D-Lactic acid is much more expensive than L-lactic acid, thus utilization of *rac*-lactide to produce polymers with different microstructures has attracted attention because *rac*-lactide can be obtained by the racemization of L-lactide generating a mixture of L-lactide, D-lactide and *meso*-lactide, followed by removal of *meso*-lactide via distillation or crystallization.[24]

1.3 Polylactide

Polylactide (PLA)-based plastics include many properties of other conventional polymers but also display biodegradability and biocompatibility, which is ideal for potential medical applications, e.g. sutures and prosthetics,[25, 26] and packing, e.g. food containers and wrapping.[27, 28] The high cost of production compared with conventional polymers and the poor thermal sustainability impede its commercial application. As the depletion of fossil fuels and the advancement of technology, the commercialization of PLA has become more economically viable. In 1997, Cargill Dow LLC, a joint venture of Cargill Inc and the Dow Chemical Company, was founded to produce PLA-based materials from annually renewable feedstock. In 2001, Cargill Dow LLC had a PLA manufacturing capacity of 140,000 metric tons per year. NatureWorks ™ launched by Cargill Dow LLC in 2002 produces PLA-based polymers for applications in food packaging, e.g. food container and cold water bottles, and applications in non-food packaging, e.g. telephone cards. Ingeo ™ launched by Cargill Dow in 2003 produces

PLA-based fibres, e.g. for pillows, mattresses, apparel, *etc*.[29] Life cycle assessment (LCA) of the PLA production of NatureWorks™ has shown that it decreases the fossil energy use and greenhouse gases released to a large extent compared to those of petrochemical-based polymers.[30]

1.4 Ring-opening Polymerization of Lactide

Polylactide can be produced by direct condensation of lactic acid; however, considering its high energy requirement and high cost of coupling agents and additives, ring-opening polymerization (ROP) of lactide becomes a good alternative.[31] ROP of lactide can yield PLA with controlled molecular weight, narrow molecular weight dispersity and controlled stereochemistry by choosing different initiators. ROP of lactide can be initiated by metal complexes or organocatalysis. This introduction focuses on ROP of lactide initiated by metal complexes.

1.4.1 Mechanisms for Ring-opening Polymerization of Lactide

There are two mechanisms reported for ring-opening polymerization of lactide: activated monomer and coordination insertion mechanisms. A coordination insertion mechanism was first suggested by Dittrich and Schulz[32] and it usually involves an organometallic complex with a nucleophilic group acting as an initiator for ROP of LA. It can be described as follows: the coordination of lactide to the metal increases the electronegativity of the carbonyl oxygen, making the carbon more electropositive to undergo nucleophilic attack by the initiating group. Then the ring is opened by acyl-

oxygen bond cleavage to generate a L_nM—$(OCH(Me)CO)_2$—Nu species. The $(OCH(Me)CO)_2$—Nu acts as a new nucleophile to attack the next coordinated monomer, resulting in the propagation of the chain (**Scheme 1-1**). The catalyst usually is an alkoxyl species, i.e. Nu is equal to ^-OR; or if not, an alcohol (ROH) is used as co-initiator, through which an alkoxyl species, L_nM—OR, is generated by protonolysis. In the case of excess of proton source, e.g. alcohol, the active species L_nM—$(OCH(Me)CO)_{2n}$—Nu undergoes proton exchange with the proton source to generate a temporary dormant species, $H(OCH(Me)CO)_{2n}$—Nu. The ROH and $H(OCH(Me)CO)_{2n}$—Nu are known as chain transfer agents. If this exchange is reversible and the rate is faster than the initiating and propagation rate, the polymerization is controlled. However, if this exchange is slow, it results in polymer chains with higher or lower molecular weights than expected values, which broaden the molecular weight dispersity.[7]

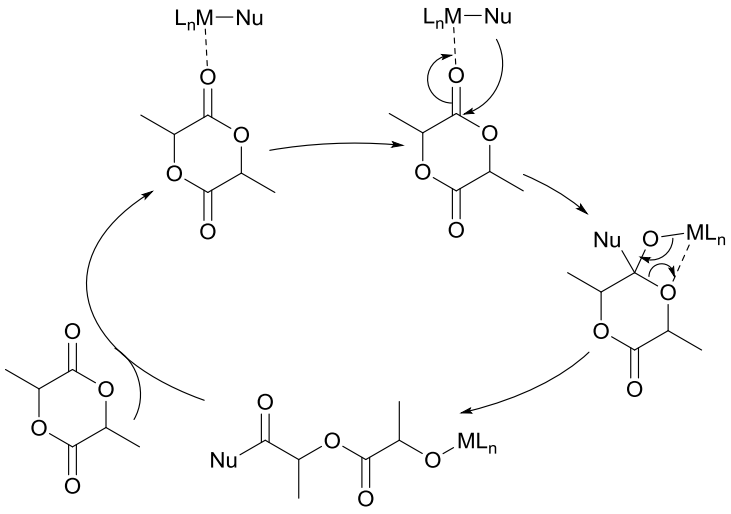

Scheme 1-1 Coordination-insertion mechanism of lactide ROP.

An activated monomer mechanism usually involves a catalyst and an external nucleophile (usually an alcohol, ROH). The external ROH ring-opens the coordinating

monomer by nucleophilic attack and acyl-oxygen cleavage, followed by the dissociation of the ring-opened monomer from the metal to generate a $H(OCHMeCO)_{2n}$—OR species, which has a hydroxyl end group acting as the new nucleophile, R'OH, to attack the next activated monomer. (**Scheme 1-2**) For a system that follows an activated monomer mechanism, the external nucleophile can interact with the catalyst causing ligand dissociation; and a large amount of proton exchange and transesterification may happen, resulting in the loss of molecular weight control and stereoselectivity.[33]

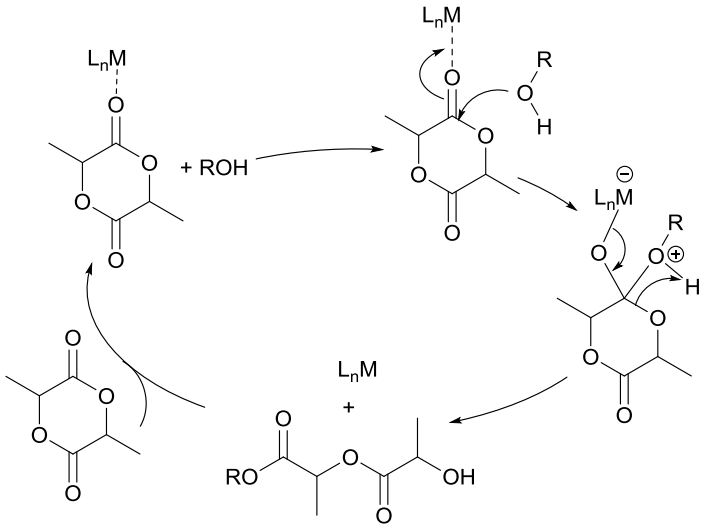

Scheme 1-2 Activated monomer mechanism of lactide ROP.

1.4.2 Stereoselectivity in ROP of Lactide

Stereoselectivity can be achieved via a chain end control mechanism or by an enantiomorphic site control mechanism. A chain end control mechanism occurs when the configuration of the incoming monomer is determined by the configuration of the last inserted monomer (usually for catalysts bearing bulky and achiral ligands). An

enantiomorphic site control mechanism is one where the orientation of the next insertion is determined by the chirality of the catalyst.

ROP of lactide using a non-stereoselective catalyst results in atactic polymers that have random chirality of the stereogenic centers of the polymer chains. ROP of enantiopure L-lactide or D-lactide can produce isotactic polymers (PLLA or PDLA) that have the same stereochemistry of two neighbouring stereogenic centers (**a**, **Figure 1-1**). ROP of *meso*-lactide can result in syndiotactic PLA with opposite stereochemistry of two neighbouring stereogenic centers having repeating units of -SRSR- via a chain-end-control mechanism when the chain end favours the same configuration or via an enantiomorphic site control mechanism. It can also generate heterotactic PLA with repeating units of -SRRS- via a chain end control mechanism that favours a monomer having an opposite configuration of the last inserted monomer (**b**, **Figure 1-1**).

ROP of *rac*-lactide, a 1:1 mixture of L- and D-lactide, can generate heterotactic PLA with repeating units of -SS-RR- by insertion of L-and D-lactide alternatively via a chain end control mechanism. Isotactic PLA can be obtained by selective insertion of one enantiomer via an enantiomorphic site control mechanism and isotactic diblock PLA (PLLA-PDLA) by preferential insertion of one enantiomer followed by insertion of the other after full consumption of the favored one via an enantiomorphic site control mechanism. There are cases when a combination of the two mechanisms is involved, or insertion errors and transesterification occur, generating isotactic multiblock PLA (**c**, **Figure 1-1**). Interestingly, isotactic multiblock PLA also can be generated from *rac*-lactide using a racemic chiral catalyst via a chain exchange mechanism, i.e. when a polymer chain incorporates an unfavoured enantiomer of monomer, this chain exchanges

to the other enantiomer of catalyst and keeps elongating with its favoured enantiomer of monomer.[34]

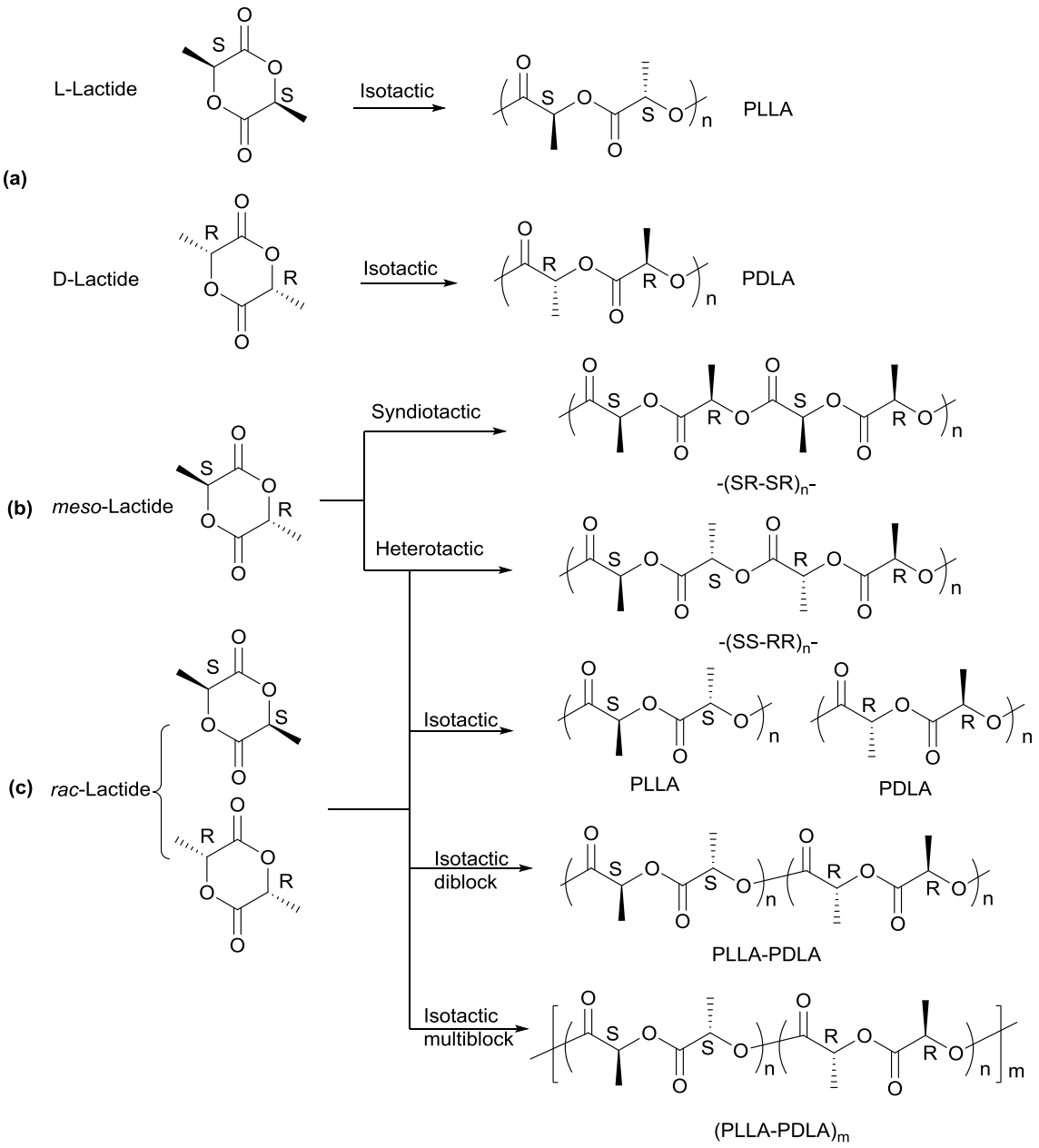

Figure 1-1 Microstructures of PLA obtained from stereocontrolled ROP of **(a)** L-lactide and D-lactide; **(b)** *meso*-lactide; and **(c)** *rac*-lactide.

1.4.3 Physical Properties of PLA

The physical properties of PLA are dominated by the stereochemistry of the polymer chains. Atactic PLA is amorphous having a glass transition temperature (T_g) of 50-60 °C and no observed melting point. Heterotactic PLA is amorphous with no glass transition temperature observed and melting point (T_m) of 130 °C. Crystalline syndiotactic PLA has T_m = 152 °C and isotactic PLLA has high crystallinity with T_m = 180 °C and T_g = 50 °C.[7] Interestingly, isotactic diblock PLA generated from *rac*-lactide shows an increased melting point, T_m = 230 °C, due to the strong interaction between PLLA and PDLA chains.[35] In recent years numerous studies have been reported on the synthesis of stereoblock copolymers from inexpensive *rac*-lactide. The incorporation of other polymers to PLA has also been broadly investigated in order to improve thermal and mechanical properties.[23, 35-39]

1.5 Recent Literature for ROP of Lactide Using Zinc Complexes

Several general and focused (immortal ROP, stereoselective, metal specific, etc.) reviews have been published, [7, 8, 10, 11, 31, 33, 40] including one in 2009 by Hayes and coworkers concerned with Ca, Mg and Zn catalysts for lactide ROP. [41] Herein, we discuss a brief account of the literature primarily since 2009 on the synthesis and catalytic activity of zinc complexes for ROP of lactide, but, important discoveries prior to 2009 will be provided as well. The following discussion focuses on zinc *β*-diiminate (BDI) complexes, zinc phenolate complexes, zinc cationic complexes, including zinc phosphinimine complexes, and zinc complexes bearing soft donor ligands for ROP of lactide.

1.6 Zinc β-Diiminate Complexes

1.6.1 Zinc Phenyl N-Substituted β-Diiminate Complexes

In 1999, Coates and coworkers utilized $Zn[N(SiMe_3)_2]_2$ as a zinc source, reacting it with a 2,6-di-isopropylphenyl (Dipp) substituted β-diimine (BDI) ligand to give a zinc amide species (**1a**) (**Figure 1-2**).[42] Further reaction of the zinc amide with *i*-PrOH yielded a dimeric zinc alkoxyl complex **1b** bridged by two alkoxyl groups. This zinc alkoxyl complex has good activity towards lactide polymerization and it still shows the best stereoselectivity to date among all the reported zinc complexes for lactide polymerization. It gives 95% conversion within 20 min at 20 °C and the polymers have reasonable molecular weights of around 37900 g/mol and narrow molecular weight dispersity, Đ = 1.10 (entry 1, **Table 1-1**). Most interestingly, it gives highly heterotactic polymers (the probability of racemic linkages between monomer units, P_r, is equal to 0.90) via a chain-end mechanism, and P_r increased to 0.94 when the polymerization was conducted at 0 °C (entry 2, **Table 1-1**). Further study found that the bulkiness of the ligand is crucial to the stereocontrol.

Changing of the isopropyl substituents on the BDI ligand to a less bulky ethyl group (**1c**) leads to a decrease of the stereocontrol of the polymerization (P_r = 0.79) (entry 3, **Table 1-1**).[43] A zinc methyl lactate complex **1d** was obtained by reaction of the zinc amide complex with *rac*-methyl lactate in order to mimic the ring-opened propagating species. X-ray diffraction characterization shows the zinc center has a distorted tetrahedral geometry with coordination of two N from the ligand and two O from the

methyl lactate group. Zinc ethyl complex **1e** was easily prepared by reacting $ZnEt_2$ with stoichiometric amount of the ligand precursor. A zinc acetate complex **1f** was obtained by reaction of the ligand with *n*-butyllithium and then transmetathesis reaction with $Zn(OAc)_2$. A study of the activities found that –O*i*-Pr and -OCH(Me)CO_2Me group are efficient initiating groups, yielding polymers with predicable molecular weights and narrow molecular weight dispersity, while -N($SiMe_3$)$_2$, -Et, and -OAc groups result in polymers with poor control (entry 4-6, **Table 1-1**).

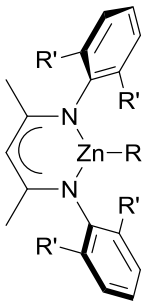

1a R' = *i*-Pr, R = N($SiMe_3$)$_2$
1b R' = *i*-Pr, R = O*i*-Pr
1c R' = Et, R = O*i*-Pr
1d R' = *i*-Pr, R = OCH(Me)CO_2Me
1e R' = *i*-Pr, R = Et
1f R' = *i*-Pr, R = OAc
1g R' = *i*-Pr, R = N(*i*-Pr)$_2$
1h R' = *i*-Pr, R =O*t*-Bu

Figure 1-2 General structure of zinc phenyl N-substituted BDI complexes.

Monomeric zinc complexes were prepared by Chisholm and coworkers in 2002.[44] Interestingly, the reaction of zinc amide complex with *tert*-butyl alcohol (*t*-BuOH) did not give the zinc alkoxyl complex (BDI)ZnO*t*-Bu using the method of Coates. Instead, they utilized a more reactive species (BDI)ZnN(*i*-Pr)$_2$ (**1g**), combined with *t*-BuOH at -78 °C in toluene to give the zinc alkoxyl complex (BDI)ZnO*t*-Bu, **1h** (**Figure 1-2**). The three

coordinate zinc center adopts a distorted trigonal planar geometry with a sum of X−Zn−X angles of 359.7°.

ROP of *rac*-lactide was studied using complex **1h** and a solvent effect was observed, i.e. at 1% catalyst loading at 20 °C, 95% conversion was obtained within 10 min in dichloromethane (DCM), while 93% conversion was obtained after 50 min in THF. Surprisingly, there was no change in stereoselectivity in DCM and in THF, giving 90% heterotacticity (entry 7-8, **Table 1-1**).

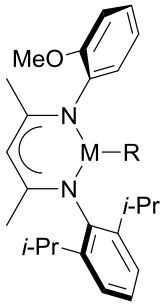

2a M = Zn, R = $N(SiMe_3)_2$
2b M = Zn, R = Et
2c M = Zn, R = $OSiPh_3$
2d M = Mg, R= N(*i*-Pr)$_2$

Figure 1-3 General structure of zinc ortho-anisole N-substituted BDI complexes.

Zinc complexes combined with ether substituted BDI ligands were explored by Gibson[45] and Chisholm.[46] Gibson and coworkers utilized a single ether substituted BDI ligand and synthesized zinc amide, zinc ethyl and zinc siloxide complexes and a magnesium amide complex (**2a-d**) (**Figure 1-3**); Chisholm and coworkers utilized a two-ether substituted BDI ligand and prepared zinc amide, zinc isopropoxyl and magnesium *tert*-butoxyl complexes (**3a-c) (Figure 1-4)**. They hypothesized that the ether group can bind to the metal center and compete with the oxygen donor of the monomer, thus increasing stereoselectivity towards ROP of lactide. Crystal structure determination found

that the pendant ether oxygen donor does not coordinate to the zinc center. Lactide ROP studies found these zinc complexes have decreased stereoselectivity but increased activity compared to the corresponding zinc complexes bearing the previous BDI ligands of **Figure 1-2** (entry 9-11, **Table 1-1**). This might be due to the lower steric hindrance of the ether group versus *i*-Pr. Interestingly, magnesium complex **3c** showed heteroselectivity in THF, giving polymers with P_r = 0.85 (entry 13, **Table 1-1**), which may indicate coordination of the pendant ether under polymerization environment in THF.

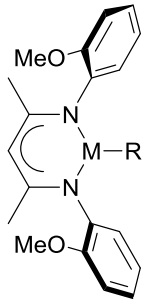

3a M = Zn, R = $N(SiMe_3)_2$
3b M = Zn, R = O*i*-Pr
3c M = Mg, R = O*t*-Bu

Figure 1-4 General structure of zinc ortho-anisole N-substituted BDI complexes.

Table 1-1 ROP of *rac*-lactide by zinc phenyl N-substituted BDI complexes.

Entry	Cat	$[LA]_0$ (M)	Loading (mol%)	Solv	Temp (°C)	t (min)	Conv (%)	Đ	P_r	Ref
1	**1b**	0.4	0.5	DCM	20	20	95	1.10	0.90	42
2	**1b**	0.4	0.5	DCM	0	120	95	1.09	0.94	42
3	**1c**	0.4	0.5	DCM	20	480	97	1.09	0.79	42
4	**1d**	0.4	0.5	DCM	20	20	97	1.14	-	43
5	**1e**	0.4	0.5	DCM	20	1200	97	1.83	-	43
6	**1f**	0.4	0.5	DCM	20	4200	92	2.07	-	43
7	**1h**	0.46	1	DCM	20	10	95	1.15	0.90	44
8	**1h**	0.46	1	THF	20	50	93	1.22	0.90	44
9	**2a**	2.8	1	$CHCl_3$	20	10	85	1.10	-	45
10	**2c**	2.8	1	$CHCl_3$	20	30	90	1.15	-	45
11	**2d**	2.8	1	C_6H_6	50	8	81	1.78	Atactic	45
12	**3b**	0.46	1	THF	20	10	91	1.19	0.68	46
13	**3c**	0.46	1	THF	20	90	90	1.70	0.85	46

DCM = dichloromethane; dashes (-) indicate no stereospecificity reported.

Chen, Zou and coworkers further modified BDI ligands by incorporating a pendant nitrogen donor in order to increase heterotactic selectivity.[47] Zinc complex **4a** and magnesium complexes **4b** and **4c** were obtained using $ZnEt_2$ and $Mg(t\text{-}Bu)_2$, respectively (**Scheme 1-3**). Treatment of **4b** and **4c** with $HN(SiMe_3)_2$ yielded magnesium amide complex **4d** and **4e**, respectively, while zinc amide complex **4f** was obtained using reaction of $Zn[N(SiMe_3)_2]_2$ with ligand precursor (**Scheme 1-4**). Also, a calcium amide complex **4g**, was prepared by treatment of ligand precursor with two equiv. of $KN(SiMe_3)_2$ and CaI_2. Unlike the phenyl ether substituted BDI derivatives,[45, 46] coordination of the amine to the metal center is observed.

All the magnesium complexes, calcium complex **4g** and zinc amide complex **4f** show good activity and control for ROP of *rac*-lactide, giving ≥ 90% conversion within 30 min at 1% catalyst loading at 25 °C (entry 2-8, **Table 1-2**). Zinc complex **4f** provides polymers with narrow molecular weight dispersity, Đ = 1.07, and expected molecular weights. Zinc ethyl complex **4a** shows slow activity due to the poor initiating ability of the ethyl group (entry 1, **Table 1-2**). Promisingly, complex **4a** and **4f** have better heterotactic selectivity (P_r = 0.69 and 0.68) than zinc complex supported by a phenyl ether substituted BDI derivative that has a rigid pendant arm (complex **3b**) (P_r = 0.59),[46] indicating the influence of the interaction of the pendant amine donor to the metal center. A calcium complex was prepared and showed high activity but poor selectivity (P_r = 0.47). Magnesium complex **4e** showed enhanced heteroselectivity in THF (P_r = 0.75) (entry 6, **Table 1-2**).

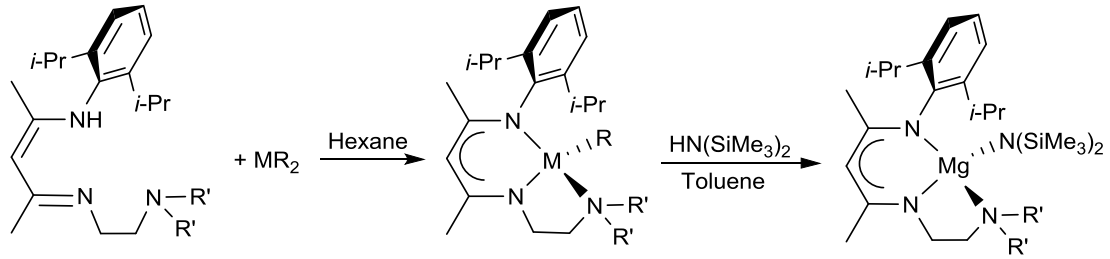

4a M = Zn, R = Et, R' = Me
4b M = Mg, R = *n*-Bu, R' = Me
4c M = Mg, R = *n*-Bu, R'-R' = $(CH_2)_5$
4d R' = Me
4e R'-R' = $(CH_2)_5$

Scheme 1-3 Synthesis of zinc and magnesium BDI complexes bearing a pendant nitrogen donor.

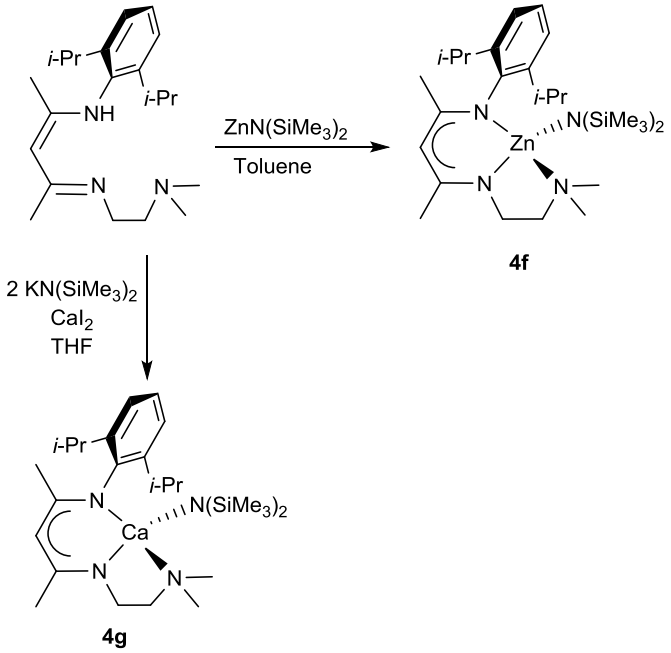

Scheme 1-4 Synthesis of zinc and calcium BDI complexes a bearing pendant nitrogen donor.

In 2011, the influence of different substituents of BDI ligands on the activity of ROP of L-lactide was studied by Chen, Lin and coworkers.[48] Zinc ethyl species, **5a-g**, were prepared by reaction of the ligand precursors with $ZnEt_2$. Further reaction of zinc ethyl species with benzyl alcohol (BnOH) resulted in different zinc alkoxyl complexes including bimetallic (**6a-e**) and trimetallic (**6f** and **6g**) zinc alkoxyl species (**Scheme 1-5**). The unpredictable nature of the reaction between zinc ethyl complexes with alcohols was reported by Coates previously when they reacted zinc ethyl species with methanol (MeOH).[49] Coates and coworkers found that trimetallic complexes were obtained when there are bulky substituents (such as *i*-Pr) on the N-aryl moieties (**8c**) or when there is an electron-withdrawing substituent such as nitriles, CN, on the N-C-C-C-N backbone of the ligand (**8e**) (**Scheme 1-6**).

Interestingly, they found that the polymerization rate is highly affected by the electronic properties of the ligand, with little effect from the number of zinc centers available. Complexes with electron-donating groups on the ortho-position of the N-aryls give high activity, ≤ 5 min was needed to reach over 90% conversion, with 1% catalyst loading at room temperature in toluene for complexes **6b**, **6f** and **6g** (entry 9, 11-12, **Table 1-2**). Although the molecular weights of the polymers are lower than expected, molecular weight dispersities are narrow, Đ = 1.05-1.20. Kinetic studies of complex **6e** found that the polymerization is first order in both monomer concentration and catalyst loading, while a trimetallic zinc alkoxyl complex reported by them previously shows a second order dependence of monomer concentration and first order dependence of the complex concentration.[50]

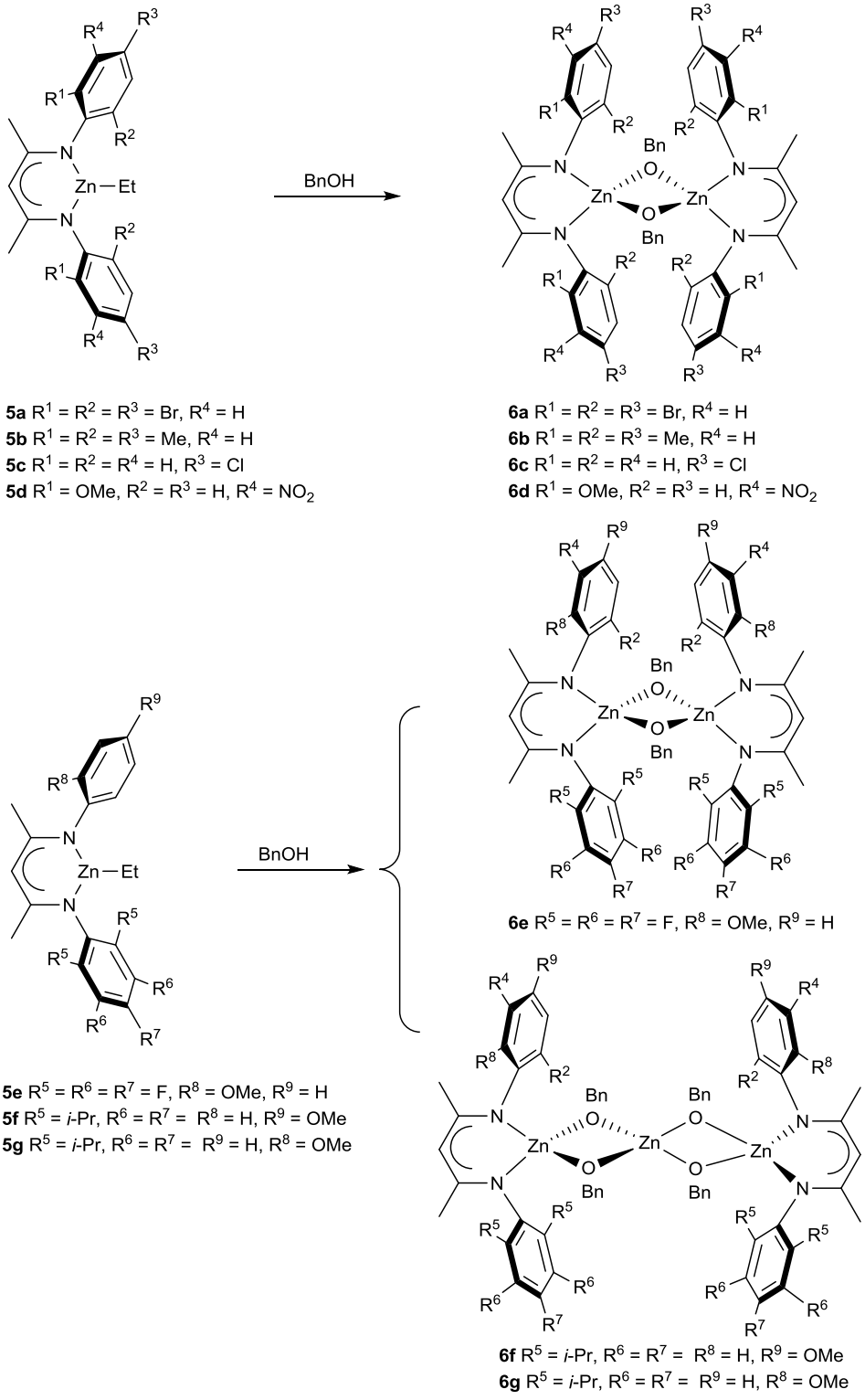

5a $R^1 = R^2 = R^3 = Br$, $R^4 = H$
5b $R^1 = R^2 = R^3 = Me$, $R^4 = H$
5c $R^1 = R^2 = R^4 = H$, $R^3 = Cl$
5d $R^1 = OMe$, $R^2 = R^3 = H$, $R^4 = NO_2$

6a $R^1 = R^2 = R^3 = Br$, $R^4 = H$
6b $R^1 = R^2 = R^3 = Me$, $R^4 = H$
6c $R^1 = R^2 = R^4 = H$, $R^3 = Cl$
6d $R^1 = OMe$, $R^2 = R^3 = H$, $R^4 = NO_2$

6e $R^5 = R^6 = R^7 = F$, $R^8 = OMe$, $R^9 = H$

5e $R^5 = R^6 = R^7 = F$, $R^8 = OMe$, $R^9 = H$
5f $R^5 = i\text{-Pr}$, $R^6 = R^7 = R^8 = H$, $R^9 = OMe$
5g $R^5 = i\text{-Pr}$, $R^6 = R^7 = R^9 = H$, $R^8 = OMe$

6f $R^5 = i\text{-Pr}$, $R^6 = R^7 = R^8 = H$, $R^9 = OMe$
6g $R^5 = i\text{-Pr}$, $R^6 = R^7 = R^9 = H$, $R^8 = OMe$

Scheme 1-5 Reaction of zinc ethyl BDI complexes with BnOH to prepare zinc alkoxyl BDI complexes.

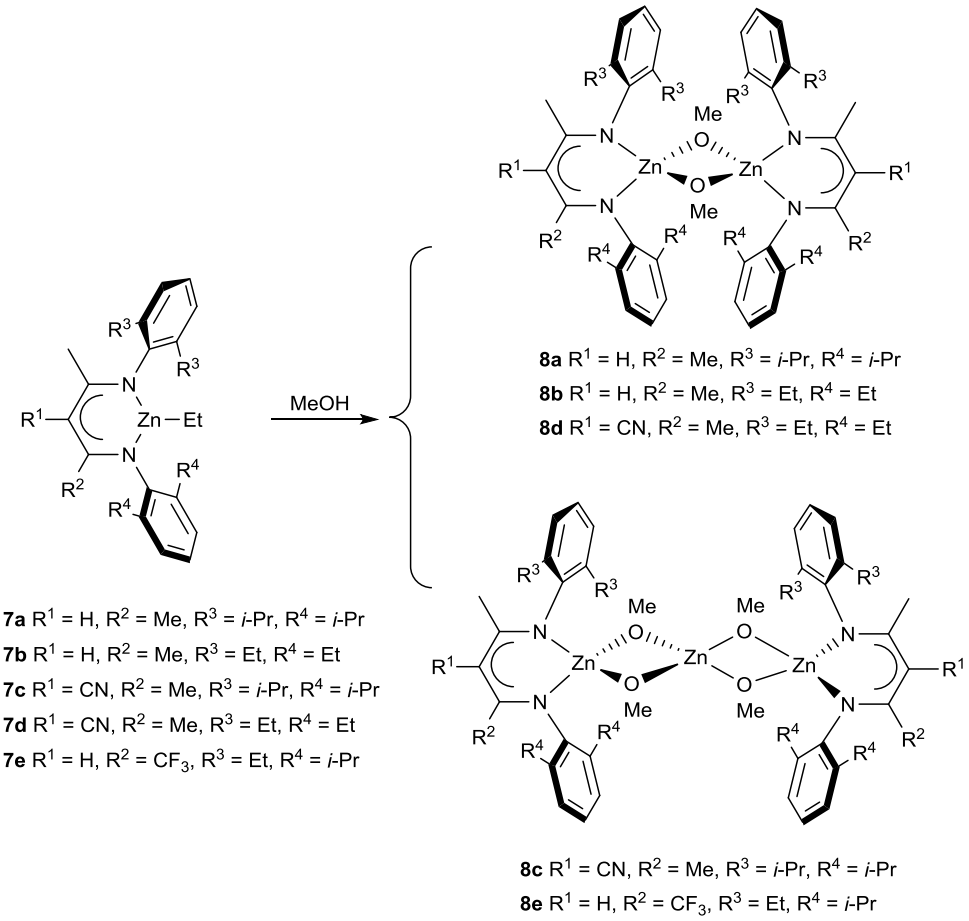

Scheme 1-6 Reaction of zinc ethyl BDI complexes with MeOH to prepare zinc alkoxyl BDI complexes.

Table 1-2 Polymerization of *rac*-lactide or L-lactide by zinc aryl-N-substituted BDI complexes.

Entry	Cat	$[LA]_o$ (M)	Loading (mol%)	Solv	Temp (°C)	t (min)	Conv (%)	Đ	P_r	Ref
1	**4a**	0.98	1	DCM	25	120	96	1.20	0.69	47
2	**4b**	0.98	1	DCM	25	30	98	1.37	0.55	47
3	**4c**	0.98	1	DCM	25	30	98	1.26	0.55	47
4	**4d**	0.98	1	DCM	25	30	98	1.72	0.55	47
5	**4e**	0.98	1	DCM	25	30	98	1.43	0.57	47
6	**4e**	0.98	1	THF	25	30	98	1.40	0.75	47
7	**4f**	0.98	1	DCM	25	30	98	1.07	0.68	47
8	**4g**	0.98	1	DCM	25	30	90	1.34	0.47	47
9*	**6b**	0.25	1	Tol.	R.T.	2	94	1.05	-	48
10*	**6e**	0.25	1	Tol.	R.T.	120	99	1.06	-	48
11*	**6f**	0.25	1	Tol.	R.T.	5	96	1.20	-	48
12*	**6g**	0.25	1	Tol.	R.T.	3	99	1.17	-	48

*ROP of L-lactide; DCM = dichloromethane; Tol. = toluene; R.T. = room temperature (no specified T given); dashes (-) indicate no stereospecificity reported.

1.6.2 Zinc Aliphatic N-Substituted β-Diiminate Complexes

For the purpose of synthesizing stereocontrolled PLA via a catalyst site control mechanism, Schaper and coworkers prepared a series of zinc aliphatic N-substituted BDI complexes.[51] Chirality can be provided by the chiral alkyl substituent of the imine of the BDI ligand, i.e. *S,S-nacnac*$^{CH(Me)PhH}$ (**9a)**, or by the prochiral alkyl substituent of the imine of the BDI ligand, i.e. *nacnac*^{BnH} (**9b**), which can generate chiral rotamers. Treatment of the ligand precursors with $ZnEt_2$ and $Zn[N(SiMe_3)_2]_2$ yielded the corresponding zinc ethyl complexes **10a, 10b** and zinc amides **12a, 12b,** respectively (**Scheme 1-7**). A possible

equilibrium between complex **10b** and homoleptic zinc species **11** is proposed. Zinc alkoxyl complexes **13a** and **13b** could be obtained by reaction of *i*-PrOH with zinc amide complexes, but not with zinc ethyl complexes. Chirality of complex **13a** is confirmed by NMR analysis, while complex **13b** shows C_{2v} symmetry, indicating fast rotation of N-benzyl bond. Crystal structure determination shows complex **13a** is a dimer with two bridging oxygens from O*i*-Pr and with two *anti*-orientated phenyl groups.

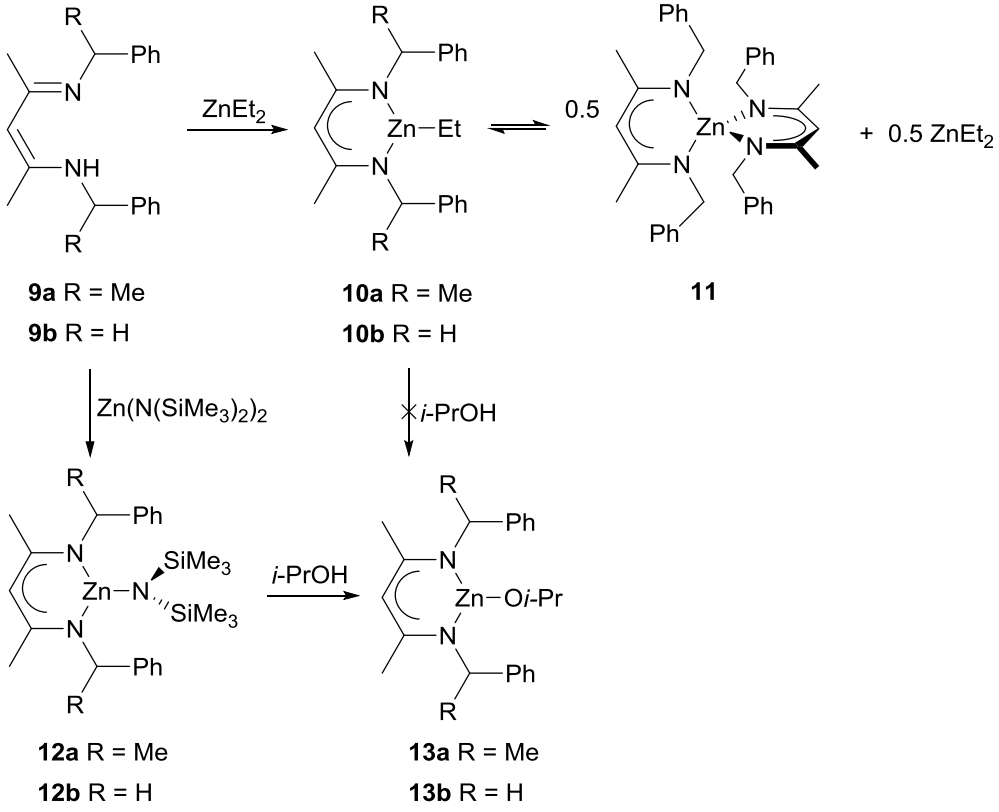

Scheme 1-7 Synthesis of zinc aliphatic N-substituted BDI complexes.

Lactide ROP catalyzed by complexes **13a** and **13b** has first-order dependence on lactide concentration, giving apparent first-order rate constants of k_{app} = 0.013-0.010 min^{-1} and k_{app} = 0.019-0.038 min^{-1}, respectively (**Table 1-3**). The polymers are predominately heterotactic property, and the P_r values of polymers obtained by **13a** (0.84-0.87) are

higher than those obtained by **13b** (0.65-0.71), which may be because **13a** is bulkier than **13b**. However, it was found by measuring the polarimetry of the remaining monomers that neither complex displays enantioselectivity for ROP of *rac*-lactide.

Table 1-3 ROP of *rac*-lactide by zinc aliphatic N-substituted BDI complexes.

Entry	Cat	$[LA]_o$ (M)	Loading (mol%)	Solv	Temp (°C)	k_{obs} (s^{-1})	Conv (%)	Đ	P_r	Ref
1	**13a**	0.17	1	DCM	23	0.013	75-85	-	0.86	51
2	**13a**	0.34	0.5	DCM	23	0.019	75-85	-	0.88	51
3	**13a**	0.51	0.33	DCM	23	0.016	75-85	-	0.85	51
4	**13a**	0.57	0.33	DCM	23	0.016	-	1.10	0.87	51
5	**13a**	0.54	0.33	DCM	23	0.015	-	1.10	0.85	51
6	**13b**	0.19	1	DCM	23	0.025	-		0.65-0.68	51
7	**13b**	0.34	0.5	DCM	23	0.038	-		0.66	51
8	**13b**	0.38	0.5	DCM	23	0.024	-	1.10	0.67-0.68	51
9	**13b**	0.60	0.33	DCM	23	0.035	-	1.10	0.68	51
10	**13b**	0.76	0.33	DCM	23	0.019	-		0.68-0.71	51

DCM = dichloromethane; dashes (-) indicate no conversion reported or no molecular weight dispersity reported.

In 2014, Schaper and coworkers further studied BDI zinc complexes with bulky anthrylmethyl substituents.[52] Zinc alkoxyl complexes **14a** and **b** were prepared using similar method as for **12** and **13** (**Scheme 1-8**). ROP of *rac*-lactide using **14a** has apparent first-order rate constants of k_{app} = 0.012-0.016 min^{-1} at 2.0 mM catalyst concentration. Promisingly, it shows increased heteroselectivity, P_r = 0.87-0.93 (entry 1-3, **Table 1-4**). The obtained polymers have higher than expected molecular weights, but the molecular weight dispersities are narrow. Catalytic-site control was not achieved due to the C_s-symmetric geometry of the complex. Complex **14b** with a chlorine substituent on the N-

C-C-C-N backbone shows lower stereoselectivity (P_r = 0.59) and lower activity than **14a** (entry 4, **Table 1-4**).

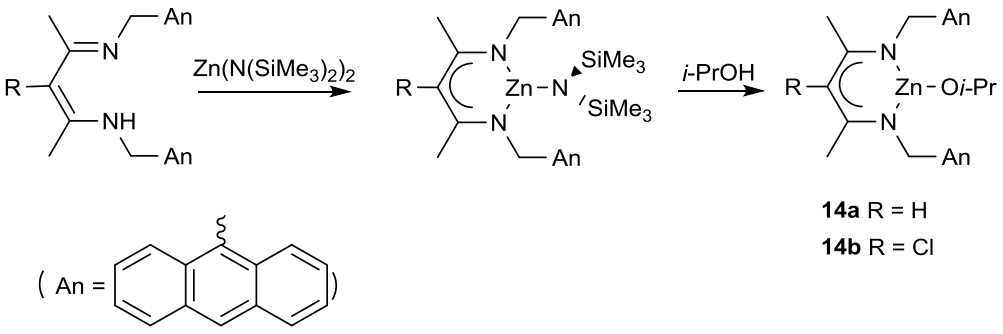

Scheme 1-8 Synthesis of zinc anthrylmethyl N-substituted BDI complexes.

Table 1-4 ROP of *rac*-lactide by zinc anthrylmethyl N-substituted BDI complexes.

Entry	Cat	$[LA]_o$ (M)	Loading (mol%)	Solv	Temp (°C)	t (min)	Conv (%)	Đ	P_r	Ref
1	**14a**	0.6	0.33	DCM	23	180	93	1.14	0.88	52
2	**14a**	0.6	0.33	DCM	23	360	95	1.16	0.93	52
3*	**14a**	0.6	0.33	DCM	23	180	87	1.04	0.87	52
4	**14b**	0.6	0.60	DCM	23	180	59	-	0.59	52

* With one equiv. of BnOH as co-initiator; DCM = dichloromethane; dashes (-) indicate no molecular weight dispersity reported.

1.7 Zinc Phenolate Complexes

1.7.1 Zinc Amino-phenolate Complexes

In 2003 Hillymer, Tolman and coworkers reported zinc complexes bearing diamino-phenolate ligands.[53] Zinc ethoxyl complex **15** was prepared by reaction of the zinc ethyl complex with 1.2 equiv. of ethanol (EtOH) (**Scheme 1-9**). Solid-state study by X-ray diffraction and laser desorption mass spectrometry (LDMS) showed complex **15** is a dimer. However, pulsed gradient spin-echo (PGSE) NMR study found the complex is

monomeric in solution. Complex **15** is the most efficient zinc catalyst for ROP of lactide to date, giving 93% *rac*-lactide conversion within 18 min at a catalyst loading of only 0.067% at 25 °C in DCM (entry 3, **Table 1-5**), but it has no stereoselectivity, giving atactic PLA from *rac*-lactide. Good control can be observed from the linear relationship between polymer molecular weight and monomer conversions with narrow molecular weight dispersities, Đ = 1.34-1.42; however, the molecular weights are lower than calculated values. Kinetic study via in situ FTIR spectroscopy (Mettler Toledo ReactIR) found the polymerization has first-order dependence of both the monomer and the complex concentration. Nonzero intercepts in plots of k_{obs} vs catalyst concentration show catalyst concentration thresholds of 0.7 mM and 2.4 mM at 25 °C and 0 °C, respectively. The catalyst may be deactivated by water to generate chain transfer agents, which causes lower than expected molecular weights.

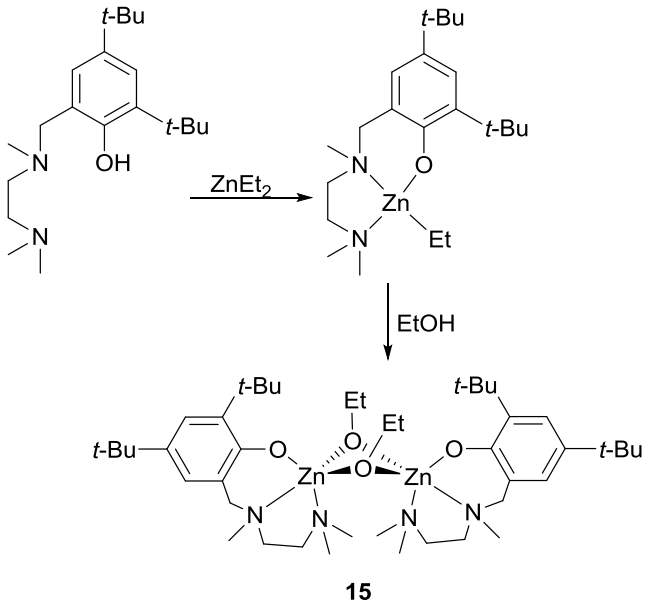

15

Scheme 1-9 Synthesis of zinc amino-phenolate complexes.

Inspired by Hillmyer and Tolman, Mehrkhodavandi and coworkers prepared a series of chiral zinc diamino-phenolate complexes in order to achieve enantiomorphic site control for ROP of lactide.[54] Enantiopure ((R,R)-**16**) and racemic ((±)-**16**) zinc ethyl complex were prepared by reaction of ligand precursors with $ZnEt_2$ (**Scheme 1-10**). An X-ray diffraction study shows that two diastereomers exist in (±)-**16** coming from the chirality of the amine. Unexpectedly, the zinc ethyl species are inert to different proton sources, e.g. methanol, ethanol, isopropyl alcohol (*i*-PrOH), and water. Protonation of complex **16** was finally achieved using phenol to yield (R,R)-**17** and (±)-**17** (**Scheme 1-10**). Unfortunately, (R,R)-**17** and (±)-**17** are not stereoselective, giving the probability of isotactic linkages between monomer units, P_m, values of 0.52 and 0.54 (entry 4-5, **Table 1-5**). Compared to the corresponding zinc ethoxyl species **15** reported by Hillmyer and Tolman, complex **17** is much less active towards ROP of *rac*-lactide. Also, complex **17** shows poor control giving broad molecular weight dispersities, Đ = 1.80-2.08.

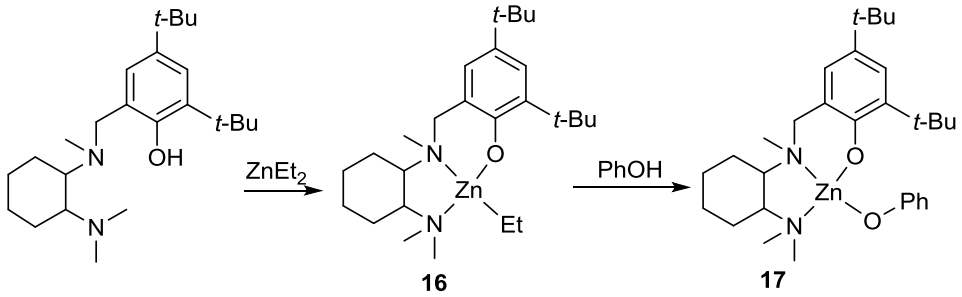

Scheme 1-10 Synthesis of chiral zinc diamino-phenolate complexes.

Lin and Chen prepared amino-phenolate ligands bearing different amine substituents, from which a series of zinc alkoxyl complexes (**18a-e**) were synthesized (**Scheme 1-11**).[55] Zinc alkoxyl **18b** was found to be dimeric in solid state but monomeric in solution. A study of L-lactide polymerization found that catalytic activity increases

with the bulkiness of the complex, resulting in that complex **18b** with the most bulky cyclohexyl substituents has the highest activity among these complexes, giving 97% conversion in 9 min (entry 6-10, **Table 1-5**). This increase in activity with steric bulkiness supports a transition state of dimer dissociation under polymerization conditions, i.e. the bulkier the complex, the faster the dissociation, resulting in an increase in polymerization rate.

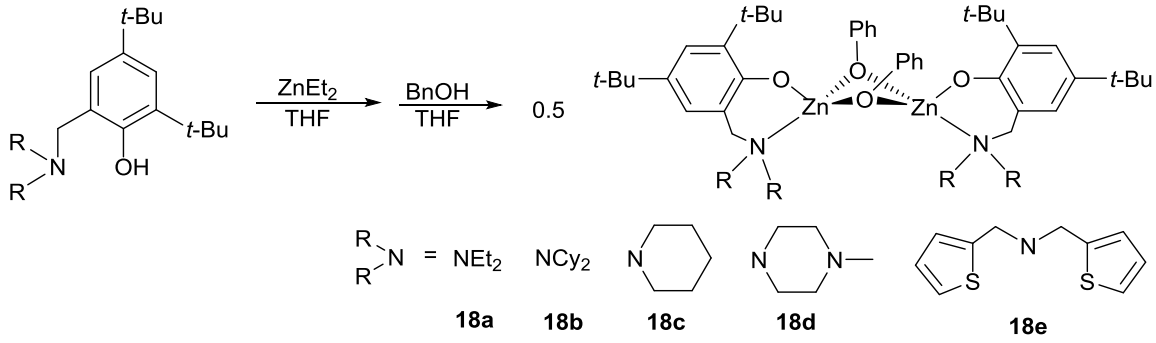

Scheme 1-11 Synthesis of zinc amino-phenolate complexes bearing different amine substituents.

Table 1-5 Polymerization of *rac*-lactide or L-lactide by zinc amino-phenolate complexes.

Entry	Cat	$[LA]_o$ (M)	Loading (mol%)	Solv	Temp (°C)	t (min)	Conv (%)	Đ	P_m	Ref
1	**15**	1	0.15	DCM	25	5	96	1.42	-	53
2	**15**	1	0.1	DCM	25	13	96	1.40	-	53
3	**15**	1	0.067	DCM	25	18	93	1.34	-	53
4	**(±)17**	0.31	0.5	DCM	20	2400	100	1.80	0.54	54
5	**(R,R)17**	0.31	0.5	DCM	20	2400	100	2.15	0.52	54
6*	**18a**	0.17	1	Tol.	R.T.	70	92	1.05	-	55
7*	**18b**	0.17	1	Tol.	R.T.	9	97	1.07	-	55
8*	**18c**	0.17	1	Tol.	R.T.	60	90	1.02	-	55
9*	**18d**	0.17	1	Tol.	R.T.	73	95	1.03	-	55
10*	**18e**	0.17	1	Tol.	R.T.	24	94	1.17	-	55

*ROP of L-lactide; DCM = dichloromethane; Tol. = toluene; R.T. = room temperature (no specified T given); dashes (-) indicate no stereospecificity reported.

Zinc bis(morpholinomethyl)-phenolate complexes were investigated by Carpentier and Sarazin.[56] A bimetallic complex **19** (**Figure 1-5**) was utilized for large-scale polymerization of lactide by utilizing low catalyst loading with a large amount of chain transfer reagent. Complex **19** in the presence of 10 equiv. of *i*-PrOH achieved 97% conversion after 60 min with 0.01% catalyst loading at 60 °C in toluene, giving polymers with expected molecular weights and narrow molecular weight dispersity (Đ = 1.10) (entry 2, **Table 1-6**). Surprisingly, controlled polymerization was achieved with 500 equiv. of *i*-PrOH and only 0.02% catalyst loading (entry 3, **Table 1-6**). This shows great potential for a non-toxic zinc complex to be the preferred catalyst for large-scale lactide polymerization.

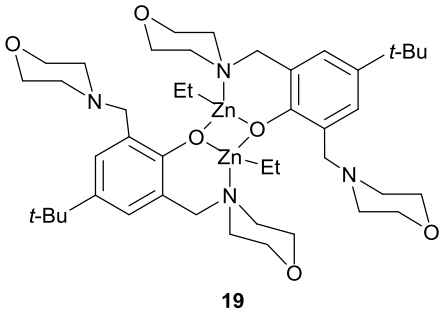

Figure 1-5 Structure of a zinc bis(morpholinomethyl)-phenolate complex.

In 2011, a series of zinc complexes with multidentate amino-phenolate ligands were prepared by Carpentier and Sarazin (**Scheme 1-12**).[57] The activity of **20** towards L-lactide polymerization was assessed and it showed similar activity to **19** as reported by them previously, which indicates the effect of the second morpholine substituent is negligible. Complex **21** is highly active for ROP of L-lactide, giving 94% conversion after only 10 min with 0.01% catalyst loading and 10 equiv. of *i*-PrOH at 60 °C in toluene (entry 4, **Table 1-6**). It was found *i*-PrOH is necessary in obtaining good activity and control. The obtained polymers are well controlled in molecular weight and molecular weight dispersity, Đ = 1.07-1.09, and PLA obtained from *rac*-lactide in THF is slightly heterotactic, $P_r = 0.63$ (entry 5, **Table 1-6**).

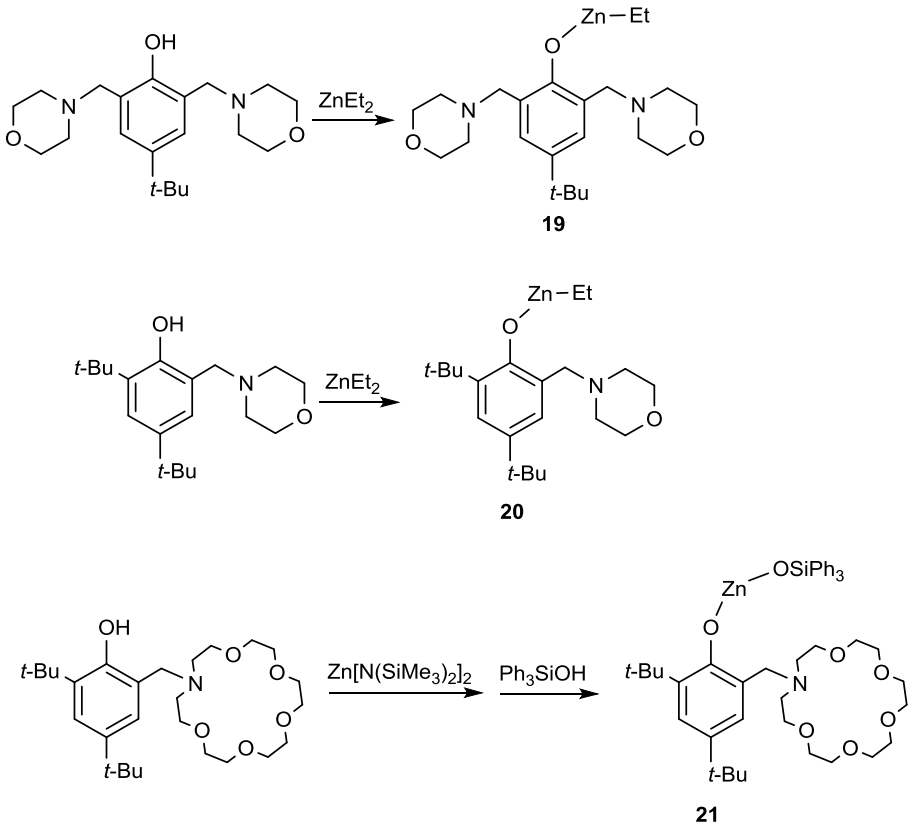

Scheme 1-12 Synthesis of zinc complexes bearing multidentate amino-phenolate ligands.

In 2011, Kerton and coworkers prepared a series of zinc complexes bearing piperazinyl amino-phenolate ligands.[58] Zinc ethyl complexes were obtained via reaction with ligand precursors and $ZnEt_2$, followed by alcoholysis with BnOH or *t*-BuOH to generate zinc alkoxyl species (**Scheme 1-13**). Compared to zinc morpholinyl complex **19** reported by Carpentier and Sarazin, the zinc piperazinyl complexes (**22b-e**) have slower activity towards ROP of lactide (entry 6-11, **Table 1-6**). Use of a microwave reactor shortened the polymerization time to 5 min to achieve over 90% conversion at 120 °C in toluene and generated PLA with good molecular weight agreement and narrow molecular weight dispersities (Đ = 1.33-1.42) (entry 8-9, **Table 1-6**). Study of the microstructure of

the PLA found these zinc complexes have no stereoselectivity, giving atactic PLA (P_r = 0.51-0.53).

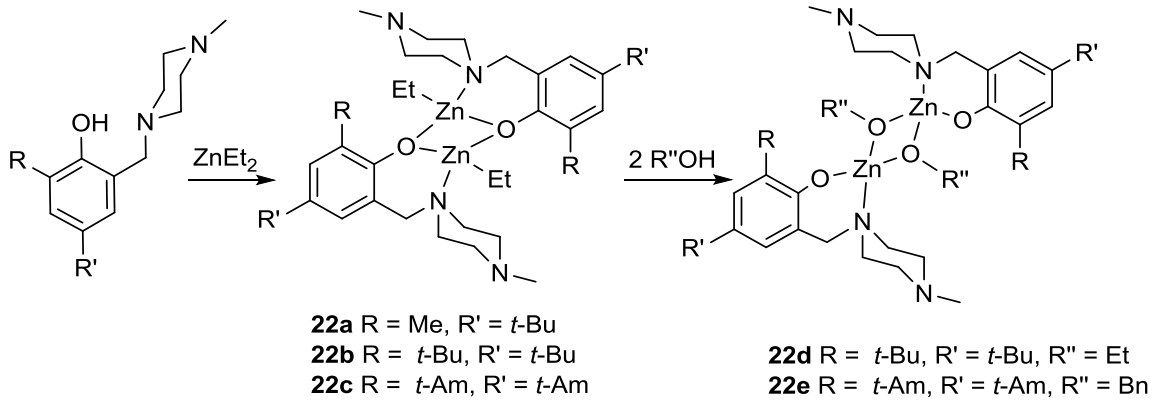

Scheme 1-13 Synthesis of zinc piperazinyl amino-phenolate complexes.

Table 1-6 ROP of rac-lactide or L-lactide by zinc morpholino-phenolate complexes.

Entry	Cat	eqv./co-initiator	$[LA]_0$ (M)	Loading (mol%)	Solv	Temp (°C)	t (min)	Conv (%)	Đ	P_r	Ref
1*	**19**	-	2	0.1	Tol.	60	60	18	2.24	-	56
2*	**19**	10/*i*-PrOH	2	0.1	Tol.	60	60	97	1.10	-	56
3*	**19**	25/*i*-PrOH	4	0.02	Tol.	60	90	94	1.16	-	56
4*	**21**	10/*i*-PrOH	2	0.1	Tol.	60	10	94	1.07	-	57
5*	**21**	10/*i*-PrOH	2	0.1	THF	60	15	88	1.09	0.63	57
6	**22b**	1/BnOH	0.44	1	Tol.	70	90	98	1.32	0.45	58
7	**22b**	1/*t*-BuOH	0.44	1	Tol.	70	120	96	1.60	0.53	58
8[a]	**22b**	1/BnOH	0.44	1	Tol.	120	5	90	1.33	0.47	58
9[a]	**22b**	1/*t*-BuOH	0.44	10	Tol.	120	5	93	1.42	0.47	58
10	**22c**	1/BnOH	0.44	1	Tol.	70	60	97	1.42	0.51	58
11	**22e**	-	0.44	1	Tol.	70	15	95	1.37	0.47	58

*ROP of L-lactide; [a] Polymerizations conducted by microwave reactor; Tol. = toluene; dashes (-) indicate no addition of co-initiator or no stereospecificity reported.

The aim of synthesizing isotactic PLA has been attempted by many groups including Ma and coworkers, who utilized tetradentate amino-phenolate ligands.[59] Zinc complexes with different substituents in the phenyl and phenoxyl moieties were prepared and all the complexes were found to have distorted tetrahedral geometry at the zinc center, with the coordination of phenoxyl oxygen, amine and the pendant amine donor, but the ether or amine substituent in the phenyl is not coordinated (**Figure 1-6**). Zinc amide complex **23a** gives 98% conversion within 4 min at 0.5% catalyst loading with one equiv. *i*-PrOH at 25 °C in THF (entry 1, **Table 1-7**). Complex **23b** with a bulky cumyl substituent on the phenoxyl has lower activity than **23a** but gives polymers with isotactic property, P_m = 0.60 in THF (entry 2, **Table 1-7**). Chloro-substituted complex **23c** is more efficient than complex **23b** and, interestingly, shows moderate heterotactic bias for ROP

of *rac*-lactide in toluene (P_r = 0.67) (entry 5, **Table 1-7**). A solvent effect was observed which shows that polymers obtained in THF have better molecular weight agreement than when using toluene. Also, it was found *i*-PrOH is required for achieving good control. Zinc ethyl complexes were prepared and those having a methoxyl substituent in the phenyl moiety (complexes **23d** and **23e**) give better activity than those having a dimethylamine substituent (complexes **23f** and **23g**) (entry 6-10, **Table 1-7**).

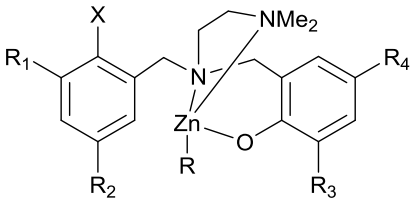

X = OMe, R = $N(SiMe_3)_2$

23a $R_1 = R_2 = H$, $R_3 = R_4 = t$-Bu

23b $R_1 = t$-Bu, R_2 = Me, $R_3 = R_4$ = Cumyl

23c $R_1 = t$-Bu, R_2 = Me, $R_3 = R_4$ = Cl

X = OMe, R = Et

23d $R_1 = R_2 = H$, $R_3 = R_4$ = Cumyl

23e $R_1 = R_2 = H$, $R_3 = R_4$ = Cl

X = NMe_2, R = Et

23f $R_1 = H$, R_2 = Me, $R_3 = R_4$ = Cumyl

23g $R_1 = H$, R_2 = Me, $R_3 = R_4$ = Cl

(Cumyl = $PhC(Me_2)$)

Figure 1-6 General structure of zinc amino-phenolate complexes.

Further modification of the pendant arm of zinc amino-phenolate complexes by replacement of the amine donor NMe_2 with bulkier NEt_2 such as in complex **24a** or by elongation of the arm with one more carbon such as complex **24b** were conducted by the same group (**Figure 1-7**).[60] Promisingly, complex **24a** with the bulkier pendent amine donor NEt_2 showed enhanced isotactic selectivity toward *rac*-lactide polymerization with P_m up to 0.65 (entry 11, **Table 1-7**). However, these modifications harm the catalytic

activity resulting in longer reaction times of 2 - 8 h to reach full conversion using the same conditions as their previous work.[59] Zinc alkoxyl complex **24c** was prepared using 1/6 equiv. of 3-*tert*-butyl-2-methoxy-5-methylbenzyl alcohol. As expected, complex **24c** showed better activity than the corresponding zinc amide complexes, giving 90% conversion after 45 min at 0.5% catalyst loading in the presence of *i*-PrOH (entry 12, **Table 1-7**). Living polymerization was observed, as shown by the linear relationship between molecular weights of the polymers and the monomer conversion. The polymers show narrow molecular weight dispersities (Đ = 1.11) and molecular weights close to the theoretical values considering both the benzyloxyl group and *i*-PrOH as initiating groups.

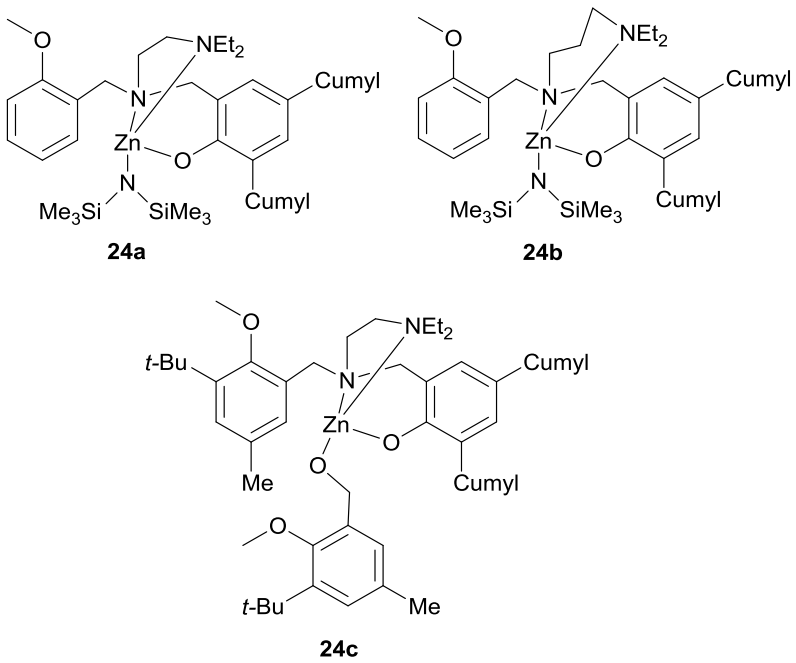

Figure 1-7 Structures of zinc amino-phenolate complexes.

Table 1-7 ROP of *rac*-lactide by zinc phenylamino-phenolate complexes.

Entry	Cat	Co-initiator	$[LA]_0$ (M)	Loading (mol%)	Solv	Temp (°C)	t (min)	Conv (%)	Đ	P_m	Ref
1	**23a**	*i*-PrOH	1.00	0.5	THF	25	4	98	1.40	0.49	59
2	**23b**	-	1.00	0.5	THF	24	50	85	1.76	0.60	59
3	**23b**	*i*-PrOH	1.00	0.5	THF	25	9	90	1.10	0.45	59
4	**23c**	*i*-PrOH	1.00	0.5	THF	24	5	95	1.22	0.37	59
5	**23c**	-	1.00	0.5	Tol.	24	30	92	1.57	0.33	59
6	**23d**	*i*-PrOH	1.00	0.5	THF	60	240	55	1.08	0.53	59
7	**23d**	*i*-PrOH	1.00	0.5	Tol.	60	100	74	1.08	0.53	59
8	**23e**	*i*-PrOH	1.00	0.5	THF	60	250	76	1.07	0.44	59
9	**23f**	*i*-PrOH	1.00	0.5	THF	60	240	62	1.17	0.54	59
10	**23g**	*i*-PrOH	1.00	0.5	THF	60	250	83	1.20	0.44	59
11	**24a**	*i*-PrOH	1.00	0.5	Tol.	24	60	98	1.46	0.65	60
12	**24c**	*i*-PrOH	1.00	0.5	Tol.	25	45	90	1.11	0.62	60

Tol. = toluene; R.T. = room temperature (no specified T given); dashes (-) indicate no addition of co-initiator.

Isotactic PLA was obtained by Ma and coworkers using chiral zinc amino-phenolate complexes.[61] Ligands with chiral N-alkylpyrrolidinyl substituents were prepared and reacted with $Zn[N(SiMe_3)_2]_2$ to generate the corresponding zinc amide complexes **25-29** (**Scheme 1-14**). Interestingly, the zinc amide complexes were shown to occur as pairs of diastereomers, and the proportion of one diastereomer decreases as the ortho-substituent of the phenoxyl becomes bulkier, as a result enantio-pure complex **29** with a bulky trityl substituted phenolate *n*-butyl pyrrolidinyl group was obtained. It was found that the activity decreases, however, with the bulkiness of the *ortho*-substituent of the phenoxyl moiety, as observed that complex **25** with only 0.067% catalyst loading provided 95% conversion of *rac*-lactide after 20 min, while 360 min is needed for complex **29** to achieve 82% conversion at 0.1% catalyst loading (entry 1-2, **Table 1-8**).

Interestingly, the tacticity of the polymers switch from heterotactic to isotactic with this increase of steric bulkiness, leading to highly isotactic PLA (P_m = 0.81) given by complex **29**.

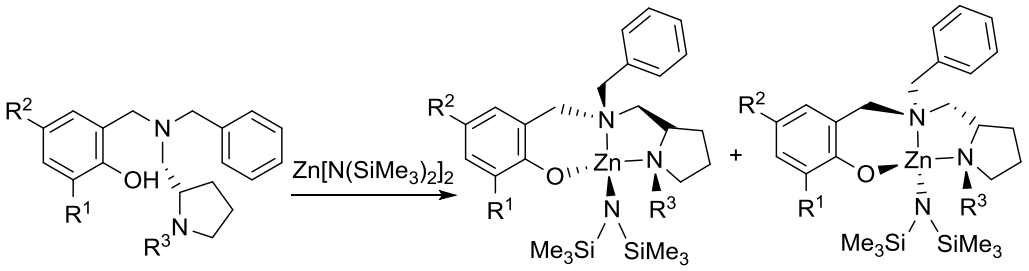

(*S*)-**L1**H: R^1 = R^2 = Cl, R^3 = Et
(*S*)-**L2**H: R^1 = R^2 = Me, R^3 = Et
(*S*)-**L3**H: R^1 = R^2 = *t*-Bu, R^3 = Et
(*S*)-**L4**H: R^1 = Trityl, R^2 = Me, R^3 = Et
(*S*)-**L5**H: R^1 = Trityl, R^2 = Me, R^3 = *n*-Bu

25: **L1**ZnN(SiMe$_3$)$_2$, **25a:25b** = 1:2.5
26: **L2**ZnN(SiMe$_3$)$_2$, **26a:26b** = 1:2
27: **L3**ZnN(SiMe$_3$)$_2$, **27a:27b** = 1:1
28: **L4**ZnN(SiMe$_3$)$_2$, **28a:28b** = 7:1
29: **L5**ZnN(SiMe$_3$)$_2$, **29** enantiopure

Scheme 1-14 Synthesis of chiral zinc amino-phenolate complexes.

Ma and coworkers further modified the phenyl moiety with a coordinating N,N-dimethylanilinyl substituent to produce tetradentate amino-phenolate ligands.[62] Besides, they changed the pendant arm with a variety of alkyl amines. Study of the complexes found that the tetradentate ligands only have three sites coordinated to the zinc center, either the alkylamine (complexes **30a-b**) or the arylamine (complexes **30c-g**) (**Scheme 1-15**). A large difference in stereoselectivity was observed: complexes **30a-b** generate heterotactic PLA (P_m = 0.40-0.46), while complexes **30c-g** generate isotactic PLA (P_m = 0.71-0.81). Impressively, complex **30g** has isotactic selectivity as high as complex **29** (P_m = 0.81) (entry 4, **Table 1-8**). The activity is increased with decreased steric bulkiness, and complex **30b** has the best activity among these complexes, converting 90% monomer in 20 min at 0.5% catalyst loading with 1 equiv. of *i*-PrOH at 25 °C in toluene (entry 3,

Table 1-8). Kinetic studies found the polymerizations have orders of 1.78-1.81 in complex concentration, suggesting a bimetallic mechanism.

Table 1-8 ROP of *rac*-lactide by zinc phenylamino-phenolate complexes.

Entry	Cat	co-initiator	$[LA]_o$ (M)	Loading (mol%)	Solv	Temp (°C)	t (min)	Conv (%)	Đ	P_m	Ref
1	**25**	*i*-PrOH	1	0.067	Tol.	25	20	95	1.13	0.41	61
2	**29**	*i*-PrOH	1	0.067	Tol.	25	360	82	1.14	0.81	61
3	**30b**	*i*-PrOH	1	0.5	Tol.	25	20	90	1.33	0.43	62
4	**30g**	*i*-PrOH	1	0.5	THF	25	120	88	1.11	0.81	62
5	**31**	*i*-PrOH	1	0.5	Tol.	25	90	99	1.12	0.80	63
6	**32**	*i*-PrOH	1	0.5	Tol.	25	90	97	1.04	0.79	63
7	**33**	-	1	0.5	Tol.	25	90	94	1.06	0.80	63
8	**34**	-	1	0.5	Tol.	25	90	96	1.05	0.79	63
9	**35**	-	1	0.5	Tol.	25	25	96	1.72	0.22	63
10	**36**	-	1	0.5	Tol.	25	25	98	1.58	0.22	63
11	**38a**	-	0.34	2	$CHCl_3$	R.T.	1400	96	1.07	-	64
12	**38b**	-	0.34	2	$CHCl_3$	R.T.	120	98	1.31	-	64
13	**38c**	-	0.34	2	$CHCl_3$	R.T.	1400	95	1.31	-	64
14	**38d**	-	0.34	2	$CHCl_3$	R.T.	1400	98	1.13	-	64
15	**38e**	-	0.34	2	$CHCl_3$	R.T.	1400	97	1.07	-	64

Tol. = toluene; R.T. = room temperature (no specified T given); dashes (-) indicate no addition of co-initiator or no stereospecify reported.

Zinc and magnesium amino-phenolate complexes with similar structures were reported by Ma (**Scheme 1-16**).[63] Zinc complexes **31-34** gave isotactic PLA (P_m = 0.79-0.80) (entry 5-8, **Table 1-8**), while magnesium complexes **35-36** gave heterotactic PLA (P_r = 0.78) (entry 9-10, **Table 1-8**). A kinetic study found that there is a large difference between the apparent rate of ROP for D-lactide and that of L-lactide catalyzed by the zinc complexes, but a negligible difference in rates for the two monomers when catalyzed by

the magnesium complexes. Zinc lactate complexes such as **37** were obtained (**Scheme 1-17**) and their structures were found to have pentacoordinate zinc centers with coordination of the carbonyl oxygen of the lactate moiety, which supports a combination of enantiomorphic site control and chain end control mechanisms for these zinc complexes to achieve isoselectivity. However, the heteroselectivity of the magnesium complexes is believed to be achieved by a chain end control mechanism.

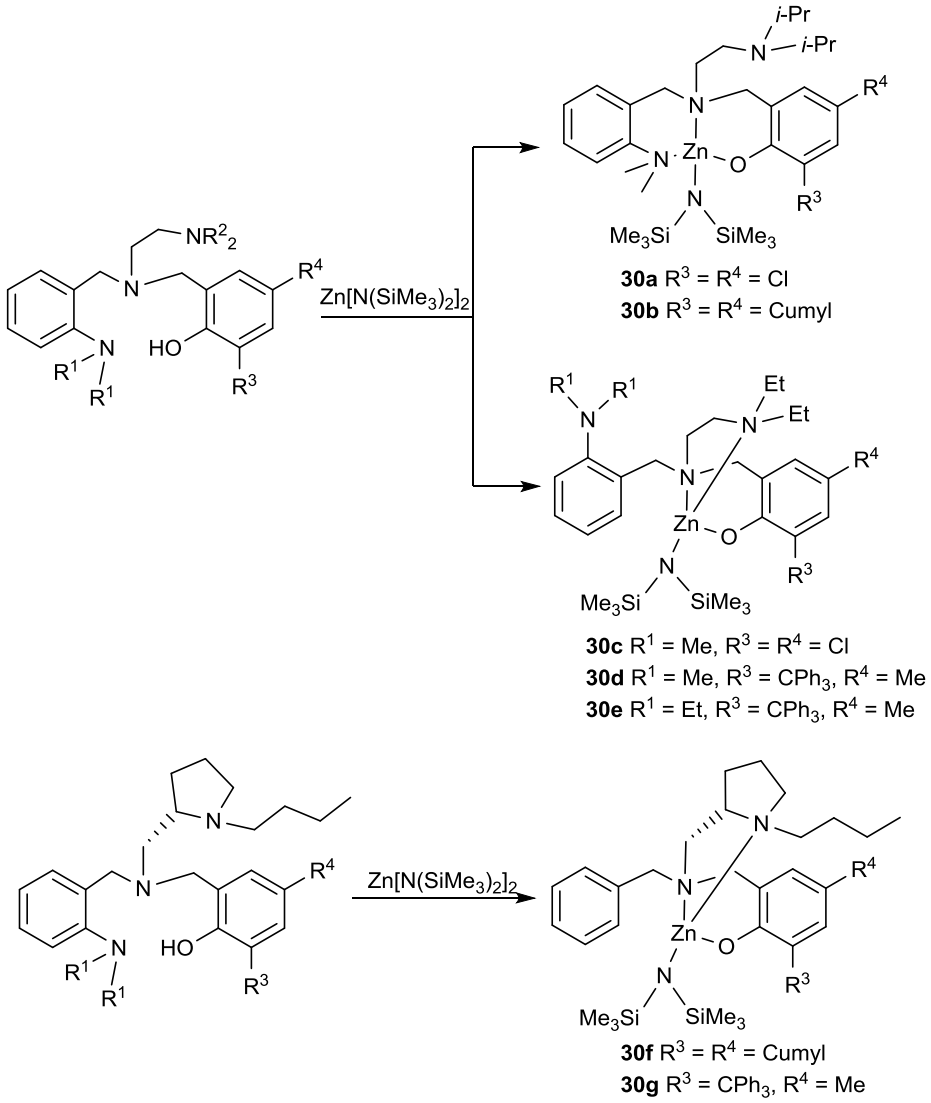

Scheme 1-15 Synthesis of zinc amino-phenolate complexes.

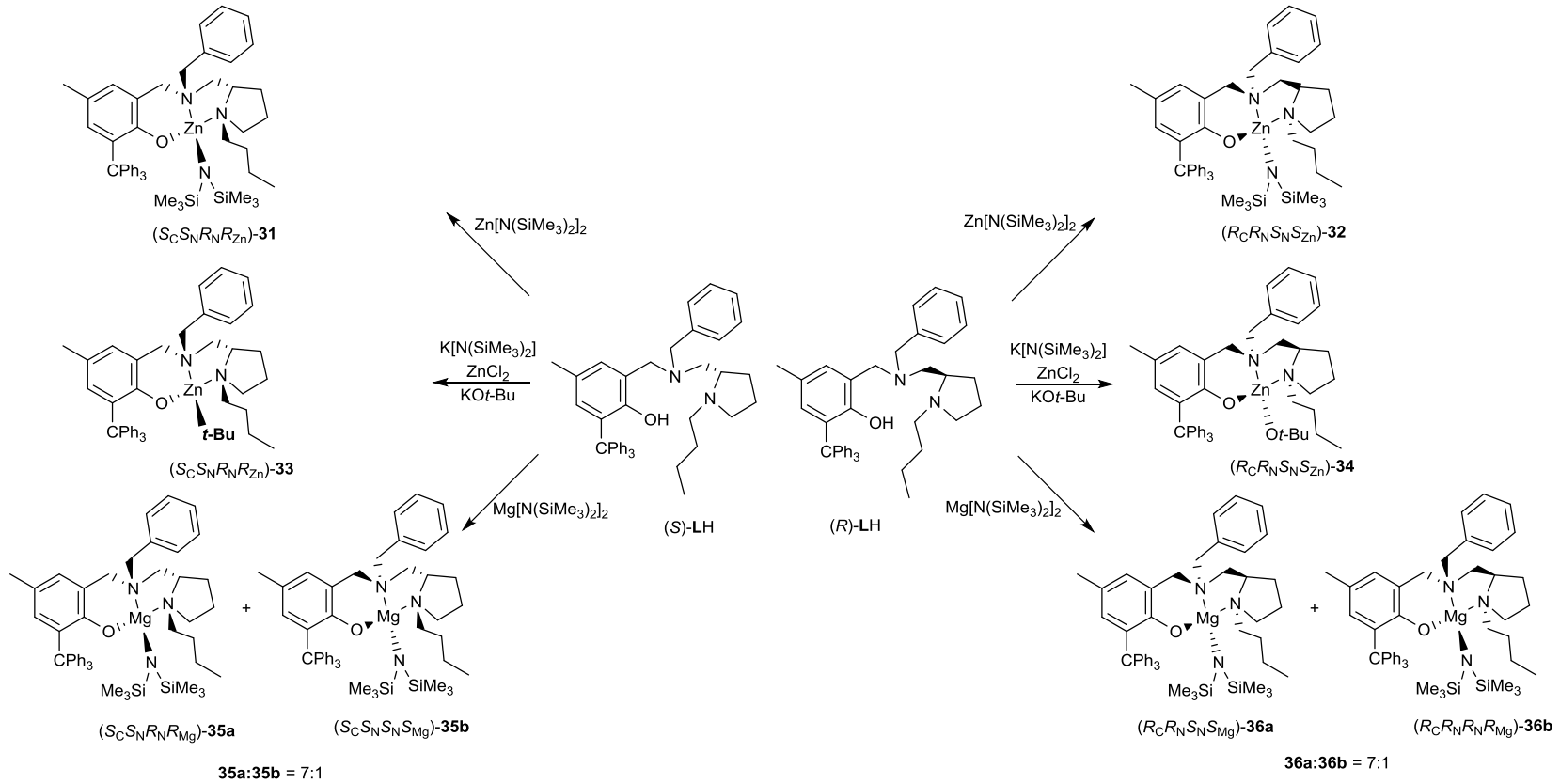

Scheme 1-16 Synthesis of zinc and magnesium amino-phenolate complexes.

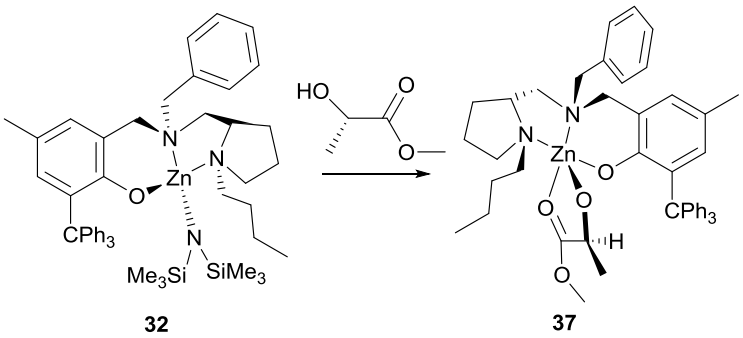

Scheme 1-17 Synthesis of a zinc methyl lactate complex bearing amino-phenolate ligand.

1.7.2 Zinc Imino-phenolate Complexes

Chiral zinc imino-phenolate complexes prepared from natural amino acids were reported by Darensbourg and coworkers.[64] They attempted to achieve enantiomorphic site control to obtain stereoselective ROP of lactide. Monomeric zinc amide complexes with different backbone substituents (**38a-d**) were prepared by reaction of the ligand precursors with $Zn[N(SiMe_3)_2]_2$ (**Scheme 1-18**). Dimeric zinc complex **38e** was obtained using *para*-fluorophenol and a study of crystal structure showed that its two zinc centers have different coordination environments. Studies of the polymerization rates towards L-lactide and D-Lactide was found that chiral complexes **38a-c** have no preference towards either enantiomers. Epimerization of lactide was observed when using non-chiral complex **38d** for ROP of L-lactide. Among these complexes, complex **38a** has the best activity for ROP of *rac*-lactide, $k_{D\text{-}LA,obs}$ = 3.13 h^{-1} and $k_{L\text{-}LA,obs}$ = 2.73 h^{-1}. The polymers obtained from these complexes have good molecular weight agreement and narrow molecular weight dispersity, Đ = 1.07-1.31 (entry 11-15, **Table 1-8**). Interestingly, these catalysts yielded heterotactic polylactides and complex **38c** shows the best heterotactic property (P_r = 0.83), which can be enhanced to P_r = 0.89 at – 30 °C.

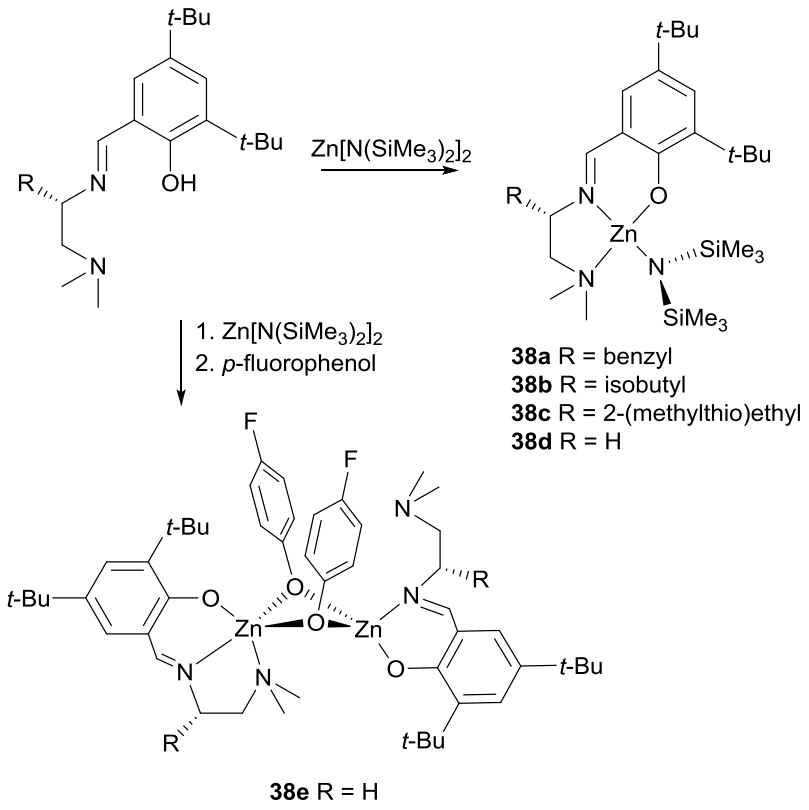

Scheme 1-18 Synthesis of zinc imino-phenolate complexes.

In 2015, Ma and coworkers utilized binaphthyl imino-phenolate ligands to prepare the corresponding zinc and magnesium complexes (**Scheme 1-19**).[65] An X-ray diffraction study found that magnesium complex **39a** is four coordinate, while zinc complex **39d** is three coordinate (without the coordination of NMe_2). Magnesium complexes **39a** gave atactic PLA (P_r =0.49) in toluene but heterotactic PLA (P_r = 0.72) in THF (entry 1-2, **Table 1-9**). Complex **39d** gave PLA with heterotactic bias (P_r = 0.80-0.84) in toluene or THF (entry 3-6, **Table 1-9**).

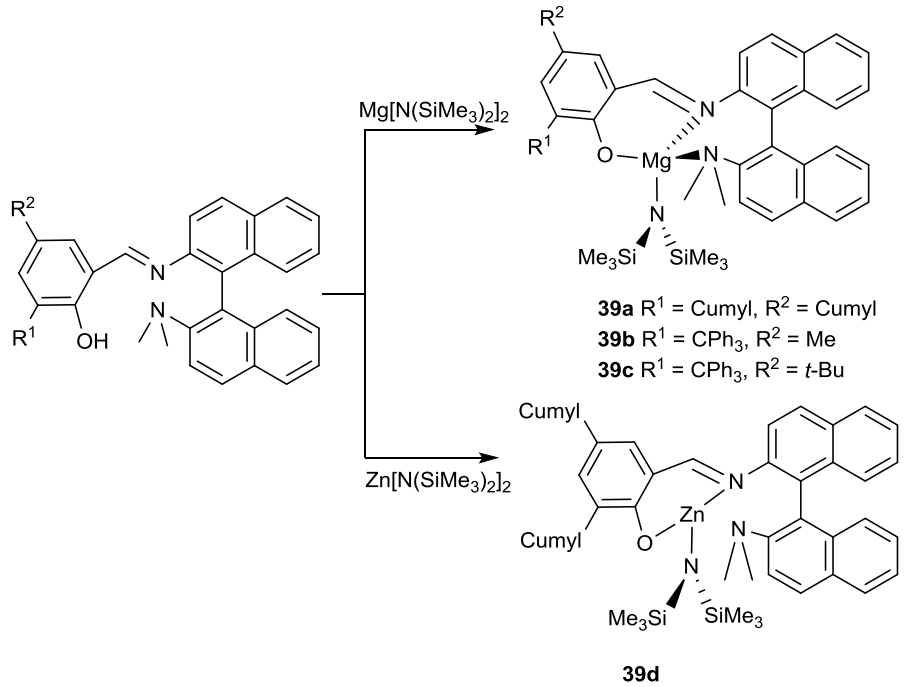

Scheme 1-19 Synthesis of zinc binaphthyl imino-phenolate complexes.

Table 1-9 ROP of *rac*-lactide by zinc imino-phenolate complexes.

Entry	Cat	eqv./co-initiator	$[LA]_0$ (M)	Loading (mol%)	Solv	Temp (°C)	t (min)	Conv (%)	Đ	P_r	Ref
1	**39a**	*i*-PrOH	1	0.5	Tol.	25	210	92	1.50	0.49	65
2	**39a**	*i*-PrOH	1	0.5	THF	25	25	98	1.47	0.72	65
3	**39d**	-	1	0.5	Tol.	50	20	96	1.70	0.80	65
4	**39d**	*i*-PrOH	1	0.5	Tol.	25	60	96	1.19	0.83	65
5	**39d**	-	1	0.5	THF	25	90	86	1.46	0.84	65
6	**39d**	*i*-PrOH	1	0.5	THF	25	60	97	1.53	0.83	65

Tol. = toluene; dashes (-) indicate no addition of co-initiator.

1.7.3 Zinc Benzotriazole Phenolate Complexes

Benzotriazole-phenolate (BTP) complexes bearing different substituents have been studied by Lin, Ko and coworkers.[66-69] The BTP aluminum complexes have been studied by them previously and showed good control for ROP of L-lactide, but the

polymerization is slow (48 h is needed to achieve full conversion).[66] Zinc BTP complexes **40** (**Scheme 1-20**) in the presence of 9-anthracenemethanol (9-AnOH) showed excellent activity for ROP of ε-caprolactone (ε-CL) (> 99% conversion with 2% catalyst loading in 5 min at 30 °C) and β-butyrolactone (> 99% conversion with 2% catalyst loading in 120 min at 55 °C) (entry 1-2, **Table 1-10**). Promisingly, block copolymer PCL-*b*-PHB (PHB: poly(3-hydroxybutyrate)) was successfully prepared by copolymerization of ε-caprolactone and β-butyrolactone using complex **40**.[67]

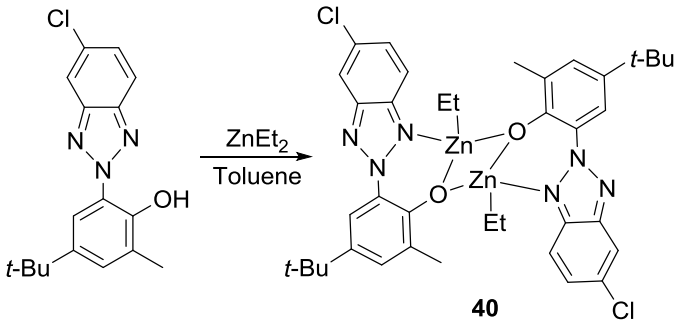

Scheme 1-20 Synthesis of a zinc benzotriazole-phenolate complex.

Zinc complex **41** with tridentate amino-benzotriazole phenolate ligand was prepared and reaction with BnOH yielded benzyloxyl complex **42** (**Scheme 1-21**).[69] In the solid state, **41** is a dimer with two bridging phenolate oxygens and **42** is a tetrametallic complex with four bridging benzyloxyl groups and one ligand per zinc. However, there are no data reported about whether the dimer of **41** and the tetramer of **42** dissociate to monomers in solution state. Complex **41** with stoichiometric amount of 9-AnOH and complex **42** showed good activity and control towards ROP of ε-caprolactone but slow rate towards ROP of β-butyrolactone (entry 3-6, **Table 1-10**). Most interestingly, they found that for complex **42** each zinc exhibits as an active site for polymerization, proven by the excellent agreement of molecular weights and narrow molecular weight

dispersities, which support the dissociation of the complex in solution state. Noticeably, these zinc complexes showed lower activity than the previously reported zinc benzotriazole-phenolate complex, **40**.

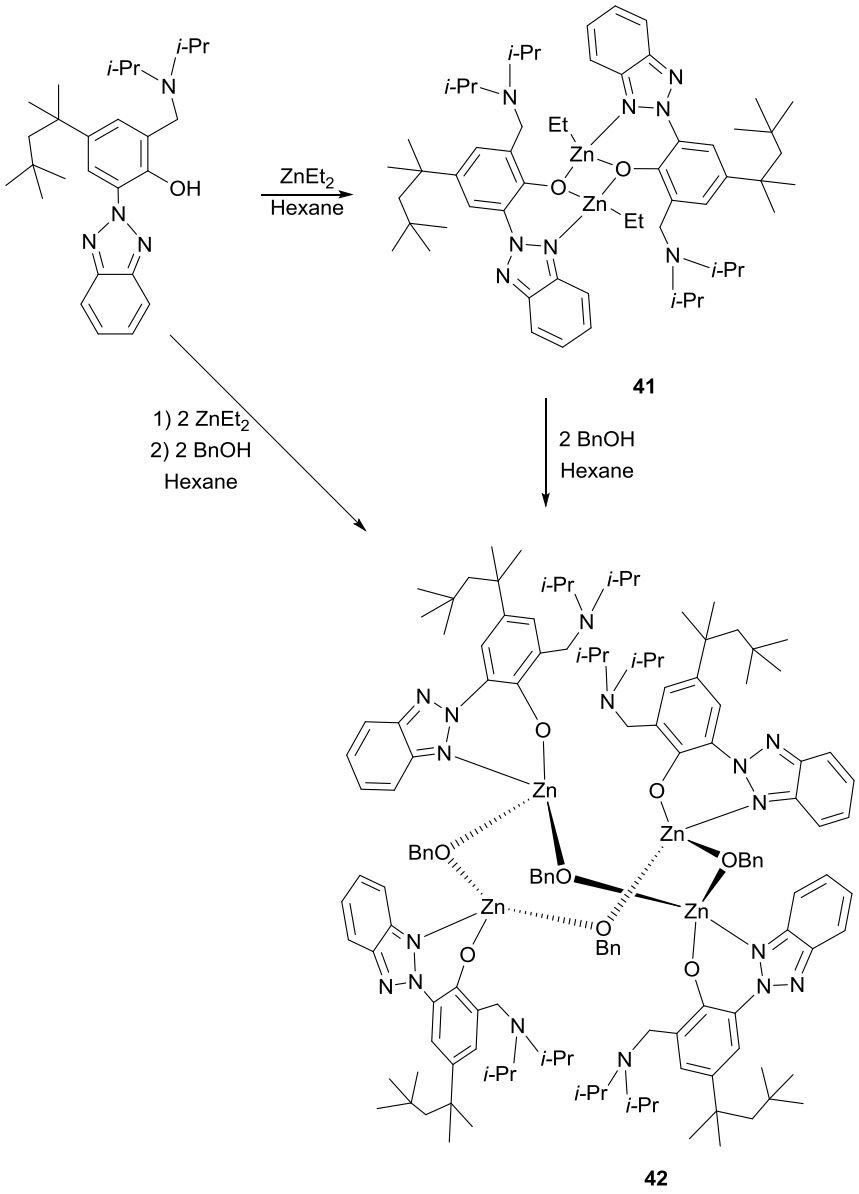

Scheme 1-21 Synthesis of zinc amino-benzotriazole-phenolate complexes.

Further utilization of bis(amino)-benzotriazole-phenolate zinc complexes for ROP of L-lactide was investigated by Ko and coworkers.[68] The tetradentate ligand coordinates

to the zinc center with only three donor atoms, resulting in a tetrahedral geometry of the monomeric complex **43** (**Scheme 1-22**). It gives 97% lactide conversion after 3 h at 0.1% catalyst loading with stoichiometric amount of 9-AnOH. The resulting polymer has higher than expected molecular weight but narrow dispersity (Đ = 1.13) (entry 7-8, **Table 1-10**). Complex **43** produces slight isotactic PLA from *rac*-lactide under long polymerization time in THF (P_m = 0.59).

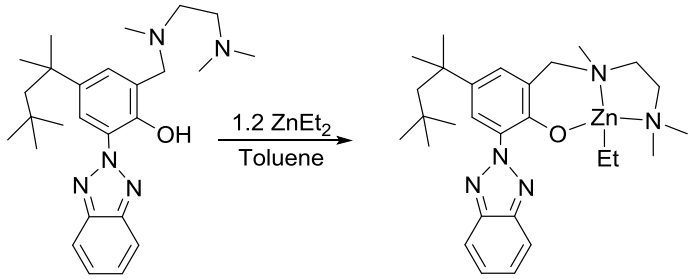

43

Scheme 1-22 Synthesis of a zinc bis(amino)-benzotriazole-phenolate complex.

Table 1-10 ROP of ε-caprolactone, β-butyrolactone and L-lactide by zinc benzotriazole-phenolate complexes.

Entry	Cat	co-initiator	$[LA]_o$ (M)	Loading (mol%)	Solv	Temp (°C)	t (min)	Conv (%)	Đ	P_m	Ref
1	**40**[a]	9-AnOH	1	2	Tol.	30	5	>99	1.04	-	67
2	**40**[b]	9-AnOH	1	2	Tol.	55	120	98	1.01	-	67
3	**41**[a]	9-AnOH	2	0.5	Tol.	30	20	99	1.07	-	69
4	**41**[b]	9-AnOH	2	0.5	Tol.	55	300	92	1.03	-	69
5	**42**[a]	-	2	0.5	Tol.	30	20	96	1.18	-	69
6	**42**[b]	-	4	0.5	Tol.	55	600	99	1.04	-	9
7	**43**[c]	9-AnOH	1	1	DCM	30	180	99	1.13	-	68
8	**43**[c]	9-AnOH	1	1	THF	30	480	94	1.16	0.59	68

[a] ROP of ε-caprolactone; [b] ROP of β-butyrolactone; [c] ROP of L-lactide, DCM = dichloromethane; Tol. = toluene; dashes (-) indicate no addition of co-initiator or no stereospecificity reported.

1.8 Cationic and Zwitterionic Zinc Complexes

1.8.1 Cationic Zinc Phosphinimine Complexes

Hayes and coworkers prepared a series of cationic zinc complexes with neutral phosphinimine ligands.[6] Direct reaction of the neutral ligand precursors with zinc sources, e.g. EtZnCl or $ZnEt_2$, failed to yield the corresponding zinc complexes because of the poor ability of the neutral ligands to stabilize the zinc complexes. The ligand precursors were protonated by the anilinium acid from $[HNMe_2Ph][B(C_6F_5)_4]$, or triflic acid HSO_3CF_3 and followed by reaction with $ZnEt_2$ to generate the cationic zinc complexes **44a** and **44b** (**Scheme 1-23**). Coordination of the $B(C_6F_5)_4$ anion to the zinc center is not observed in **44a,** while weak coordination of the SO_3CF_3 anion to the zinc center in **44b** is observed in the crystal structures. **44a** gives 90% L-lactide conversion after 6 h at 100 °C at 1% catalyst loading (entry 1, **Table 1-11**); **44b** shows slower activity giving 85% conversion after 9 h under the same conditions (entry 2, **Table 1-11**).

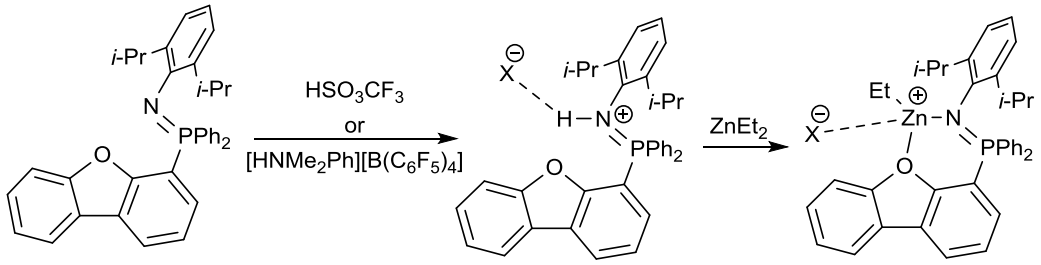

Scheme 1-23 Synthesis of cationic zinc phosphinimine complexes.

Cationic zinc complexes with chiral phosphinimine ligands were further studied by the same group.[70] A zinc methyl lactate species **45** (**Figure 1-8**) gives 90% *rac*-lactide

conversion after 9 h at ambient temperature with 1% catalyst loading in bromobenzene-d_5 (entry 3, **Table 1-11**). Unfortunately, the stereoselectivity is poor and the obtained polymer is atactic, which is often seen for cationic zinc systems. However, interestingly, the molecular weights (17,000 – 36,000 g/mol) are higher than those obtained by the non-chiral cationic zinc phosphinimine complexes **44a** and **44b** (2500-5000 g/mol).

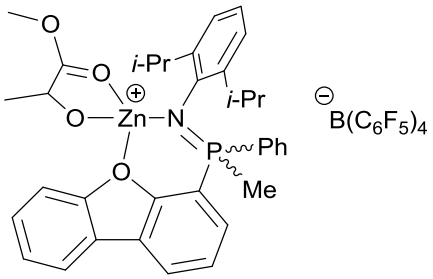

45

Figure 1-8 Structure of a cationic zinc methyl lactate complex bearing neutral phosphinimine ligand.

A tridentate bis(phosphinimine) ligand was used to synthesis zinc complexes and the obtained complexes have coordination of the two imine N atoms but no coordination of the oxygen atom from the dibenzofuran (dbf) backbone.[71] Zinc methyl complex **46a** was obtained by reaction of protonated ligand precursor with $ZnMe_2$, and zinc acetate complex **46d** was obtained by reaction with MeZnOAc (**Scheme 1-24**). Zinc methyl lactate complex **46b** together with 15% **46c** were obtained using EtZn-methyl-(S)-lactate but separation of pure complex **46b** failed. Complexes **46a** and zinc acetate complex **46d** proved to be inactive toward ROP of *rac*-lactide. Zinc methyl lactate complex **46b** gives 90% conversion after 3.5 h at 60 °C with 2% catalyst loading in C_6D_5Br (entry 7-8, **Table 1-11**). This complex gives narrower molecular weight dispersities (Đ = 1.2-1.3) than those of the previously reported complex **45**, even though the molecular weights are

higher than expected and the polymers are atactic. Stoichiometric reaction of 1:10 ratio of complex **46b**/**46c** to *rac*-lactide was monitored by $^{31}P\{^{1}H\}$ NMR and ^{1}H NMR spectroscopy. Complex **46b** was found to be converted to a new species, indicating a coordination-insertion mechanism, and **46c** shows no reactivity under the polymerization conditions.

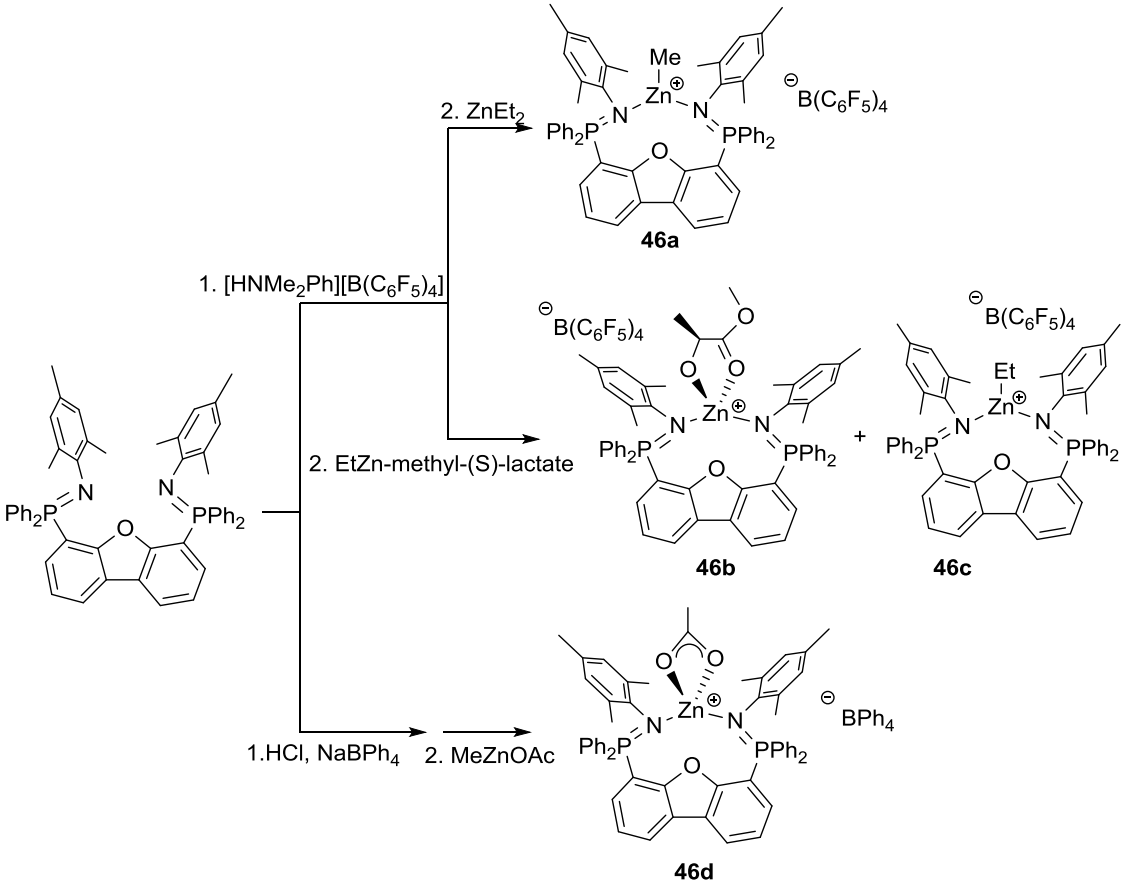

Scheme 1-24 Synthesis of cationic zinc bis(phosphinimine) complexes.

The steric properties of the bis(phosphinimine) system were further studied and a less bulky *p*-isopropylphenyl (Pipp) substituent was used on the phosphinimine.[9] Zinc methyl complexes **47a**, **47b** and zinc methyl lactate complex **47c** were synthesized (**Scheme 1-25**). They differed from complexes with bulky mesityl substituents (**46a-d**) as

coordination from the oxygen of the dibenzofuran (dbf) backbone was observed. Complex **47c** showed good activity for ROP of *rac*-lactide, giving 90% conversion after 50 min at 0.5% catalyst loading at 25 °C in CD_2Cl_2 ($k_{obs} = 8.65\times10^{-4}\ s^{-1}$) (entry 9, **Table 1-11**). The polymers show heterotactic preference with P_r value of 0.63. The molecular weights agree with theoretical values and the molecular weight dispersities are narrow, ranging from 1.08 to 1.34 (entry 10-13, **Table 1-11**).

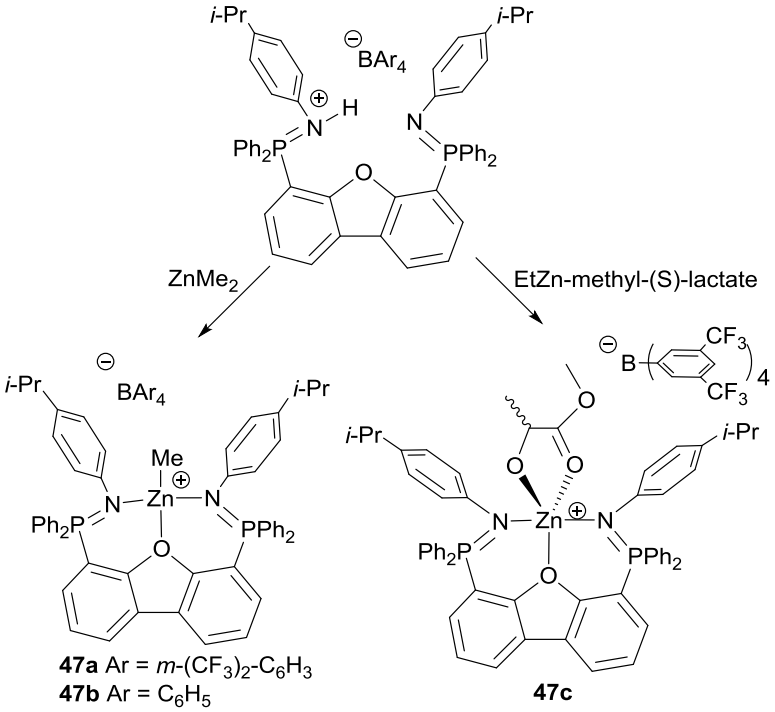

Scheme 1-25 Synthesis of cationic zinc bis(phosphinimine) complexes.

Further study of the steric and electronic effects of bis(phosphinimine) ligand towards ROP of *rac*-lactide was conducted by Hayes and coworkers.[72] Complex **48a** (**Figure 1-9**) bearing *O*-methylphenyl substituent shows no coordination from the dbf backbone, while a weak coordination of dbf was observed in complex **48b**. Zinc complex **48b** gives better ROP activity ($k_{obs} = 5.11\times10^{-4}\ s^{-1}$ at 25 °C) than complex **48a** ($k_{obs} = 3.65\times10^{-4}\ s^{-1}$ at 60 °C), but slightly lower activity than the Pipp species **47d**, from which

they concluded that an increase of the electron density of the imine site and the coordination of dbf decrease the electrophilic ability of the zinc center, thus increasing the activity. They also concluded that reducing of the steric bulk of the complex results in increased activity. Analysis of the polymers obtained by **48b** showed enhanced heterotactic property (P_r = 0.70) (entry 15, **Table 1-11**).

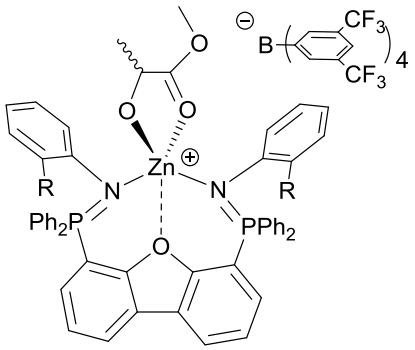

48a R = CH_3
48b R = H

Figure 1-9 Structure of cationic zinc bis(phosphinimine) complexes.

Table 1-11 ROP of *rac*-lactide and L-lactide or by zinc phosphinimine complexes.

Entry	Cat	$[LA]_0$ (M)	Loading (mol%)	Solv	Temp (°C)	t (min)	Conv (%)	Đ	P_r	Ref
1*	**44a**	1	1	C_6D_6/C_6D_5Br	100	360	90	-	-	6
2*	**44b**	1	1.	C_6D_6/C_6D_5Br	100	540	85	-	-	6
3	**45**	0.5	1	C_6D_5Br	100	540	90	-	-	70
4	**45**	1	0.5	C_6H_5Br	100	540	74	1.98	-	70
5	**45**	1	0.33	C_6H_5Br	100	540	69	1.89	-	70
6	**45**	1	0.25	C_6H_5Br	100	540	69	1.81	-	70
7	**46b**	0.25	2	C_6D_5Br	60	210	90	-	-	71
8	**46b**	0.25	2	C_6H_5Br	60	210	≈90	1.2-1.3	-	71
9	**47c**	1	0.5	CD_2Cl_2	25	50	90		-	9
10	**47c**	1	1	DCM	26	60	99	1.34	0.63	9
11	**47c**	1	0.5	DCM	26	60	98	1.15	0.63	9
12	**47c**	1	0.33	DCM	26	90	92	1.08	0.63	9
13	**47c**	1	0.1	DCM	26	360	99	1.30	0.63	9
14	**48a**	1	0.5	DCM	40	480	90	1.37	0.61	72
15	**48b**	1	0.5	DCM	25	75	96	1.35	0.70	72

* ROP of L-lactide; DCM = dichloromethane; dashes (-) indicate no molecular weight dispersity or no stereospecificity reported.

1.8.2 Cationic Zinc Amino-phenolate Complexes

Guillaume, Bourissou and coworkers utilized a cationic zinc complex (**49**, **Scheme 1-27**) combined with a amine base, pentamethylpiperidine (PMP), with *neo*-pentanol (*neo*-PentOH) for ROP of L-lactide and *rac*-lactide.[73] They proposed that PMP assisted the initiation of lactide ROP by hydrogen bonding with *neo*-PentOH (**Scheme 1-27**). Polymerization studies revealed that the system has good activity toward ROP of *rac*-lactide, giving 92% conversion after 3 h with 0.2% catalyst loading ([LA]:[*neo*-PentOH]:[**49**]:[amine] = 200:2:1:1) at 25 °C in DCM (entry 2, **Table 1-12**). This system proved to have good control, producing polymers with molecular weights close to the theoretical values and a linear relationship between molecular weight and lactide-to-*neo*-pentanol ratio. Polymerizations in toluene and DCM give polymers with dispersity (Đ) ranging from 1.17 to 1.34 (entry 1-3, **Table 1-12**), while polymerization in THF exhibits slower rate and the dispersity increases 1.70 (entry 4, **Table 1-12**). $PhNMe_2$ with lower basicity than PMP was tested but showed to be inactive. The polymers produced in high co-initiator loading have molecular weights in agreement with theoretical values and narrow molecular weight dispersity. Homonuclear decoupled $^1H\{^1H\}$ NMR analysis shows this system gives isotactic polymers from L-lactide (as expected) and atactic polymers from *rac*-lactide. Even though no stereoselectivity was achieved, this is the first exploration of an organic/organometallic binary system for ROP of lactide.

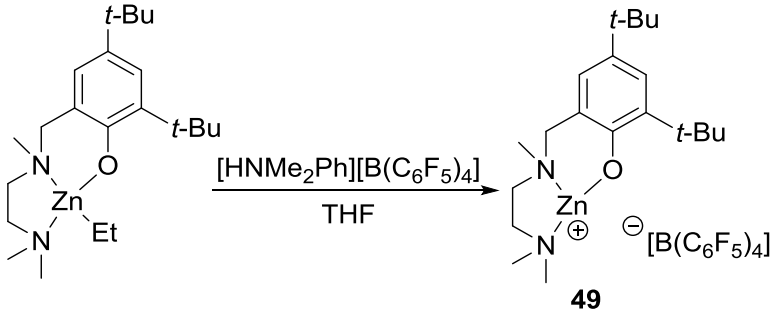

Scheme 1-26 Synthesis of a cationic zinc diamino-phenolate complex.

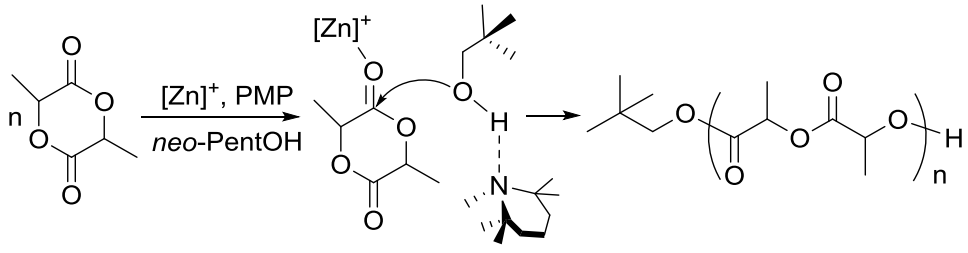

Scheme 1-27 Proposed mechanism for PMP associated initiating of ROP of lactide.

1.8.3 Heteroscorpionate Zwitterionic Zinc Complexes

Cui and coworkers reported zwitterionic zinc complexes supported by a heteroscorpionate ligand in 2014.[74] The ligand precursor was treated with KH or $LiCH_2SiMe_3$ followed by saltmetathesis to generate a zinc chloride complex. Treatment of the zinc chloride complex with $KN(SiHMe_2)_2$ or KOBn generates zwitterionic zinc amide complex **50a** and zinc benzyloxyl complex **50b**, respectively (**Scheme 1-28**). Complex **50a** coverts 90% *rac*-lactide in 1.5 h at 70 °C (entry 5, **Table 1-12**) in THF, while **50b** can initiate polymerization at ambient temperature, coverting 90% *rac*-lactide within 3 h at 30 °C (entry 9, **Table 1-12**). Interestingly, both **50a** and **50b** provide polymers with isotactic bias, P_m = 0.70-0.74, and the isotacticity increased when using toluene (P_m = 0.85) or benzene (P_m = 0.83) as polymerization solvent (entry 7-8, **Table**

1-12). Unfortunately, there is no enantioselectivity as they found the polymerization rates of D-lactide and L-lactide are identical. Studies support a chain-end mechanism for these complexes.

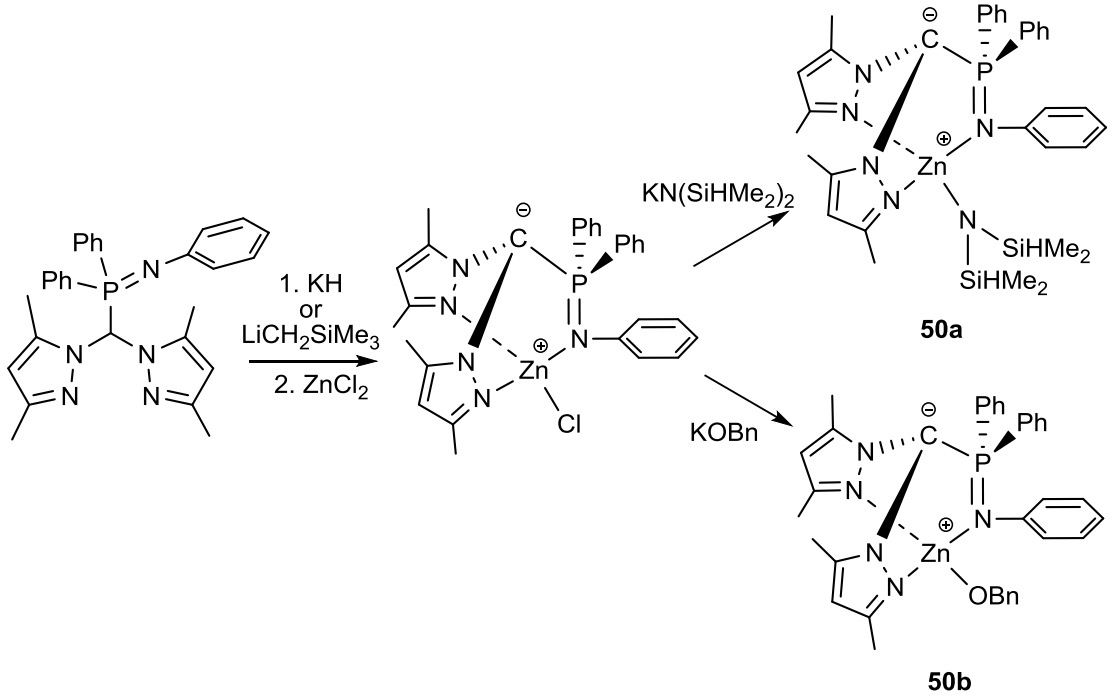

Scheme 1-28 Synthesis of zwitterionic zinc complexes supported by heteroscorpionate ligand.

1.8.4 Cationic Zinc *N*-Heterocyclic Carbene Complexes

N-Heterocyclic carbene (NHC) complexes have attracted attention from many groups for ROP of cyclic esters and reviewed by Waymouth, Hedrick and coworkers in 2010.[75] Recently, Dagorne investigated NHC zinc complexes and reported the first cationic NHC zinc complexes.[76] Cationic zinc complexes **51a** and **51b** were obtained by reaction of NHC with $ZnMe_2$ and followed by ionization with $B(C_6F_5)_3$ in THF (**Scheme 1-29**). Neutral zinc complex **52a** and **52b** were obtained by reaction of NHC with $Zn(C_6F_5)_2$ in toluene (**Scheme 1-30**). ROP of cyclic ester, e.g. β-butyrolactone, *rac*-lactide, and trimethylene carbonate (TMC), were tested using these complexes. While **51a** and **51b** show no activity, neutral complexes **52a** and **52b** slowly initiate ROP of *rac*-lactide, giving 100% conversion after 20 h at room temperature in DCM (entry 10-11, **Table 1-12**). Unfortunately, the complexes have poor control, producing PLA with molecular weights lower than theoretical values and broad molecular weight dispersities, Đ = 1.96-2.13.

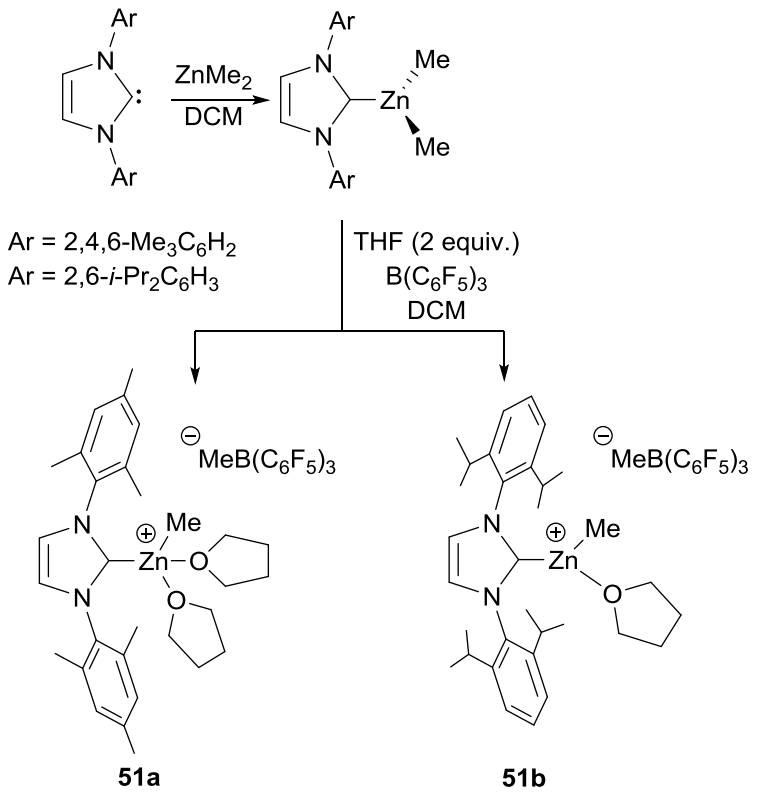

Scheme 1-29 Synthesis of cationic zinc *N*-heterocyclic carbene complexes.

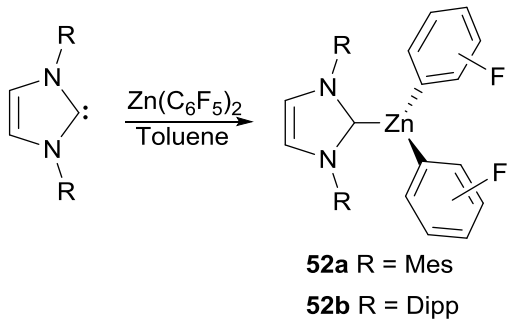

Scheme 1-30 Synthesis of zinc *N*-heterocyclic carbene complexes.

Table 1-12 ROP of *rac*-lactide by cationic and zwitterionic zinc complexes.

Entry	Cat	eqv./co-initiator	$[LA]_0$ (M)	Loading (mol%)	Solv	Temp (°C)	t (min)	Conv (%)	Đ	P_m	Ref
1	**49**	1/*neo*-PentOH, 0.5/PMP	-	0.5	Tol.	50	180	98	1.34	-	73
2	**49**	1/*neo*-PentOH, 0.5/PMP	0.5	0.5	DCM	25	180	92	1.34	-	73
3	**49**	2/*neo*-PentOH, 0.5/PMP	0.5	0.5	DCM	25	300	87	1.17	-	73
4	**49**	1/*neo*-PentOH, 0.5/PMP	-	0.5	THF	50	1440	94	1.70	-	73
5	**50a**	-	0.8	0.5	THF	70	90	90	1.96	0.70	74
6	**50a**	-	0.8	0.5	THF	30	600	91	1.98	0.74	74
7	**50a**	-	0.8	0.5	Tol.	30	480	96	1.37	0.85	74
8	**50a**	-	0.8	0.5	C_6H_6	30	240	92	1.27	0.83	74
9	**50b**	-	0.8	0.5	THF	30	180	90	1.56	0.74	74
10	**52a**	-	1	1	DCM	R.T.	1200	100	2.13	-	75
11	**52b**	-	1	1	DCM	R.T.	1200	100	1.96	-	75

Dashes (-) indicate no addition of co-initiator or no stereospecificity reported; DCM = dichloromethane; Tol. = toluene.

1.9 Zinc Complexes with Soft Heteroatom Donors

1.9.1 Zinc Phenoxy-thioether Complexes

Lamberti and Mazzeo prepared a series of zinc and magnesium complexes bearing phenoxy-thioether ligands.[77] Zinc (**53a** and **53b**) and magnesium complexes (**53c**) were synthesized using $Zn[N(SiMe_3)_2]_2$, $ZnEt_2$, or $Mg(n\text{-}Bu)_2$ as metal sources (**Scheme 1-31**). Characterization of complexes **53b** and **53c** by VT ^1H NMR and Diffusion-Ordered Spectroscopy (DOSY) reveal that they are dimeric in solution. Zinc complex **53a** converts 92% *rac*-lactide after 14 h at 0.5% catalyst loading in the presence of one equiv. of *i*-PrOH at 70 °C in toluene (entry 1, **Table 1-13**), and zinc complex **53b** gives full conversion after 7 h at the same conditions (entry 2, **Table 1-13**). The obtained PLA is atactic having molecular weights slightly higher than expected values and Đ values of 1.29-1.34. Magnesium complex **53c** gives 95% conversion after 5 h at 25 °C and the obtained polymers have a modest isotactic bias, $P_m = 0.63$ (entry 3, **Table 1-13**).

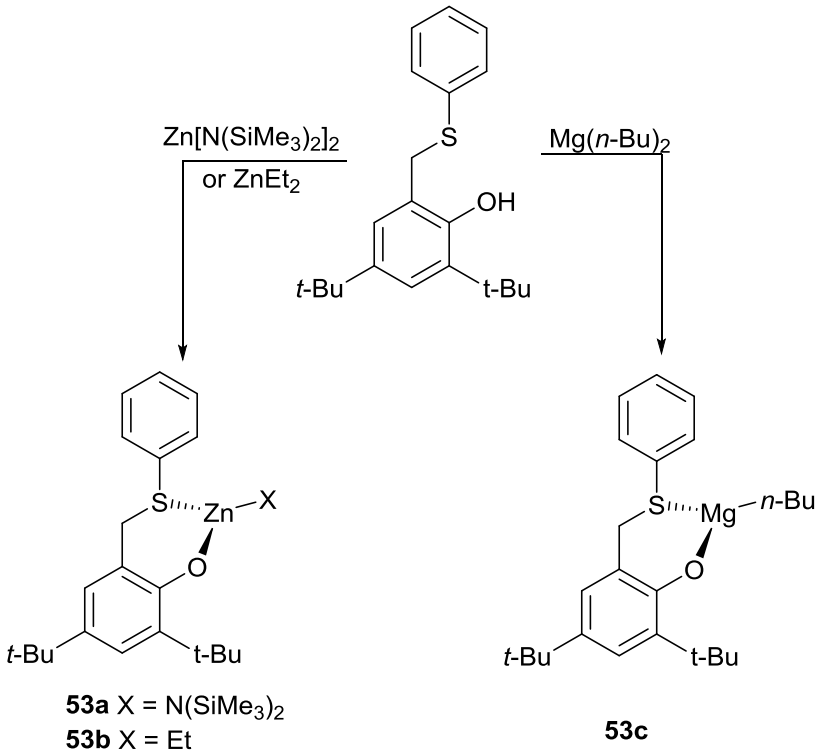

Scheme 1-31 Synthesis of zinc and magnesium complexes bearing phenoxy-thioether ligands.

Table 1-13 ROP of *rac*-lactide by zinc phenoxy-thioether and zinc phosphine-phenolate complexes.

Entry	Cat	co-initiator	$[LA]_0$ (M)	Loading (mol%)	Solv	Temp (°C)	T (min)	Conv (%)	Đ	P_m	Ref
1	**53a**	*i*-PrOH	1	0.5	Tol.	70	840	92	1.34	0.55	77
2	**53b**	*i*-PrOH	1	0.5	Tol.	70	840	100	1.29	0.46	77
3	**53c**	*i*-PrOH	1	0.5	Tol.	25	300	97	1.14	0.63	77
4	**54c**	-	1	1	DCM	R.T.	120	97	1.02	-	78

Dashes (-) indicate no addition of co-initiator or no stereospecificity reported; DCM = dichloromethane; Tol. = toluene.

1.9.2 Zinc Phosphino-phenolate Complexes

Avilés and Dagorne utilized phosphine-phenolate zinc complexes with soft phosphine donors for ROP of *rac*-lactide.[78] Dimeric zinc complexes **54a** and **54b** were obtained by reaction of the ligand precursors and $ZnEt_2$ through alkane elimination (**Scheme 1-32**). Reaction of the zinc ethyl complex with BnOH yields zinc alkoxyl species **54c** and **54d** with two bridging benzyloxyl groups. Reaction of $ZnEt_2$ with two equiv. of ligand precursor gives homoleptic complex **54e**. Noticeably, complex **54d** can slowly aggregate to yield homoleptic complex **54e** after 8 days in DCM/pentane. The activity of ROP of *rac*-lactide was studied and showed complex **54c** is highly active giving 97% conversion after 120 min (entry 4, **Table 1-13**). Also, it shows good control giving polymer with good molecular weight agreement and Đ value of 1.02. The homoleptic complex **54e** is inactive towards ROP of lactide.

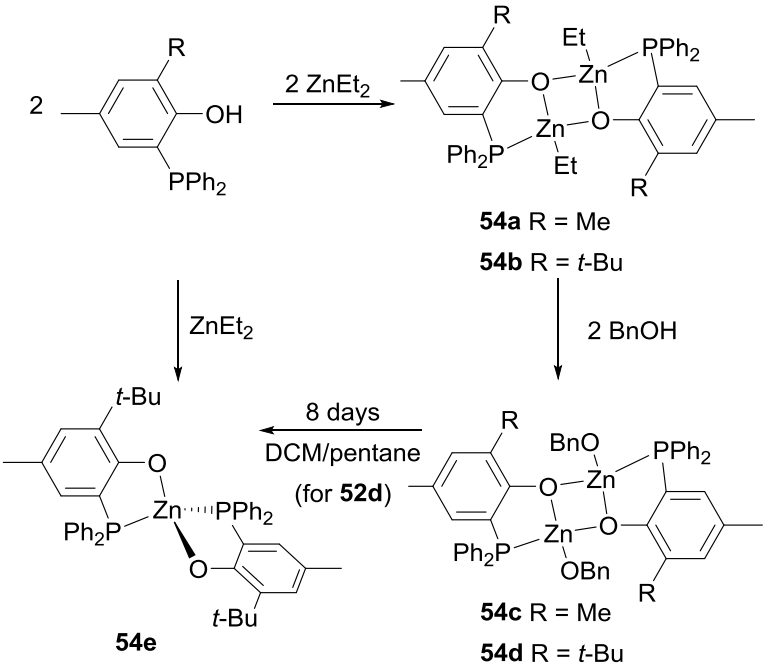

Scheme 1-32 Synthesis of zinc phosphine-phenolate complexes.

1.10 Zinc Amino-bis(phenolate) Complexes and Scope of this Research

A chiral bimetallic zinc complex was prepared by Schaper using a chiral amino-bis(phenolate) ligand (**Scheme 1-33**).[79] This complex showed low activity at ambient temperature achieving 91% conversion after 20 h with 1% catalyst loading at 50 °C in $CDCl_3$. It produces polymers with slightly heterotactic bias, P_r = 0.59, which may be because of the fast rotation of N-C bond or not enough chiral induction from the methyl and phenyl substituents on the amine.

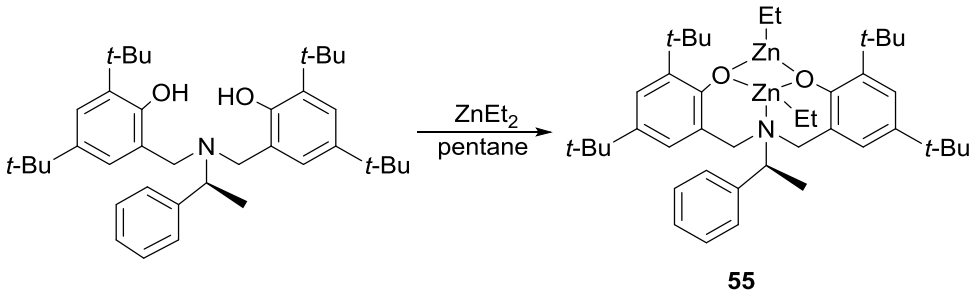

Scheme 1-33 Synthesis of a zinc amino-bis(phenolate) complex.

Considering the low activity of **55** might also be due to the steric crowding of the zinc center, hindering the coordination of lactide, replacement of the methylphenyl substituent of the amine with a less bulky group may improve its activity for lactide polymerization. Also, the lactide ROP activity of complex **55** was studied in very low detail and with no conclusions to the reaction mechanism. The research in this thesis involved tridentate amine-bis(phenolate) ligands (**Figure 1-10**) with a *n*-propyl substituent on the amine and focused on synthesis, characterization and study of zinc amino-bis(phenolate) complexes bearing different initiating groups towards ROP of *rac*-lactide. The synthesis and characterization of zinc amino-bis(phenolate) complexes bearing different initiating groups will be discussed in Chapter 2; the catalytic study

towards ROP of *rac*-lactide, including kinetic studies, studies of polymers, determination of thermodynamic parameters and a reaction mechanism, will be discussed in Chapter 3; and the experimental procedures will be presented in Chapter 4.

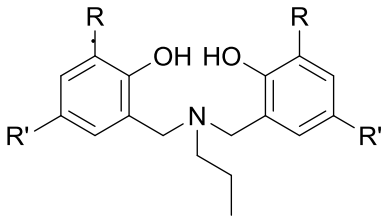

H_2[**L1**], R=R'=*t*-Bu
H_2[**L2**], R=*t*-Bu, R'=Me

Figure 1-10 General structure of amino-bis(phenolate) ligands.

1.11 References

1. Jensen, W. B. *J. Chem. Educ.* **2003,** *80*, 952-961.

2. Stahl, L.; Smoliakova, I. P., 2.06 - Zinc Organometallics. In *Comprehensive Organometallic Chemistry III*, Crabtree, D. M. P. M. H., Ed. Elsevier: Oxford, 2007; pp 309-418.

3. Burgess, J.; Prince, R. H., Zinc: Inorganic & Coordination Chemistry. In *Encyclopedia of Inorganic Chemistry*, John Wiley & Sons, Ltd. 2006.

4. Berg, J. M. *Annu. Rev. Biophys. and Biophys. Chem.* **1990,** *19*, 405-421.

5. Seyferth, D. *Organometallics* **2001,** *20*, 2940-2955.

6. Wheaton, C. A.; Ireland, B. J.; Hayes, P. G. *Organometallics* **2009,** *28*, 1282-1285.

7. Stanford, M. J.; Dove, A. P. *Chem. Soc. Rev.* **2010,** *39*, 486-494.

8. Thomas, C. M. *Chem. Soc. Rev.* **2010,** *39*, 165-173.

9. Wheaton, C. A.; Hayes, P. G. *Chem. Commun.* **2010,** *46*, 8404-8406.

10. Buffet, J.-C.; Okuda, J. *Polym. Chem.* **2011,** *2*, 2758-2763.

11. Dijkstra, P. J.; Du, H.; Feijen, J. *Polym. Chem.* **2011,** *2*, 520-527.

12. Li, J.-Y.; Li, C.-Y.; Tai, W.-J.; Lin, C.-H.; Ko, B.-T. *Inorg. Chem. Commun.* **2011,** *14*, 1140-1144.

13. Chuang, H. J.; Chen, H. L.; Huang, B. H.; Tsai, T. E.; Huang, P. L.; Liao, T. T.; Lin, C. C. *J. Polym. Sci., Part A: Polym. Chem.* **2013,** *51*, 1185-1196.

14. Cheng, M.; Moore, D. R.; Reczek, J. J.; Chamberlain, B. M.; Lobkovsky, E. B.; Coates, G. W. *J. Am. Chem. Soc.* **2001,** *123*, 8738-8749.

15. Darensbourg, D. J.; Wildeson, J. R.; Yarbrough, J. C. *Inorg. Chem.* **2002,** *41*, 973-980.

16. Darensbourg, D. J.; Lewis, S. J.; Rodgers, J. L.; Yarbrough, J. C. *Inorg. Chem.* **2003,** *42*, 581-589.

17. Moore, D. R.; Cheng, M.; Lobkovsky, E. B.; Coates, G. W. *J. Am. Chem. Soc.* **2003,** *125*, 11911-11924.

18. Coates, G. W.; Moore, D. R. *Angew. Chem. Int. Ed.* **2004,** *43*, 6618-6639.

19. Jutz, F.; Buchard, A.; Kember, M. R.; Fredriksen, S. B.; Williams, C. K. *J. Am. Chem. Soc.* **2011,** *133*, 17395-17405.

20. Klaus, S.; Lehenmeier, M. W.; Anderson, C. E.; Rieger, B. *Coord. Chem. Rev.* **2011,** *255*, 1460-1479.

21. Lehenmeier, M. W.; Kissling, S.; Altenbuchner, P. T.; Bruckmeier, C.; Deglmann, P.; Brym, A. K.; Rieger, B. *Angew. Chem. Int. Ed.* **2013,** *52*, 9821-9826.

22. Vaidya, A.; Pandey, R.; Mudliar, S.; Kumar, M. S.; Chakrabarti, T.; Devotta, S. *Crit. Rev. Environ. Sci. Technol.* **2005,** *35*, 429-467.

23. Mohapatra, A. K.; Mohanty, S.; Nayak, S. K. *J. Thermoplast. Compos. Mater.* **2014,** *27*, 699-716.

24. Paetz, C.; Hagen, R. *Chem. Ing. Tech.* **2014,** *86*, 519-523.

25. Hoffman, A. S. *Adv. Drug Del. Rev.* **2012,** *64*, 18-23.

26. Dev, A.; Binulal, N.; Anitha, A.; Nair, S.; Furuike, T.; Tamura, H.; Jayakumar, R. *Carbohydr. Polym.* **2010,** *80*, 833-838.

27. Capra, P.; Briasco, B.; Sorrenti, M.; Catenacci, L.; Sachet, M.; Perugini, P. *J. Appl. Polym. Sci.* **2014,** *131*.

28. Tawakkal, I. S.; Cran, M. J.; Miltz, J.; Bigger, S. W. *J. Food Sci.* **2014,** *79*, R1477-R1490.

29. Vink, E. T.; Rábago, K.; Glassner, D. A.; Springs, B.; O'Connor, R. P.; Kolstad, J.; Gruber, P. R. *Macromol. Biosci.* **2004,** *4*, 551-564.

30. Vink, E. T. H.; Rábago, K. R.; Glassner, D. A.; Gruber, P. R. *Polym. Degrad. Stab.* **2003,** *80*, 403-419.

31. Platel, R. H.; Hodgson, L. M.; Williams, C. K. *Polym. Rev.* **2008,** *48*, 11-63.

32. Dittrich, V. W.; Schulz, R. C. *Angew. Makromol. Chem.* **1971,** *15*, 109-126.

33. Ajellal, N.; Carpentier, J.-F.; Guillaume, C.; Guillaume, S. M.; Helou, M.; Poirier, V.; Sarazin, Y.; Trifonov, A. *Dalton Trans.* **2010,** *39*, 8363-8376.

34. Ovitt, T. M.; Coates, G. W. *J. Polym. Sci., Part A: Polym. Chem.* **2000,** *38*, 4686-4692.

35. Othman, N.; Xu, C.; Mehrkhodavandi, P.; Hatzikiriakos, S. G. *Polymer* **2012,** *53*, 2443-2452.

36. Khorsand Sourkohi, B.; Cunningham, A.; Zhang, Q.; Oh, J. K. *Biomacromolecules* **2011,** *12*, 3819-3825.

37. Sinha Ray, S. *Acc. Chem. Res.* **2012,** *45*, 1710-1720.

38. Li, X.; Kang, H.; Shen, J.; Zhang, L.; Nishi, T.; Ito, K.; Zhao, C.; Coates, P. *Polymer* **2014,** *55*, 4313-4323.

39. Torres-Giner, S.; Martinez-Abad, A.; Lagaron, J. M. *J. Appl. Polym. Sci.* **2014,** *131*.

40. Wu, J.; Yu, T.; Chen, C.; Lin, C. *Coord. Chem. Rev.* **2006,** *250*, 602-626.

41. Wheaton, C. A.; Hayes, P. G.; Ireland, B. J. *Dalton Trans.* **2009**, 4832-4846.

42. Cheng, M.; Attygalle, A. B.; Lobkovsky, E. B.; Coates, G. W. *J. Am. Chem. Soc.* **1999,** *121*, 11583-11584.

43. Chamberlain, B. M.; Cheng, M.; Moore, D. R.; Ovitt, T. M.; Lobkovsky, E. B.; Coates, G. W. *J. Am. Chem. Soc.* **2001,** *123*, 3229-3238.

44. Chisholm, M. H.; Gallucci, J.; Phomphrai, K. *Inorg. Chem.* **2002,** *41*, 2785-2794.

45. Dove, A. P.; Gibson, V. C.; Marshall, E. L.; White, A. J.; Williams, D. J. *Dalton Trans.* **2004**, 570-578.

46. Chisholm, M. H.; Gallucci, J. C.; Phomphrai, K. *Inorg. Chem.* **2005,** *44*, 8004-8010.

47. Xu, X.; Chen, Y.; Zou, G.; Ma, Z.; Li, G. *J. Organomet. Chem.* **2010,** *695*, 1155-1162.

48. Chen, H.-Y.; Peng, Y.-L.; Huang, T.-H.; Sutar, A. K.; Miller, S. A.; Lin, C.-C. *J. Mol. Catal. A: Chem.* **2011,** *339*, 61-71.

49. Allen, S. D.; Moore, D. R.; Lobkovsky, E. B.; Coates, G. W. *J. Organomet. Chem.* **2003,** *683*, 137-148.

50. Chen, H.-Y.; Huang, B.-H.; Lin, C.-C. *Macromolecules* **2005,** *38*, 5400-5405.

51. Drouin, F.; Oguadinma, P. O.; Whitehorne, T. J.; Prud'homme, R. E.; Schaper, F. *Organometallics* **2010,** *29*, 2139-2147.

52. Whitehorne, T. J.; Vabre, B.; Schaper, F. *Dalton Trans.* **2014,** *43*, 6339-6352.

53. Williams, C. K.; Breyfogle, L. E.; Choi, S. K.; Nam, W.; Young, V. G.; Hillmyer, M. A.; Tolman, W. B. *J. Am. Chem. Soc.* **2003,** *125*, 11350-11359.

54. Labourdette, G.; Lee, D. J.; Patrick, B. O.; Ezhova, M. B.; Mehrkhodavandi, P. *Organometallics* **2009,** *28*, 1309-1319.

55. Chuang, H. J.; Weng, S. F.; Chang, C. C.; Lin, C. C.; Chen, H. Y. *Dalton Trans.* **2011,** *40*, 9601-9607.

56. Poirier, V.; Roisnel, T.; Carpentier, J. F.; Sarazin, Y. *Dalton Trans.* **2009**, 9820-9827.

57. Poirier, V.; Roisnel, T.; Carpentier, J. F.; Sarazin, Y. *Dalton Trans.* **2011,** *40*, 523-534.

58. Ikpo, N.; Saunders, L. N.; Walsh, J. L.; Smith, J. M. B.; Dawe, L. N.; Kerton, F. M. *Eur. J. Inorg. Chem.* **2011,** *2011*, 5347-5359.

59. Wang, L.; Ma, H. *Dalton Trans.* **2010,** *39*, 7897-7910.

60. Song, S.; Zhang, X.; Ma, H.; Yang, Y. *J. Chem. Soc., Dalton Trans.* **2012,** *41*, 3266-3277.

61. Wang, H.; Ma, H. *Chem. Commun.* **2013,** *49*, 8686-8688.

62. Yang, Y.; Wang, H.; Ma, H. *Inorg. Chem.* **2015,** *54*, 5839-5854.

63. Wang, H.; Yang, Y.; Ma, H. *Macromolecules* **2014,** *47*, 7750-7764.

64. Darensbourg, D. J.; Karroonnirun, O. *Inorg. Chem.* **2010,** *49*, 2360-2371.

65. Huang, M.; Pan, C.; Ma, H. *Dalton Trans.* **2015,** *44*, 12420-12431.

66. Li, C. Y.; Tsai, C. Y.; Lin, C. H.; Ko, B. T. *Dalton Trans.* **2011,** *40*, 1880-1887.

67. Tai, Y.-E.; Li, C.-Y.; Lin, C.-H.; Liu, Y.-C.; Ko, B.-T.; Sun, Y.-S. *J. Polym. Sci., Part A: Polym. Chem.* **2011,** *49*, 4027-4036.

68. Sung, C. Y.; Li, C. Y.; Su, J. K.; Chen, T. Y.; Lin, C. H.; Ko, B. T. *Dalton Trans.* **2012,** *41*, 953-961.

69. Wang, J. H.; Tsai, C. Y.; Su, J. K.; Huang, B. H.; Lin, C. C.; Ko, B. T. *Dalton Trans.* **2015,** *44*, 12401-12410.

70. Sun, H.; Ritch, J. S.; Hayes, P. G. *Inorg. Chem.* **2011,** *50*, 8063-8072.

71. Wheaton, C. A.; Hayes, P. G. *Dalton Trans.* **2010,** *39*, 3861-3869.

72. Wheaton, C. A.; Hayes, P. G. *Catal. Sci. Tech.* **2012,** *2*, 125-138.

73. Piedra-Arroni, E.; Brignou, P.; Amgoune, A.; Guillaume, S. M.; Carpentier, J. F.; Bourissou, D. *Chem. Commun.* **2011,** *47*, 9828-9830.

74. Mou, Z.; Liu, B.; Wang, M.; Xie, H.; Li, P.; Li, L.; Li, S.; Cui, D. *Chem. Commun.* **2014,** *50*, 11411-11414.

75. Kiesewetter, M. K.; Shin, E. J.; Hedrick, J. L.; Waymouth, R. M. *Macromolecules* **2010,** *43*, 2093-2107.

76. Schnee, G.; Fliedel, C.; Avilés, T.; Dagorne, S. *Eur. J. Inorg. Chem.* **2013,** *2013*, 3699-3709.

77. Pilone, A.; Lamberti, M.; Mazzeo, M.; Milione, S.; Pellecchia, C. *Dalton Trans.* **2013,** *42*, 13036-13047.

78. Fliedel, C.; Rosa, V.; Alves, F. M.; Martins, A. M.; Aviles, T.; Dagorne, S. *Dalton Trans.* **2015,** *44*, 12376-12387.

79. Pastor, M. F.; Whitehorne, T. J.; Oguadinma, P. O.; Schaper, F. *Inorg. Chem. Commun.* **2011,** *14*, 1737-1741.

Chapter 2 Synthesis and Characterization of Zinc Amino-bis(phenolate) Complexes

2.1 Introduction

Amino-bis(phenolate) ligands exhibit tunable electronic effects and flexible steric properties, and the catalytic activities of amino-bis(phenolate) complexes have been well studied.[1-12] Zinc amino-phenolate complexes for ring-opening polymerization (ROP) of lactide (LA) have been widely investigated [14-28] and Tolman and Hillmyer reported the most efficient zinc ethoxyl complex to date.[13]

Schaper *et al.* synthesized a bimetallic zinc complex with a chiral N-substituted amino-bis(phenolate) ligand that offers poor activity for ROP of *rac*-lactide (*rac*-LA), possibly because of the steric bulkiness of the complex.[8] Consequently, we synthesized less bulky zinc amino-bis(phenolate) complexes and the ROP of *rac*-lactide was tested in the presence and absence of exogenous alcohol. Zinc alkoxyl complexes in which the alkoxyl group usually acts as initiating group have better catalytic activities than zinc ethyl complexes towards ROP of lactide.[13, 29, 30]

Recently, Hayes *et al.* prepared a zinc lactate complex with a methyl lactate moiety coordinated to a zinc center and this complex initiates polymerization of lactide with a coordination-insertion mechanism at ambient conditions.[31] Inspired by these works, attempts were made to isolate zinc alkoxyl complexes and the activity of zinc amino-bis(phenolate)s for ROP of *rac*-lactide was studied.

This chapter discusses the preparation and characterization of zinc amino-bis(phenolate) complexes bearing different initiating groups. Their catalytic activity for ROP of *rac*-lactide will be discussed in Chapter 3.

2.2 Results and Discussion

2.2.1 Synthesis of Zinc Ethyl Complexes in Non-coordinating Solvent

The tridentate amino-bis(phenolate) ligand precursors H_2**[L1]** and H_2**[L2]** (where [**L1**] = *n*-propylamine-*N*,*N*-bis(2-methylene-4,6-di-*t*-butylphenolate) and [**L2**] = *n*-propylamine-*N*,*N*-bis(2-methylene-6-*t*-butyl-4-methylphenolate) were synthesized using a modified Mannich condensation reaction in water as previously reported.[32] Alkane elimination reaction under nitrogen of the ligand precursors H_2**[L1]** and H_2**[L2]** with two equiv. of $ZnEt_2$ in pentane afforded the bimetallic zinc complexes **1a** and **1b**, respectively (**Scheme 2-1**). It was found that one ethyl group of $ZnEt_2$ is easily protonated by the ligand precursor; however the second ethyl group resists removal possibly due to the more stable C-Zn bond after the coordination of the oxygen from the ligand.[35] Reaction of H_2**[L1]** with one equiv. of $ZnEt_2$ yielded a mixture of products. Multiple NCH_2, *t*-Bu and aromatic proton assignments were observed in ^{1}H NMR spectra (**Figure A-6 and 7**).

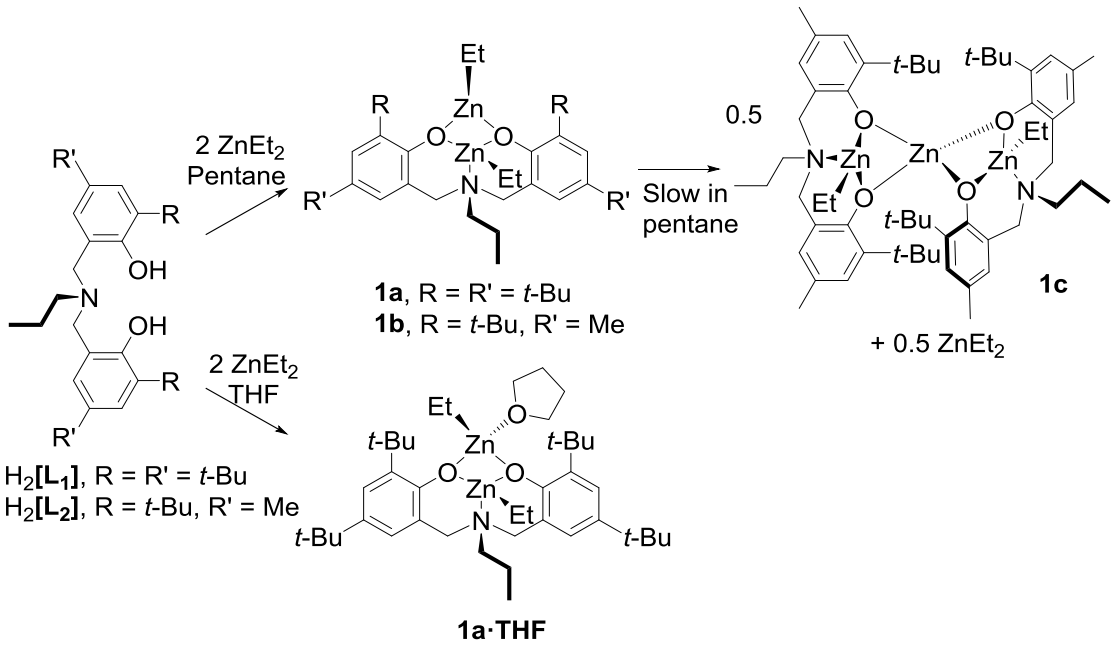

Scheme 2-1 Synthesis of zinc ethyl complexes.

2.2.2 Characterization of Zinc Ethyl Complexes

2.2.2.1 NMR Spectroscopy

The zinc complexes were characterized by ^{1}H and ^{13}C NMR spectroscopy. The ^{1}H NMR spectra of complexes **1a** and **1b** in $CDCl_3$ show two zinc ethyl environments (two triplets, at δ 0.96 and δ 0.75, arising from two different $ZnCH_2CH_3$ methylene groups and two quartets, at δ 0.35 and δ -0.12, arising from two methyl environments). ^{13}C NMR spectroscopy assisted by an attached proton test (APT) (Figure A-1) confirmed the presence of two methylene and two methyl carbon environments. The diastereotopic NCH_2Ar protons appear as a pair of doublets, confirming the coordination of the ligand to the zinc center. The assignments of the ^{1}H NMR (**Figure 2-1**) and ^{13}C NMR (**Figure 2-2**) spectra are listed in **Table 2-1** and **Table 2-2**, respectively.

Table 2-1 Assignment of resonances in the ^{1}H NMR spectrum of **1a** in $CDCl_3$.

Proton types	Number of protons	Chemical shift (δ)	Peak	*J* (Hz)
ArH	2	7.29	d	2.5
ArH	2	6.91	d	2.5
$ArCH_2$	2	4.15	d	14.0
$ArCH_2$	2	3.74	d	14.0
$NCH_2CH_2CH_3$	2	2.63	m	-
$NCH_2CH_2CH_3$	2	1.59	m	-
$C(CH_3)_3$	18	1.48	s	-
$C(CH_3)_3$	18	1.30	s	-
$ZnCH_2CH_3$	3	0.96	t	8.1
$NCH_2CH_2CH_3$	3	0.82	t	7.3
$ZnCH_2CH_3$	3	0.75	t	8.1
$ZnCH_2CH_3$	2	0.32	q	8.1
$ZnCH_2CH_3$	2	-0.12	q	8.1

Table 2-2 Assignment of resonances in the ^{13}C NMR spectrum of **1a** in $CDCl_3$.

Carbon types	Chemical shift (δ)			
Ar	158.75	140.64	139.25	125.13
ArH	125.10	124.74		
$ArCH_2$	64.07			
$NCH_2CH_2CH_3$	60.14			
$C(CH_3)_3$	35.51	34.30		
$C(CH_3)_3$	31.82	30.47		
$NCH_2CH_2CH_3$	18.68			
$NCH_2CH_2CH_3$	11.86			
$ZnCH_2CH_3$	12.20	11.46		
$ZnCH_2CH_3$	1.00	-2.07		

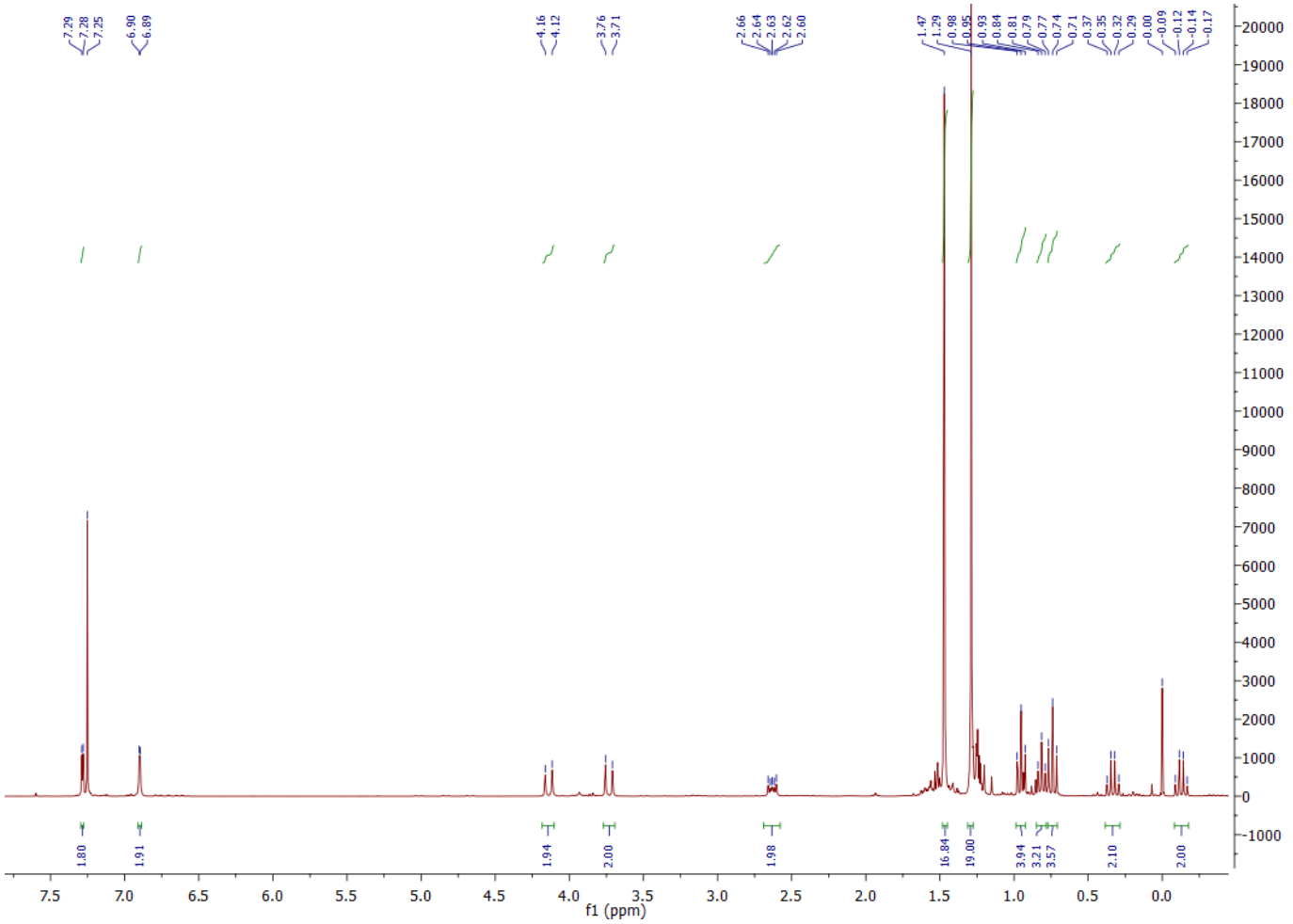

Figure 2-1 ^{1}H NMR spectrum of complex **1a** (300 MHz, $CDCl_3$, 298 K).

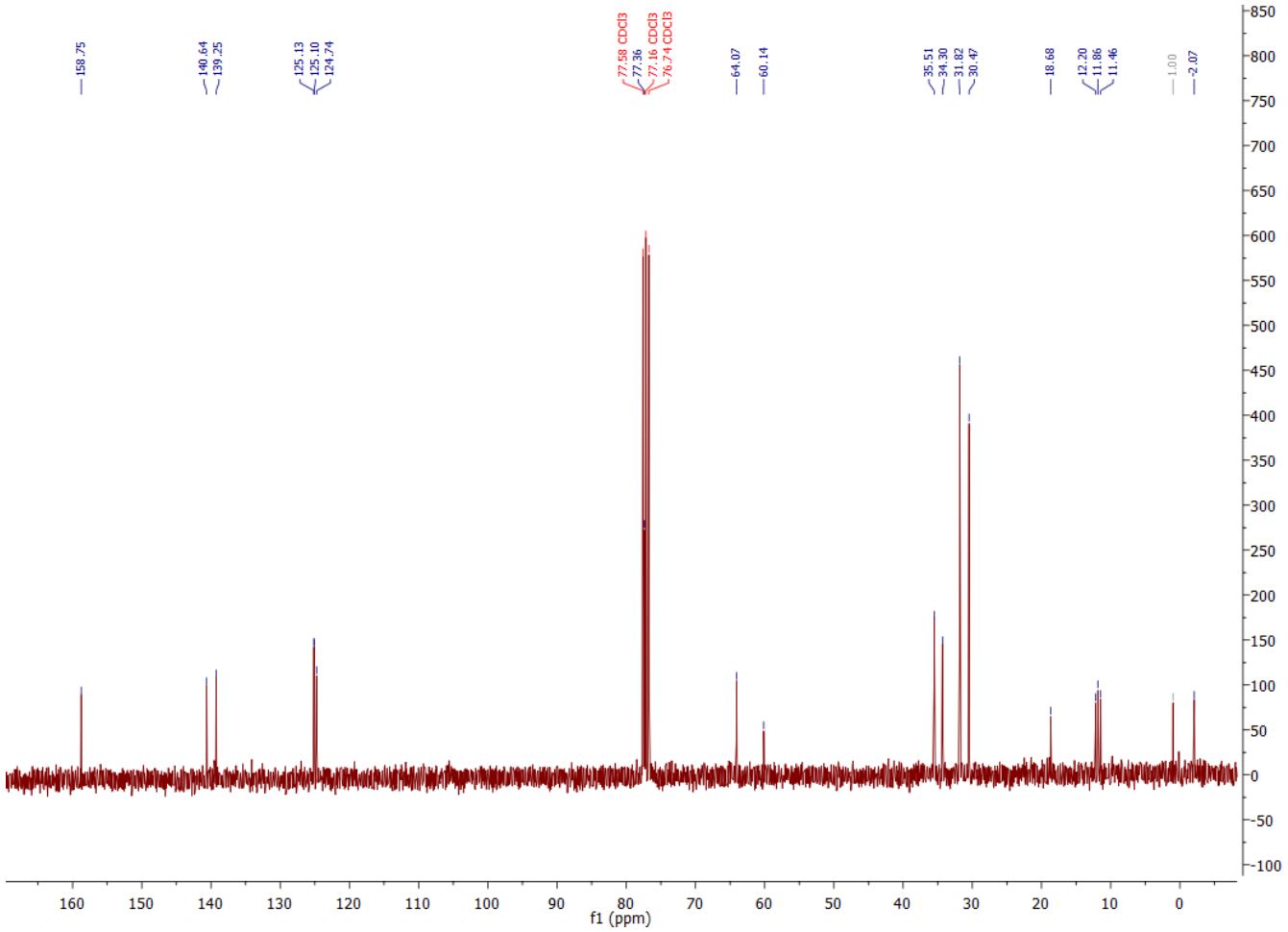

Figure 2-2 ^{13}C NMR spectum of complex **1a** (75 MHz, $CDCl_3$, 298 K).

2.2.2.2 MALDI-TOF MS

MALDI-TOF MS, which is a soft ionization technique that minimizes fragmentation of the complex, is a valuable tool for characterization of organometallic compounds.[33] Anthracene was chosen as matrix for zinc complexes. In the glove box, complex **1a** was mixed with anthracene in a ratio of 1:1 in toluene. 1 μL of this solution was spotted on the MALDI plate and allowed to dry. The plate was sealed under nitrogen in a Ziploc bag for transport to the instrument. A fragment possibly coming from $[Zn_3Et[\mathbf{L1}]_2]^+$, was observed at *m/z* = 1211.6 (**Figure 2-3**, **B**); a fragment corresponding to $[Zn_2[\mathbf{L1}]_2]^+$ was observed at *m/z* = 1118.7 (**Figure 2-3**, **C**); and a fragment possibly from $[Zn_3Et_2[\mathbf{L1}]CH_3]H^+$, was observed at *m/z* = 763.3 (**Figure 2-3**, **D**). These fragments support a trimetallic structure in solid state, which is similar to **1c** (**Figure 2-4**) that will be discussed later. It is possible that, in solid state, two equiv. of bimetallic complex **1a** aggregate to form the trimetallic complex and eliminate $ZnEt_2$ (**Scheme 2-1**). It is also possible that the trimetallic complex is obtained from the decomposition of **1a** under MALDI conditions. The bimetallic complex **1a** with the loss of one methyl group, $[Zn_2Et[\mathbf{L1}]CH_3]H^+$, was observed at *m/z* = 669.3 (**Figure 2-3**, **E**); two additional fragments, i.e. $[ZnEt[\mathbf{L1}]]^+$ at *m/z* = 652.3 and $[Zn[\mathbf{L1}]]^+$ at 557.3 were observed under MALDI conditions (**Figure 2-3**, **F** and **G**). The experimental mass spectra were found to match well with the theoretical isotopic patterns. In order to see these matches clearly, **Figure 2-3** is spread out over the next four pages.

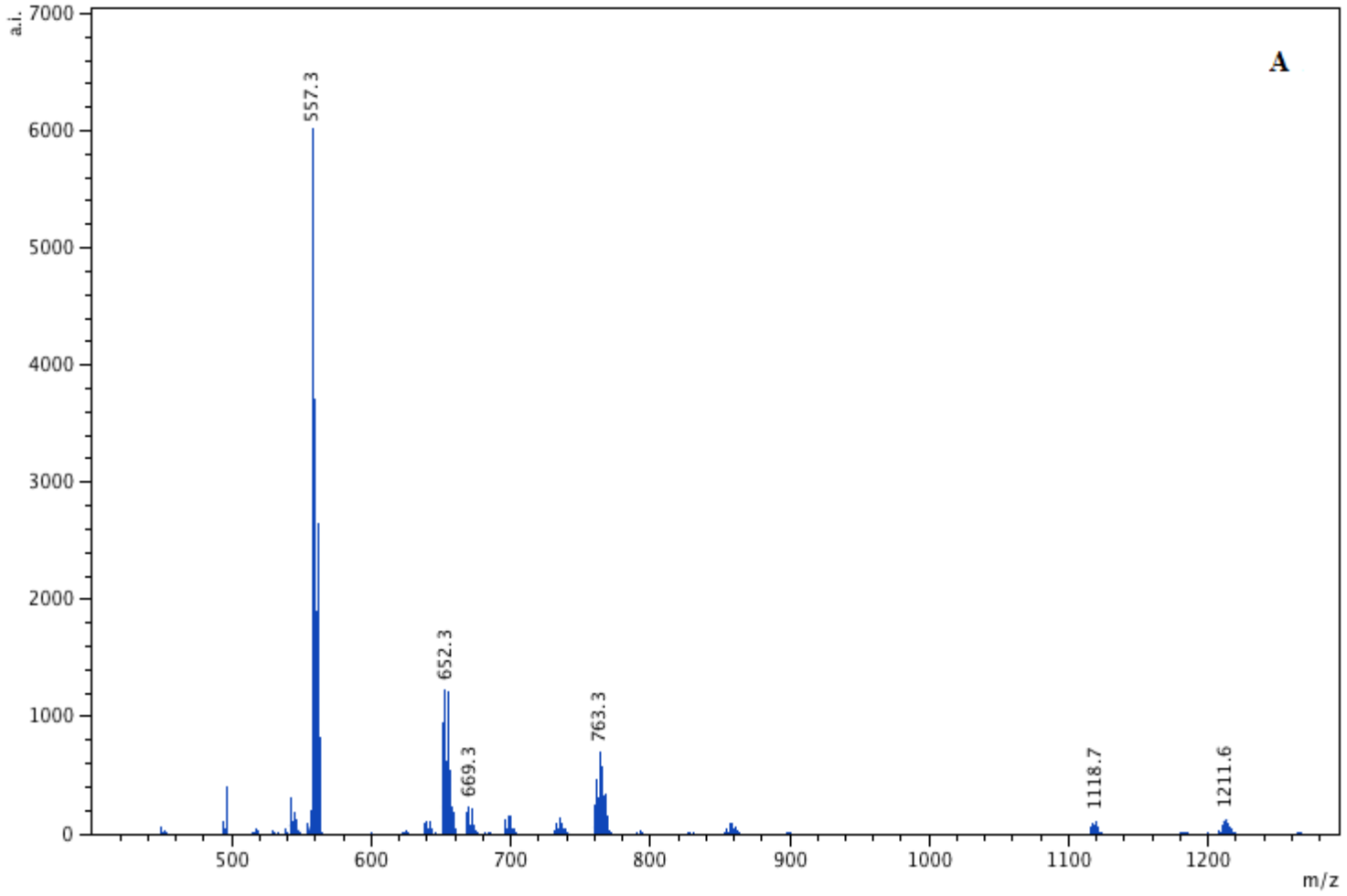
A
a.i.
7000
6000
5000
4000
3000
2000
1000
0
557.3
652.3
669.3
763.3
1118.7
1211.6
500
600
700
800
900
1000
1100
1200
m/z

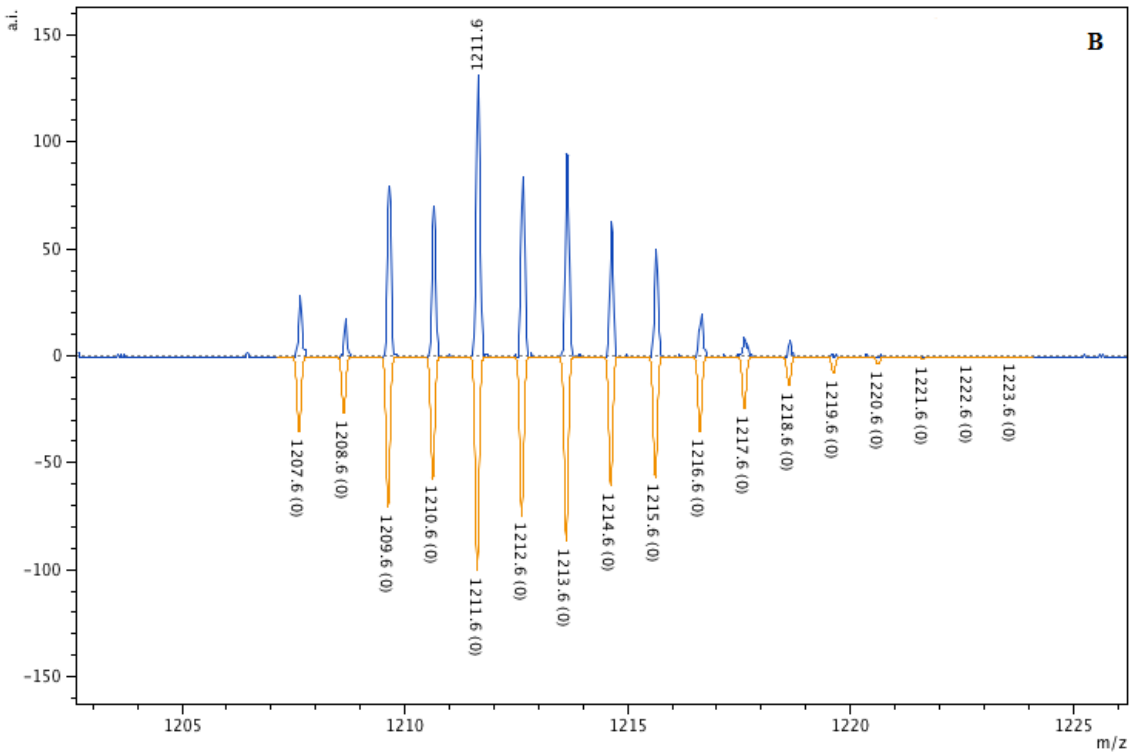
B
a.i.
150
100
50
0
-50
-100
-150
1211.6
1207.6 (0)
1208.6 (0)
1209.6 (0)
1210.6 (0)
1211.6 (0)
1212.6 (0)
1213.6 (0)
1214.6 (0)
1215.6 (0)
1216.6 (0)
1217.6 (0)
1218.6 (0)
1219.6 (0)
1220.6 (0)
1221.6 (0)
1222.6 (0)
1223.6 (0)
1205
1210
1215
1220
1225
m/z

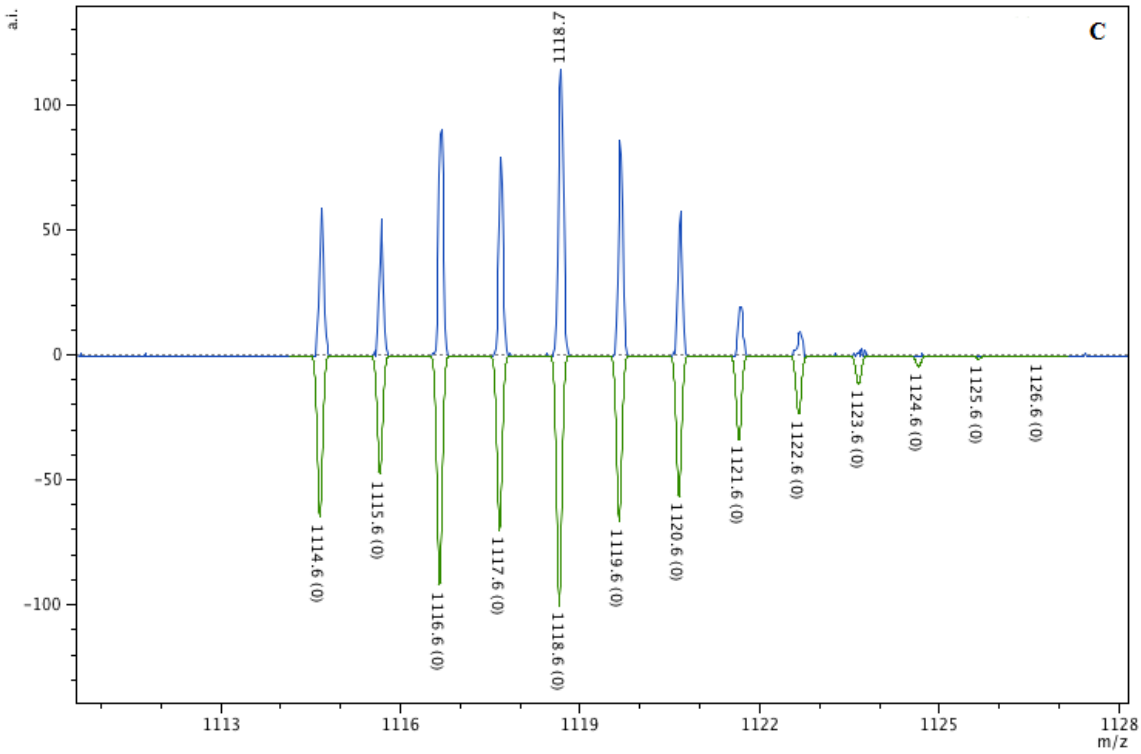
C
a.i.
100
50
0
-50
-100
1118.7
1114.6 (0)
1115.6 (0)
1116.6 (0)
1117.6 (0)
1118.6 (0)
1119.6 (0)
1120.6 (0)
1121.6 (0)
1122.6 (0)
1123.6 (0)
1124.6 (0)
1125.6 (0)
1126.6 (0)
1113
1116
1119
1122
1125
1128
m/z

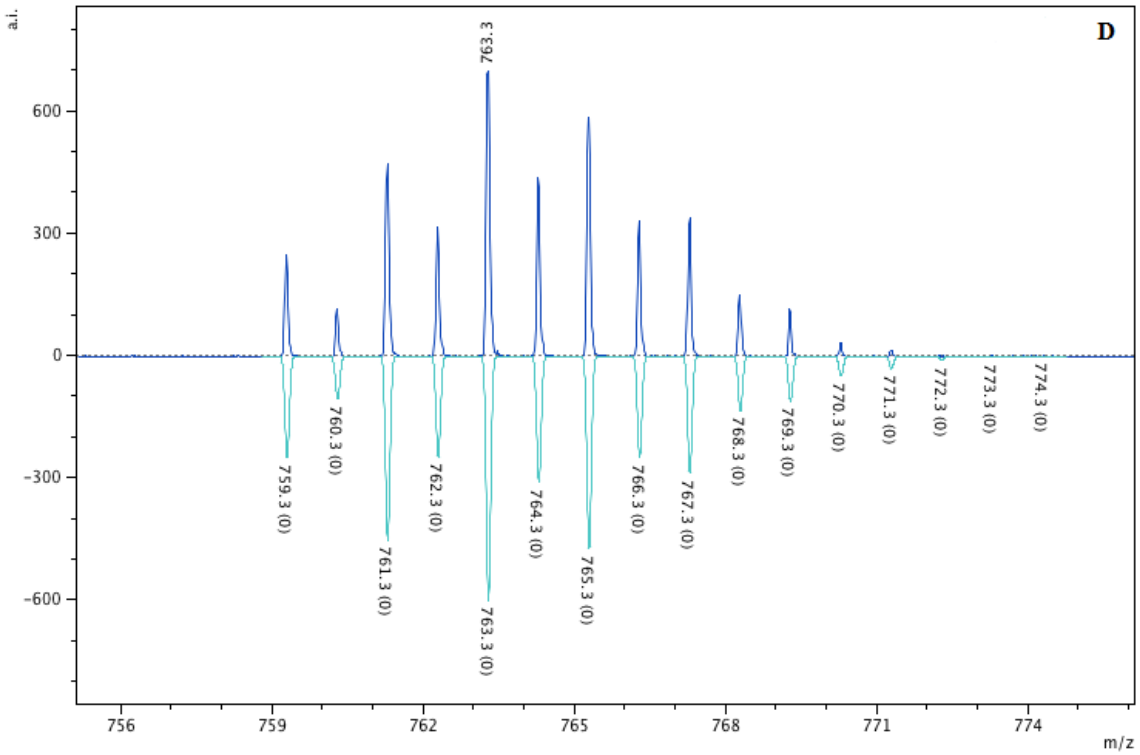
D
a.i.
600
300
0
-300
-600
763.3
759.3 (0)
760.3 (0)
761.3 (0)
762.3 (0)
763.3 (0)
764.3 (0)
765.3 (0)
766.3 (0)
767.3 (0)
768.3 (0)
769.3 (0)
770.3 (0)
771.3 (0)
772.3 (0)
773.3 (0)
774.3 (0)
756
759
762
765
768
771
774
m/z

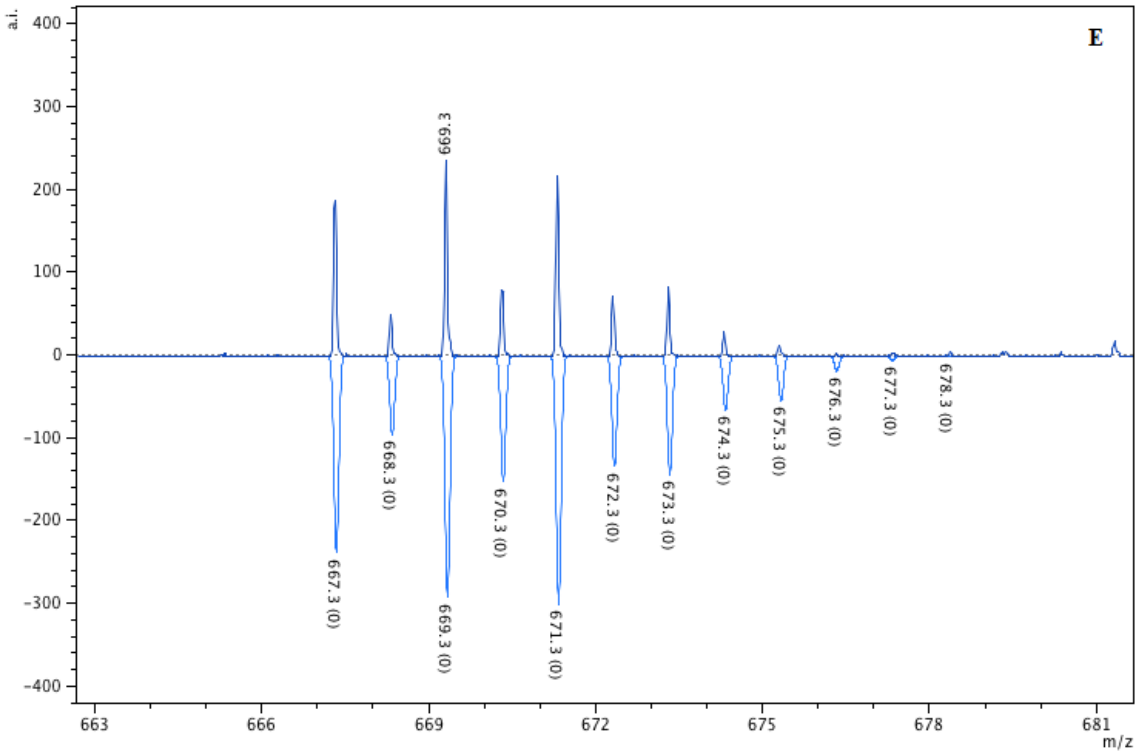
E
a.i.
400
300
200
100
0
-100
-200
-300
-400
669.3
667.3 (0)
668.3 (0)
669.3 (0)
670.3 (0)
671.3 (0)
672.3 (0)
673.3 (0)
674.3 (0)
675.3 (0)
676.3 (0)
677.3 (0)
678.3 (0)
663
666
669
672
675
678
681
m/z

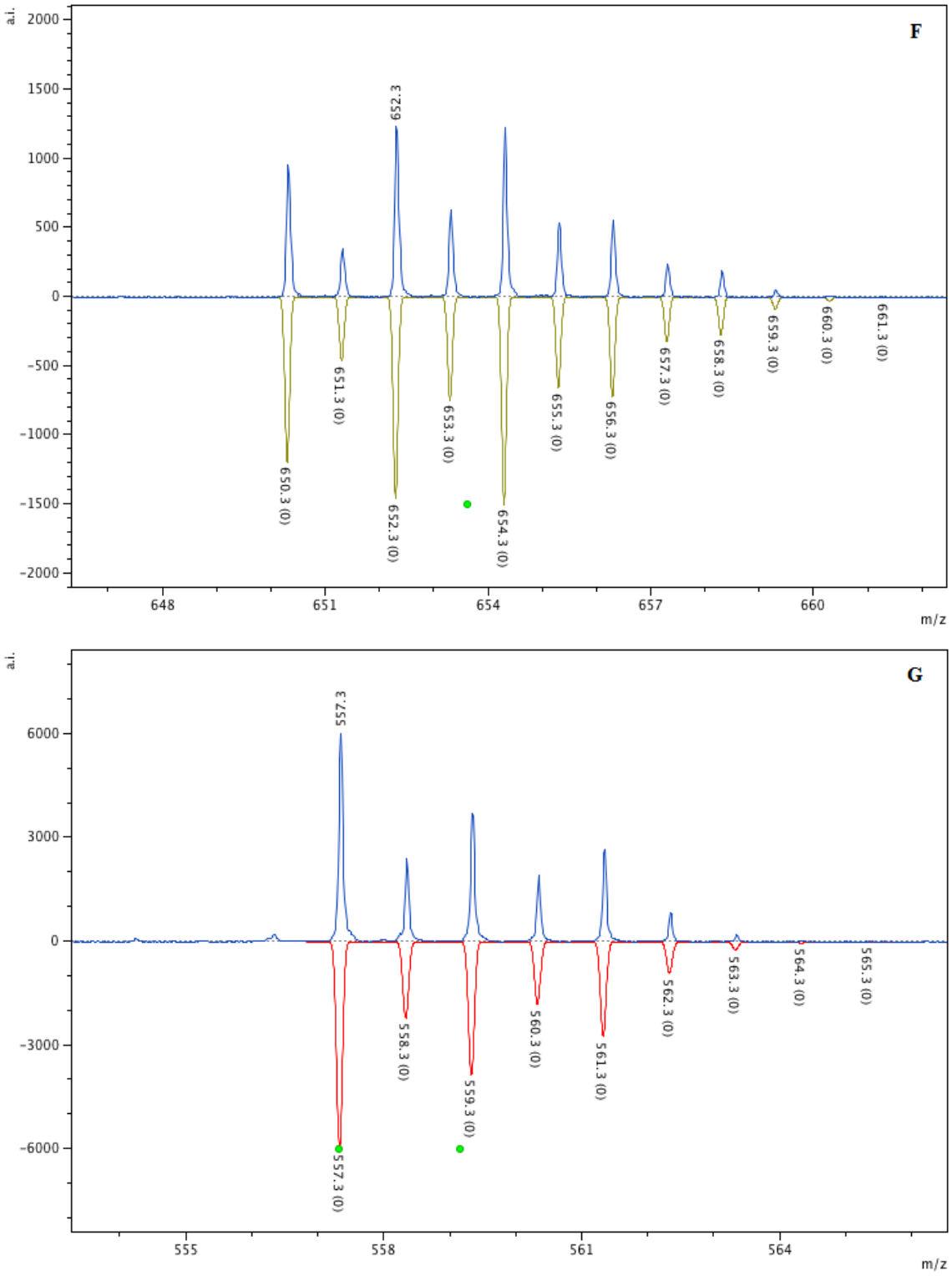

Figure 2-3 MALDI-TOF mass spectra for complex **1a**: full spectrum (**A**) and expanded spectra with experimental and theoretical (flipped) isotopic distribution patterns (**B-G**).

2.2.2.3 Elemental Analysis

Complexes **1a** and **1b** were characterized by elemental analysis. Complex **1a** and **1b** were dried under vacuum for 4 h for removal of the residual pentane. Experiments were conducted using air-free techniques and were found to have good agreement with the theoretical values, as shown in **Table 2-3**.

Table 2-3 Elemental analysis of complexes **1a** and **1b**.

Complex	Experimental (theoretical) C%	Experimental (theoretical) H%	Experimental (theoretical) N%
1a	65.25 (65.10)	8.93 (9.01)	2.10 (2.05)
1b	62.50 (62.21)	8.30 (8.25)	2.50 (2.34)

2.2.2.4 Single Crystal X-ray Diffraction

Colorless needle-like crystals were obtained by recrystallization of **1b** in pentane at room temperature, and the crystals changed to colorless blocklike crystals after a month. However their analysis by X-ray diffraction gave a molecular structure showing a trimetallic complex with two **[L2]** ligands and two ethyl groups, **1c** (**Figure 2-4**). The selected bond lengths and angles are shown in **Table 2-4**. Crystallographic details are given in **Table 2-5**. This structure is inconsistent with the NMR spectra and elemental analysis results obtained for **1b** and is likely from decomposition of the bimetallic species in non-coordinating solvents (**Scheme 2-1**). Unfortunately, sufficient quantities of **1c** could not be obtained for acceptable NMR characterization. Each zinc atom has a tetrahedral geometry with the two outer zinc atoms having the same coordination environment; each possesses an amine donor, an ethyl group and two phenolate oxygens bridging a pair of zinc atoms. The central zinc atom occupies a distorted tetrahedral geometry bonded to the four bridging oxygen atoms and shows O(1)-Zn(2)-O(2) and O(3)-Zn(2)-O(4) angles of 85.02(12)° and 86.96(12)°, respectively.

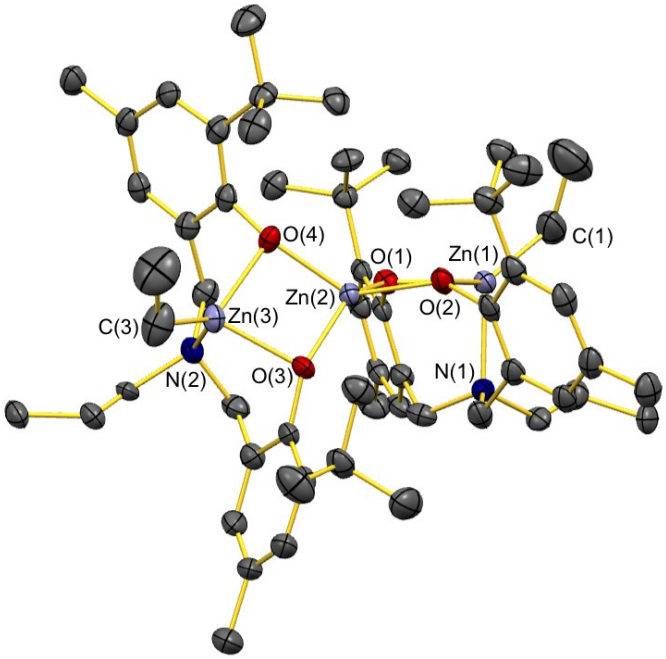

Figure 2-4 Partially labeled molecular structure (ORTEP) of Zn_3Et_2[**L2**]$_2$, **1c**. Thermal ellipsoids are drawn at 50% probability and H atoms are excluded for clarity.

Table 2-4 Selected bond lengths (Å) and angles (°) for Zn_3Et_2[**L2**]$_2$, **1c**.

Atoms	Distance (Å)	Atoms	Angle (°)
Zn(1)-O(1)	2.050(3)	O(1)-Zn(1)-O(2)	80.58(11)
Zn(1)-O(2)	2.055(3)	O(1)-Zn(1)-N(1)	89.45(12)
Zn(1)-N(1)	2.159(3)	O(2)-Zn(1)-N(1)	90.18(13)
Zn(1)-C(1)	1.973(6)	C(1)-Zn(1)-O(1)	121.81(17)
Zn(2)-O(1)	1.951(3)	C(1)-Zn(1)-O(2)	135.3(3)
Zn(2)-O(2)	1.977(3)	C(1)-Zn(1)-N(1)	124.7(2)
Zn(2)-O(3)	1.954(3)	O(1)-Zn(2)-O(2)	85.02(12)
Zn(2)-O(4)	1.988(3)	O(1)-Zn(2)-O(3)	134.56(14)
Zn(3)-O(3)	2.056(3)	O(1)-Zn(2)-O(4)	113.12(11)
Zn(3)-O(4)	2.065(3)	O(2)-Zn(2)-O(4)	129.25(14)
Zn(3)-N(2)	2.167(4)	O(3)-Zn(2)-O(2)	114.15(11)
Zn(3)-C(3)	1.960(6)	O(3)-Zn(2)-O(4)	86.96(12)
		O(3)-Zn(3)-O(4)	82.34(10)
		O(3)-Zn(3)-N(2)	87.96(13)
		O(4)-Zn(3)-N(2)	90.81(13)
		C(3)-Zn(3)-O(3)	122.04(17)
		C(3)-Zn(3)-O(4)	129.5(2)
		C(3)-Zn(3)-N(2)	129.4(2)

Table 2-5 Crystal data and structure refinement for **1c**, **1a·THF** and **2**.

Complex	**1c**	**1a·THF**	**2**
Empirical formula	$C_{58}H_{88}N_2O_4Zn_3$	$C_{41}H_{69}NO_3Zn_2$	$C_{72}H_{116}N_2O_6Zn_3$
Formula weight	1073.41	754.71	1301.77
Temperature/K	124.98	125.03	125.02
Crystal system	monoclinic	monoclinic	monoclinic
Space group	$P2_1$	$P2_1/c$	$P2_1/c$
a/Å	13.1456(11)	12.9102(11)	13.4644(9)
b/Å	18.2114(15)	10.9571(10)	28.1652(19)
c/Å	13.3495(11)	28.288(3)	20.0841(14)
α/°	90	90	90
β/°	119.0050(10)	93.6070(10)	104.2080(10)
γ/°	90	90	90
Volume/Å^3	2795.0(4)	3993.6(6)	7383.5(9)
Z	2	4	4
ρ_{calc}g/cm^3	1.275	1.255	1.171
μ/mm^{-1}	1.322	1.237	1.014
F(000)	1144.0	1624.0	2800.0
Crystal size/mm^3	0.362 × 0.253 × 0.173	0.401 × 0.335 × 0.231	0.354 × 0.251 × 0.226
Radiation, λ (MoKα)	0.71073	0.71073	0.71073
2Θ range for data collection/°	4.144 to 56.606	3.988 to 57.406	4.184 to 56.584
Index ranges	-16 ≤ h ≤ 17, -18 ≤ k ≤ 24, -17 ≤ l ≤ 17	-16 ≤ h ≤ 16, -14 ≤ k ≤ 12, -37 ≤ l ≤ 38	-17 ≤ h ≤ 17, -36 ≤ k ≤ 37, -26 ≤ l ≤ 24
Reflections collected	16956	31734	60031
Independent reflections	8130 [R_{int} = 0.0293, R_{sigma} = 0.0690]	9708 [R_{int} = 0.0263, R_{sigma} = 0.0292]	17705 [R_{int} = 0.0533, R_{sigma} = 0.0621]
Data/restraints/parameters	8130/7/658	9708/0/439	17705/102/840
Goodness-of-fit on F^2	0.905	1.027	1.013
R_1, wR_2 [I/2σ (I)]	0.0322, 0.0604	0.0289, 0.0683	0.0426, 0.0871
R_1, wR_2 [all data]	0.0387, 0.0619	0.0382, 0.0721	0.0805, 0.0995
Largest diff. peak/hole / e Å^{-3}	0.47/-0.35	0.37/-0.22	0.41/-0.40
CCDC Reference	1412176	1412177	1412178

[a]$R_1 = \Sigma(|F_o| - |F_c|)/\Sigma|F_o|$; $wR_2 = [\Sigma/(w(F_o^2 - F_c^2)^2)/\Sigma w(F_o^2)^2]^{1/2}$, where $w = 1/\sigma^2(F_o^2) + (aP)^2 + bP$.

2.2.3 Synthesis of Zinc Ethyl Complexes in THF

Reaction of H_2**[L1]** with two equiv. of $ZnEt_2$ in THF yielded the corresponding bimetallic complex with one THF molecule coordinating to a zinc center, $[Zn_2Et_2(THF)]$**[L1]**, **1a·THF** (**Scheme 2-1**). The reaction mixture was stirred for 2 h followed by removal of the solvent under vacuum to gain a colorless solid. The product was dissolved in pentane and soon precipitated out. The solid was washed twice with pentane and dried under vacuum.

2.2.4 Characterization of Zinc Ethyl THF Complex

2.2.4.1 NMR Spectroscopy

The ^{1}H NMR spectrum (**Figure 2-5**) of complex **1a·THF** is similar to that of **1a**, with the appearance of two extra multiplets at δ 3.92 and δ 1.93 assigned to the coordinated THF, moving to upfield comparing with free THF in $CDCl_3$, at δ 3.76 and δ 1.85.[34] Correlation spectroscopy (COSY) (**Figure 2-6**) confirmed the coordination of THF by showing the two multiplets are coupled. The COSY spectrum also confirmed the existence of two different ethyl groups. Comparison of **1a** and **1a·THF** found the chemical shift of one $ZnCH_2CH_3$ shifts from δ 0.11 to δ 0.35.

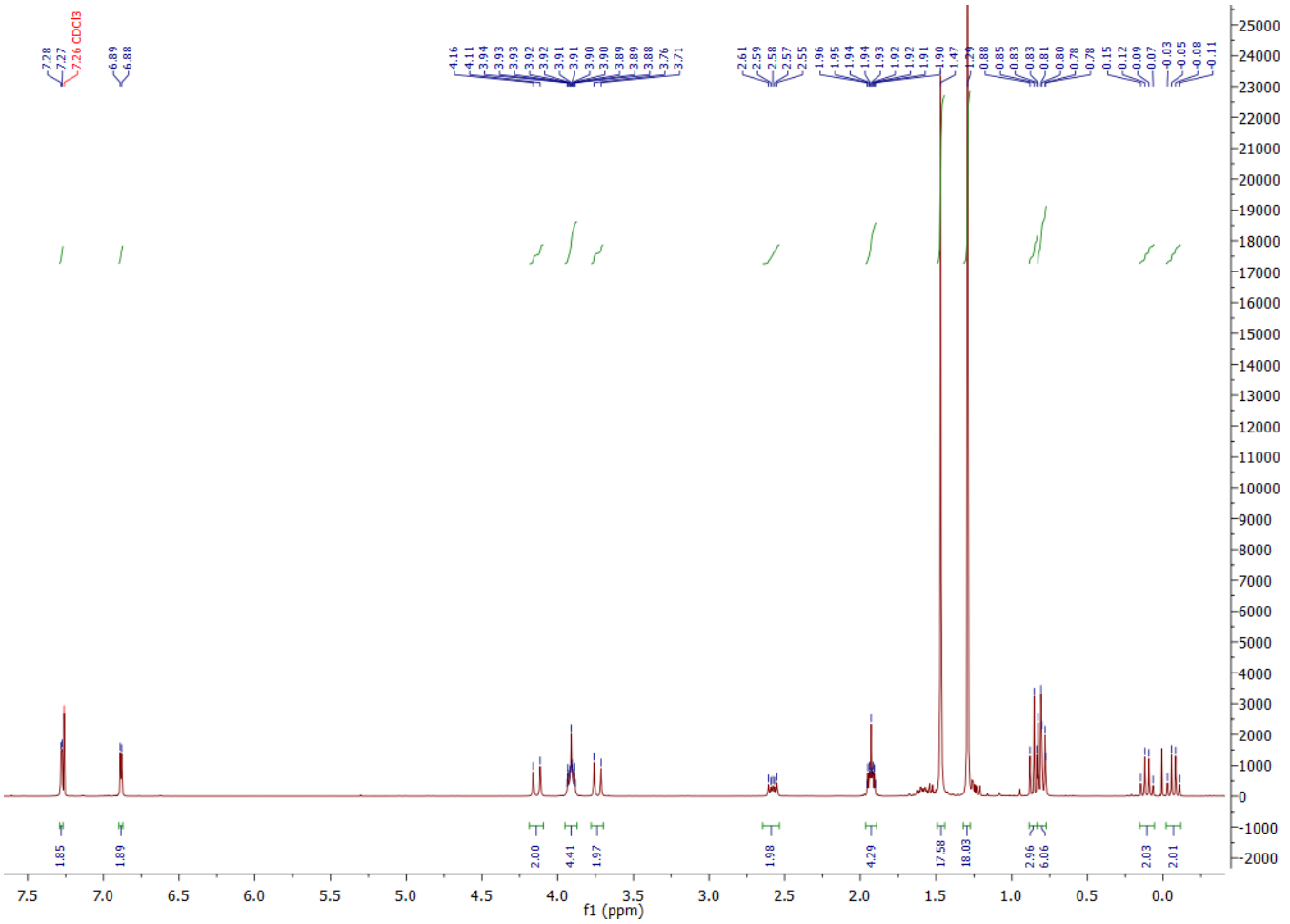

Figure 2-5 ^{1}H NMR spectrum of **1a·THF** (300 MHz, $CDCl_3$, 298 K).

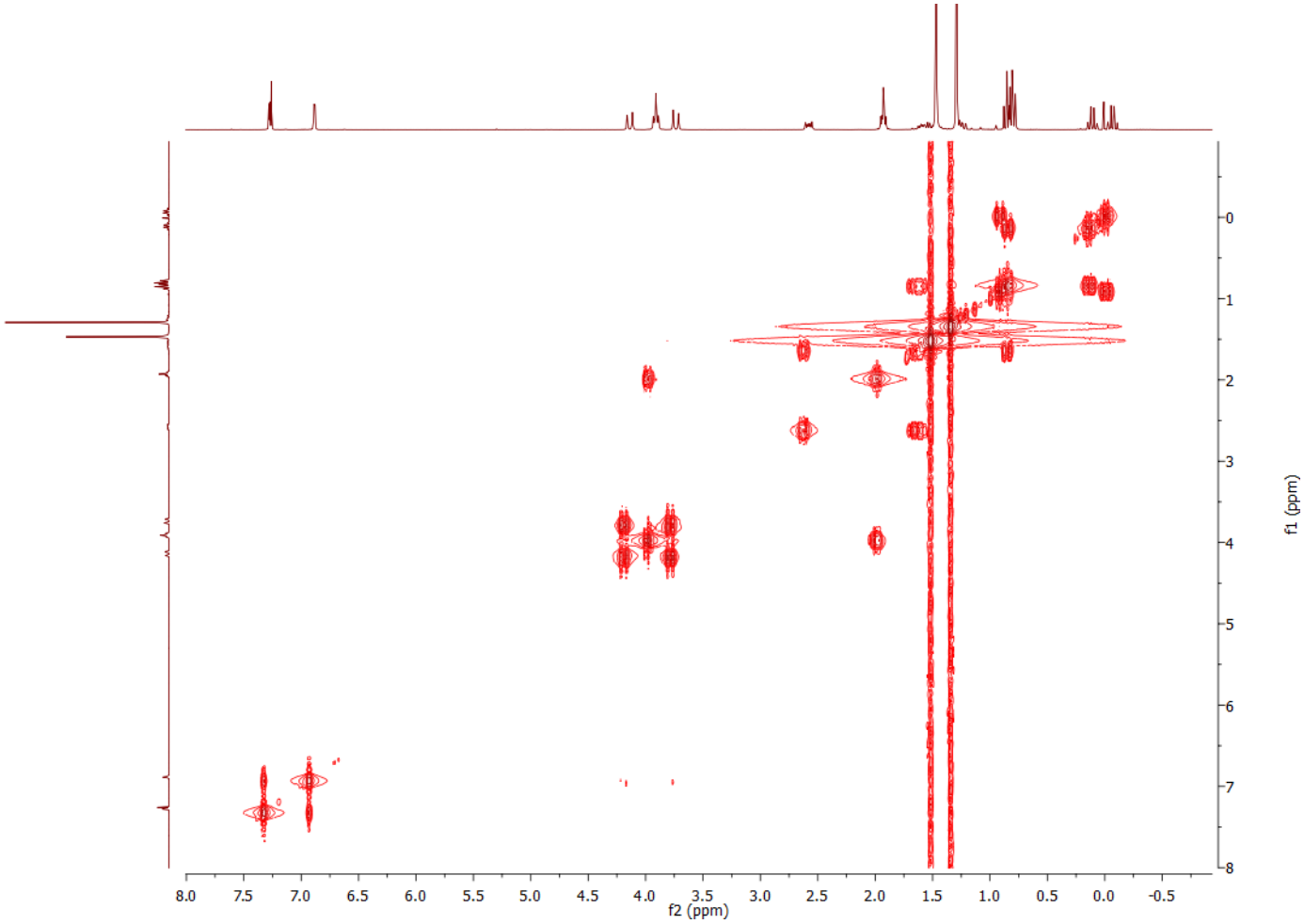

Figure 2-6 COSY spectrum of **1a·THF** (300 MHz, $CDCl_3$, 298 K).

2.2.4.2 X-ray Diffraction

Crystals suitable for X-ray diffraction were obtained in pentane at room temperature and the single crystal molecular structure is shown in **Figure 2-7**, with selected bond lengths and angles shown in **Table 2-6**. Each zinc center adopts a four-coordinate geometry. The nearly planar Zn_2O_2 core possesses a sum of angles of 359.8° and a O(1)-Zn(1)-O(2) angle of 84.87(4)°. One zinc atom is coordinated by two bridging phenolates, the neutral donor amine and an ethyl group. The other zinc atom is coordinated by two bridging phenolates, an ethyl group and one THF molecule. The bonds between the two bridging oxygen atoms and the zinc atoms are similar, with Zn(1)-O(1) = 2.0570(11), Zn(1)-O(2) = 2.0435(10), Zn(2)-O(1) = 2.0031(10) and Zn(2)-O(2) = 2.0444(11) Å. These zinc phenolate bonds have similar length as those reported in literature.[17-20] The Zn(2)-O(3) bond length is expectedly longer at 2.1581(11) Å. Crystallographic details are given in **Table 2-5**.

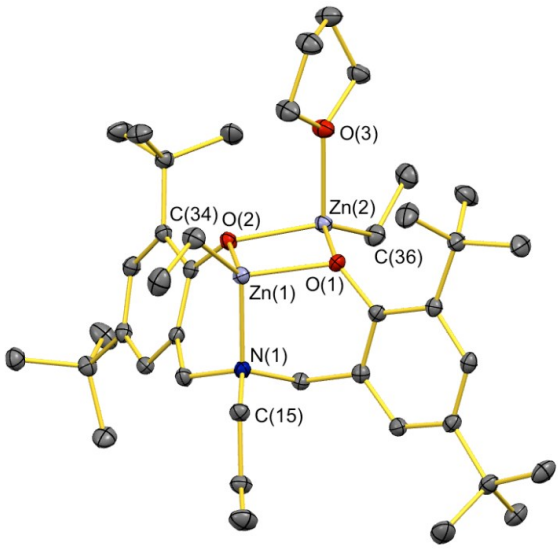

Figure 2-7 Partially labeled molecular structure (ORTEP) of Zn_2Et_2(THF)**[L1]**, **1a·THF**. Thermal ellipsoids are drawn at 50% probability and H atoms are excluded for clarity.

Table 2-6 Selected bond lengths (Å) and angles (°) for $Zn_2Et_2(THF)$**[L1]**, **1a·THF**.

Atoms	Distance (Å)	Atoms	Angle (°)
Zn(1)-O(1)	2.0570(11)	O(1)-Zn(1)-N(1)	92.80(4)
Zn(1)-O(2)	2.0435(10)	O(2)-Zn(1)-O(1)	84.87(4)
Zn(1)-N(1)	2.0860(12)	O(2)-Zn(1)-N(1)	91.54(5)
Zn(1)-C(34)	1.9708(16)	C(34)-Zn(1)-O(1)	125.78(6)
Zn(2)-O(1)	2.0031(10)	C(34)-Zn(1)-O(2)	120.18(6)
Zn(2)-O(2)	2.0444(11)	C(34)-Zn(1)-N(1)	129.34(6)
Zn(2)-O(3)	2.1581(11)	O(1)-Zn(2)-O(2)	86.24(4)
Zn(2)-C(36)	1.9707(16)	O(1)-Zn(2)-O(3)	91.72(4)
		O(2)-Zn(2)-O(3)	96.09(4)
		C(36)-Zn(2)-O(1)	128.40(6)
		C(36)-Zn(2)-O(2)	129.02(6)
		C(36-)Zn(2)-O(3)	115.62(6)

2.2.5 Synthesis of Zinc Alkoxyl Complexes

Reaction of zinc ethyl complex **1a** with isopropyl alcohol (*i*-PrOH) in pentane resulted in the precipitation of the zinc isopropoxyl complex, $Zn_3(i\text{-PrO})_2$**[L1]**$_2$, **2** (**Scheme 2-2**). Two equiv. of *i*-PrOH were added to the solution of complex **1a** in pentane. A white precipitate was obtained and the reaction mixture was stirred for 4 h at ambient temperature. The stirring was then stopped to allow the precipitate to settle and the upper solution was removed using a pipet. The remaining solid was then washed twice with pentane, followed by removal of the solvent to yield a colorless solid. It was found that utilization of one equiv. of *i*-PrOH with complex **1a** also generates complex **2** (**Scheme 2-2**). The reaction of complex **1a** with *i*-PrOH was also carried out in THF, which yielded the same product, without any coordination of THF.

Reactions of complex **1a** or **1a·THF** with benzyl alcohol (BnOH) were conducted in pentane or THF; however, no pure product was obtained based on NMR analysis. Stoichiometric reactions of **1a·THF** with one equiv. of BnOH or two equiv. of BnOH were monitored by ^{1}H NMR (**Figure 3-30**) and detailed discussion is given in Chapter 3.

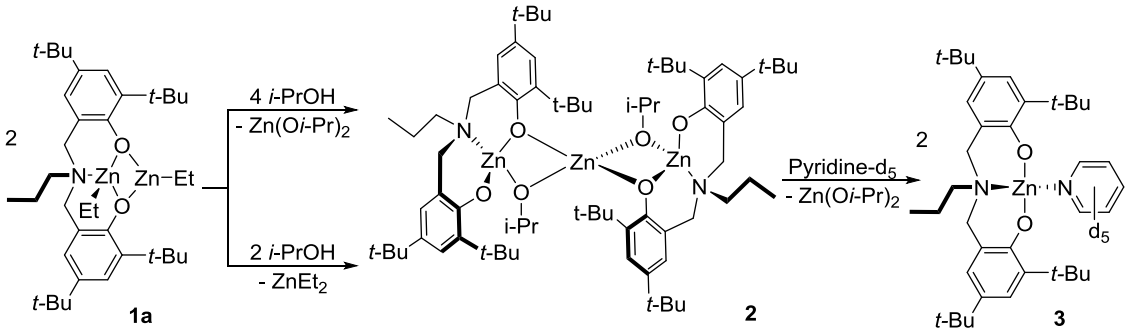

Scheme 2-2 Synthesis of zinc isopropoxyl complex.

2.2.6 Characterization of Zinc Alkoxyl Complex

2.2.6.1 NMR Spectroscopy

The ^{1}H NMR spectrum (**Figure 2-8**) of complex **2** in $CDCl_3$ indicates four different environments of aromatic protons and four different *t*-Bu group environments. The multiplet at δ 4.32 corresponds to the isopropoxyl tertiary carbon proton. Four doublets of the NCH_2 protons appeared in the spectrum with chemical shifts at δ 3.51, 3.12, 2.70, and 2.55. Two doublets appeared at δ 1.42 and δ 1.23 corresponding to the methyl protons of the isopropoxyl groups. Integration of the *i*-Pr resonances shows one isopropyl group occurs per amino-bis(phenolate) ligand. The COSY spectrum (**Figure 2-9**) shows the coupling of the methine proton of isopropoxyl at δ 4.32 with the methyl protons of isopropoxyl at δ 1.42 and δ 1.23, which confirms the proposed structure. It is noticeable that there was a multiplet at δ 4.13 and weak resonances indicating the

existence of *i*-PrOZnEt species. After further purification of the product by washing with pentane, the *i*-PrOZnEt resonances disappeared. The summary of the ^{1}H NMR and ^{13}C NMR spectra are listed in **Table 2-7** and **Table 2-8**, respectively.

NMR analysis of complex **2** in pyridine-d_5 shows the formation of the monometallic pyridine adduct, Zn(py)**[L1]** (**Figure A-6**). A white precipitate, possibly Zn(*i*-PrO)$_2$, was observed in the NMR tube, and weak resonances assigned to the *i*-PrO groups of Zn(*i*-PrO)$_2$ were still observable. The two doublets of the NCH_2 protons confirm the amino-bis(phenolate) ligand is still coordinated to the zinc center. This suggests the trimetallic compounds dissociate into mono- or dimetallic (formulated as Zn(solvent)**[L]** or Zn_2R_2(solvent)**[L]**) molecules in coordinating solvents.

Table 2-7 Assignment of resonances in the ^{1}H NMR spectrum of **2** in $CDCl_3$.

Proton types	Number of protons	Chemical shift (δ)	Peak	*J* (Hz)
ArH	2	7.26	d	2.5
ArH	2	7.15	d	2.6
ArH	2	6.60	d	2.6
ArH	2	6.54	d	2.5
CH	2	4.32	m(septet)	6.0
$ArCH_2$	2	3.51	d	13.4
$ArCH_2$	2	3.12	d	13.4
$ArCH_2$	2	2.70	d	13.2
$ArCH_2$	2	2.55	d	13.2
$NC\mathit{H}_2CH_2CH_3$	4	2.59	m	-
$C(CH_3)_3$	18	1.50	s	-
$CH(C\mathit{H}_3)_2$	6	1.42	d	6.0
$C(CH_3)_3$	18	1.39	s	-
$C(CH_3)_3$	18	1.30	s	-
$NCH_2C\mathit{H}_2CH_3$	4	1.29	m	7.3
$CH(C\mathit{H}_3)_2$	6	1.23	d	-
$C(CH_3)_3$	18	1.19	s	-
$NCH_2CH_2C\mathit{H}_3$	6	0.73	t	7.3

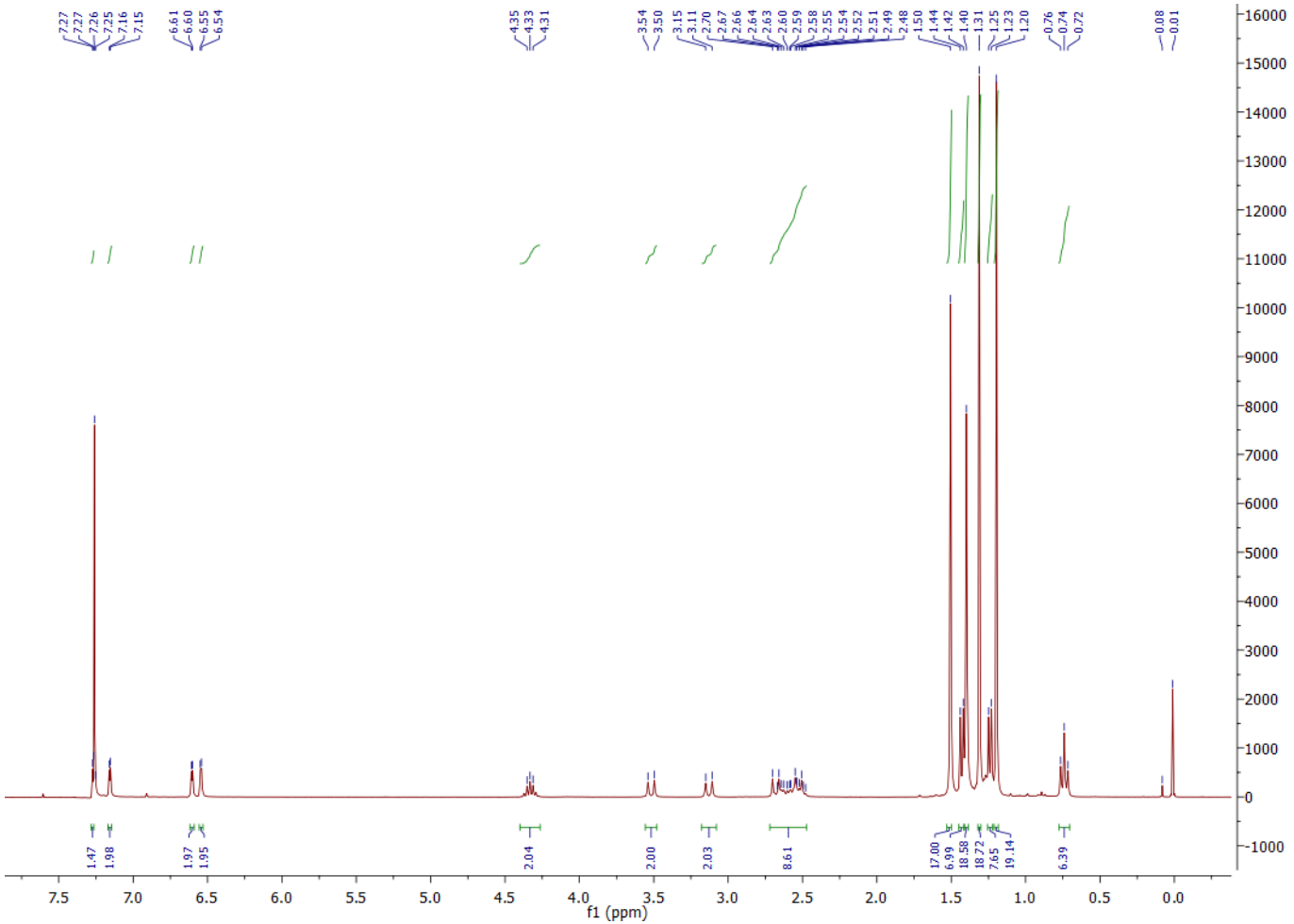

Figure 2-8 ^{1}H NMR spectrum of **2** (300 MHz, $CDCl_3$, 298 K).

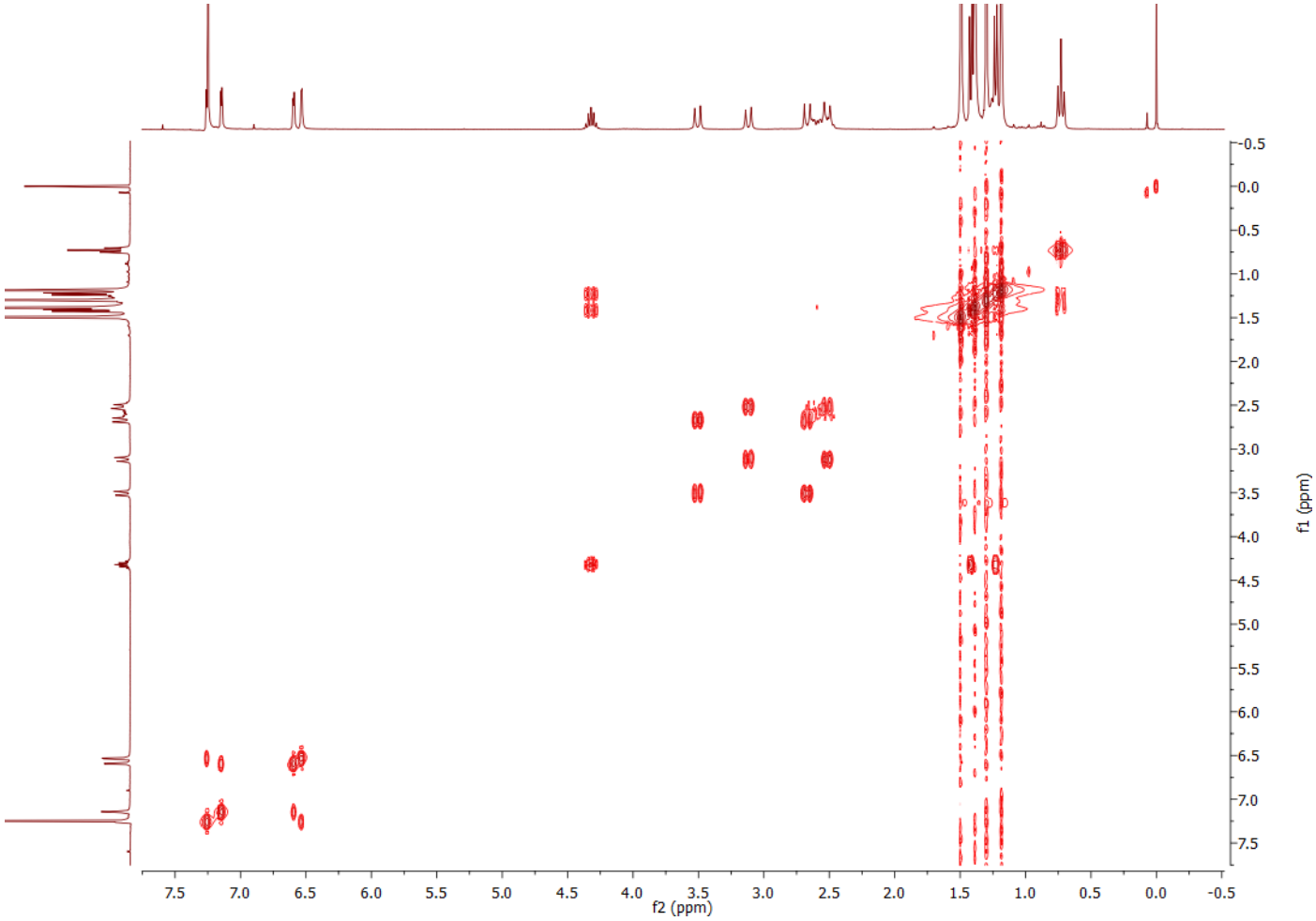

Figure 2-9 COSY spectrum of **2** (300 MHz, $CDCl_3$, 298 K).

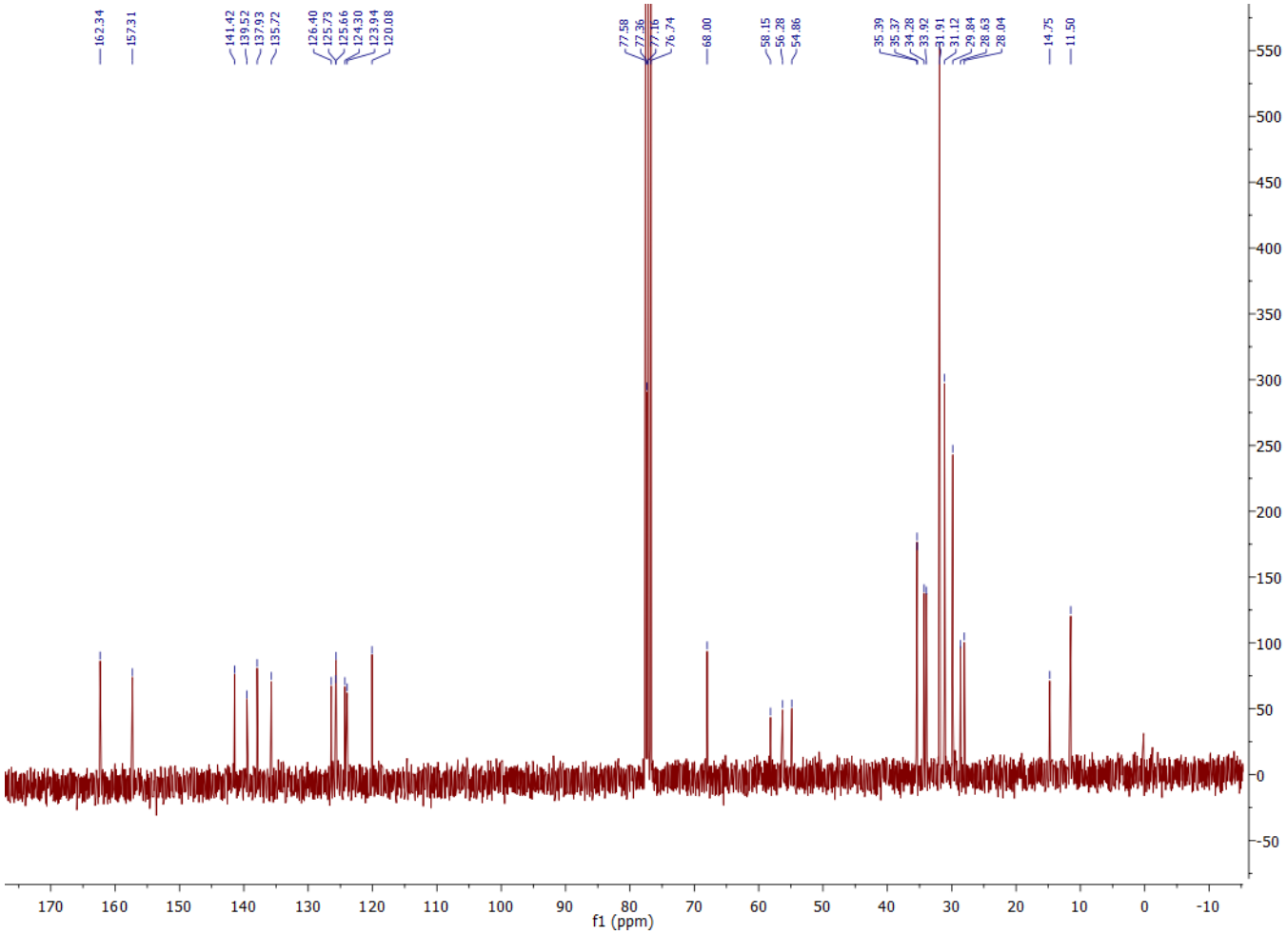

Figure 2-10 ^{13}C NMR spectrum of **2** (75 MHz, $CDCl_3$, 298 K).

Table 2-8 Assignment of resonances in the ^{13}C NMR spectrum of **2** in $CDCl_3$.

Carbon types	**Chemical shift (δ)**					
Ar	162.34	157.31	141.42	139.52	137.93	135.72
Ar	126.4	125.73	125.66	124.3	123.94	120.08
CH	68					
Ar*C*H_2	58.15	56.28				
N*C*$H_2CH_2CH_3$	54.86					
C$(CH_3)_3$	35.39	35.37	34.28	33.92		
C(*C*$H_3)_3$	31.91	31.12	29.84			
NCH_2*C*H_2CH_3	18.53					
CH(*C*$H_3)_2$	28.63	28.04				
NCH_2CH_2*C*H_3	14.75	11.5				

2.2.6.2 Elemental Analysis

Complex **2** was dried overnight under vacuum for removal of any solvent residual. Experiments were conducted using air-free techniques. The experimental results agrees with the theoretical values, as shown in **Table 2-9**

Table 2-9 Elemental analysis of complex **2**.

Complex	**Experimental (theoretical) C%**	**Experimental (theoretical) H%**	**Experimental (theoretical) N%**
2	62.50 (62.21)	8.30 (8.25)	2.50 (2.34)

2.2.6.3 Singel Crystal X-ray Diffraction

Crystals suitable for X-ray diffraction were obtained in pentane at room temperature. Complex **2** was characterized by single crystal X-ray diffraction, which confirmed complex **2** is a trimetallic complex possessing two amino-bis(phenolate) ligands and two isopropoxyl groups (**Figure 2-11**). Selected bond lengths and angles are shown in **Table 2-10**. Each zinc atom possesses a distorted tetrahedral geometry. The central Zn(2) atom is coordinated by two bridging phenolate oxygen donors and two bridging isopropoxyl groups. These zinc alkoxyl bonds have similar length with those reported in literature.[13,16,19] Crystallographic details are given in **Table 2-5**.

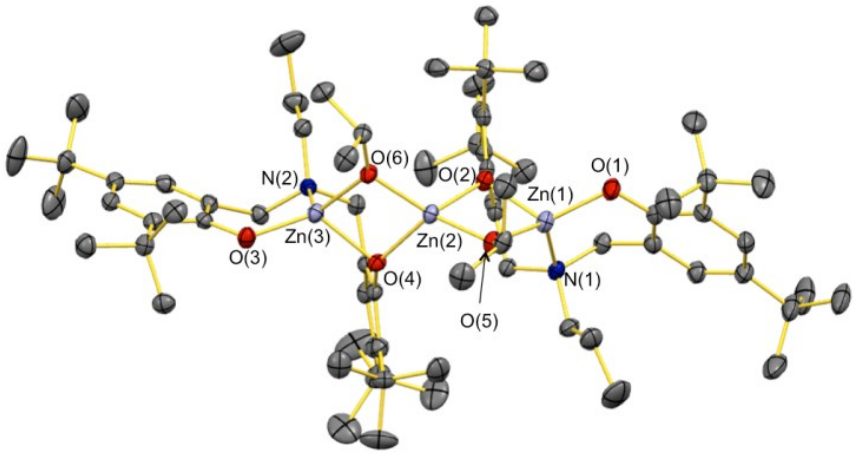

Figure 2-11 Partially labeled molecular structure (ORTEP) of $Zn_3(i\text{-PrO})_2$[**L1**]$_2$, **2**. Thermal ellipsoids are drawn at 50% probability and H atoms are excluded for clarity.

Table 2-10 Selected bond lengths (Å) and angles (°) for $Zn_3(i\text{-PrO})_2$[**L1**]$_2$, **2**.

Atoms	Distance (Å)	Atoms	Angle (°)
Zn(1)-O(1)	1.8664(16)	O(1)-Zn(1)-O(2)	119.18(7)
Zn(1)-O(2)	1.9966(15)	O(1)-Zn(1)-O(5)	131.97(7)
Zn(1)-O(5)	1.9405(16)	O(1)-Zn(1)-N(1)	101.73(7)
Zn(1)-N(1)	2.0726(19)	O(2)-Zn(1)-N(1)	95.43(6)
Zn(2)-O(2)	1.9940(15)	O(5)-Zn(1)-O(2)	83.50(6)
Zn(2)-O(4)	1.9944(15)	O(5)-Zn(1)-N(1)	118.67(7)
Zn(2)-O(5)	1.9360(15)	O(2)-Zn(2)-O(4)	118.66(6)
Zn(2)-O(6)	1.9358(14)	O(5)-Zn(2)-O(2)	83.68(6)
Zn(3)-O(3)	1.8746(16)	O(5)-Zn(2)-O(4)	120.54(7)
Zn(3)-O(4)	2.0083(15)	O(6)-Zn(2)-O(2)	119.96(7)
Zn(3)-O(6)	1.9444(15)	O(6)-Zn(2)-O(4)	83.38(6)
Zn(3)-N(2)	2.0744(19)	O(6)-Zn(2)-O(5)	134.91(6)
		O(3)-Zn(3)-O(4)	122.54(7)
		O(3))-Zn(3)-O(6)	134.48(7)
		O(3)-Zn(3)-N(2)	101.66(7)
		O(4)-Zn(3)-N(2)	96.11(6)
		O(6)-Zn(3)-O(4)	82.80(6)
		O(6)-Zn(3)-N(2)	113.27(7)

2.2.7 Attempted Synthesis of Zinc Methyl Lactate Complexes

Reactions of complex **1a** with L-methyl lactate to generate the corresponding zinc methyl lactate species were attempted. The proposed reactions for obtaining the desired products of $Zn_2Et(OCHMeCO)$[**L1**] (**3a**) and $Zn_2(OCHMeCO)_2$[**L1**] (**3b**) are shown in **Scheme 2-3**.

One equiv. or two equiv. of methyl lactate was added to a solution of complex **1a** in pentane. White precipitate formed after stirring for 1 h. The reaction mixture was stirred for 4 h at ambient temperature and then filtered to give a clear solution. A colorless solid was obtained after the removal of the solvent under vacuum and drying overnight. The products show complicated ^{1}H NMR spectra that could not be assigned. Therefore, they were characterized using MALDI-TOF MS and elemental analysis.

Attempted synthesis of zinc methyl lactate complex by treatment of complex **1a** with an excess of methyl lactate per ethyl group, i.e. 2.2 equiv., or by lengthier reaction time was conducted. However, pure complex **3b** failed to be obtained.

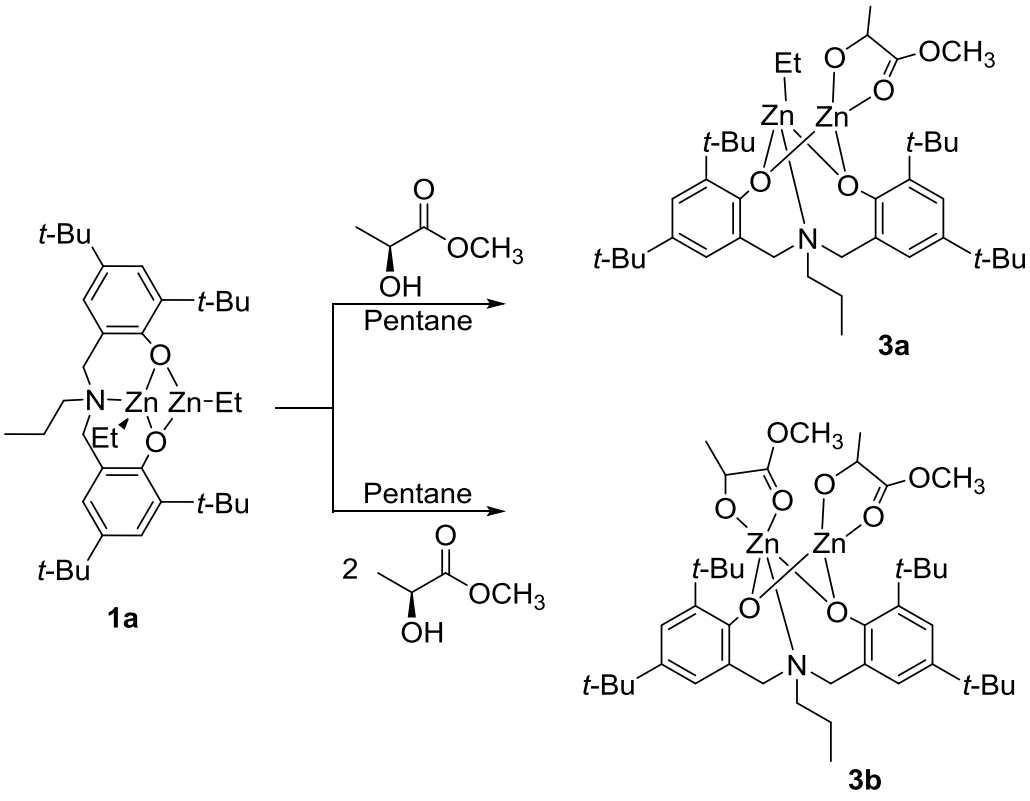

Scheme 2-3 Proposed reactions of complex **1a** with L-methyl lactate.

2.2.8 Characterization of Zinc Methyl Lactate complexes

2.2.8.1 NMR Spectroscopy

The ^{1}H NMR spectra of the two reaction products were difficult to assign. Noticeably, the product of using one equiv. of L-methyl lactate shows two different environments of the methine region at δ 4.67 and δ 4.20 with an integration ratio of 3:1, which may belong to two isomers of the zinc methyl lactate species (**Figure A – 9 and 10**). For the product obtained by reacting **1a** with two equiv. of L-methyl lactate, multiple methine environments were observed, which indicate more than one methyl lactate moiety (**Figure A – 11**).

2.2.8.2 MALDI-TOF MS

The MALDI mass spectra of these two products showed peaks at *m/z* 757.4 and *m/z* 831.4 (**Figure 2-12**, **Figure 2-13**), corresponding to a complex with one ethyl and one methyl lactate group, and a complex with two methyl lactate groups, respectively. Other peaks at *m/z* 557.4, corresponding to Zn[**L1**] were observed.

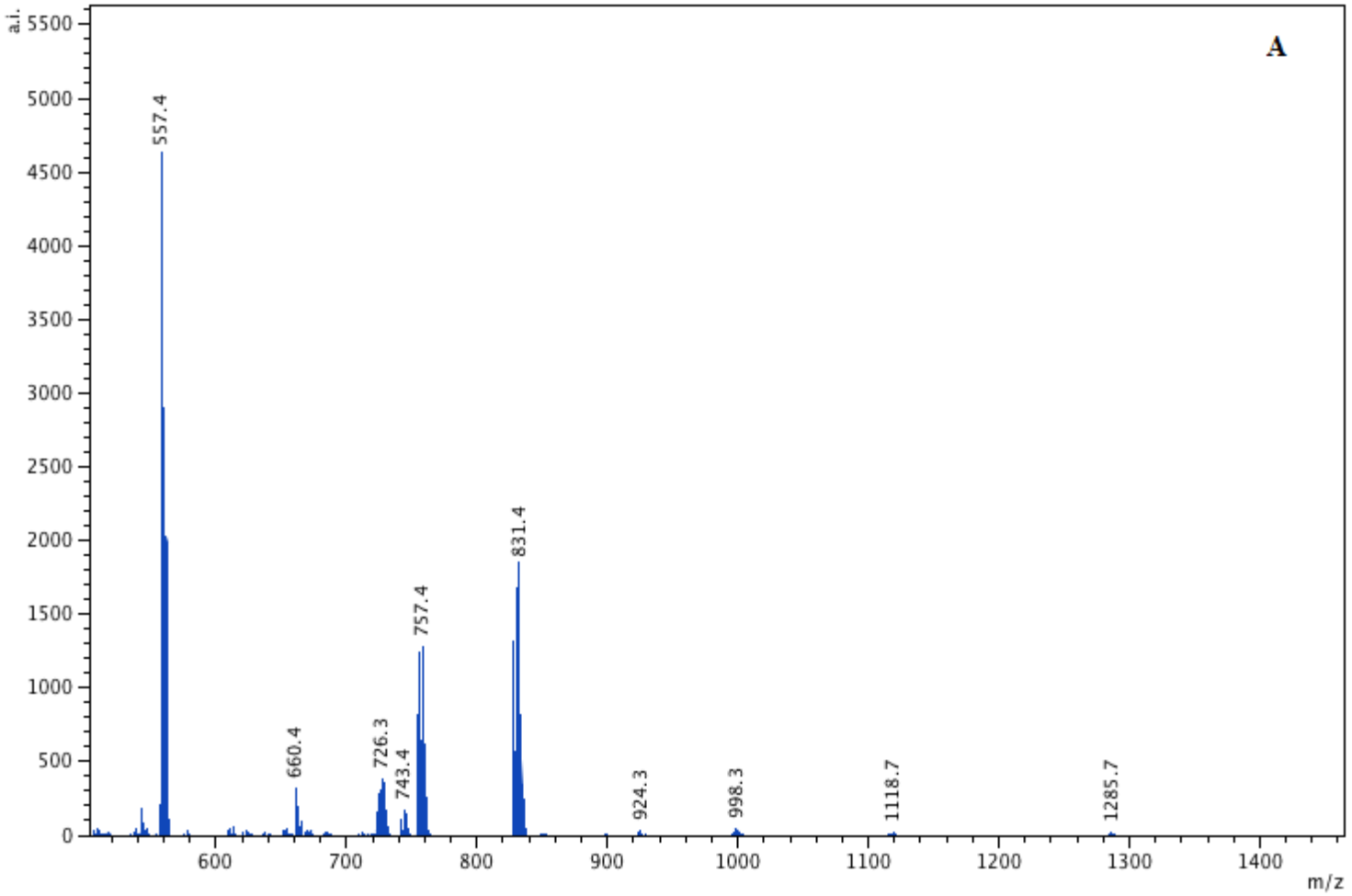
A
a.i.
5500
5000
4500
4000
3500
3000
2500
2000
1500
1000
500
0
557.4
660.4
726.3
743.4
757.4
831.4
924.3
998.3
1118.7
1285.7
600
700
800
900
1000
1100
1200
1300
1400
m/z

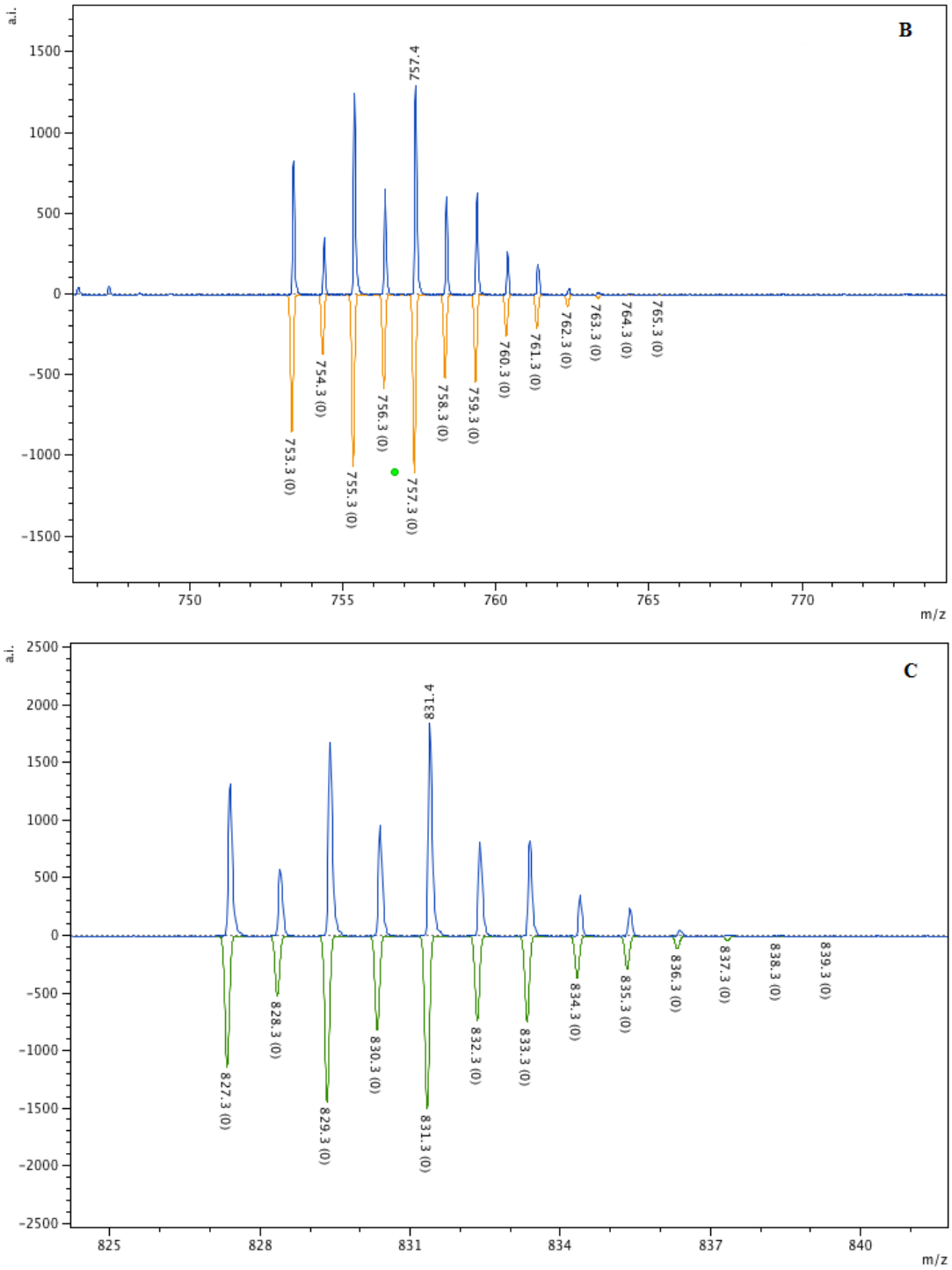

Figure 2-12 MALDI-TOF mass spectra for the reaction product of complex **1a** and one equiv. of methyl lactate: full spectrum (**A**) and expanded spectra with experimental and theoretical (flipped) isotopic distribution patterns (**B** and **C**).

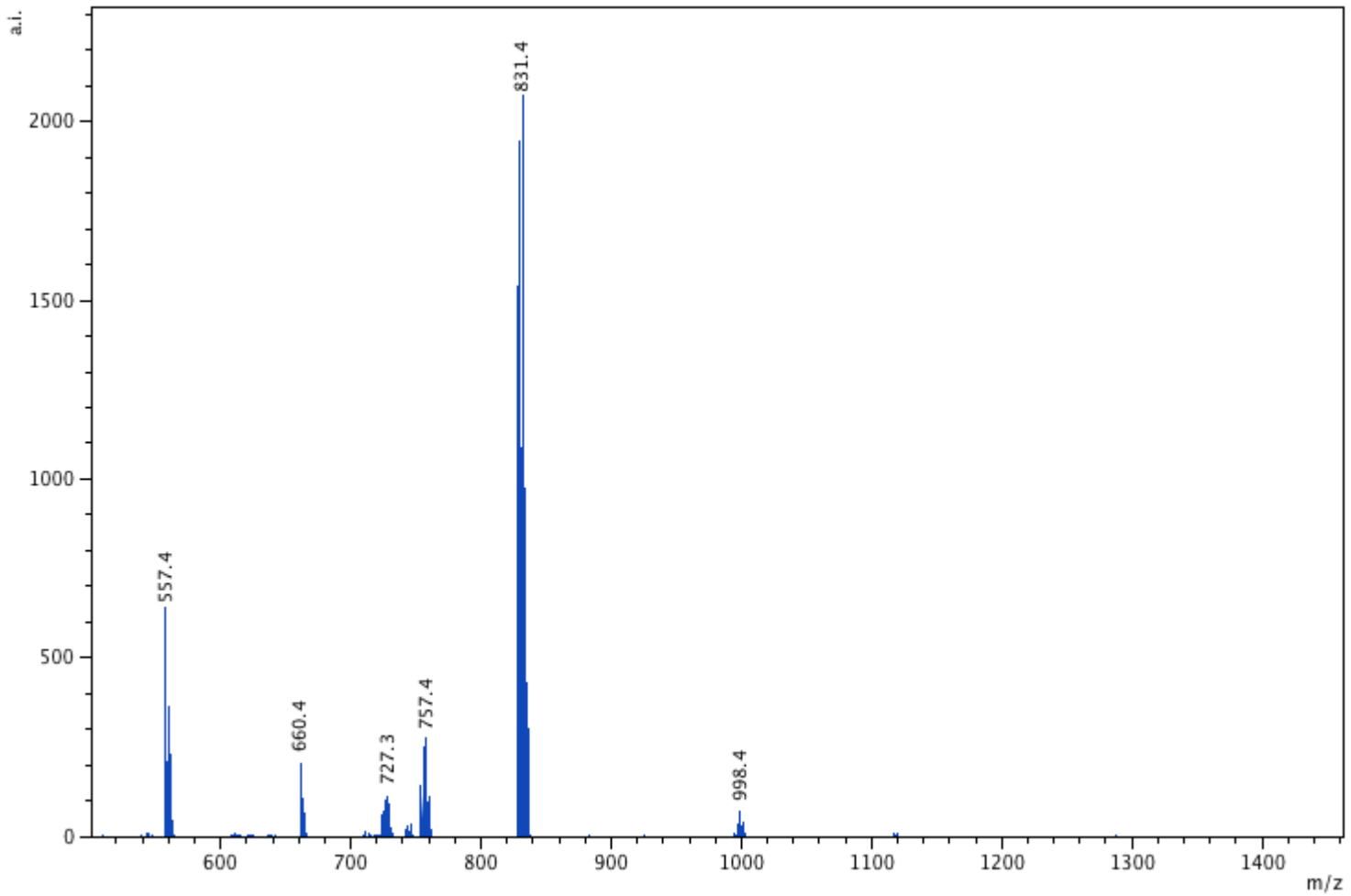

Figure 2-13 MALDI-TOF mass spectrum for the reaction product of complex **1a** and two equiv. of methyl lactate.

2.2.8.3 Elemental Analysis

Elemental analysis samples of proposed compounds **3a** and **3b** were prepared by drying under vacuum overnight. The experimental results are shown in **Table 2-11**. Product **3a** showed good agreement of experimental and theoretical values; however, there is non-negligible difference (> 0.4 %) between those of **3b**. A mixture of complex **3a** and **3b** at a ratio of 1:0.85 has theoretical elemental analysis values that agree with the experimental values for **3b**. The product may therefore be a mixture of complexes **3a** and **3b**.

Table 2-11 Elemental analysis of products **3a** and **3b**.

Complex	Formula	Experimental (theoretical) C%	Experimental (theoretical) H%	Experimental (theoretical) N%
3a	$C_{39}H_{63}NO_5Zn_2$	62.05 (61.90)	8.23 (8.39)	1.86 (1.85)
3b	$C_{41}H_{65}NO_8Zn_2$	60.54 (59.28)	7.99 (7.89)	1.83 (1.69)
3a, 0.85 3b	$C_{39}H_{63}NO_5Zn_2$ 0.85($C_{41}H_{65}NO_8Zn_2$)	60.54 (60.64)	7.99 (8.15)	1.83 (1.77)

2.3 Conclusions

A series of bimetallic and trimetallic zinc complexes of amino-bis(phenolate) ligands were synthesized and characterized. Bimetallic complexes $(ZnEt)_2$**[L1]** (**1a**) and $(ZnEt)_2$**[L2]** (**1b**) were prepared via reaction of the proligands H_2[**L1**] and H_2[**L2**] with $ZnEt_2$ in pentane. A THF adduct $(ZnEt)_2$**[L1]**·THF (**1a·THF**) was obtained by using THF as solvent. Treatment of **1a** with one or two equiv. of isopropyl alcohol gave a trimetallic zinc complex Zn_3(*i*-PrO)$_2$**[L1]$_2$** (**2**). The obtained complexes were characterized by NMR spectroscopy, MALDI-TOF MS, elemental analysis and X-ray diffraction. The crystal structure of trimetallic complex **1c** was obtained and believed to come from the decomposition of complex **1b** in a non-coordination solvent. The THF adduct **1a·THF** is also bimetallic having a similar structure to **1a** but with one THF molecule loosely coordinated to one zinc, which makes both zinc centers have tetrahedral geometry. Zinc isopropoxyl complex **2** is found to be trimetallic, with two amino-bis(phenolate) ligands and three zinc centers. All of the zinc centers are in tetrahedral environments and the zinc in the center is highly distorted by the Zn_2O_2 ring strain. Treatment of complex **1a** with methyl lactate to obtain the corresponding zinc methyl lactate complex was attempted. The reaction products were characterized by NMR spectroscopy, MALDI-TOF MS and elemental analysis. ^{1}H NMR spectrum of **3a** shows complicated peaks, which could come from numerous isomers. Elemental analysis suggests that complex **3a** is pure but the product of **1a** with two equiv. of methyl lactate is a mixture of **3a** and **3b**. Unfortunately, crystals of **3a** and **3b** suitable for X-ray diffraction were not obtained.

2.4 References

1. Bonnet, F.; Cowley, A. R.; Mountford, P. *Inorg. Chem.* **2005,** *44*, 9046-9055.

2. Dean, R. K.; Reckling, A. M.; Chen, H.; Dawe, L. N.; Schneider, C. M.; Kozak, C. M. *Dalton Trans.* **2013,** *42*, 3504-3520.

3. Devaine-Pressing, K.; Lehr, J. H.; Pratt, M. E.; Dawe, L. N.; Sarjeant, A. A.; Kozak, C. M. *Dalton Trans.* **2015,** *44*, 12365-12375.

4. Dyer, H. E.; Huijser, S.; Susperregui, N.; Bonnet, F.; Schwarz, A. D.; Duchateau, R.; Maron, L.; Mountford, P. *Organometallics* **2010,** *29*, 3602-3621.

5. Liu, X.; Jian, C.; Yu, D.; Zhang, J.; Tang, N.; Wang, C.; Wu, J. *Inorg. Chem. Commun.* **2013,** *36*, 206-211.

6. Liu, X.; Shang, X.; Tang, T.; Hu, N.; Pei, F.; Cui, D.; Chen, X.; Jing, X. *Organometallics* **2007,** *26*, 2747-2757.

7. Nie, K.; Fang, L.; Yao, Y.; Zhang, Y.; Shen, Q.; Wang, Y. *Inorg. Chem.* **2012,** *51*, 11133-11143.

8. Pastor, M. F.; Whitehorne, T. J.; Oguadinma, P. O.; Schaper, F. *Inorg. Chem. Commun.* **2011,** *14*, 1737-1741.

9. Saunders, L. N.; Dawe, L. N.; Kozak, C. M. *J. Organomet. Chem.* **2014,** *749*, 34-40.

10. Sinenkov, M. A.; Fukin, G. K.; Cherkasov, A. V.; Ajellal, N.; Roisnel, T.; Kerton, F. M.; Carpentier, J.-F.; Trifonov, A. A. *New J. Chem.* **2011,** *35*, 204-212.

11. Yang, S.; Du, Z.; Zhang, Y.; Shen, Q. *Chem. Commun.* **2012,** *48*, 9780-9782.

12. Yang, S.; Nie, K.; Zhang, Y.; Xue, M.; Yao, Y.; Shen, Q. *Inorg. Chem.* **2013,** *53*, 105-115.

13. Williams, C. K.; Breyfogle, L. E.; Choi, S. K.; Nam, W.; Young, V. G.; Hillmyer, M. A.; Tolman, W. B. *J. Am. Chem. Soc.* **2003,** *125*, 11350-11359.

14. Silvernail, C. M.; Yao, L. J.; Hill, L. M.; Hillmyer, M. A.; Tolman, W. B. *Inorg. Chem.* **2007,** *46*, 6565-6574.

15. Labourdette, G.; Lee, D. J.; Patrick, B. O.; Ezhova, M. B.; Mehrkhodavandi, P. *Organometallics* **2009,** *28*, 1309-1319.

16. Chuang, H. J.; Weng, S. F.; Chang, C. C.; Lin, C. C.; Chen, H. Y. *Dalton Trans.* **2011,** *40*, 9601-9607.

17. Poirier, V.; Roisnel, T.; Carpentier, J. F.; Sarazin, Y. *Dalton Trans.* **2009**, 9820-9827.

18. Poirier, V.; Roisnel, T.; Carpentier, J. F.; Sarazin, Y. *Dalton Trans.* **2011,** *40*, 523-534.

19. Ikpo, N.; Saunders, L. N.; Walsh, J. L.; Smith, J. M. B.; Dawe, L. N.; Kerton, F. M. *Eur. J. Inorg. Chem.* **2011,** *2011*, 5347-5359.

20. Wang, L.; Ma, H. *Dalton Trans.* **2010,** *39*, 7897-7910.

21. Song, S.; Zhang, X.; Ma, H.; Yang, Y. *J. Chem. Soc., Dalton Trans.* **2012,** *41*, 3266-3277.

22. Wang, H.; Ma, H. *Chem. Commun.* **2013,** *49*, 8686-8688.

23. Yang, Y.; Wang, H.; Ma, H. *Inorg. Chem.* **2015,** *54*, 5839-5854.

24. Wang, H.; Yang, Y.; Ma, H. *Macromolecules* **2014,** *47*, 7750-7764.

25. Darensbourg, D. J.; Karroonnirun, O. *Inorg. Chem.* **2010,** *49*, 2360-2371.

26. Huang, M.; Pan, C.; Ma, H. *Dalton Trans.* **2015,** *44*, 12420-12431.

27. Li, C. Y.; Tsai, C. Y.; Lin, C. H.; Ko, B. T. *Dalton Trans.* **2011,** *40*, 1880-1887.

28. Sung, C. Y.; Li, C. Y.; Su, J. K.; Chen, T. Y.; Lin, C. H.; Ko, B. T. *Dalton Trans.* **2012,** *41*, 953-961.

29. Drouin, F.; Oguadinma, P. O.; Whitehorne, T. J.; Prud'homme, R. E.; Schaper, F. *Organometallics* **2010,** *29*, 2139-2147.

30. Whitehorne, T. J.; Vabre, B.; Schaper, F. *Dalton Trans.* **2014,** *43*, 6339-6352.

31. Wheaton, C. A.; Hayes, P. G. *Chem. Commun.* **2010,** *46*, 8404-8406.

32. Qian, X.; Dawe, L. N.; Kozak, C. M. *Dalton Trans.* **2011,** *40*, 933-943.

33. Eelman, M. D.; Blacquiere, J. M.; Moriarty, M. M.; Fogg, D. E. *Angew. Chem.* **2008,** *120*, 309-312.

34. Fulmer, G. R.; Miller, A. J.; Sherden, N. H.; Gottlieb, H. E.; Nudelman, A.; Stoltz, B. M.; Bercaw, J. E.; Goldberg, K. I. *Organometallics* **2010**, *29*, 2176-2179.

35. Herold, R.; Aggarwal, S.; Neff, V. *Can. J. Chem.* **1963**, *41*, 1368-1380.

Chapter 3 Ring-opening Polymerization of *rac*-Lactide Using Zinc Amino-bis(phenolate) Complexes

3.1 Introduction

Polylactide (PLA) is a promising sustainable polymer because of its biocompatibility, flexible waste management (e.g. recycling and composting)[1], and monomer renewability (e.g. corn and corn waste).[2] PLA has potential medical applications, such as sutures and prosthetics.[3, 4] At present, it is considered a potential alternative to traditional petrochemical-based polymers in packaging applications, especially food containers and wrapping.[5, 6]

Ring-opening polymerization (ROP) of lactide (LA) has been widely studied using different metal complexes.[7-16] Zinc complexes have attracted attention because they are cheap, abundant, nontoxic, colorless and can be monitored by NMR spectroscopy as they are diamagnetic.[10] A variety of zinc complexes bearing different ligand scaffolds such as β-diiminate (BDI),[17-28] tris(pyrazolyl)borate (TPB),[29] bis(pyrazolyl)amide (BPA),[30] phenolate,[31-49] N-heterocyclic carbenes,[50, 51] and recently phosphinimine ligands[52-55] have been investigated for ROP of lactide.

This chapter discusses ring-opening polymerization of *rac*-lactide using zinc amino-bis(phenolate) complexes **1a**, **1a·THF** and **2**. ROP of *rac*-lactide was studied in melt phase and in solution with and without the addition of benzyl alcohol (BnOH) or isopropyl alcohol (*i*-PrOH). The polymers obtained were characterized by NMR

spectroscopy, gel permeation chromatograpy (GPC), differential scanning calorimetry (DSC) and MALDI-TOF MS. Kinetic data were obtained by monitoring the polymerization reaction using ^{1}H NMR spectroscopy. Further studies of the mechanism were conducted by monitoring stoichiometric and low lactide concentration reactions of lactide, complex **1a·THF** and BnOH at various temperatures. Thermodynamic activation parameters were also obtained.

3.2 Results and Discussion

3.2.1 Ring-opening Polymerization of *rac*-Lactide Using Complex 1a

3.2.1.1 Kinetic Studies

Polymerization of *rac*-lactide was conducted using complex **1a** in toluene and CH_2Cl_2 but low activity was observed in both of these solvents at room temperature and at 80 °C in toluene (**Figure 3-1**). Good activity was, however, observed in neat lactide under melt conditions. Catalyst loadings of 1% and 0.5% gave nearly quantitative conversion of lactide after 100 minutes, but decreasing catalyst loading to 0.2% and 0.1% results in 65% and 17% conversion, respectively, after this time. (**Table 3-1**) A study of lactide conversion over time was conducted using 0.5% catalyst loading at 130 °C (**Table 3-2**). After 15 minutes, 92% lactide conversion was observed (entry 5). The melt phase polymerization shows an approximate first order dependence on the monomer concentration (**Figure 3-2**).

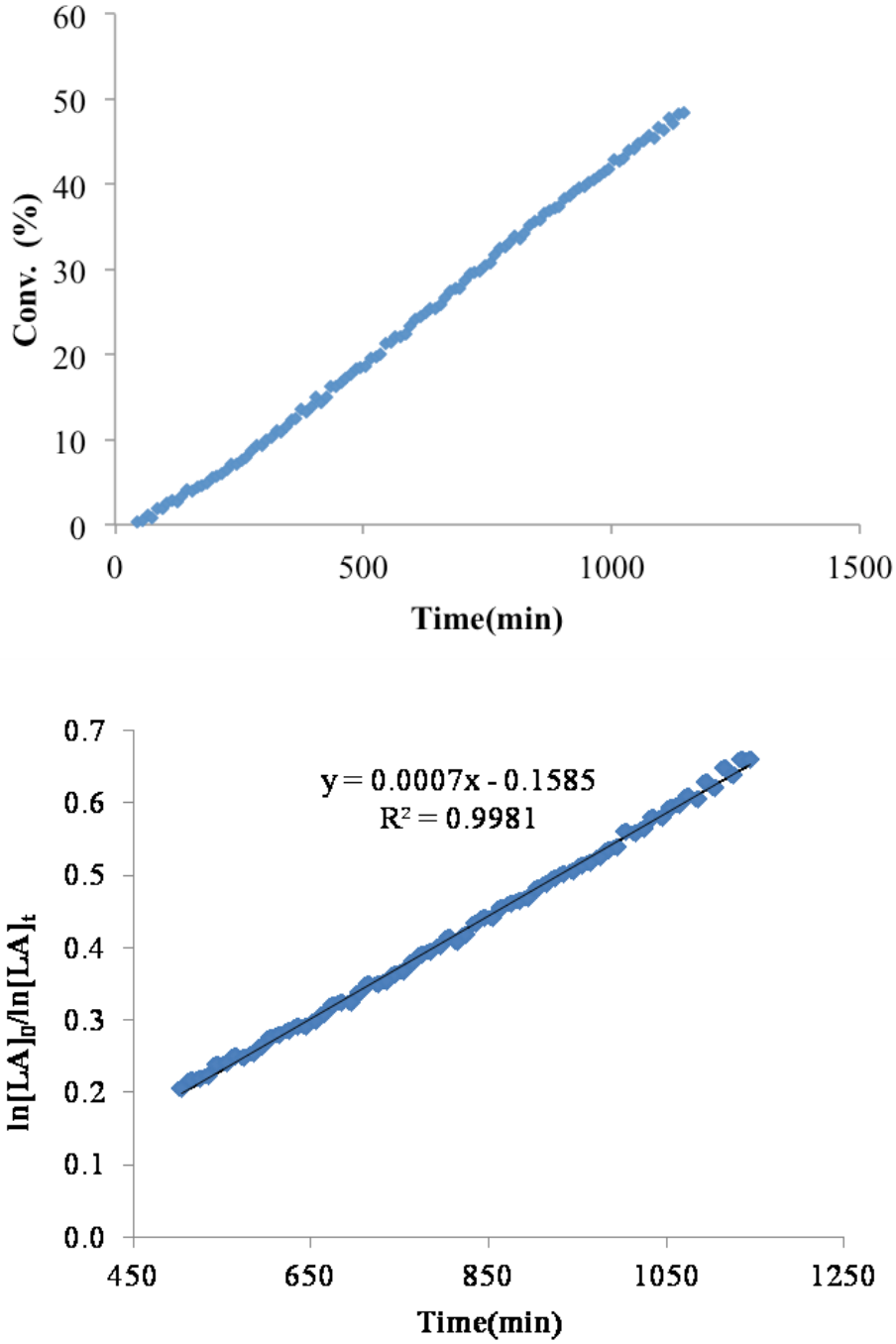

Figure 3-1 Plots of monomer conversion vs. time (top) and Plots of $\ln[LA]_0/[LA]_t$ vs. time excluding induction period (bottom) for ROP of *rac*-lactide catalyzed by complex **1a** ([LA]:[**1a**] = 100:1, [LA] = 0.11 M in toluene-d_8, 80 °C). The solid lines are the best linear fits.

Table 3-1 Melt phase ROP of *rac*-lactide using complex **1a**, 125 °C

Entry	[LA]:[1a]	t (min)	Conv (%)
1	100:1	100	98.4
2	200:1	100	97.6
3	500:1	100	64.7
4	1000:1	100	17.4

*Calculated via integration of the methine resonances of *rac*-lactide and polylactide.

Table 3-2 ROP of *rac*-LA using complex **1a** ([LA]:[**1a**] = 200:1, 130 °C).

Entry	t (min)	Conv (%)[a]	T_g (°C)	M_n (Theor)[b] (kg/mol)	M_n (GPC)[c] (kg/mol)	M_w/M_n
1	3	2.9	-	-	-	-
2	5	27.0	-	-	-	-
3	7	69.7	42.9	20.0	-	-
4	10	86.8	46.4	25.0	36.4	1.52
5	15	92.2	45.6	26.6	37.3	1.40
6	20	94.4	44.2	27.2	27.6	1.17
7	30	97.3	47.5	28.0	28.6	1.24
8	40	97.4	-	28.1	26.1	1.29
9	60	96.3	-	-	-	-
10	80	96.6	-	-	-	-

[a] Calculated via integration of the methine resonances of *rac*-LA and PLA. [b] M_n (cal.) = $[LA]_0/[\mathbf{1a}]_0 \times$ conv. × M (LA). [c] Determined by gel permeantion chromatography (GPC) in THF using dn/dc = 0.046 mL g^{-1}.

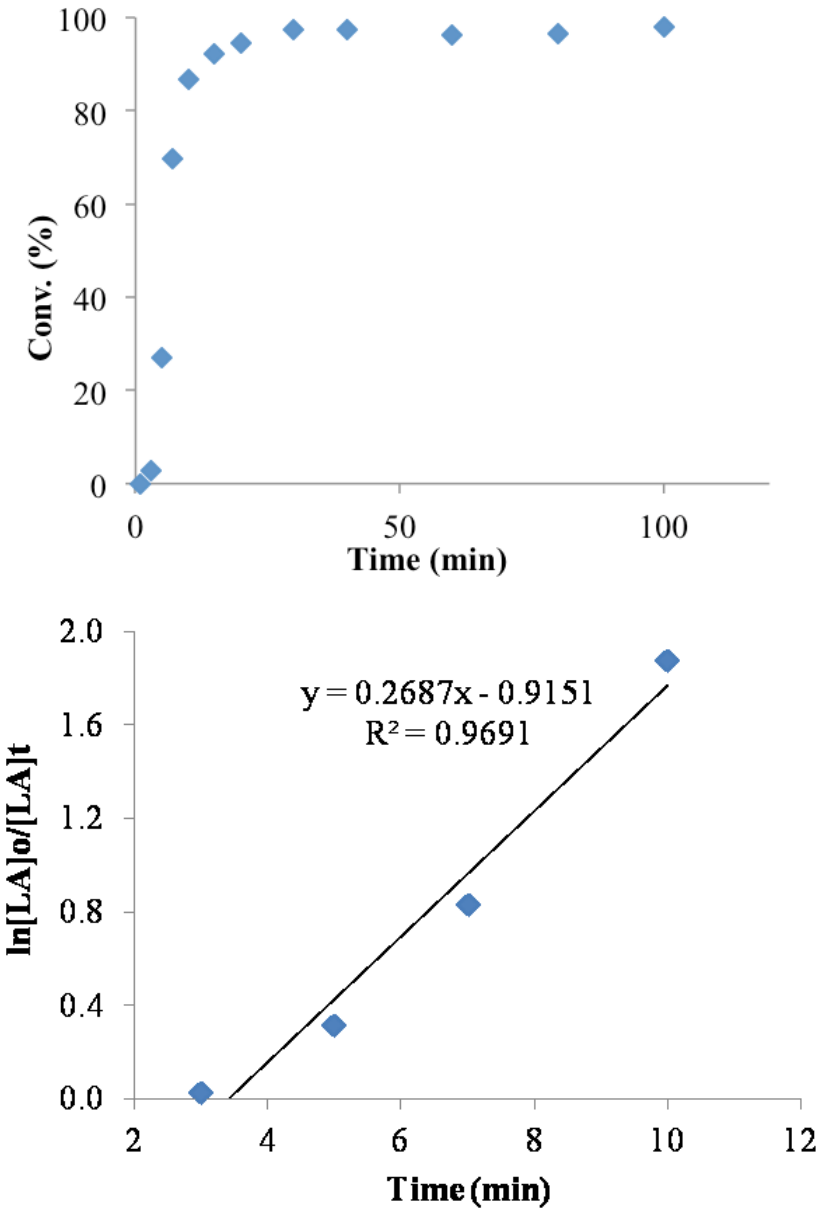

Figure 3-2 Plots of monomer conversion vs. time (top) and Plots of $\ln[LA]_0/[LA]_t$ vs. time (bottom) for melt phase ROP of *rac*-lactide catalyzed by complex **1a** ([LA]:[**1a**] = 200:1, 130 °C).

3.2.1.2 Study of the Polymers

The conversion of monomer to polymer was obtained by NMR analysis of the crude product. The crude products were then purified by dissolving in $CHCl_3$ and precipitating out with cold methanol. Upon removing the methanol, colorless polymer was obtained and its molecular weights, dispersity, end group characterization and glass transition temperatures were measured.

3.2.1.2.1 NMR Spectroscopy

A typical ^1H NMR spectrum of the melt polymerization product is shown in **Figure 3-3**. The quartet at δ 5.12 corresponds to the methine proton of unreacted LA; and the multiplet at δ 5.17 corresponds to the methine protons of PLA. Conversion of monomer to polymer was obtained based on the methine regions, given by a ratio of the integration of PLA to the sum of the integrations of LA and PLA, i.e. $I_{PLA}/(I_{PLA}+I_{LA})$.

Typical ^1H NMR spectra and peak assignments of polymerization products conducted in toluene at room temperature in the presence and absence of BnOH after quenching with methanol are shown in **Figure 3-4**. The OMe peak is also present in polymers initiated in the presence of BnOH, which possibly because of the opening of cyclic oligomers on quenching, or because of remaining MeOH solvent in the polymer.

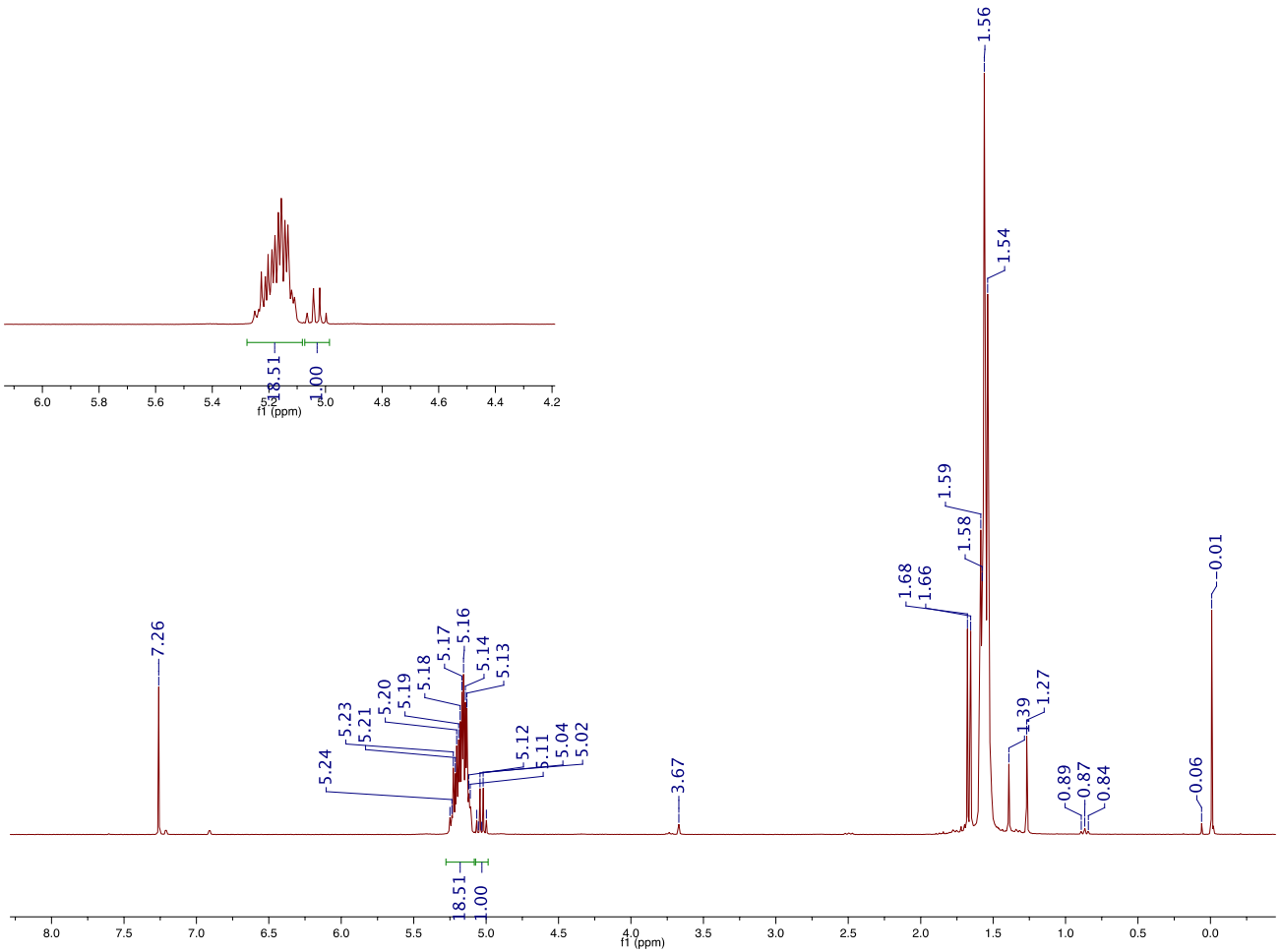

Figure 3-3 ^{1}H NMR spectrum of product mixture, [LA]:[complex **1a**] = 200:1, 130 °C, 15 min, measured in $CDCl_3$

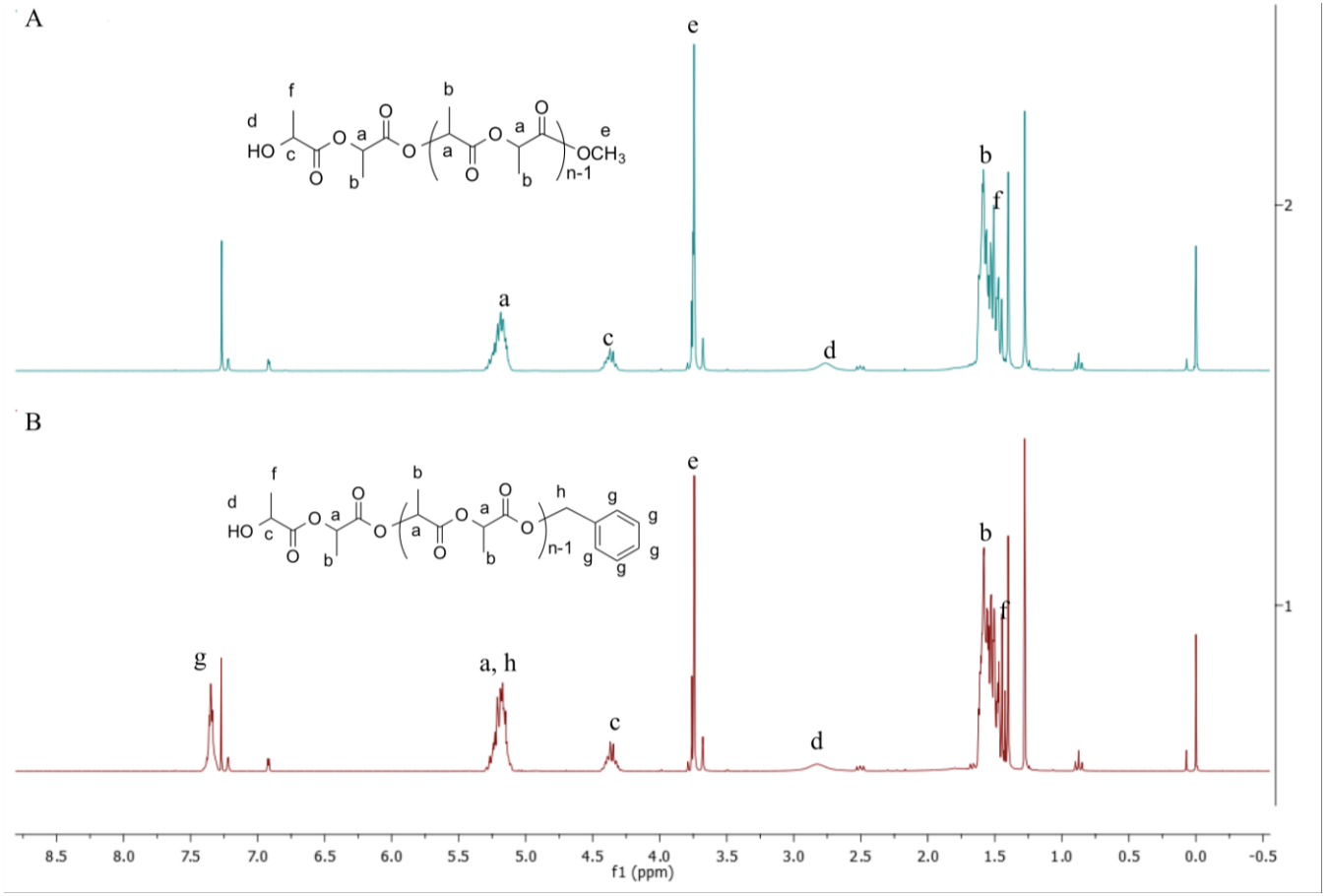

Figure 3-4 ^{1}H NMR spectra of polymerization products conducted in toluene at room temperature after quenching by methanol. Polymerization conditions: A: [LA]:[complex **1a**] = 100:1; B: [LA]:[complex **1a**]:[BnOH] = 100:1:1.

3.2.1.2.2 Gel Permeation Chromatography

The polymers were characterized by gel permeation chromatography (GPC) to determine the molecular weight (M_n) and molecular weight distribution (Đ). The molecular weights of the polymers are in good agreement with the expected values and the molecular weight distributions (M_w/M_n) range from 1.17 to 1.52 (**Table 3-2**). The active catalyst may result from reaction of the zinc alkyl complex with impurities in the lactide, e.g. lactic acid.[56] The polymer obtained during shorter reaction times (entries 4 and 5) show slightly higher than expected molecular weights, but for reactions allowed to run longer the M_n values are as expected. The higher M_n values and slightly broader dispersities may be a result of a slow initiation rate versus propagating rate.[57]

It is possible that the decomposition of complex **1a** at high temperatures (near 130 °C) generates the active species for lactide polymerization, therefore, the stability of the compound at these temperatures was evaluated by heating a solution of **1a** in toluene-d_8 to 150 °C for 10 min in a microwave reactor. The ^{1}H NMR spectrum of this solution was identical before and after heating and showed no evidence of compound decomposition.

3.2.1.2.3 MALDI-TOF MS

MALDI-TOF MS provides valuable information for the study of the repeating units and the end groups of polymers.[58, 59] Polymer obtained using the conditions of entry 7 in **Table 3-2** was analyzed using 2,5-dihydroxybenzoic acid (DHBA) as matrix. MALDI-TOF mass spectrometry of the polymers showed series of peaks with repeating units of *m/z* 72, corresponding to a half of lactide: –(C=O)CH(CH_3)O- unit, which is consistent with transesterification.[42] There are two dominant series of peaks corresponding to *cyclo*-

$(C_3H_4O_2)_n \cdot Na^+$ (A) and *cyclo*-$(C_3H_4O_2)_n \cdot K^+$ (B) (**Figure 3-5**). The absence of a co-initiator and the slow polymerization rate allows for backbiting to occur.[42] Following purification of the polymer by precipitation from methanol, one more series of peaks is observed in the mass spectrum corresponding to polymers with OCH_3 end groups arising from the methanol, $H[(C=O)CH(CH_3)O]_nOCH_3Na^+$ (C) (**Figure 3-6**). The mass spectra using reflectron mode (**Figure 3-7**, **Figure 3-8**) give better resolution than linear mode. However, the reflectron mode spectrum of purified polymer (**Figure 3-8**) shows the appearance of some unknown species spaced by *m/z* 72, which might come from methanolysis of the polymers during purification.[18]

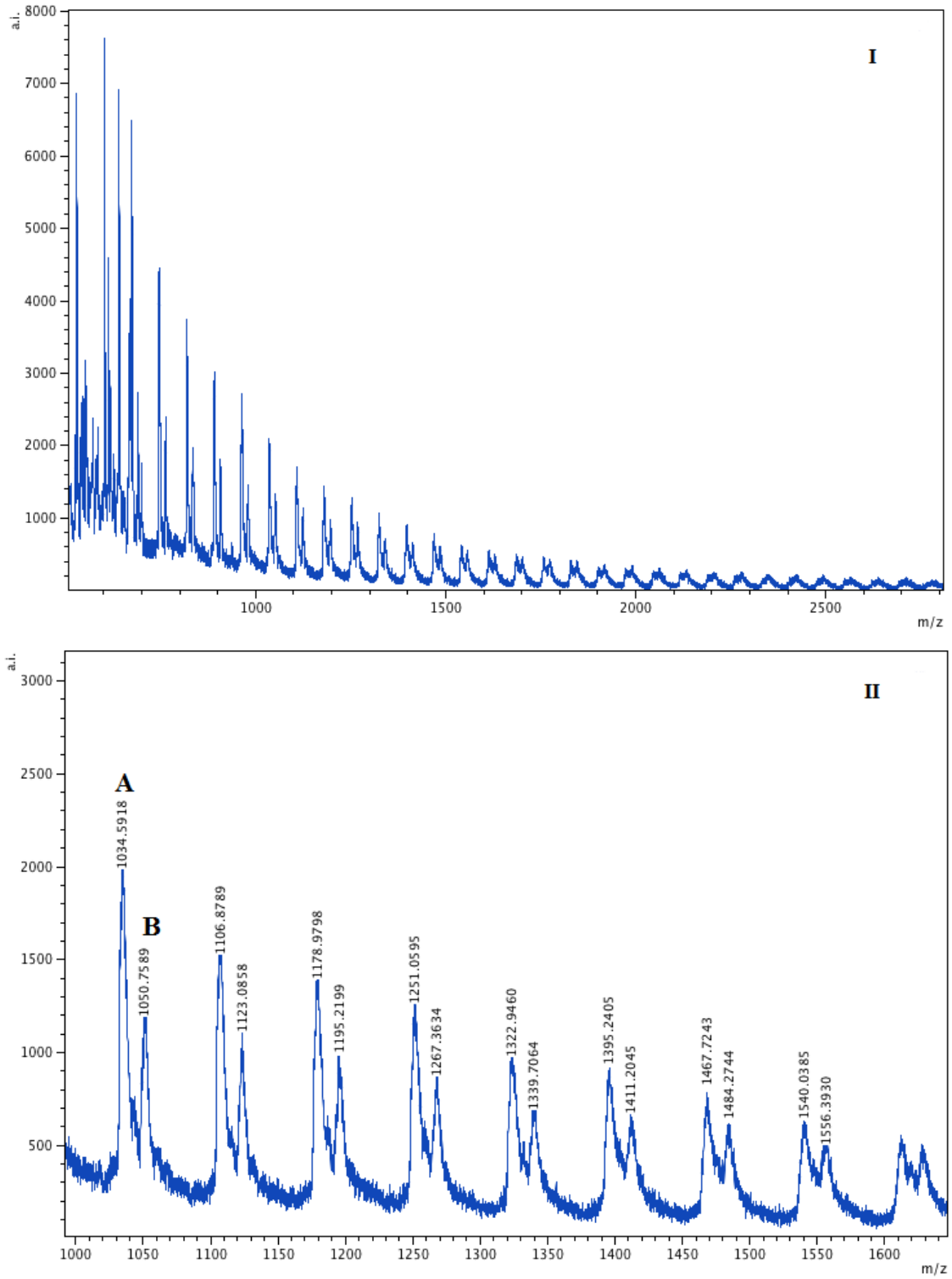

Figure 3-5 MALDI-TOF mass spectra (linear mode) of crude product obtained under the condition of entry 7, **Table 3-2** (**I**: full spectrum; **II**: expanded spectrum).

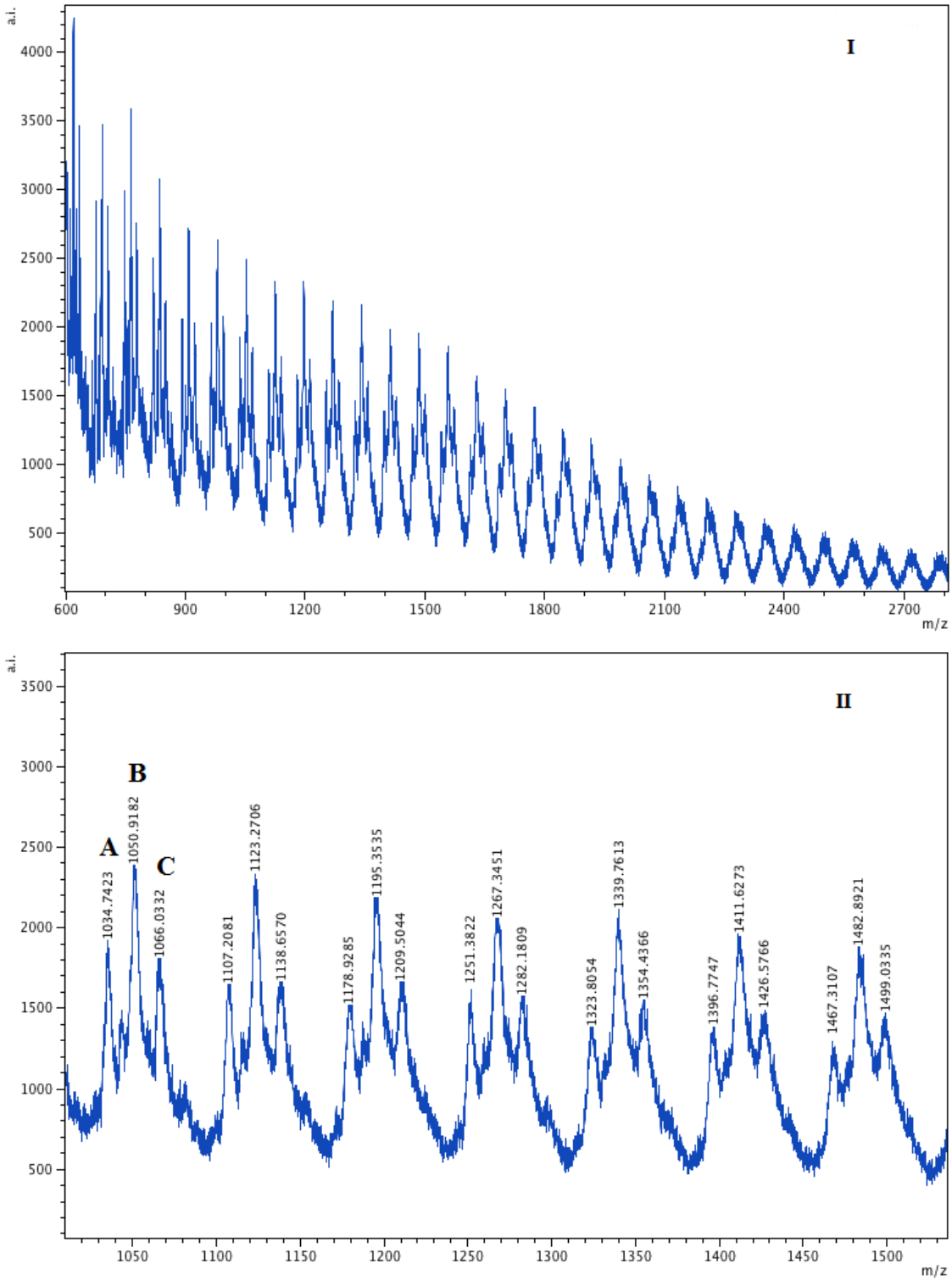

Figure 3-6 MALDI-TOF mass spectra (linear mode) of purified polymer obtained under the condition of entry 7, **Table 3-2** (**I**: full spectrum; **II**: expanded spectrum).

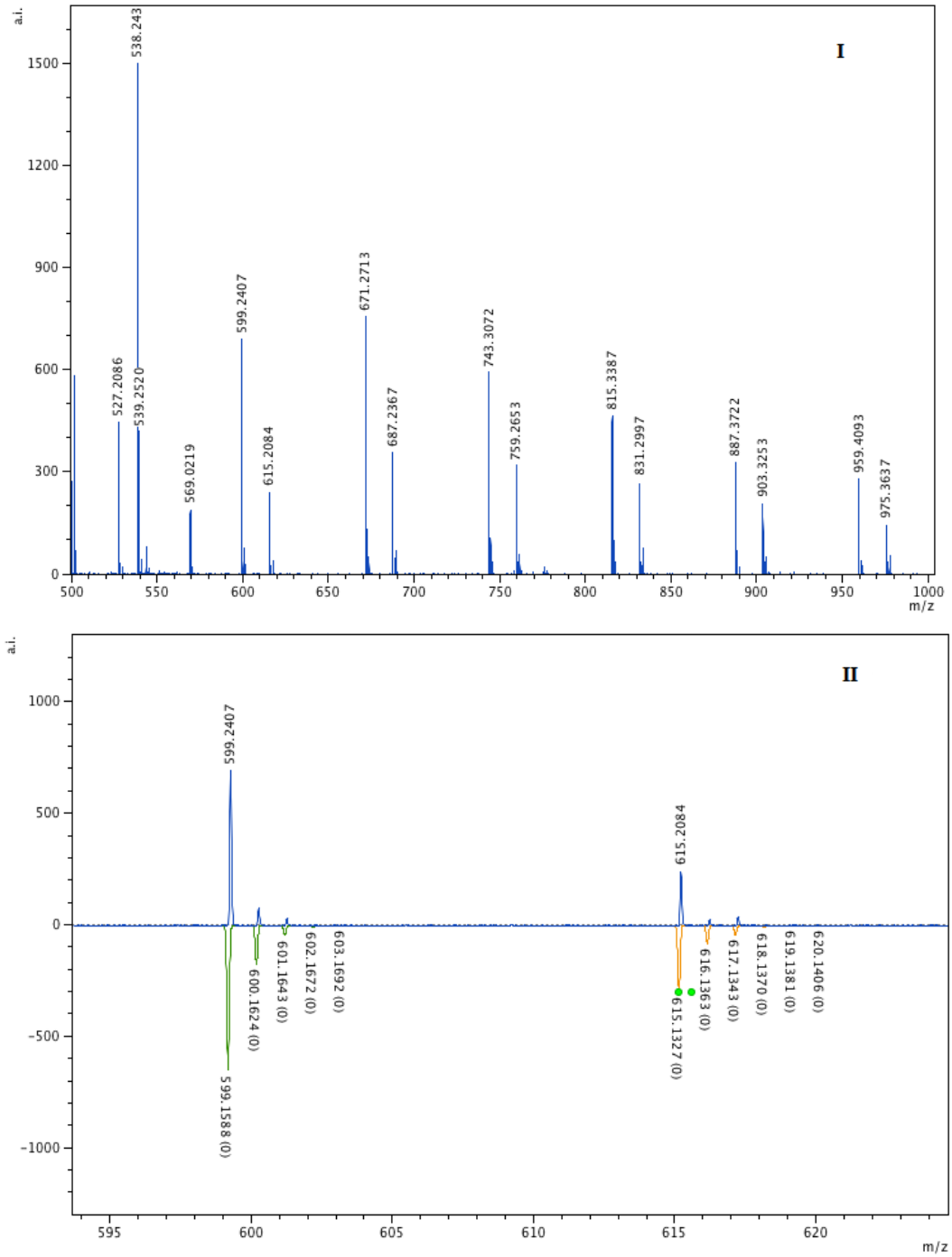

Figure 3-7 MALDI-TOF mass spectra (reflectron mode) of crude product obtained under the condition of entry 7, **Table 3-2** (**I**: full spectrum; **II**: expanded spectrum with experimental andcalculated peaks).

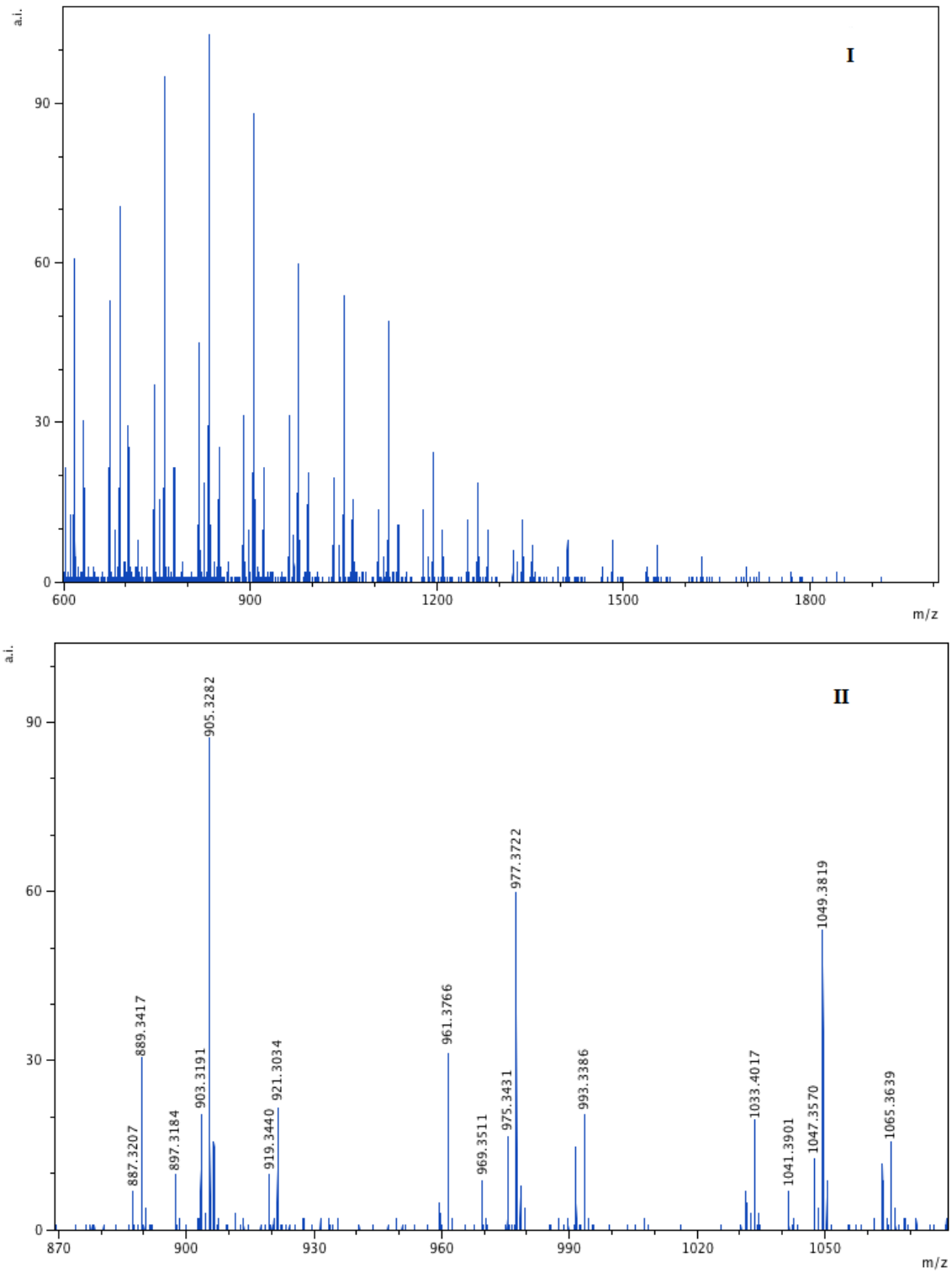

Figure 3-8 MALDI-TOF mass spectra (reflectron mode) of purified polymer obtained under the condition of entry 7, **Table 3-2** (**I**: full spectrum; **II**: expanded spectrum).

3.2.1.2.4 Differential Scanning Calorimetry

Glass transition temperatures (T_g) were measured using Differential Scanning Calorimetry (DSC) for the purified polymers obtained under conditions described in **Table 3-2**, entries 4-8. The obtained T_g values of 43 – 48 °C for the PLA agree with that reported in the literature.[12] A representative DSC trace of PLA obtained by complex **1a** is shown in **Figure 3-9**.

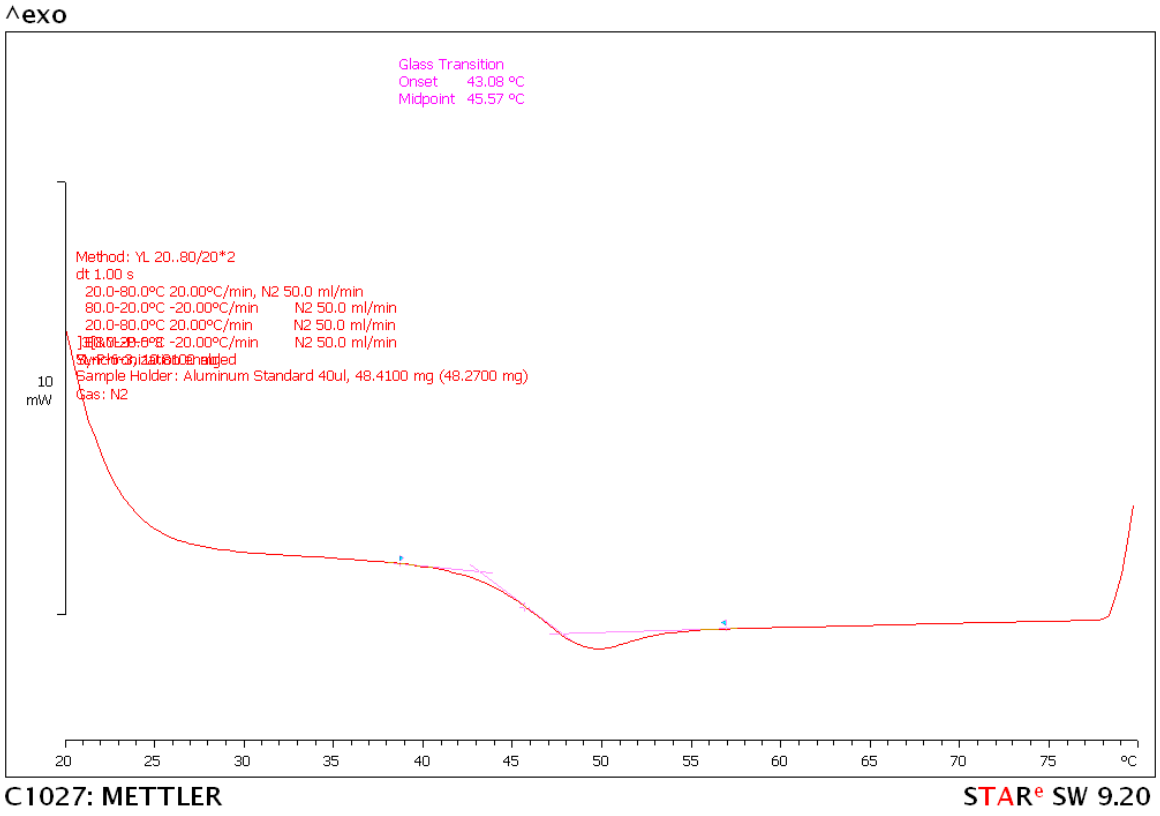

Figure 3-9 Measurement of glass transition temperature of purified polymer, entry 6 of **Table 3-2**.

3.2.2 Ring-opening Polymerization of *rac*-Lactide Using Complex 1a·THF

3.2.2.1 Kinetic Study

Polymerization of *rac*-lactide in solution with addition of benzyl alcohol (BnOH) was further studied using complex **1a·THF** since it is better characterized than complex **1a**. Better activity and controllability were obtained for **1a·THF** than using complex **1a**, either with or without addition of BnOH to both complexes (**Figure 3-10**). Kinetic data were obtained by monitoring the reaction via ^{1}H NMR. The plots of $\ln[LA]_0/[LA]_t$ vs. time shows first order dependence on monomer concentration (**Figure 3-11**). The reaction rate can be expressed as $-d[LA]/d[t] = k_{obs}[LA] = k[\mathbf{1a{\cdot}THF}]^x[LA]^1$. If the reaction has a first order dependence on catalyst concentration, both the plot of $\ln k_{obs}$ vs. ln[**1a**·THF] and the plot of k_{obs} vs. [**1a·THF**] should have linear fits. The dependence on catalyst concentration, however, is complicated. The plot of $\ln k_{obs}$ vs. ln[**1a·THF**] (**Figure 3-12**) deviates from an ideal first order dependence, possibly from the bimetallic nature of the zinc complex, or from incomplete formation of an active species through reaction with BnOH. A direct plot of k_{obs} vs. [**1a·THF**] also indicates deviation from an ideal first order dependence having an equation of $y = 0.278x + 6.9966 \times 10^{-5}$.

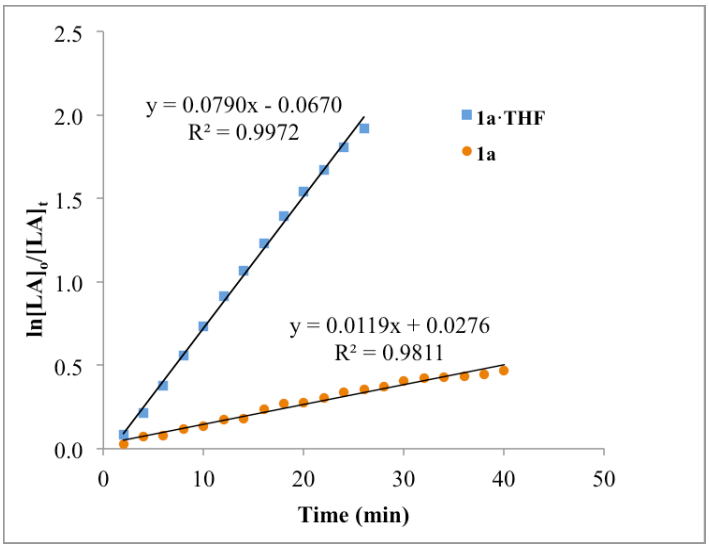

Figure 3-10 Plots of $\ln[LA]_0/[LA]_t$ vs. time for ROP of *rac*-LA catalyzed by complex **1a·THF**/BnOH and **1a** /BnOH ([LA]:[complex]:[BnOH] = 200:1:1, [LA] = 0.66 M in toluene-d_8, 80 °C).

The ROP of *rac*-LA initiated by **1a·THF** was investigated under immortal conditions using benzyl alcohol or isopropyl alcohol as chain-transfer agents. The polymerization rate increased with increasing BnOH concentration (**Figure 3-13**) and a linear dependence of the reaction rate on [Polymer chain]:[**1a·THF**] (i.e. [BnOH]:[**1a·THF**]) is observed, which indicates an activated monomer mechanism.

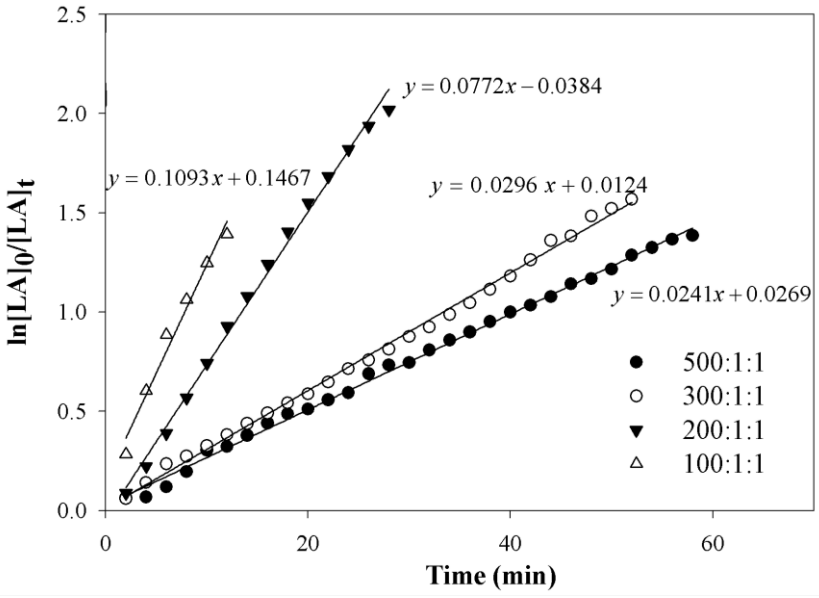

Figure 3-11 Plots of $\ln[LA]_0/[LA]_t$ vs. time for ROP of *rac*-LA catalyzed by complex **1a·THF**/BnOH ([LA]:[**1a·THF**]:[BnOH] = 100:1:1, 200:1:1 , 300:1:1 or 500:1:1; [LA] = 0.66 M in toluene-d_8, 80 °C).

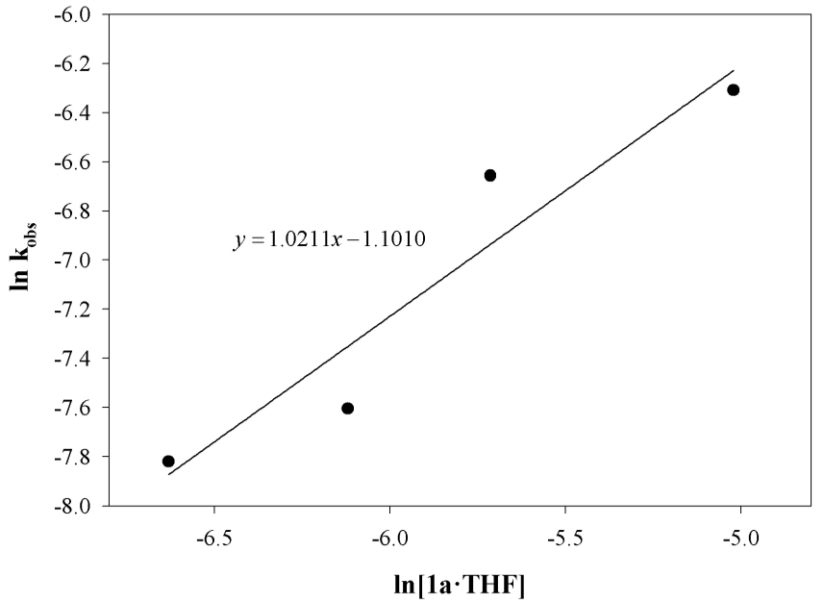

Figure 3-12 Plots of ln k_{obs} vs. ln[**1a·THF**]. Polymerization conditions: [LA]:[**1a·THF**]:[BnOH] = 100:1:1, 200:1:1, 300:1:1 or 500:1:1; [LA] = 0.66 M in toluene-d_8, 80 ºC).

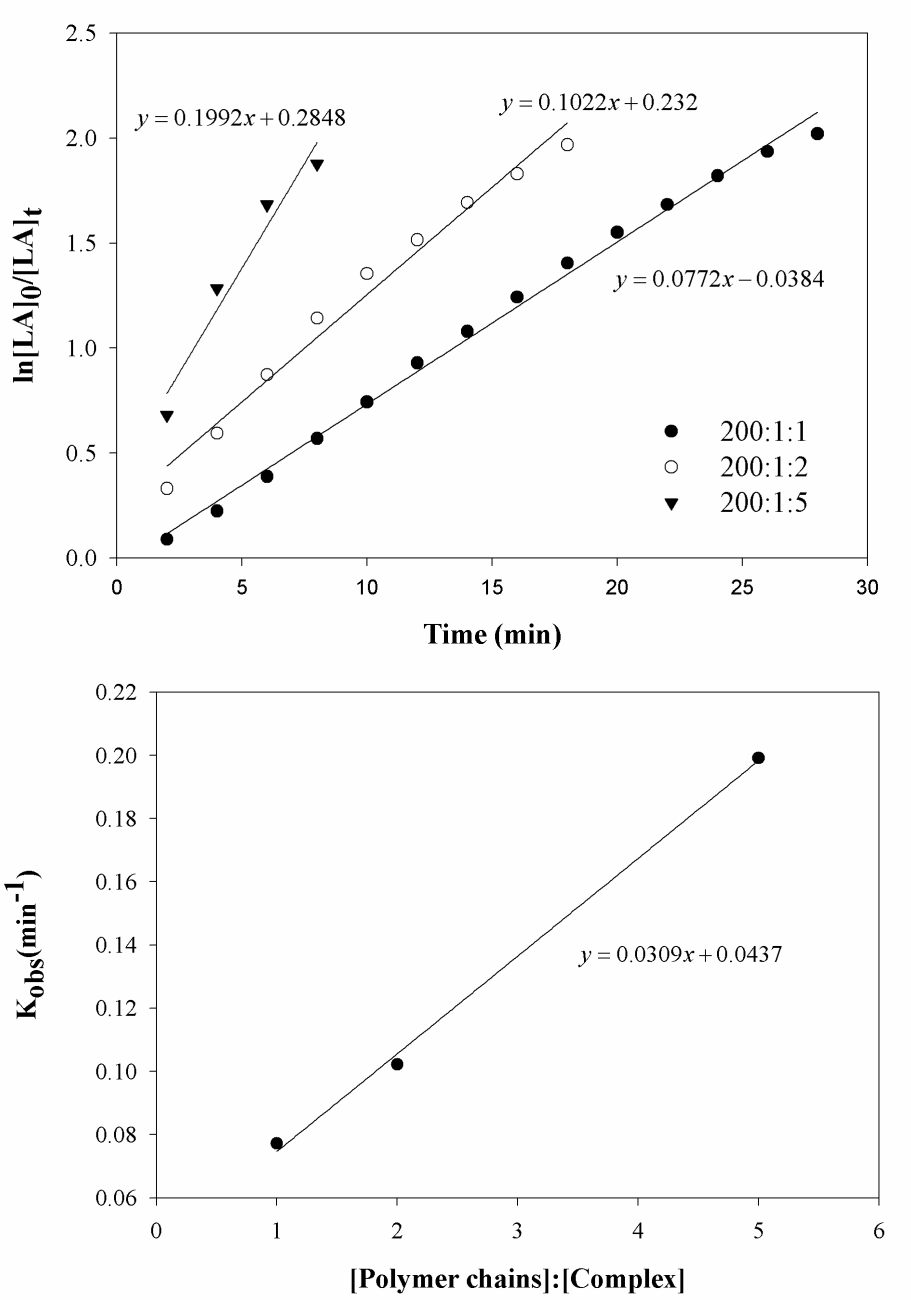

Figure 3-13 Plots of $\ln[LA]_0/[LA]_t$ vs. time (top) and corresponding observed rate constant k_{obs} vs. [Polymer chains]:[Complex] plots (bottom) for the ROP of *rac*-LA catalyzed by complex **1a·THF**/BnOH ([LA]:[**1a·THF**]:[BnOH] = 200:1:1, 200:1:2 or 200:1:5; [LA] = 0.66 M in toluene-d_8, 80 °C). The solid lines are the best linear fits.

3.2.2.2 Study of the Polymers

3.2.2.2.1 Gel Permeation Chromatography

Polymer molecular weight determination by gel permeation chromatography (GPC) showed a proportional increase in molecular weight with increasing lactide-to-catalyst ratio (100:1, 200:1 and 500:1) and equimolar ratios of **1a·THF** and alcohol (**Figure 3-14**). Similarly, polymer molecular weight decreased with increasing BnOH to lactide ratio (**Figure 3-15**). The molecular weight distributions of the polymers are narrow, Đ = 1.04 – 1.16, except polymers obtained using a lactide to complex ratio of 500:1, which showed only slightly broader molecular weight distributions (Đ = 1.25), likely due to transesterification by impurities in the *rac*-LA or adventitious water and the longer reaction time required (**Table 3-3**). A representative polymerization where [LA]:[**1a·THF**]:[BnOH] = 200:1:1 in toluene at 80 °C shows good control with polymer molecular weights increasing linearly with conversion and narrow dispersities ranging from 1.03 to 1.10 indicating living polymerization (**Figure 3-16**).

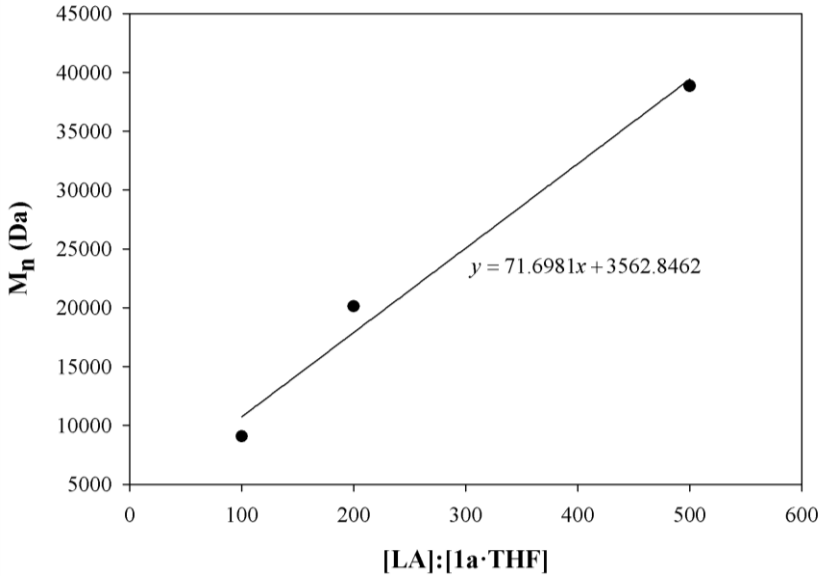

Figure 3-14 Plot of $M_{n(GPC)}$ vs. [LA]:[**1a·THF**] for ROP of *rac*-LA catalyzed by complex **1a·THF**/BnOH ([LA]:[**1a·THF**]:[BnOH] = 100:1:1, 200:1:1 or 500:1:1; [LA] = 0.66 M in toluene-d_8, 80 °C).

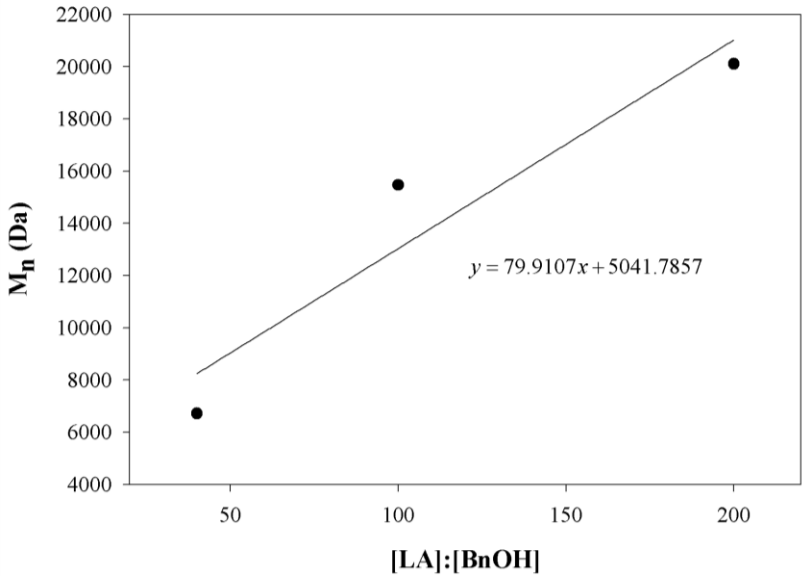

Figure 3-15 Plot of $M_{n(GPC)}$ vs. [LA]:[BnOH] for ROP of *rac*-LA catalyzed by complex **1a·THF**/BnOH ([LA]:[**1a·THF**]:[BnOH] = 200:1:1, 200:1:2 or 200:1:5; [LA] = 0.66 M in toluene-d_8, 80 °C).

Table 3-3 ROP of *rac*-LA using complex **1a·THF** ([LA] = 0.66 M in toluene, 80 °C).

Entry	[LA]:[1a·THF]:[BnOH]	t (min)	Conv (%)[a]	M_n (Theor)[b] (kg/mol)	M_n (GPC)[c] (kg/mol)	M_w/M_n	P_r[d]
1	100:1:1	40	99.1	14.3	9.1	1.16	0.53
2	200:1:1	60	97.8	28.2	20.1	1.11	0.53
3	200:1:2	40	99.5	14.3	15.5	1.16	-
4	200:1:5	40	99.5	5.73	6.72	1.04	-
5	500:1:1	140	83.1	59.8	38.9	1.25	-

[a] Calculated via integration of the methine resonances of *rac*-LA and PLA. [b] M_n (cal.) = $[LA]_0/[\mathbf{1a{\cdot}THF}]_0 \times$ conv. × M (LA). [c] Determined by gel permeation chromatography (GPC) in THF by triple detection using dn/dc = 0.049 mL g^{-1}. [d] Determined from homonuclear decoupled ^{1}H NMR by $P_r = 2I_1/(I_1 + I_2)$, with I_1 = δ 5.19-5.24 (*rmr, mmr/rmm*), I_2 = δ 5.13-5.19 (*mmr/rmm, mmm, mrm*).

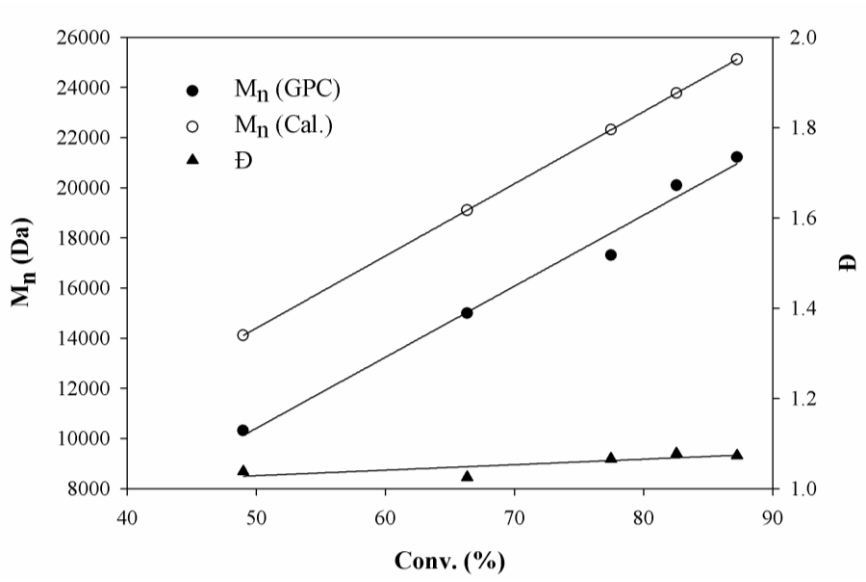

Figure 3-16 Plots of molecular weight and molecular weight distribution vs. lactide conversion for the ROP of *rac*-LA catalyzed by complex **1a·THF**/BnOH ([LA]:[**1a·THF**]:[BnOH] = 200:1:1, [LA] = 0.66 M in toluene, 80 °C).

3.2.2.2.2 MALDI-TOF MS

The MALDI-TOF mass spectra of the polymers produced using complex **1a·THF** in the presence of BnOH were obtained. Polymers obtained using ratios of [LA]:[**1a·THF**]:[BnOH] = 100:1:1, 200:1:1, 200:1:2 or 200:1:5 have repeating units of *m/z* 72, indicating the occurrence of transesterification during the polymerization. The linear mode spectra show three dominant series of peaks corresponding to *cyclo*-$(C_3H_4O_2)_n \cdot Na^+$ (A) and *cyclo*-$(C_3H_4O_2)_n \cdot K^+$ (B) and $BnO(C_3H_4O_2)_nH \cdot Na^+$ (C) (**Figure 3-17**). The reflectron mode spectra gave better resolution in the lower mass range and show additional peaks corresponding to $HO(C_3H_4O_2)_nH \cdot Na^+$ (**Figure 3-18**). The mass spectrum of polymer obtained using a lower catalyst loading of 500:1:1 [LA]:[**1a·THF**]:[BnOH] shows two dominant series of peaks corresponding to *cyclo*-$(C_3H_4O_2)_n \cdot Na^+$ (A) and *cyclo*-$(C_3H_4O_2)_n \cdot K^+$ (B) (**Figure 3-19** and **Figure 3-20**).

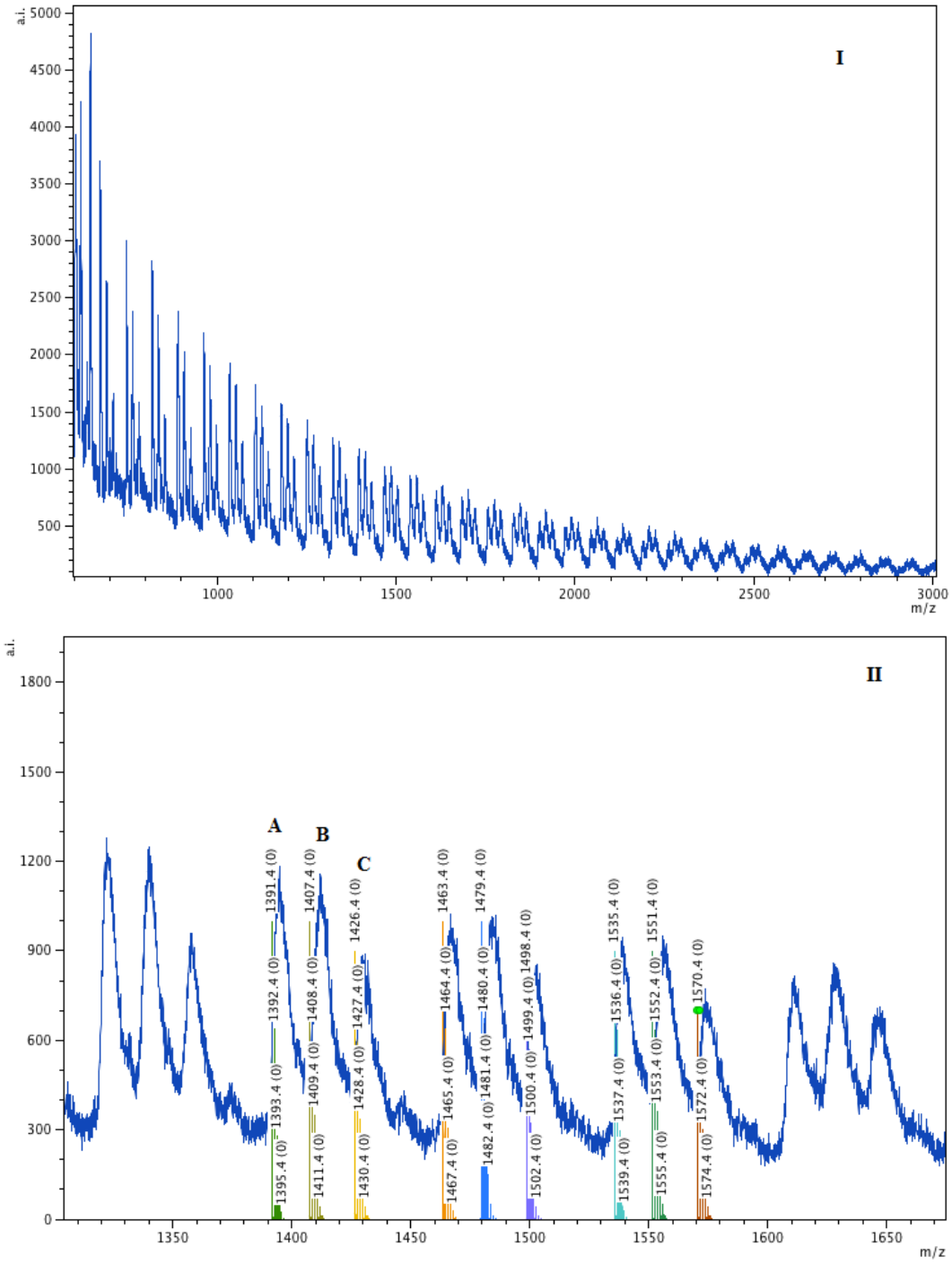

Figure 3-17 MALDI-TOF mass spectra (linear mode) of PLA obtained using complex **1a·THF** ([LA]:[**1a·THF**]:[BnOH] = 100:1:1, 80 °C in toluene), (**I**: full spectrum; **II**: expanded spectrum with experimental calculated peaks).

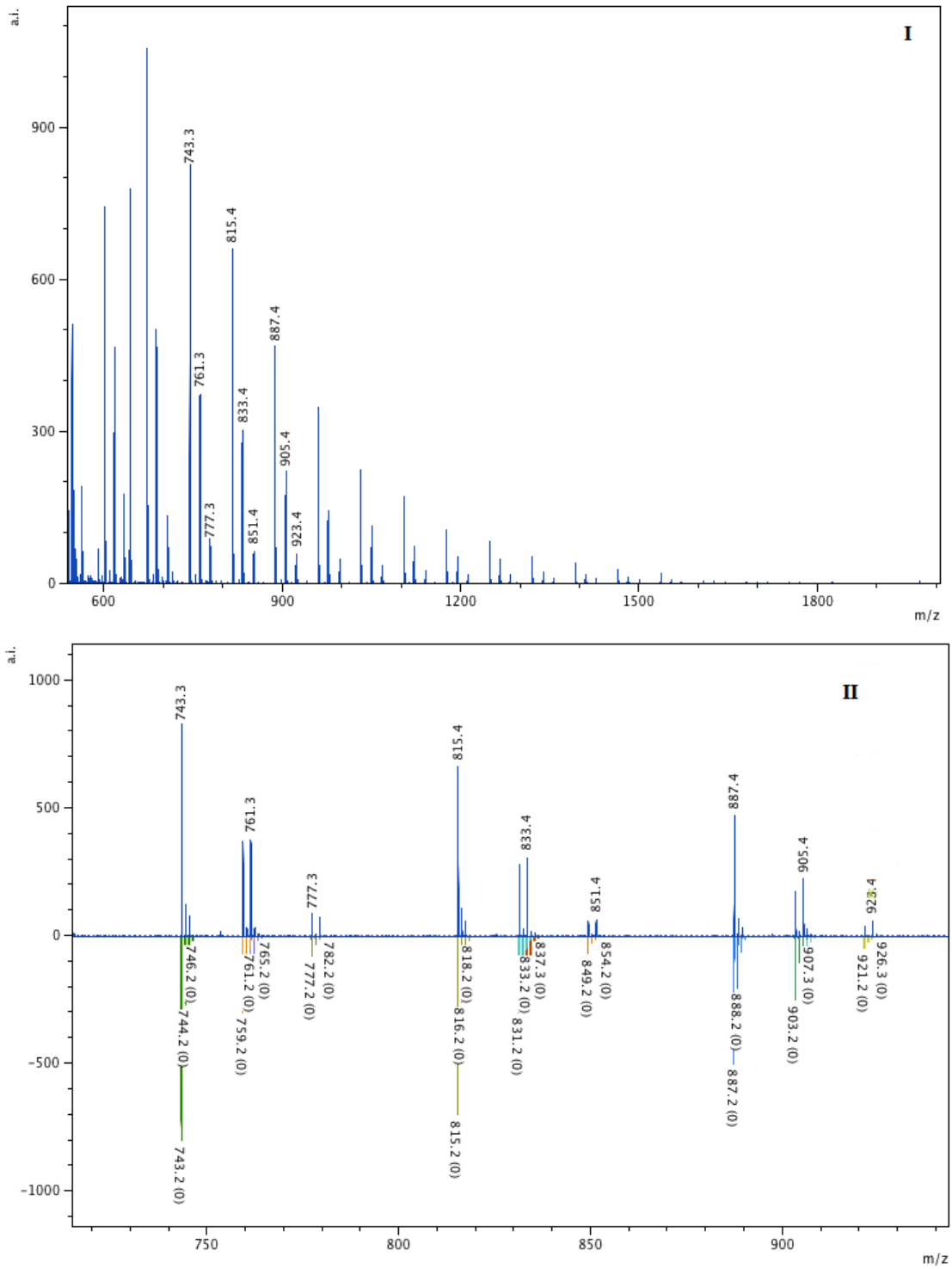

Figure 3-18 MALDI MALDI-TOF mass spectra (reflectron mode) of PLA obtained using complex **1a·THF** ([LA]:[**1a·THF**] :[BnOH] = 100:1:1, 80 °C in toluene), (**I**: full spectrum; **II**: expanded spectrum with experimental and calculated peaks).

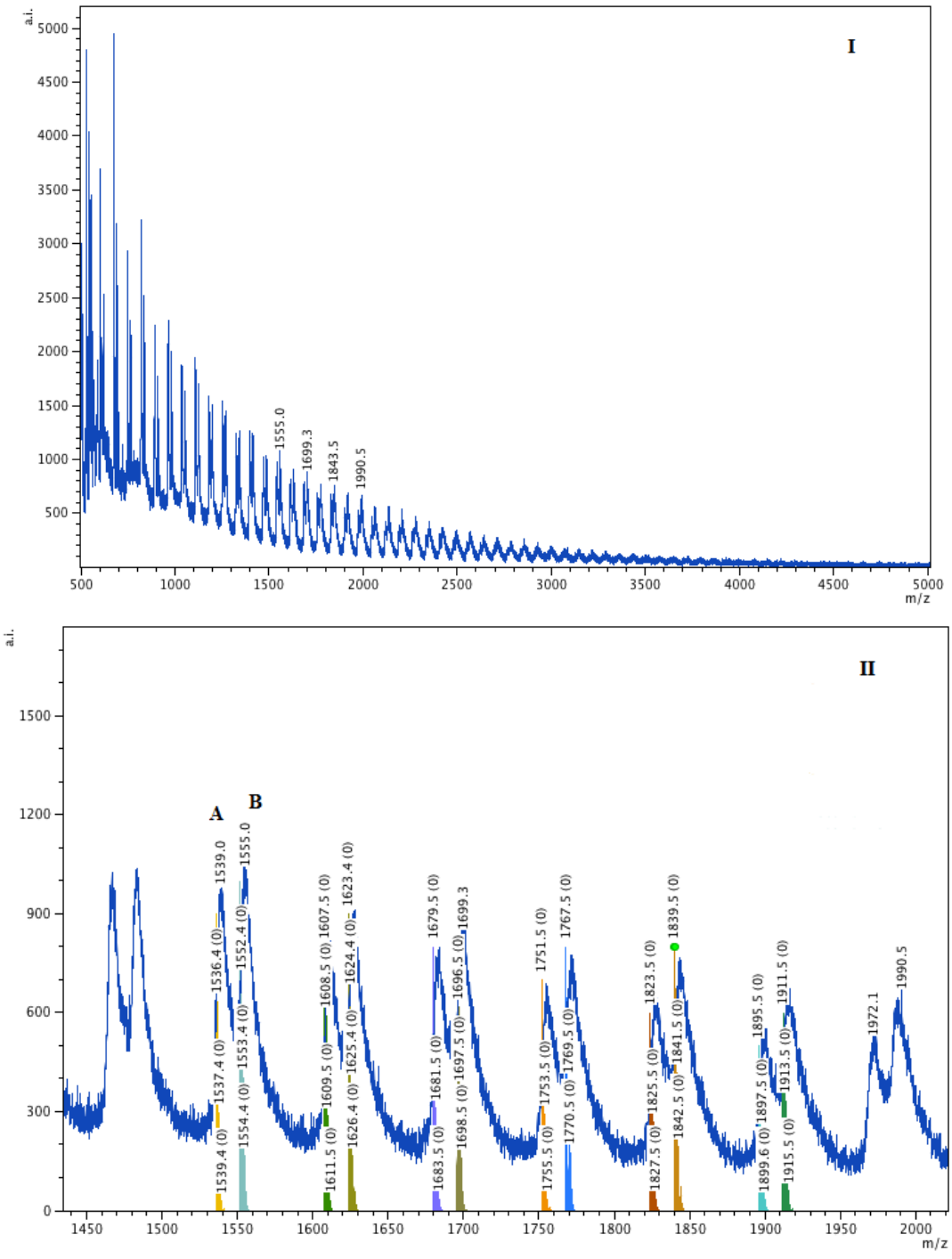

Figure 3-19 MALDI- MALDI-TOF mass spectra (linear mode) of PLA obtained using complex **1a·THF** ([LA]:[**1a·THF**] :[BnOH] = 500:1:1, 80 °C in toluene), (**I**: full spectrum; **II**: expanded spectrum with experimental and calculated peaks).

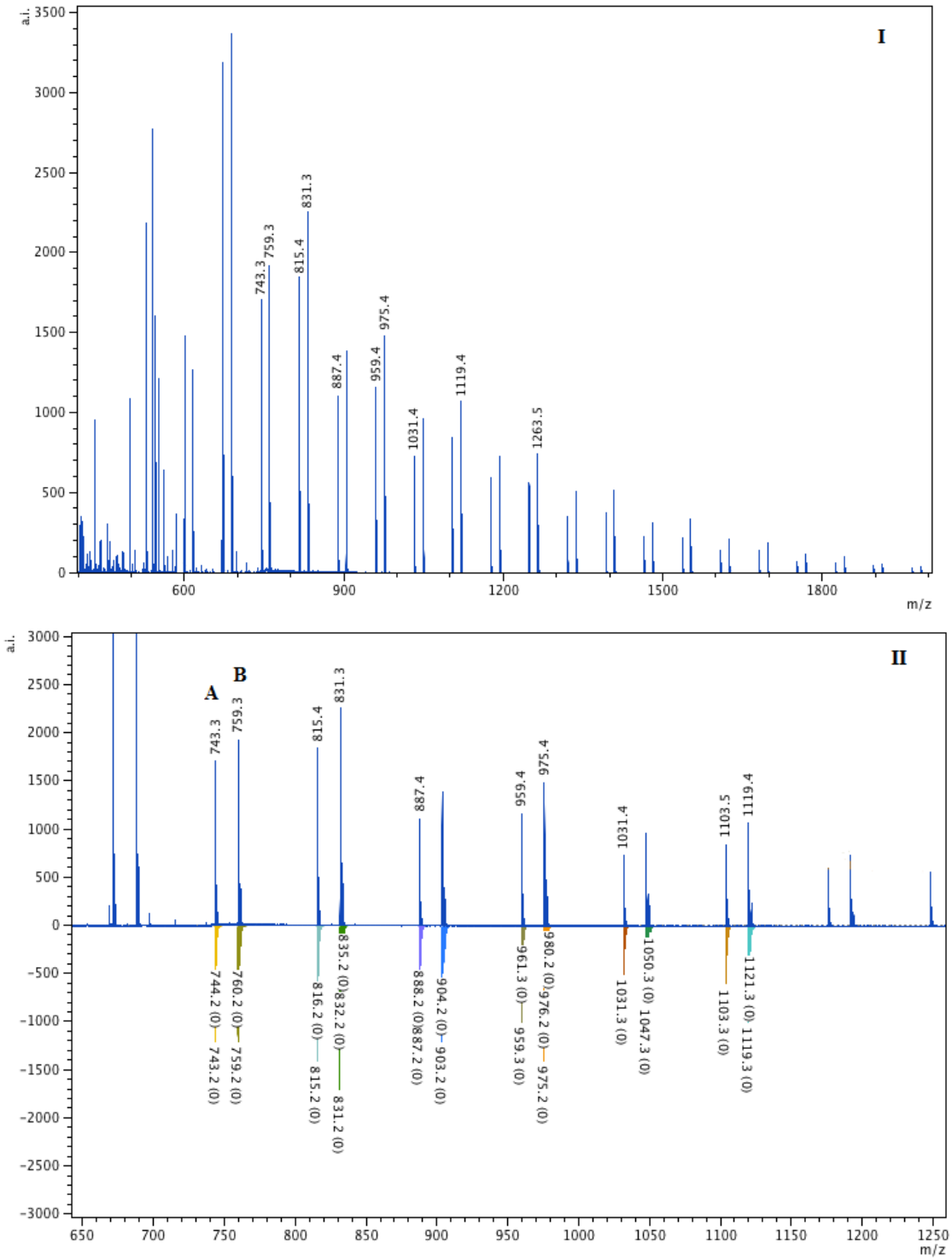

Figure 3-20 MALDI MALDI-TOF mass spectra (reflectron mode) of PLA obtained using complex **1a·THF** ([LA]:[**1a·THF**] :[BnOH] = 500:1:1, 80 °C in toluene), (**I**: full spectrum; **II**: expanded spectrum with experimental and calculated peaks).

3.2.2.2.3 Homonuclear Decoupled ^{1}H NMR

The stereochemistry of the obtained polymers (**Table 3-3**, entries 1 and 2) was studied using homonuclear decoupled ^{1}H NMR. The probabilities of racemic enchainment of monomer units (P_r) of the PLA were found to be 0.53, which indicates the polymers are atactic. P_r values are calculated by $P_r = 2I_1/(I_1 + I_2)$, with I_1 = δ 5.19-5.24 (*rmr, mmr/rmm*), I_2 = δ 5.13-5.19 (*mmr/rmm, mmm, mrm*) (**Figure 3-21**).[25]

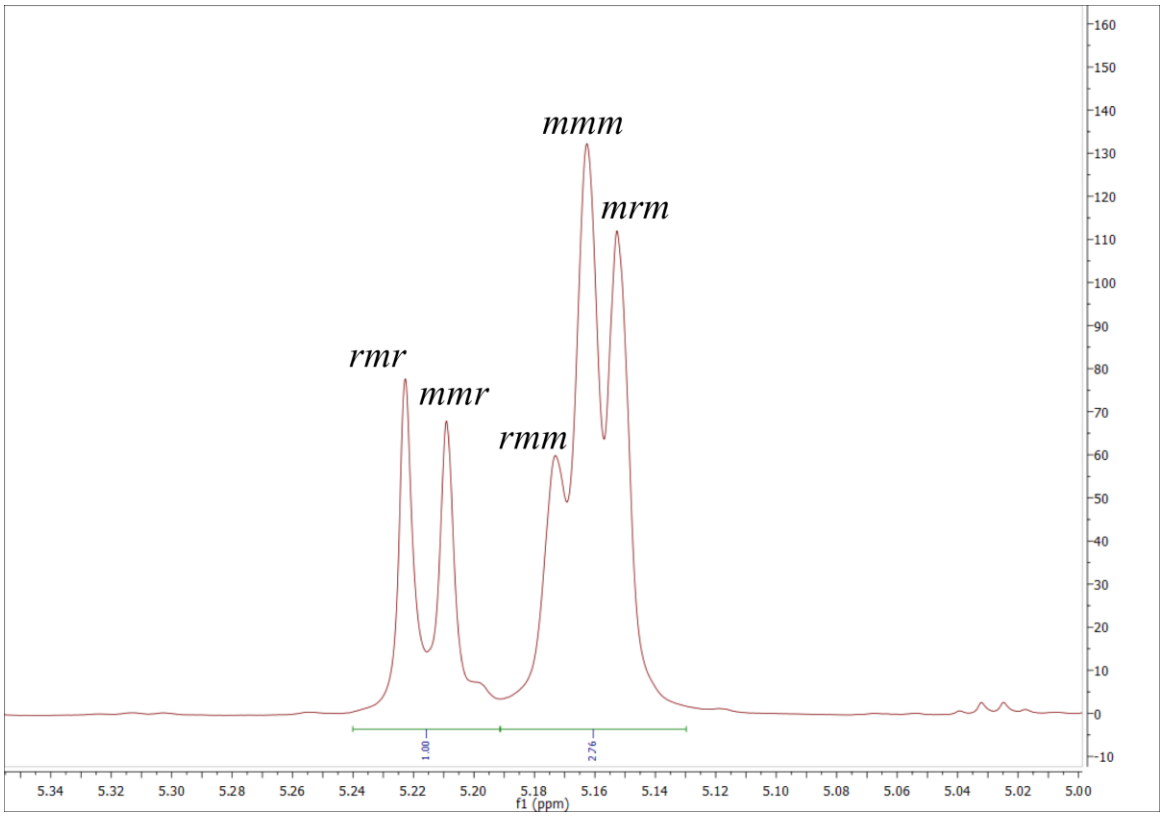

Figure 3-21 Homonuclear decoupled ^{1}H NMR spectrum of the methine region of PLA prepared from *rac*-LA with **1a·THF**/BnOH ([LA]:[**1a·THF**]:[BnOH]=100:1:1), at 80 °C for 40 min. (500 MHz, $CDCl_3$).

3.2.3 Ring-opening Polymerization of *rac*-Lactide Using Complex 2

3.2.3.1 Kinetic Studies

Polymerization of *rac*-lactide using the zinc alkoxyl derivative, **2**, was found to exhibit slower activity than the zinc ethyl species. For **2**, k_{obs} was found to be 0.665×10^{-3} s^{-1} whereas **1a·THF** exibits a k_{obs} of 1.833×10^{-3} s^{-1} under identical conditions ([LA]:[complex]:[BnOH] = 100:1:1 in toluene-d_8 at 80 °C). This may be because zinc complex **2** is more sterically hindered than complex **1a·THF**, which has a labile THF that can dissociate from the zinc center and allow the coordination of BnOH or lactide. It is also possible that complex **2** must undergo a dissociation process in solution first, followed by the coordination of *rac*-lactide. This would lead to the formation of two equiv. of a Zn(solv)[**L**] species, where (solv) represents a coordinating solvent, alcohol or lactide monomer.[56] ROP of *rac*-lactide using *i*-PrOH or BnOH as co-initiator was studied and kinetic data were obtained for polymerization performed at various temperatures in toluene-d_8. The polymerization rate appears to be independent of the amount of *i*-PrOH used (**Figure 3-22**) whereas increasing [BnOH] increases the rate significantly, as for **1a·THF** (**Figure 3-13**).

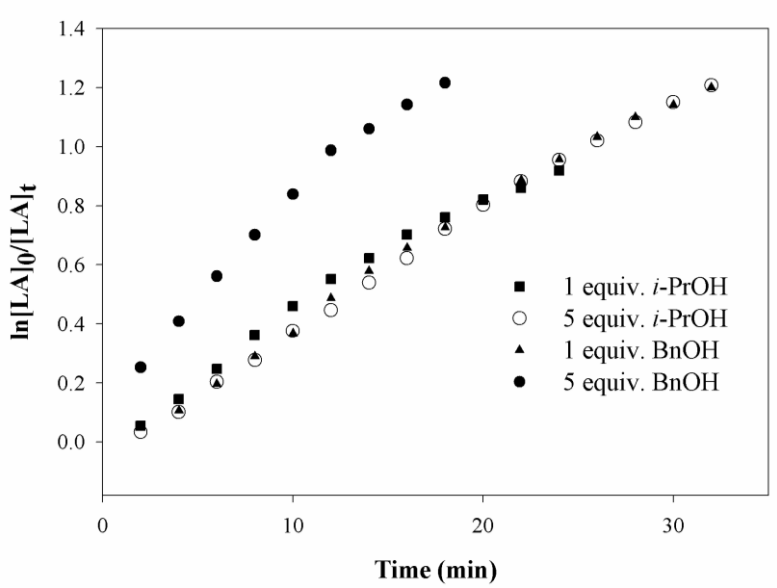

Figure 3-22 Plots of $\ln[LA]_0/[LA]_t$ vs. time for ROP of *rac*-LA catalyzed by complex **2**/*i*-PrOH or /BnOH ([LA]:[**2**]:[*i*-PrOH] = 100:1:1, or 100:1:5; [LA]:[**2**]:[BnOH] = 100:1:1, or 100:1:5; [LA] = 0.66 M in toluene-d_8, 80 °C).

The influence of co-initiator concentration, [ROH], on the reaction rate of ROP of *rac*-lactide was studied. Increasing the [*i*-PrOH]:[**2**] ratio from 1:1 to 5:1 has only very little effect on the polymerization rate, but a more significant increase in the reaction rate is observed with a 10:1 ratio of alcohol to zinc complex. **Figure 3-23** presents the dependence of the reaction rate on the number of polymer chains per complex, reflecting the influence of [*i*-PrOH]. Zinc complex **2** contains two –*i*-PrO groups that can act as initiating units and three zinc centers. Thus the number of polymer chains generated per complex can be expressed as (2[**2**] + [*i*-PrOH])/[**2**] and the number of polymer chains generated per zinc center is equal to (2[**2**] + [*i*-PrOH])/3[**2**]).[57]

3.2.3.2 Thermodynamic Activation Parameters

The influence of temperature on reaction rate shows the anticipated increase on going from 70 to 90 °C. Arrhenius analysis gave an activation energy (E_a) of 83.19 ± 15.29 $kJ \cdot mol^{-1}$ for *rac*-lactide polymerization in the presence of one equiv. of BnOH (**Figure 3-24**). Eyring analysis of the data (**Figure 3-25**) gave thermodynamic activation parameters of $\Delta H^{\ddagger}$ = 80.25 ± 15.31 $kJ \cdot mol^{-1}$ and $\Delta S^{\ddagger}$ = – 78.71 ± 43.35 $J \cdot K^{-1} \cdot mol^{-1}$, which are consistent with an ordered transition state and a coordination insertion mechanism, but also do not exclude an activated monomer mechanism. [60-62]

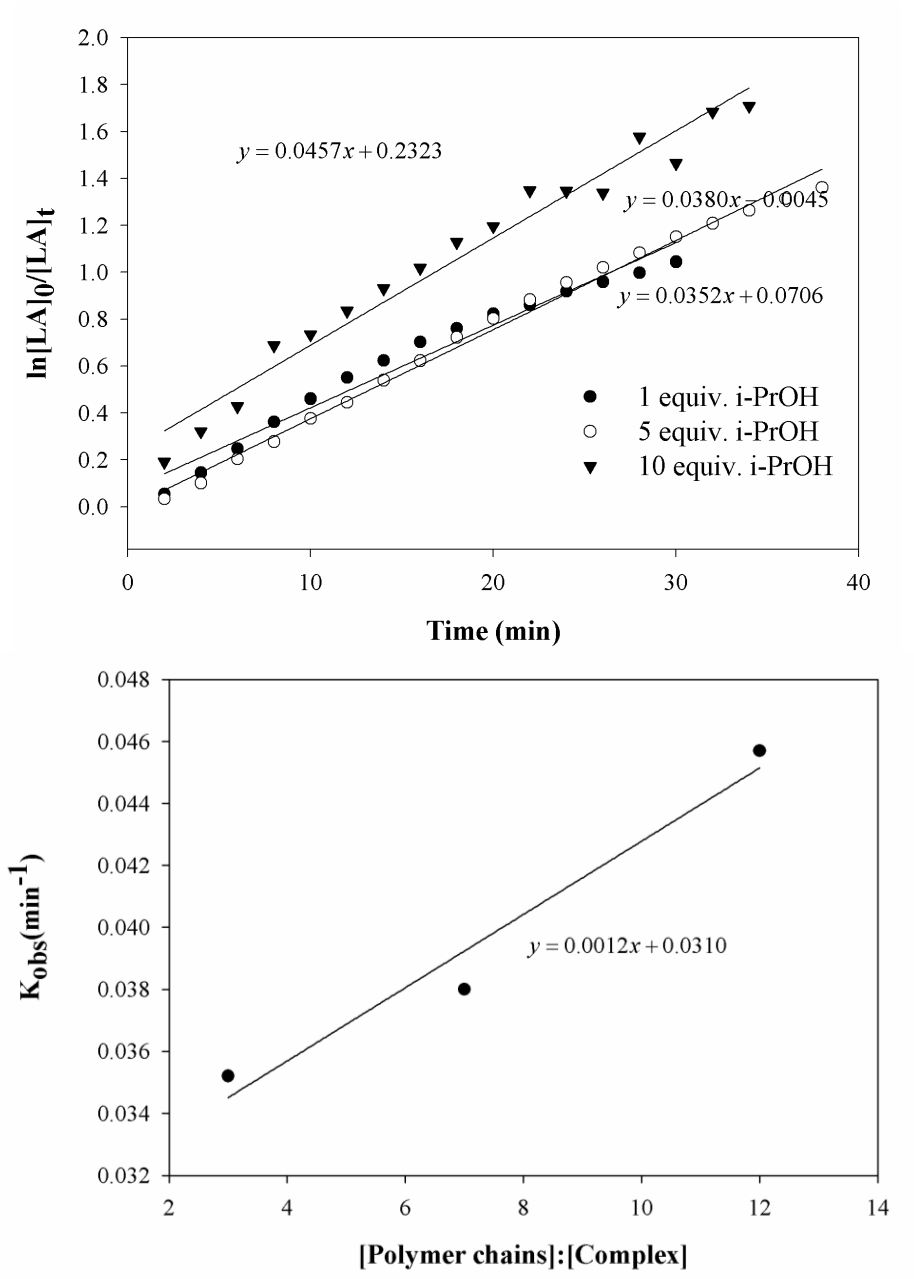

Figure 3-23 Plots of $\ln[LA]_0/[LA]_t$ vs. time (top) and corresponding observed rate constant k_{app} vs. [Polymer chains]:[Complex] plots (bottom) for the immortal ROP of *rac*-LA catalyzed by complex **2**/*i*-PrOH to determine the dependence on [*i*-PrOH]([LA]:[**2**]:[*i*-PrOH] = 100:1:1, 5, 10; [LA] = 0.66 M in toluene-d_8, 80 °C). The solid lines are the best linear fits.

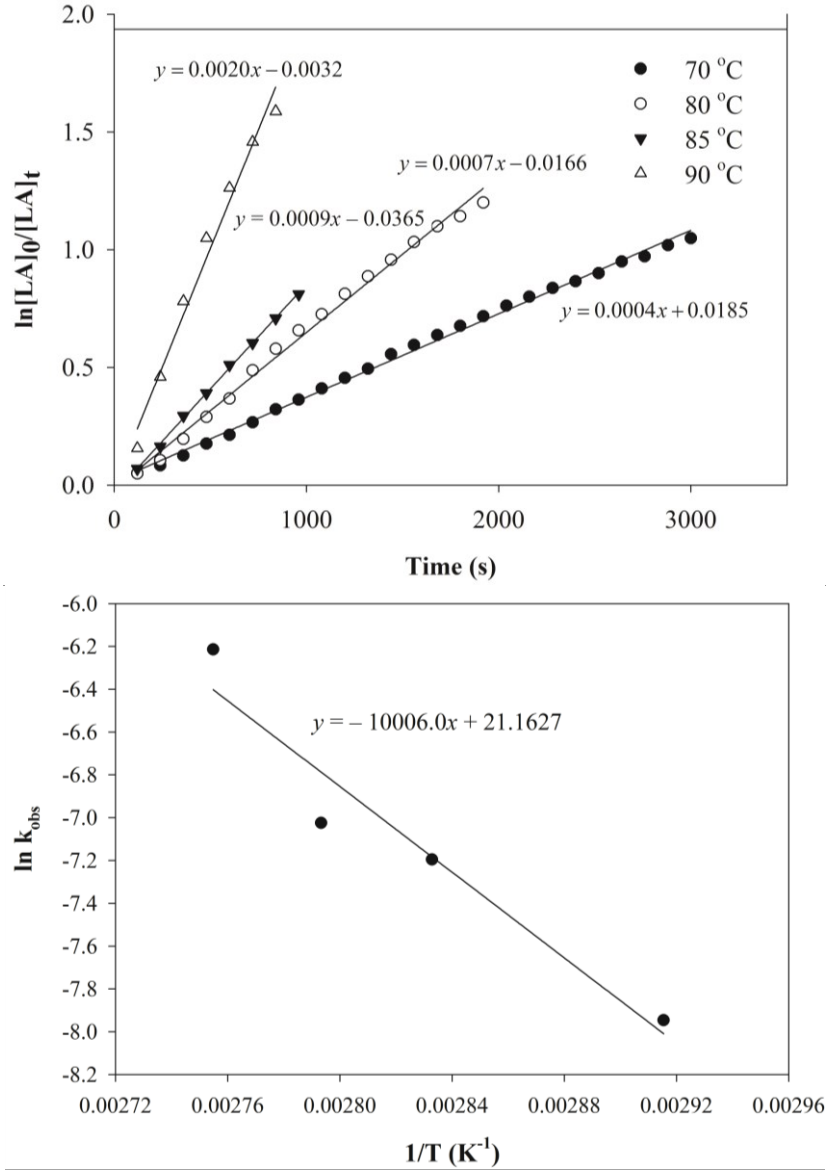

Figure 3-24 Plots of $\ln[LA]_0/[LA]_t$ vs. time and corresponding Arrhenius plots of $\ln k_{obs}$ vs. 1/T for ROP of *rac*-LA catalyzed by complex **2**/BnOH ([LA]:[**2**]:[BnOH] = 100:1:1, [LA] = 0.66 M in toluene-d_8) in the temperature range of 70 to 90 °C. The solid line is the best linear fit.

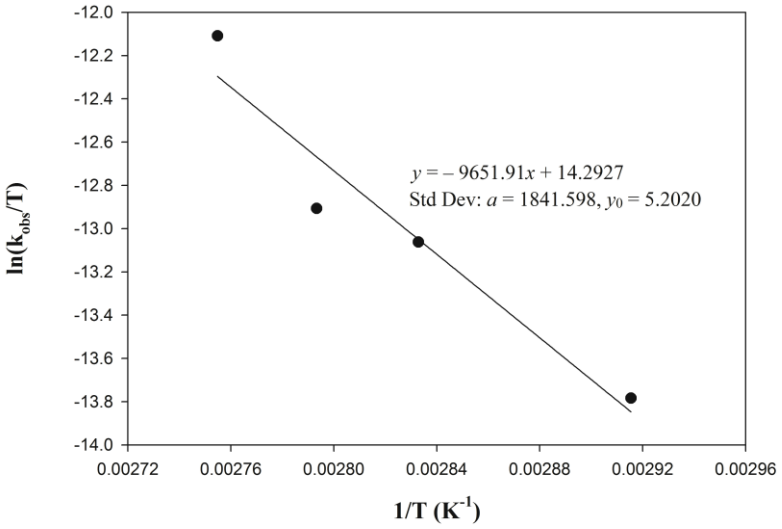

Figure 3-25 Eyring analysis for ROP of *rac*-LA catalyzed by complex **2**/*i*-PrOH ([LA]:[**2**]:[*i*-PrOH] = 100:1:1, [LA] = 0.66 M in toluene-d_8) in the temperature range of 70 to 90 °C. The solid line is the best linear fit.

3.2.3.3 Study of the Polymers

3.2.3.3.1 MALDI-TOF MS

MALDI mass spectra were obtained for the polymers produced by complex **2** in the presence of *i*-PrOH. The most intense peaks show intervals of *m/z* 72 corresponding to *i*-PrO$(C_3H_4O_2)_nH\cdot Na^+$ (**Figure 3-26**). The MALDI mass spectrum of the polymer obtained using complex 2 in the presence of BnOH is shown in **Figure 3-27**. The spectrum shows a mixture of polymers with either BnO– or *i*-PrO– end groups and the main series of peaks can be assigned as BnO/*i*-PrO$(C_3H_4O_2)_nH\cdot Na^+$. The linear mode spectrum shows peaks arising from K^+ cationized polymer fragments as well (**Figure 3-28**).

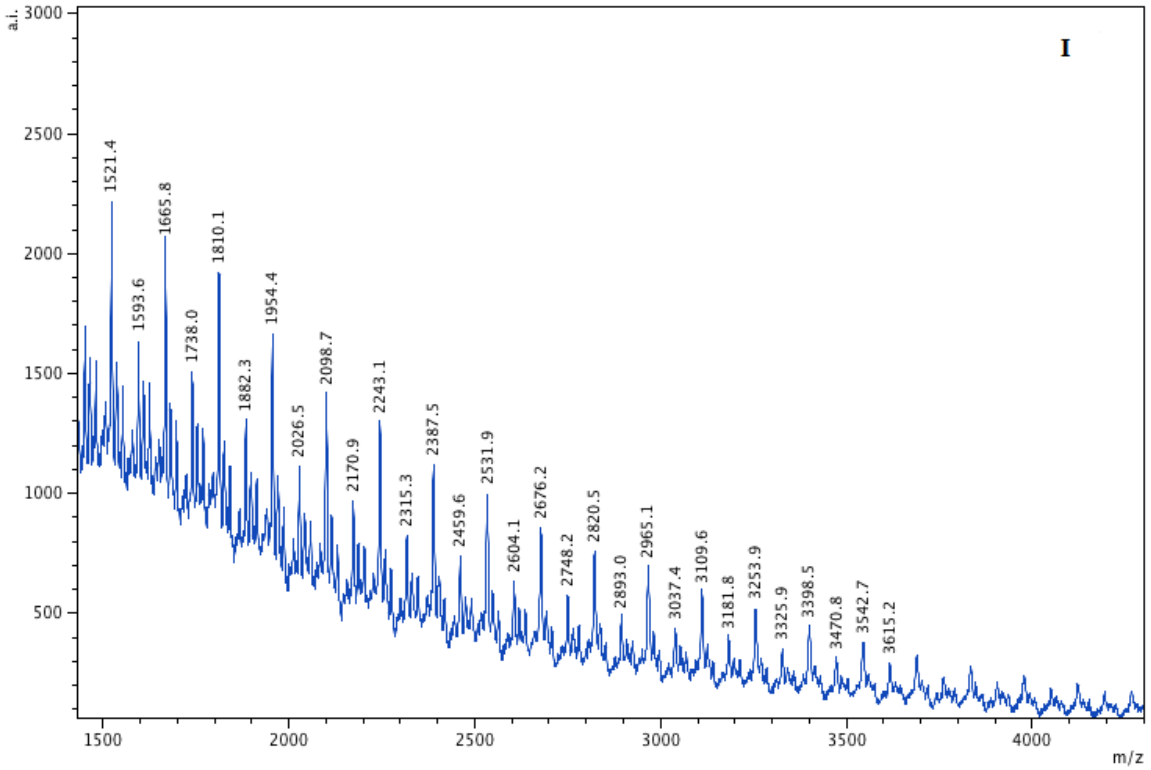
I
a.i.
m/z
1521.4
1593.6
1665.8
1738.0
1810.1
1882.3
1954.4
2026.5
2098.7
2170.9
2243.1
2315.3
2387.5
2459.6
2531.9
2604.1
2676.2
2748.2
2820.5
2893.0
2965.1
3037.4
3109.6
3181.8
3253.9
3325.9
3398.5
3470.8
3542.7
3615.2

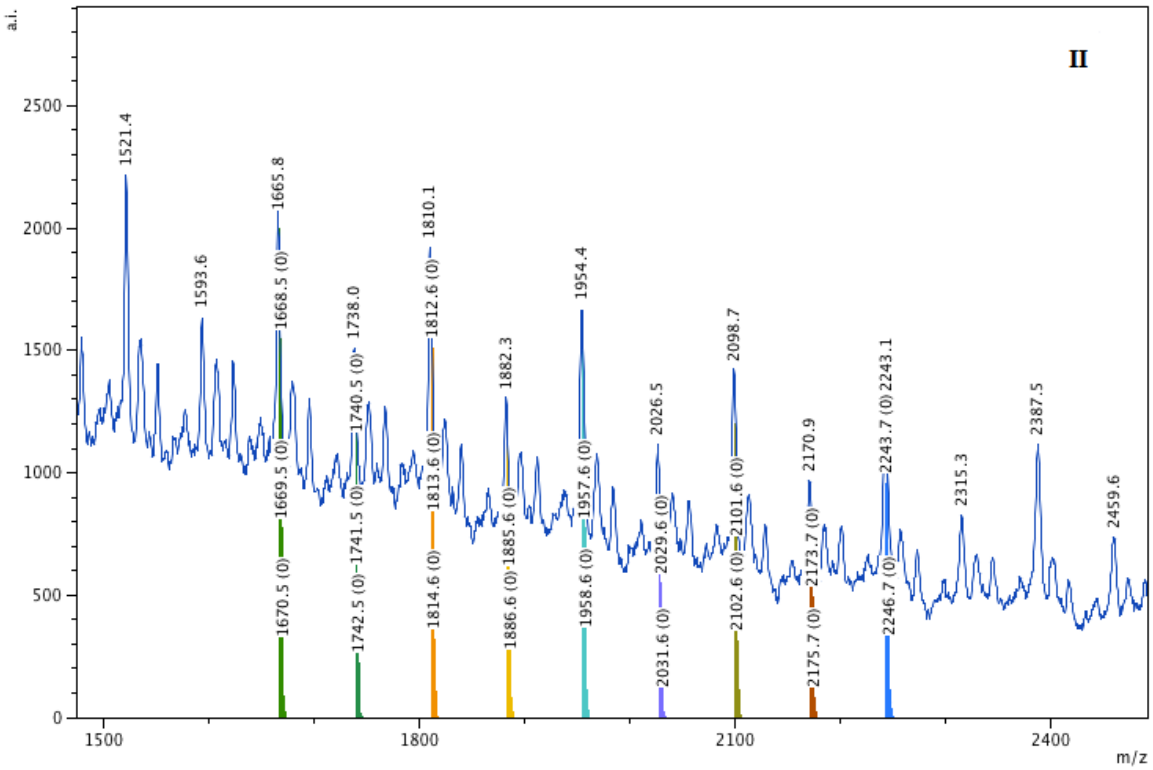
II
a.i.
m/z
1521.4
1593.6
1665.8
1668.5 (0)
1669.5 (0)
1670.5 (0)
1738.0
1740.5 (0)
1741.5 (0)
1742.5 (0)
1810.1
1812.6 (0)
1813.6 (0)
1814.6 (0)
1882.3
1885.6 (0)
1886.6 (0)
1954.4
1957.6 (0)
1958.6 (0)
2026.5
2029.6 (0)
2031.6 (0)
2098.7
2101.6 (0)
2102.6 (0)
2170.9
2173.7 (0)
2175.7 (0)
2243.1
2243.7 (0)
2246.7 (0)
2315.3
2387.5
2459.6

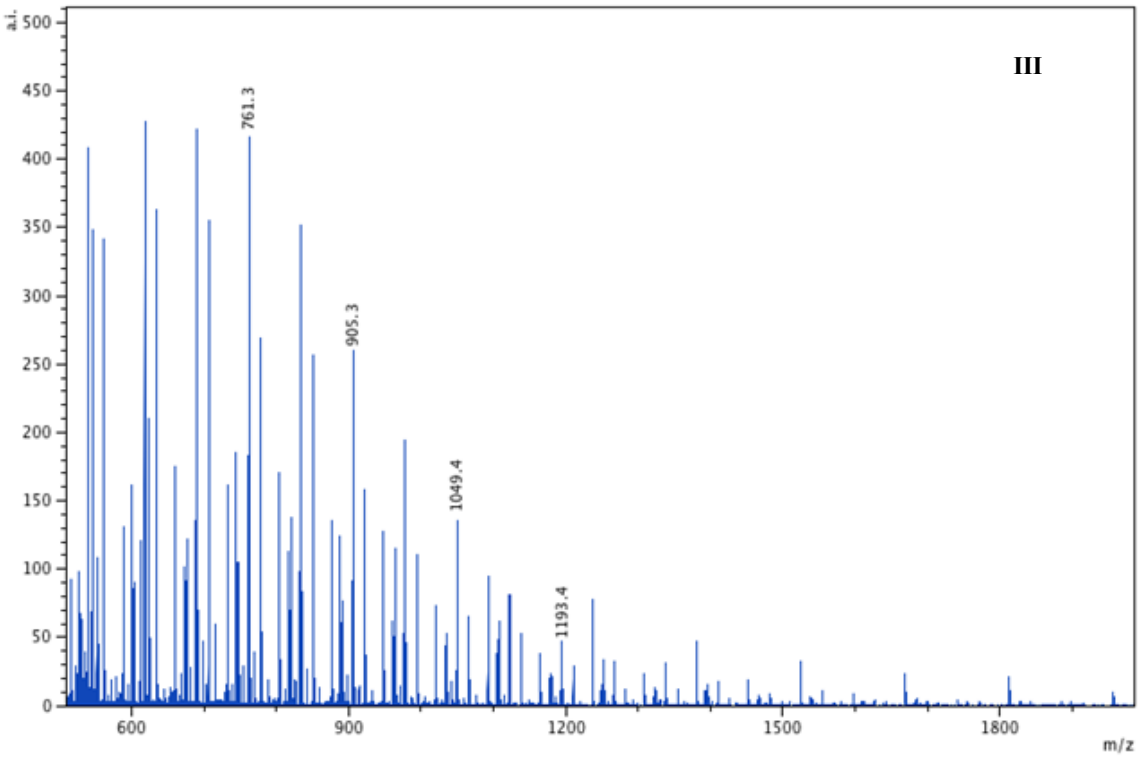

Figure 3-26 MALDI-TOF mass spectra of PLA obtained using complex **2**/*i*-PrOH ([LA]:[**2**]:[*i*-PrOH] = 100:1:1, [LA] = 0.66 M in toluene-d_8, 90 °C), (**I**: linear mode, full spectrum; **II**: linear mode, expanded spectrum with experimental and theoretical modelled peaks; **III**: reflectron mode, full spectrum).

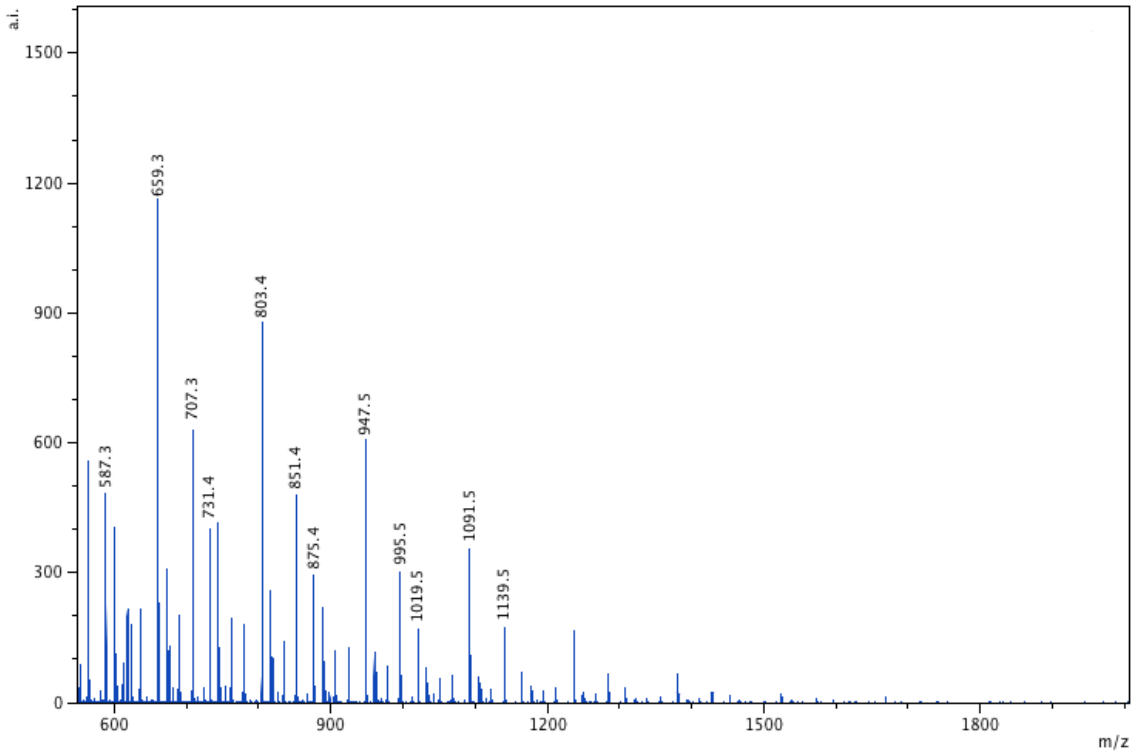

Figure 3-27 MALDI-TOF mass spectrum (reflectron mode) of PLA obtained using complex **2**/BnOH ([LA]:[**2**]:[BnOH] = 100:1:1, [LA] = 0.66 M in toluene-d_8, 80 °C)

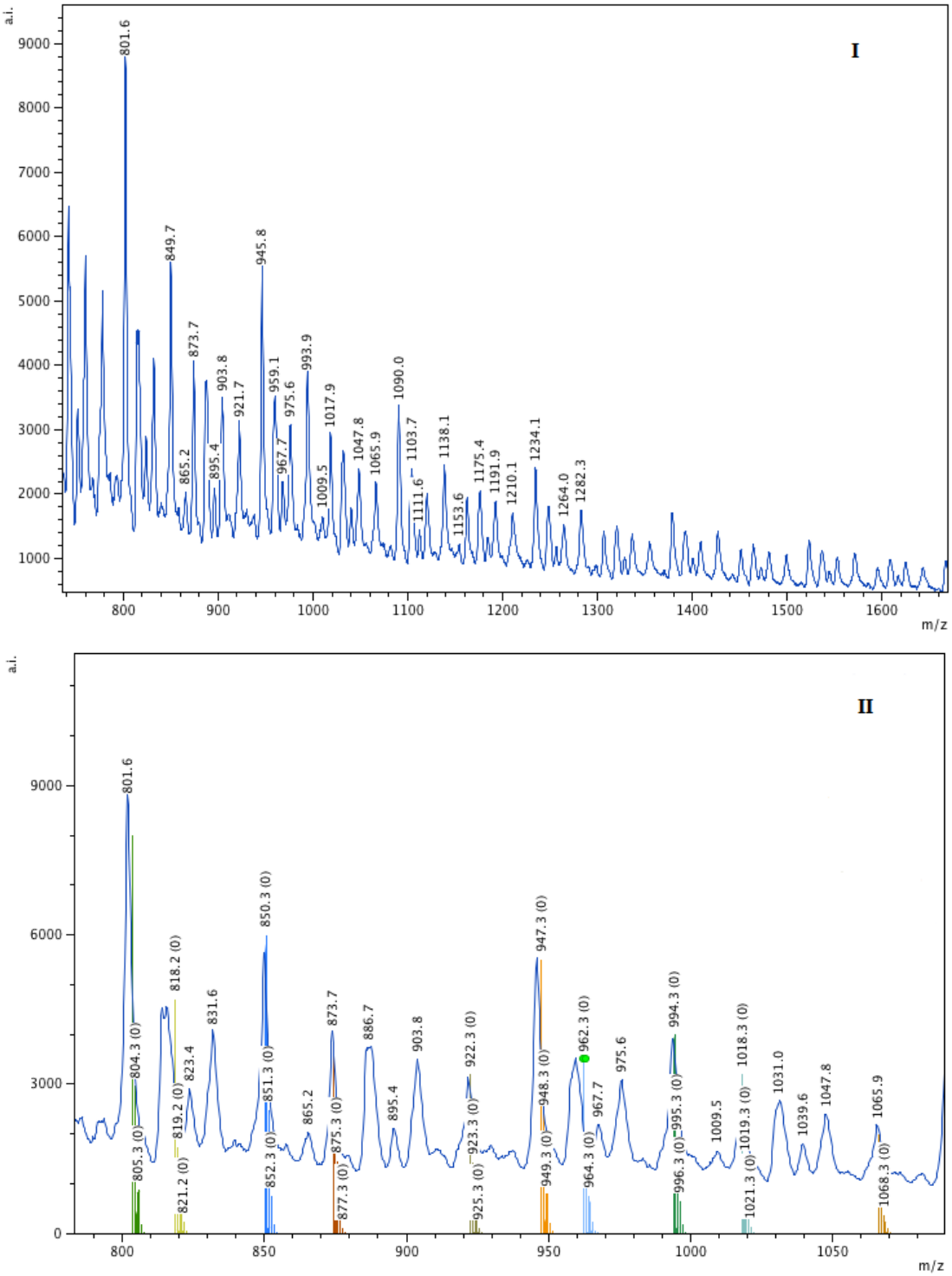

Figure 3-28 MALDI-TOF mass spectra (linear mode) of PLA obtained using complex **2**/BnOH ([LA]:[**2**]:[BnOH] = 100:1:1, [LA] = 0.66 M in toluene-d_8, 80 °C), (**I**: full spectrum; **II**: expanded spectrum with experimental and theoretical modelled peaks).

3.2.4 Mechanistic Study of Ring-opening Polymerization of *rac*-Lactide

NMR scale experiments were conducted to monitor the reactions in toluene-d_8 at 353 K in order to model polymerization conditions. Spectra were collected upon cooling after heating the reaction mixture for set times because the resonances were broad and not readily assignable at 353 K. The ^{1}H NMR spectrum of BnOH in toluene-d_8 was first obtained. The hydroxyl proton appeared as a triplet at δ 4.70 and the methylene protons coupling with the hydroxyl H appeared as a doublet at δ 4.37. A 1:1 ratio of [LA]:[BnOH] was heated for 30 min and the ^{1}H NMR spectrum was collected at 298 K after cooling (**Figure 3-29**). The peaks corresponding to *rac*-lactide showed little change; however, the methylene protons of the BnOH appeared as a singlet at δ 4.29 and the hydroxyl proton was absent. A new weak peak appeared at δ 1.03, which may be the hydroxyl proton resulting from reaction of BnOH with lactide or possibly due to hydrogen bonding between BnOH and LA. In any case, a reaction is clearly observed between BnOH and lactide upon heating to 353 K.

Reactions of 1:1 or 1:2 mixtures of **1a·THF** and BnOH were conducted using the same NMR monitoring conditions. ^{1}H NMR spectra were collected immediately after mixing and heating (**Figure 3-30**). Complex **1a·THF** reacted with 1 equiv. BnOH following heating to 353 K and showed that the THF peaks had shifted upfield (e.g. from δ 3.91 to 3.54) indicating dissociation from the zinc center. A new peak is observed at δ 0.81 corresponding to ethane resulting from protonolysis of an ethyl group. The presence of one set of sharp ethyl resonances is observed as well as a singlet at δ 4.52, which is attributed to zinc-bound benzyloxide. Reaction of a 1:2 ratio of **1a·THF** and BnOH showed a more

intense ethane resonance and broading of the remaining resonances including those of the aromatic groups. The diagnostic methylene doublets of **1a·THF** are no longer clearly visible, implying the complete conversion of **1a·THF** to another species, likely one containing two benzyloxide groups. This is consistent with an increasing number of polymer chain growth sites per complex and the decrease in observed PLA M_n with increased BnOH loading (**Table 3-3**, entries 2-4). Hence, it is likely that reaction of **1a·THF** with BnOH gives a product related to **2**, however, it is more fluxional than **2** at these conditions. Disproportionation of zinc-benzyloxides supported by β-diketiminate ligands to give trimetallic alkoxyl-bridged zinc complexes similar to **2** has been previously reported.[27]

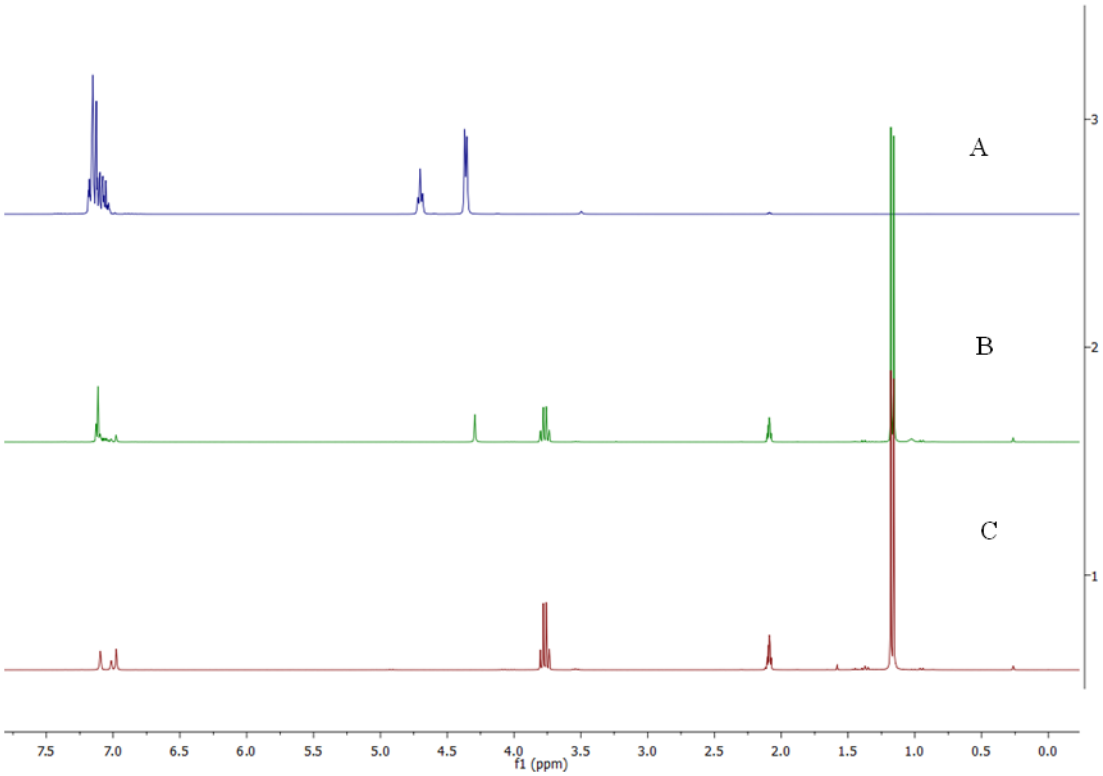

Figure 3-29 ^{1}H NMR spectra in toluene-d_8 of A: BnOH; B: *rac*-LA and BnOH (1:1 ratio) following heating to 353 K then cooling to 298 K; and C: *rac*-LA.

Reaction of *rac*-lactide with **1a·THF** followed by addition of BnOH in a 1:1:1 ratio was then monitored by ^{1}H NMR (**Figure 3-31**). Comparison of the spectrum of the pure complex with that of the mixture after heating showed that there were only slight shifts of the THF peaks, i.e. from δ 3.90 and δ 1.54 to δ 3.87 and δ 1.53, respectively, and slight chemical shift changes of one of the ethyl groups, from δ 0.92 and δ 0.16 to δ 0.91 and δ 0.14, respectively. Therefore, it is unlikely that THF dissociation occurs in this case, or if displacement does occur at 353 K, the zinc site is not sufficiently hindered to prevent re-coordination of the displaced THF upon cooling to 298 K. Comparison of the spectra before and after heating showed the ring-opening of the cyclic lactide monomer based on the chemical shift change of the methine peak from δ 3.80 downfield to coincident with the THF peak near δ 3.90. A peak at δ 0.81 is observed corresponding to ethane even before heating to 353 K. Interestingly, when lactide is present the ethyl group(s) of **1a·THF** do not appear to undergo protonation by the alcohol as readily as when **1a·THF** and BnOH are heated without LA as described above.

Reaction of a 1:1:2 mixture of *rac*-lactide, **1a·THF**, and BnOH was investigated under the same conditions as above. A spectrum was collected after mixing and showed slight broadening of the THF, lactide and ethyl group peaks (**Figure 3-32**). Comparison of the spectra of the pure complex and the mixture after heating showed negligible shifting of the THF peaks as mentioned above, from δ 3.90 and δ 1.54 to δ 3.83 and δ 1.52, respectively. Ethane is observed as before, but again one ZnEt group appears to remain intact; however, the intensity of the ethane peak increases upon heating (**Figure 3-32**, spectra A and B) and increasing BnOH loading (**Figure 3-33**, spectra A and B). Therefore, protonolysis of one ethyl group does not proceed fully even with excess BnOH when

lactide is present and displacement of both ethyl groups by BnOH is clearly unfavored. The ^{1}H NMR spectrum of the reaction of 2:1:1 of *rac*-lactide: **1a·THF**:BnOH showed one of the ethyl groups shifted downfield very slightly after heating (**Figure 3-33**, spectrum C). Also, when more than one equiv. of lactide is present, protonation of an ethyl group still proceeds even though LA and BnOH are shown to undergo ring-opening at 353 K. Since the presence of lactide was found to hinder the reaction of BnOH with **1a·THF**, the experiment was repeated but now lactide was added after the addition of BnOH to a solution of **1a·THF** in toluene-d_8 (**Figure 3-34**). It is apparent that a zinc-ethyl group is lost along with the appearance of PLA resonances between δ 4.5 and δ 5.5 upon heating the solution (**Figure 3-34**, spectra B and C). A coordination-insertion mechanism requires formation of a ZnOBn complex via protonolysis of a Zn-Et bond and evidence for this has been observed in ^{1}H NMR spectra. Unfortunately, crystalline product of this reaction suitable for X-ray diffraction could not be obtained. In the case of complex **2**, which already possesses ZnOR sites and is likely stabilized by the presence of an additional zinc centre, a coordination-insertion mechanism is likely favored. The low solubility of (*i*-PrO)$_2$Zn in toluene likely makes it unavailable to act as an initiator, but its presence in low concentrations cannot be ignored and it may play a role in the activity of that system. Benzyl alcohol concentration does, however, exhibit an influence on reaction rates, therefore the nature of the alcohol coinitiator may be an important factor in the mechanism.

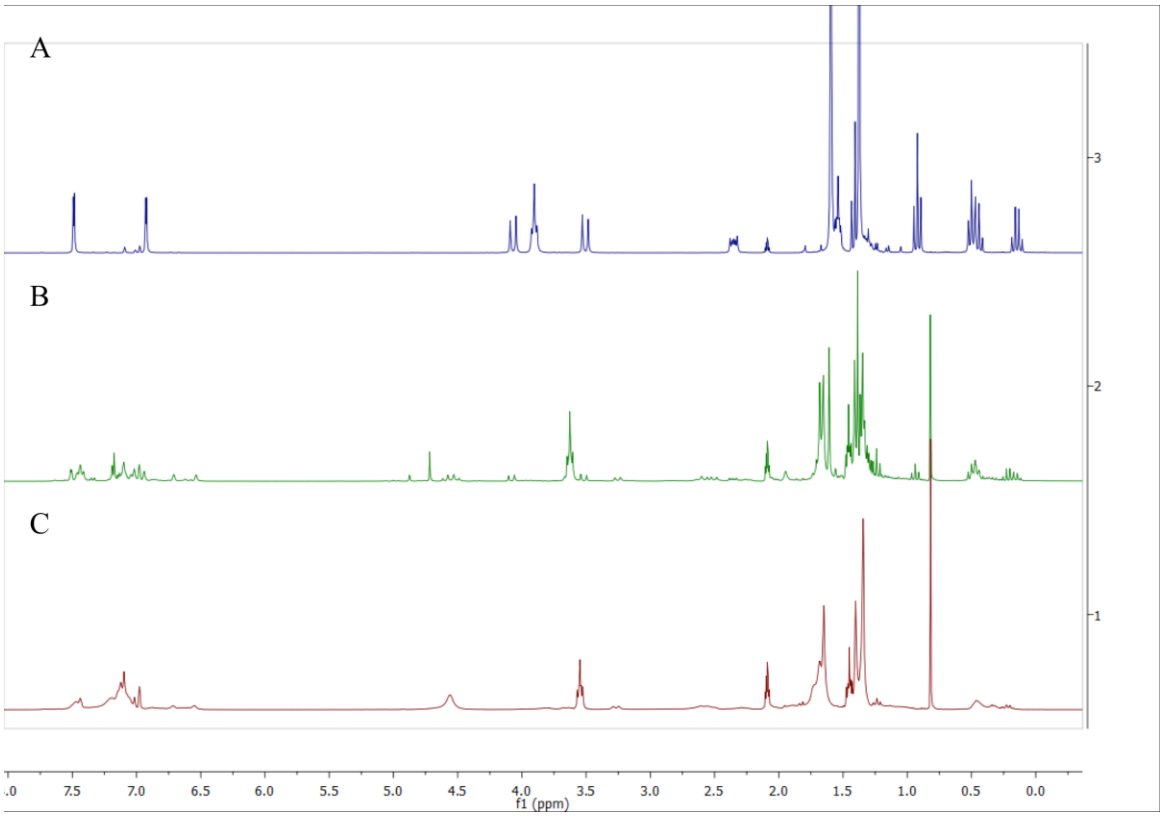

Figure 3-30 ^{1}H NMR spectra in toluene-d_8 of A: **1a·THF**; B: **1a·THF** with one equiv. BnOH; C: **1a·THF** with two equiv. BnOH.

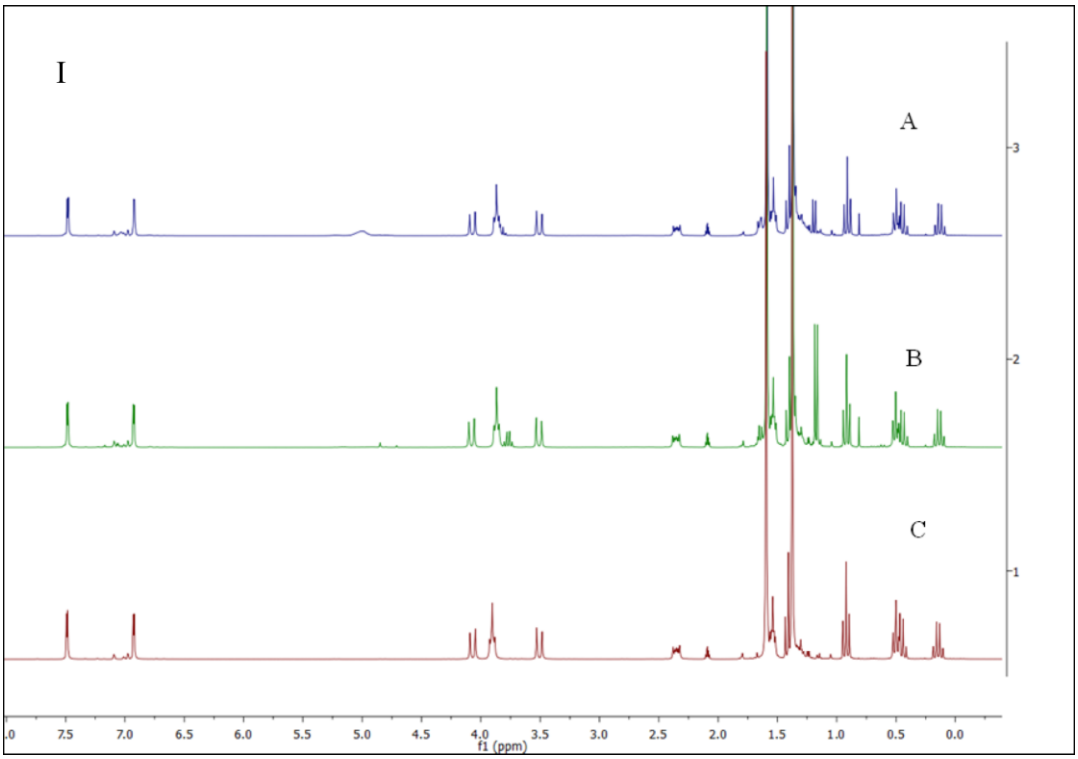
I
A
B
C
f1 (ppm)

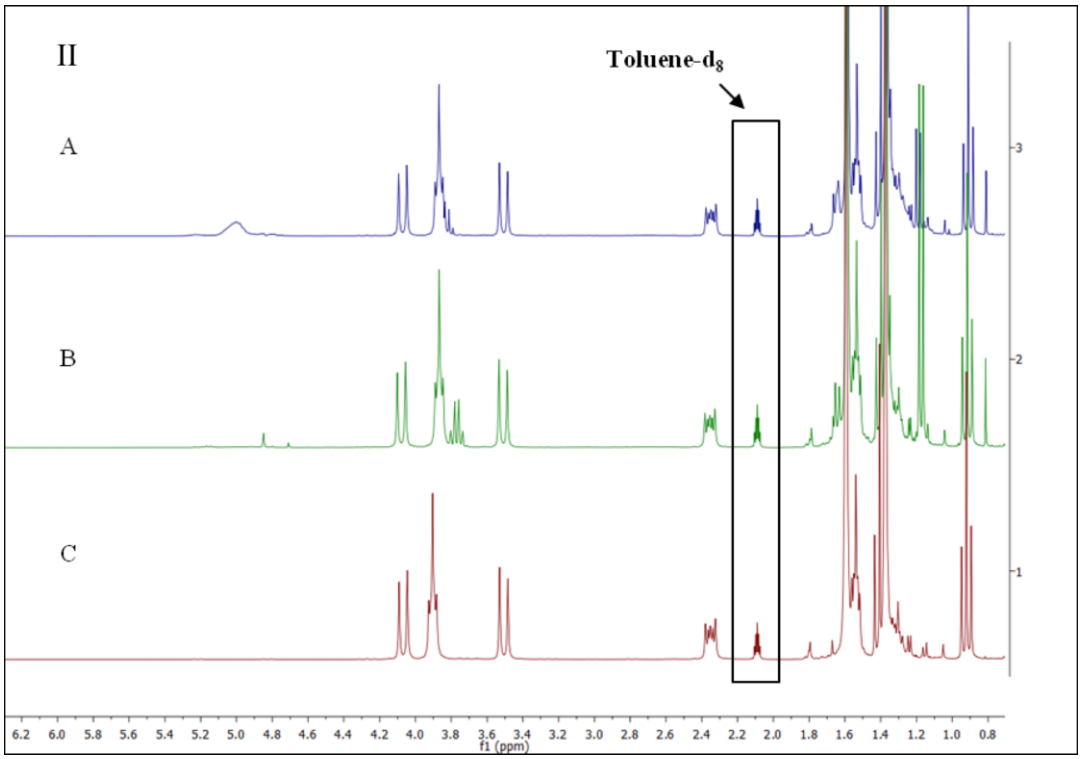
II
Toluene-d8
A
B
C
f1 (ppm)

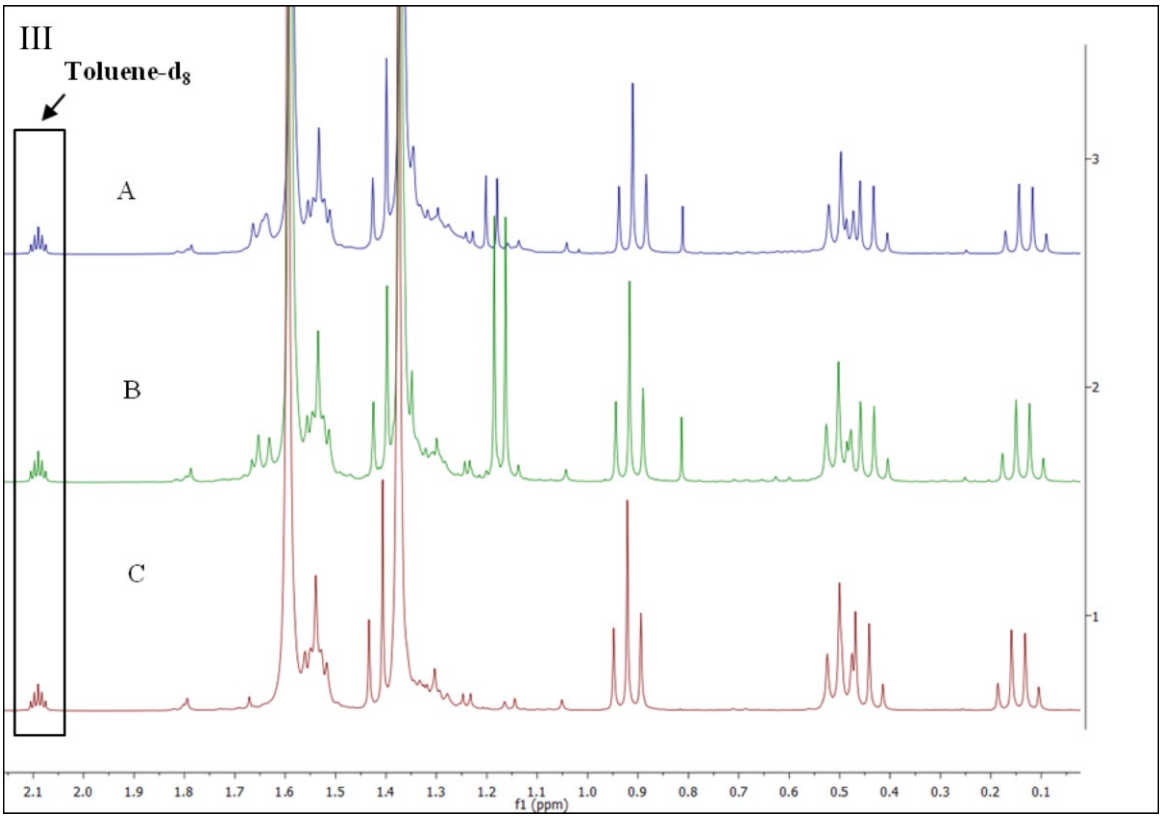

Figure 3-31 Complete ^{1}H NMR spectra (**I**), expansion of the THF peak region (**II**), and expansion of the ethyl group region (**III**) in toluene-d_8. A: [LA]:[**1a·THF**]:[BnOH]=1:1:1 after heating to 353 K for 60 min; B: mixture of [LA]:[**1a·THF**]:[BnOH]=1:1:1 before heating; C: **1a·THF** alone.

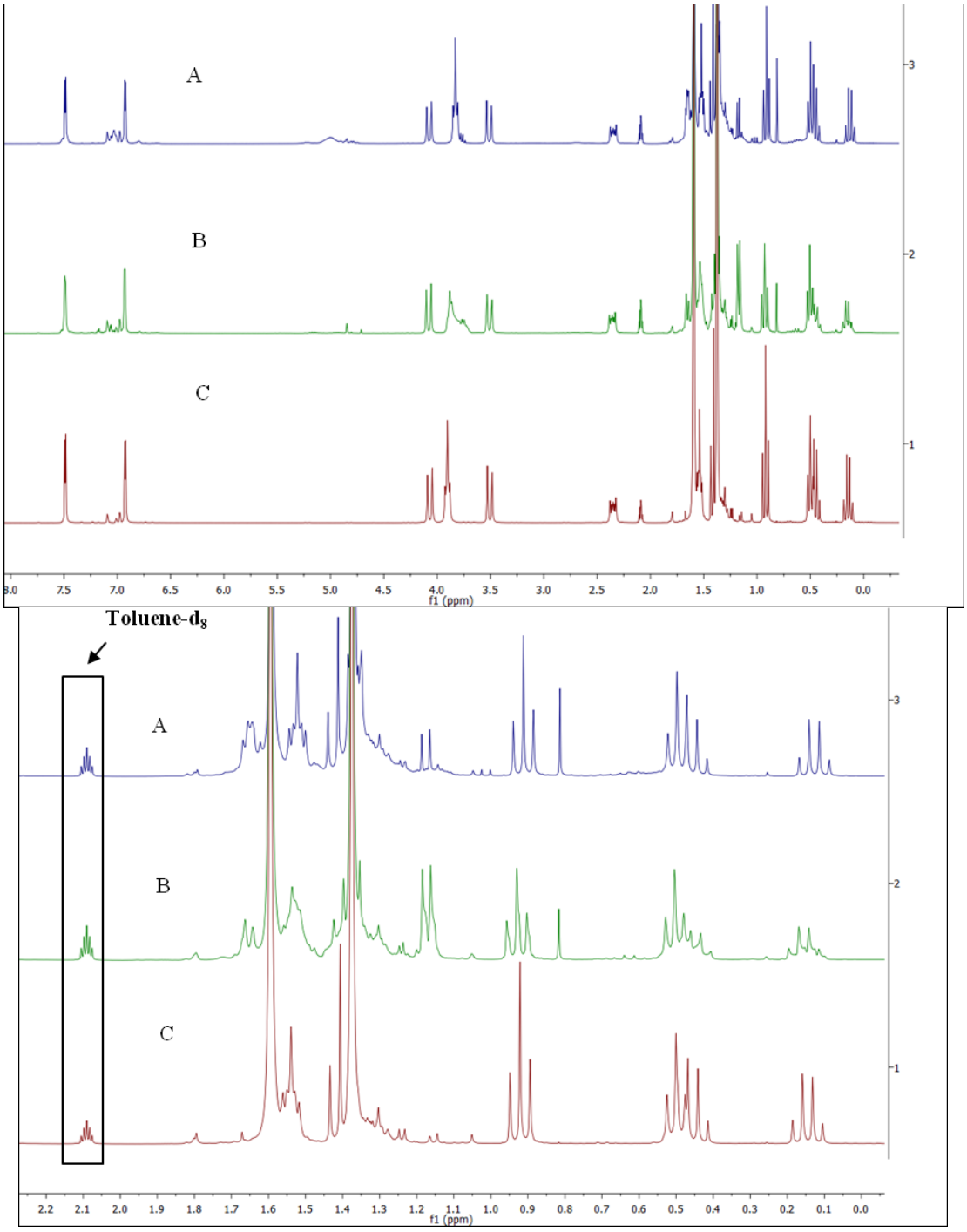

Figure 3-32 ^{1}H NMR spectra (top) and expanded spectra of ethyl group region (bottom), in toluene-d_8. A: [LA]:[**1a·THF**]:[BnOH] = 1:1:2 after heating for 72 min; B: mixture of [LA]:[**1a·THF**]:[BnOH]=1:1:2 before heating; C: **1a·THF**.

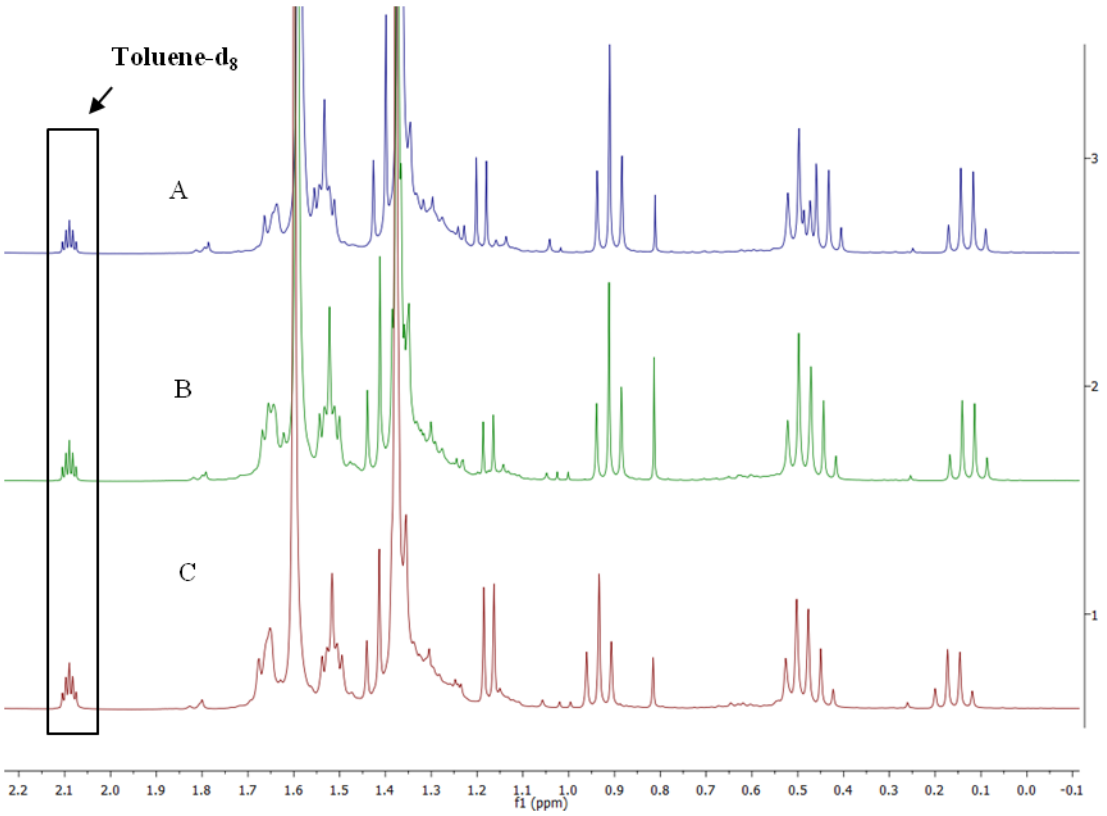

Figure 3-33 Expanded ^{1}H NMR spectra in toluene-d_8 of A: [LA]:[**1a·THF**]:[BnOH] = 1:1:1 after heating for 72 min; B: mixture of [LA]:[**1a·THF**]:[BnOH] = 1:1:2 after heating for 60 min; C: mixture of [LA]:[**1a·THF**]:[BnOH] = 2:1:1 after heating for 60 min.

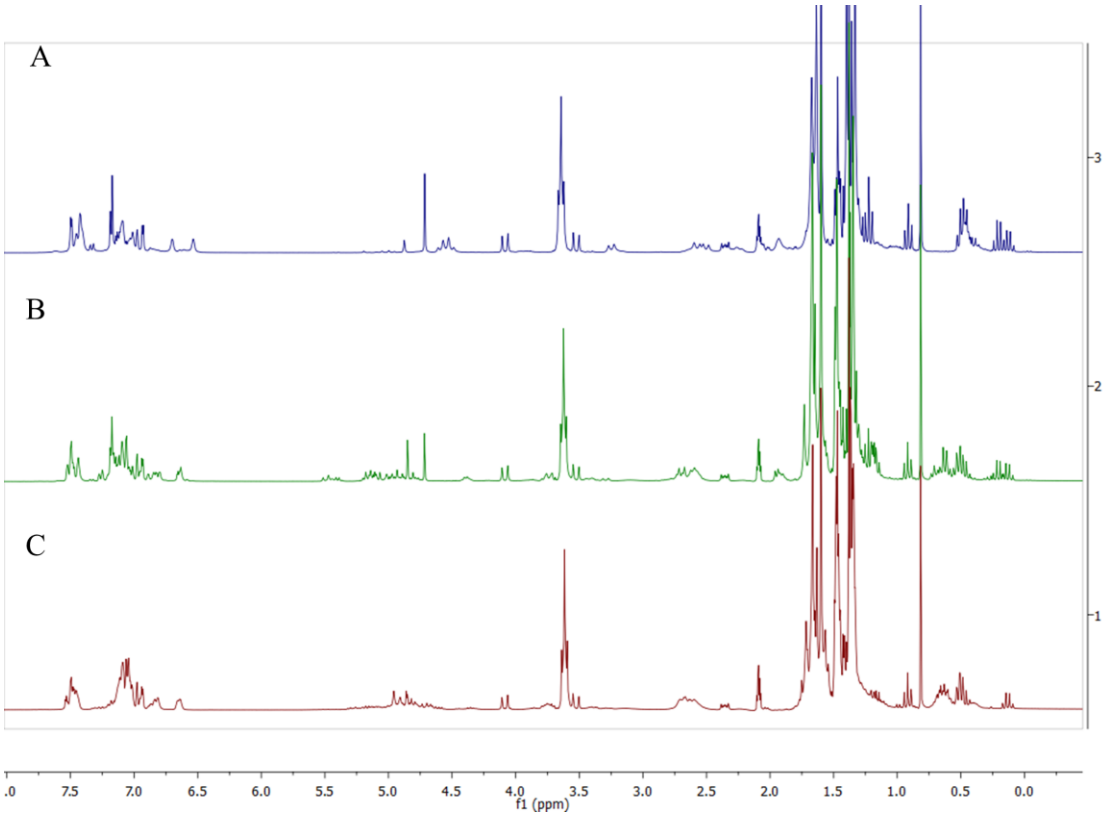

Figure 3-34 ^{1}H NMR spectra in toluene-d_8, of A: **1a·THF** with one equiv. of BnOH; B: **1a·THF** with one equiv. BnOH then addition of one equiv. of LA; C: the mixture of B after heating for 1 h.

3.3 Conclusions

Zinc complexes of tridentate amino-bis(phenolate) ligands for ring-opening of *rac*-lactide were studied. Zinc complex **1a** showed activity in melt phase *rac*-lactide polymerization, giving 92% conversion after only 15 min producing polymers with narrow molecular weight distributions. ROP of *rac*-lactide using **1a·THF** in the presence of BnOH was studied by ^{1}H NMR spectroscopy in toluene-d_8. Kinetic data showed that the reaction is first order in monomer concentration and the rate is proportional to the concentration of added benzyl alcohol. The reaction appears pseudo-first order in metal complex concentration, but the bimetallic nature of the complex and the presence of two possible reaction sites with BnOH prevent definitive confirmation of reaction order. A linear relationship of reaction rate to [polymer chain]:[complex] ratio was obtained in the presence of BnOH. Complex **1a·THF** provides polymers with moderate molecular weight distributions, and polymerization has a linear relationship of M_n vs. lactide conversion, M_n vs. lactide to complex ratio, and M_n vs lactide to ROH ratio, thus indicating immortal polymerization. However, cyclic oligomers due to back-biting were also obtained. Activity of complex **2** for ROP of *rac*-lactide in the presence of BnOH or *i*-PrOH was studied and the thermodynamic activation parameters were determined. Investigations of **1a·THF** with stoichiometric amounts of BnOH suggest the formation of ZnOBn groups; however, the increased rate upon addition of BnOH argues for an activated monomer mechanism. Thus, the mechanisms in this system remain ambiguous, possibly following a combination of activated monomer and coordination insertion mechanisms. Unfortunately, further mechanistic studies were limited by the poor solubility of *rac*-lactide in toluene. The

viscosity change over the polymerization time may affect the reaction rates and it may also affect the aggregation state of zinc complexes, which makes the actual mechanism complicated to study.

3.4 References

1. Drumright, R. E.; Gruber, P. R.; Henton, D. E. *Adv. Mater.* **2000,** *12*, 1841-1846.

2. Vennestrom, P. N.; Osmundsen, C. M.; Christensen, C. H.; Taarning, E. *Angew. Chem. Int. Ed.* **2011,** *50*, 10502-10509.

3. Hoffman, A. S. *Adv. Drug Del. Rev.* **2012,** *64*, 18-23.

4. Dev, A.; Binulal, N.; Anitha, A.; Nair, S.; Furuike, T.; Tamura, H.; Jayakumar, R. *Carbohydr. Polym.* **2010,** *80*, 833-838.

5. Capra, P.; Briasco, B.; Sorrenti, M.; Catenacci, L.; Sachet, M.; Perugini, P. *J. Appl. Polym. Sci.* **2014,** *131*.

6. Tawakkal, I. S.; Cran, M. J.; Miltz, J.; Bigger, S. W. *J. Food Sci.* **2014,** *79*, R1477-R1490.

7. Dechy-Cabaret, O.; Martin-Vaca, B.; Bourissou, D. *Chem. Rev.* **2004,** *104*, 6147-6176.

8. Wu, J.; Yu, T.; Chen, C.; Lin, C. *Coord. Chem. Rev.* **2006,** *250*, 602-626.

9. Platel, R. H.; Hodgson, L. M.; Williams, C. K. *Polym. Rev.* **2008,** *48*, 11-63.

10. Wheaton, C. A.; Hayes, P. G.; Ireland, B. J. *Dalton Trans.* **2009**, 4832-4846.

11. Ajellal, N.; Carpentier, J.-F.; Guillaume, C.; Guillaume, S. M.; Helou, M.; Poirier, V.; Sarazin, Y.; Trifonov, A. *Dalton Trans.* **2010,** *39*, 8363-8376.

12. Stanford, M. J.; Dove, A. P. *Chem. Soc. Rev.* **2010,** *39*, 486-494.

13. Thomas, C. M. *Chem. Soc. Rev.* **2010,** *39*, 165-173.

14. Buffet, J.-C.; Okuda, J. *Polym. Chem.* **2011,** *2*, 2758-2763.

15. Dijkstra, P. J.; Du, H.; Feijen, J. *Polym. Chem.* **2011,** *2*, 520-527.

16. Tschan, M. J.-L.; Brulé, E.; Haquette, P.; Thomas, C. M. *Polym. Chem.* **2012,** *3*, 836-851.

17. Cheng, M.; Attygalle, A. B.; Lobkovsky, E. B.; Coates, G. W. *J. Am. Chem. Soc.* **1999,** *121*, 11583-11584.

18. Chamberlain, B. M.; Cheng, M.; Moore, D. R.; Ovitt, T. M.; Lobkovsky, E. B.; Coates, G. W. *J. Am. Chem. Soc.* **2001,** *123*, 3229-3238.

19. Chisholm, M. H.; Gallucci, J. C.; Zhen, H.; Huffman, J. C. *Inorg. Chem.* **2001,** *40*, 5051-5054.

20. Chisholm, M. H.; Huffman, J. C.; Phomphrai, K. *Dalton Trans.* **2001**, 222-224.

21. Chisholm, M. H.; Phomphrai, K. *Inorg. Chim. Acta* **2003,** *350*, 121-125.

22. Dove, A. P.; Gibson, V. C.; Marshall, E. L.; White, A. J.; Williams, D. J. *Dalton Trans.* **2004**, 570-578.

23. Chisholm, M. H.; Gallucci, J. C.; Phomphrai, K. *Inorg. Chem.* **2005,** *44*, 8004-8010.

24. Marshall, E. L.; Gibson, V. C.; Rzepa, H. S. *J. Am. Chem. Soc.* **2005,** *127*, 6048-6051.

25. Drouin, F.; Oguadinma, P. O.; Whitehorne, T. J.; Prud'homme, R. E.; Schaper, F. *Organometallics* **2010,** *29*, 2139-2147.

26. Xu, X.; Chen, Y.; Zou, G.; Ma, Z.; Li, G. *J. Organomet. Chem.* **2010,** *695*, 1155-1162.

27. Chen, H.-Y.; Peng, Y.-L.; Huang, T.-H.; Sutar, A. K.; Miller, S. A.; Lin, C.-C. *J. Mol. Catal. A: Chem.* **2011,** *339*, 61-71.

28. Whitehorne, T. J.; Vabre, B.; Schaper, F. *Dalton Trans.* **2014,** *43*, 6339-6352.

29. Chisholm, M. H.; Eilerts, N. W.; Huffman, J. C.; Iyer, S. S.; Pacold, M.; Phomphrai, K. *J. Am. Chem. Soc.* **2000,** *122*, 11845-11854.

30. Lian, B.; Thomas, C. M.; Casagrande, O. L.; Lehmann, C. W.; Roisnel, T.; Carpentier, J.-F. *Inorg. Chem.* **2007,** *46*, 328-340.

31. Breyfogle, L. E.; Williams, C. K.; Young Jr, V. G.; Hillmyer, M. A.; Tolman, W. B. *Dalton Trans.* **2006**, 928-936.

32. Chen, H.-Y.; Tang, H.-Y.; Lin, C.-C. *Macromolecules* **2006,** *39*, 3745-3752.

33. Chisholm, M. H.; Lin, C.-C.; Gallucci, J. C.; Ko, B.-T. *Dalton Trans.* **2003**, 406-412.

34. Chuang, H. J.; Weng, S. F.; Chang, C. C.; Lin, C. C.; Chen, H. Y. *Dalton Trans.* **2011,** *40*, 9601-9607.

35. Darensbourg, D. J.; Choi, W.; Richers, C. P. *Macromolecules* **2007,** *40*, 3521-3523.

36. Darensbourg, D. J.; Karroonnirun, O. *Macromolecules* **2010,** *43*, 8880-8886.

37. Dong, Q.; Ma, X.; Guo, J.; Wei, X.; Zhou, M.; Liu, D. *Inorg. Chem. Commun.* **2008,** *11*, 608-611.

38. Ejfler, J.; Szafert, S.; Mierzwicki, K.; Jerzykiewicz, L. B.; Sobota, P. *Dalton Trans.* **2008**, 6556-6562.

39. Huang, B.-H.; Lin, C.-N.; Hsueh, M.-L.; Athar, T.; Lin, C.-C. *Polymer* **2006,** *47*, 6622-6629.

40. Knight, P. D.; White, A. J.; Williams, C. K. *Inorg. Chem.* **2008,** *47*, 11711-11719.

41. Labourdette, G.; Lee, D. J.; Patrick, B. O.; Ezhova, M. B.; Mehrkhodavandi, P. *Organometallics* **2009,** *28*, 1309-1319.

42. Pastor, M. F.; Whitehorne, T. J.; Oguadinma, P. O.; Schaper, F. *Inorg. Chem. Commun.* **2011,** *14*, 1737-1741.

43. Piedra-Arroni, E.; Brignou, P.; Amgoune, A.; Guillaume, S. M.; Carpentier, J. F.; Bourissou, D. *Chem. Commun.* **2011,** *47*, 9828-9830.

44. Poirier, V.; Roisnel, T.; Carpentier, J. F.; Sarazin, Y. *Dalton Trans.* **2011,** *40*, 523-534.

45. Song, S.; Zhang, X.; Ma, H.; Yang, Y. *Dalton Trans.* **2012,** *41*, 3266-3277.

46. Wang, L.; Ma, H. *Dalton Trans.* **2010,** *39*, 7897-7910.

47. Williams, C. K.; Breyfogle, L. E.; Choi, S. K.; Nam, W.; Young, V. G.; Hillmyer, M. A.; Tolman, W. B. *J. Am. Chem. Soc.* **2003,** *125*, 11350-11359.

48. Wu, J.-C.; Huang, B.-H.; Hsueh, M.-L.; Lai, S.-L.; Lin, C.-C. *Polymer* **2005,** *46*, 9784-9792.

49. Fliedel, C.; Rosa, V.; Alves, F. M.; Martins, A. M.; Aviles, T.; Dagorne, S. *Dalton trans.* **2015,** *44*, 12376-12387.

50. Jensen, T. R.; Breyfogle, L. E.; Hillmyer, M. A.; Tolman, W. B. *Chem. Commun.* **2004**, 2504-2505.

51. Jensen, T. R.; Schaller, C. P.; Hillmyer, M. A.; Tolman, W. B. *J. Organomet. Chem.* **2005,** *690*, 5881-5891.

52. Wheaton, C. A.; Ireland, B. J.; Hayes, P. G. *Organometallics* **2009,** *28*, 1282-1285.

53. Wheaton, C. A.; Hayes, P. G. *Chem. Commun.* **2010,** *46*, 8404-8406.

54. Sun, H.; Ritch, J. S.; Hayes, P. G. *Inorg. Chem.* **2011,** *50*, 8063-8072.

55. Wheaton, C. A.; Hayes, P. G. *Catal. Sci. Tech.* **2012,** *2*, 125-138.

56. Silvernail, C. M.; Yao, L. J.; Hill, L. M.; Hillmyer, M. A.; Tolman, W. B. *Inorg. Chem.* **2007,** *46*, 6565-6574.

57. Wang, L.; Poirier, V.; Ghiotto, F.; Bochmann, M.; Cannon, R. D.; Carpentier, J.-F. o.; Sarazin, Y. *Macromolecules* **2014,** *47*, 2574-2584.

58. Li, Y.; Hoskins, J. N.; Sreerama, S. G.; Grayson, M. A.; Grayson, S. M. *J. Mass Spectrom.* **2010,** *45*, 587-611.

59. Weidner, S. M.; Trimpin, S. *Anal. Chem.* **2010,** *82*, 4811-4829.

60. Chisholm, M. H.; Delbridge, E. E. *New J. Chem.* **2003,** *27*, 1177-1183.

61. Douglas, A. F.; Patrick, B. O.; Mehrkhodavandi, P. *Angew. Chem.* **2008,** *120*, 2322-2325.

62. Sun, H.; Ritch, J. S.; Hayes, P. G. *Dalton Trans.* **2012,** *41*, 3701-3713.

Chapter 4 Experimental

4.1 General Methods

Unless otherwise stated, all manipulations were performed under an atmosphere of dry oxygen-free nitrogen by means of Schlenk techniques or using an MBraun LabmasterDP glove box. Anhydrous diethyl ether was purified using an MBraun Solvent Purification System. THF was stored over sieves and distilled from sodium benzophenone ketyl under nitrogen. Diethylzinc (1.0 M in hexanes) was purchased from Sigma-Aldrich. *rac*-Lactide was purchased from either Aldrich or Alfa Aesar and dried over sodium sulphate in THF, recrystallized and stored under an inert atmosphere prior to use. Benzyl alcohol was purchased from Alfa Aesar and dried over activated 4 Å molecular sieves, distilled under reduced pressure and stored under nitrogen in an ampule prior to use. Other reagents were purchased from Strem, Aldrich or Alfa Aesar and used without further purification. The proligands H_2**[L1]** and H_2**[L2]** were prepared according to the previously reported procedure.[1]

4.2 Instrumentation

MALDI-TOF MS was performed using an Applied Biosystems 4800 MALDI TOF/TOF Analyzer equipped with a reflectron, delayed ion extraction and high performance nitrogen laser (200 Hz operating at 355 nm). Samples were prepared in the glove box and sealed under nitrogen in a Ziploc bag for transport to the instrument.

Anthracene was used as the matrix for the zinc compounds and 2,5-dihydroxybenzoic acid (DHBA) was used as the matrix for the polymers. The matrix was dissolved in THF at a concentration of 10 $mg \cdot mL^{-1}$. Polymer was dissolved in THF at approximately 1 $mg \cdot mL^{-1}$. The matrix and polymer solutions were mixed together at ratios of 3 to 1; 1 μL of this was spotted on the MALDI plate and left to dry. Images of mass spectra were prepared using mMass software (www.mmass.org).

GPC analysis was performed on a Wyatt Triple Detection (triple angle light scattering, viscometry and refractive index) system with Agilent 2600 series sample and solvent handling and two Phenogel columns (10^3 Å 300 × 4.60 mm and 10^4 Å 300 × 4.60 mm). Samples were prepared at a concentration of 2 $mg \cdot mL^{-1}$ in $CHCl_3$ and left to equilibrate for ~2 h before being filtered through 0.2 μm nylon syringe filters and eluted with HPLC grade solvents ($CHCl_3$ or THF) at flow rates of 0.25 $mL \cdot min^{-1}$ with 100 μL injection volumes. The appropriate dn/dc values were employed for polylactide in $CHCl_3$ (dn/dc = 0.0237 $mL \cdot g^{-1}$) and for THF (0.049 $mL \cdot g^{-1}$).

NMR spectra were recorded at 300 MHz for ^1H and 75.5 MHz for ^{13}C or at 500 MHz for ^1H NMR kinetic studies. $CDCl_3$ and C_6D_6 were purchased from Cambridge Isotope Laboratories and toluene-d_8, pyridine-d_5 from Aldrich. Deuterated solvents used in the analysis of the zinc complexes were dried over calcium hydride ($CDCl_3$ and pyridine-d_5) or sodium/potassium alloy (C_6D_6 and toluene-d_8), vacuum transferred and stored under nitrogen in ampules fitted with Teflon valves. Glass transition temperatures (T_g) were measured using a Mettler Toledo DSC 1 S**TA**R^e System equipped with a Julabo FT 100 immersion cooling system, using R1150 refrigerant in an EtOH bath with a

working range of −100 to +20 °C. Samples (~5 mg) were weighed into 40 μL aluminum pans and subjected to three heating cycles. The first heating cycle consisted of heating from 0 to 100 °C at a rate of 10 °C·min^{-1}, held for 2 min at 100 °C and then cooled back to 0 °C at 10 °C·min^{-1}. The sample was held at this temperature for 2 min and subjected to a two heating cycles from 0 to 190 °C at a rate of 10 °C·min^{-1}. Elemental analyses were performed at Canadian Microanalytical Service Ltd., Delta, British Columbia, Canada.

4.3 Synthesis of Zinc Complexes

4.3.1 $(ZnEt)_2$[L1], 1a

$ZnEt_2$ (1.00 g, 8.06 mmol) in hexane was added to a solution of H_2**[L1]** (2.00 g, 4.03 mmol) in pentane. The reaction mixture was stirred for 2 h at ambient temperature. The solvent was removed under vacuum to yield a pale yellow solid (yield: 2.78 g, 99%). Anal. Calc'd for $C_{37}H_{61}NO_2Zn_2$: C 65.10, H 9.01, N 2.05%; Found: C 65.25, H 8.93, N 2.10%. ^{1}H NMR (300 MHz, $CDCl_3$) δ 7.29 (d, *J* = 2.6 Hz, 2H, ArH), 6.91 (d, *J* = 2.5 Hz, 2H, ArH), 4.15 (d, *J* = 14.0 Hz, 2H, $ArCH_2$), 3.74 (d, *J* = 14.0 Hz, 2H, $ArCH_2$), 2.72 – 2.55 (m, *J* = 4.6 Hz, *J* = 3.7 Hz, 2H, $NCH_2CH_2CH_3$), 1.65 – 1.54 (m, 2H, $NCH_2CH_2CH_3$), 1.48 (s, 18H, $C(CH_3)_3$), 1.30 (s, 18H, $C(CH_3)_3$), 0.96 (t, *J* = 8.1 Hz, 3H, $ZnCH_2CH_3$), 0.82 (t, *J* = 7.3 Hz, 3H, $NCH_2CH_2CH_3$), 0.75 (t, *J* = 8.1 Hz, 3H, $ZnCH_2CH_3$), 0.35 (q, *J* = 8.1 Hz, 2H, $ZnCH_2CH_3$), -0.12 (q, *J* = 8.1 Hz, 2H, $ZnCH_2CH_3$). ^{13}C NMR (75 MHz, $CDCl_3$) δ 158.75 (Ar), 140.64 (Ar), 139.25 (Ar), 125.13 (Ar), 125.10 (Ar), 124.74 (Ar), 64.07 ($ArCH_2$), 60.14 ($NCH_2CH_2CH_3$), 35.51 ($C(CH_3)_3$), 34.30 ($C(CH_3)_3$), 31.82 ($C(CH_3)_3$),

30.47 (C(*C*H$_3$)$_3$), 18.68 (NCH$_2$*C*H$_2$CH$_3$), 12.20 (ZnCH$_2$*C*H$_3$), 11.86 (NCH$_2$CH$_2$*C*H$_3$), 11.46 (ZnCH$_2$*C*H$_3$), 1.00 (Zn*C*H$_2$CH$_3$), -2.07 (Zn*C*H$_2$CH$_3$).

4.3.2 (ZnEt)$_2$[L2], 1b

ZnEt$_2$ (1.00 g, 8.06 mmol) in hexane was added to a solution of H$_2$**[L2]** (1.66 g, 4.03 mmol) in pentane. The reaction mixture was stirred for 2 h at ambient temperature. The solvent was removed under vacuum to yield a pale yellow solid (yield: 2.36 g, 98%). Anal. Calc'd for $C_{31}H_{49}NO_2Zn_2$: C 62.21, H 8.25, N 2.34%; Found: C 62.50, H 8.30, N 2.50%. ^{1}H NMR (300 MHz, $CDCl_3$) δ 7.08 (d, *J* = 2.1 Hz, 2H, ArH), 6.74 (d, *J* = 1.9 Hz, 2H, ArH), 4.15 (d, *J* = 14.1 Hz, 2H, ArCH$_2$), 3.69 (d, *J* = 14.1 Hz, 2H, ArCH$_2$), 2.74 – 2.58 (t, *J* = 7.3 Hz, 2H, NC*H*$_2$CH$_2$CH$_3$), 2.27 (s, 6H, ArCH$_3$), 1.69 – 1.57 (m, 2H, NCH$_2$C*H*$_2$CH$_3$), 1.47 (s, 18H, C(C*H*$_3$)$_3$), 1.03 (t, 3H, *J* = 8.0 Hz, ZnCH$_2$C*H*$_3$), 0.84 (t, *J* = 7.3 Hz, 3H, NCH$_2$CH$_2$C*H*$_3$), 0.75 (t, *J* = 8.0 Hz, 3H, ZnCH$_2$C*H*$_3$), 0.41 (q, *J* = 8.1 Hz, 2H, ZnC*H*$_2$CH$_3$), -0.12 (q, *J* = 8.1 Hz, 2H, ZnC*H*$_2$CH$_3$). ^{13}C NMR (75 MHz, $CDCl_3$) δ 159.00 (Ar), 140.00 (Ar), 128.83 (Ar), 128.57 (Ar), 127.33 (Ar*C*H$_2$), 125.99 (Ar*C*H$_2$), 64.35 (Ar*C*H$_2$), 60.58 (N*C*H$_2$CH$_2$CH$_3$), 35.53 (*C*(CH$_3$)$_3$), 35.21 (*C*(CH$_3$)$_3$), 31.58 (Ar*C*H$_3$), 30.40 (C(*C*H$_3$)$_3$), 20.98 (C(*C*H$_3$)$_3$), 19.26 (NCH$_2$*C*H$_2$*C*H$_3$), 12.21 (ZnCH$_2$*C*H$_3$), 12.01 (NCH$_2$CH$_2$*C*H$_3$), 11.52 (ZnCH$_2$*C*H$_3$), 0.88 (Zn*C*H$_2$CH$_3$), -2.08 (Zn*C*H$_2$CH$_3$).

4.3.3 (ZnEt)$_2$[L1](THF), 1a·THF

ZnEt$_2$ (1.00 g, 8.06 mmol) in hexane was added to a solution of H$_2$**[L1]** (2.00 g, 4.03 mmol) in THF. The reaction mixture was stirred for 2 h at ambient temperature. The solvent was removed under vacuum to yield a white solid. The solid was then washed

with pentane (yield: 3.00 g, 99%). ^{1}H NMR (300 MHz, Toluene-d_8) δ 7.49 (d, J = 2.6 Hz, 2H, ArH), 6.93 (d, J = 2.6 Hz, 2H, ArH), 4.07 (d, J = 13.7 Hz, 2H, $ArCH_2$), 3.94 – 3.86 (m, 4H, THF CH_2), 3.51 (d, J = 13.7 Hz, 2H, $ArCH_2$), 2.42 – 2.31 (t, J = 7.3 Hz, 2H, $NCH_2CH_2CH_3$), 1.59 (s, 18H, $C(CH_3)_3$), 1.57 – 1.51 (m, 4H, THF CH_2), 1.38 (s, 18H, $C(CH_3)_3$), 0.92 (t, J = 8.1 Hz, 3H, $ZnCH_2CH_3$), 0.50 (t, J = 7.3 Hz, 3H, $NCH_2CH_2CH_3$), 0.44 (t, J = 8.1 Hz, 3H, $ZnCH_2CH_3$), 0.15 (q, J = 8.1 Hz, 2H, $ZnCH_2CH_3$). ^{1}H NMR (300 MHz, $CDCl_3$) δ 7.28 (d, J = 2.6 Hz, 2H, ArH), 6.88 (d, J = 2.6 Hz, 2H, ArH), 4.14 (d, J = 13.8 Hz, 2H, $ArCH_2$), 3.95 – 3.87 (m, 4H, THF CH_2), 3.74 (d, J = 13.8 Hz, 2H, $ArCH_2$), 2.64 – 2.53 (m, 2H, $NCH_2CH_2CH_3$), 1.97 – 1.89 (m, 4H, THF CH_2), 1.64 – 1.52 (m, 2H, $NCH_2CH_2CH_3$), 1.47 (s, 18H, $C(CH_3)_3$), 1.29 (s, 18H, $C(CH_3)_3$), 0.85 (t, J = 8.0 Hz, 3H, $ZnCH_2CH_3$), 0.81 (t, J = 8.0 Hz, 3H, $ZnCH_2CH_3$), 0.80 (t, J = 7.3 Hz, 3H, $NCH_2CH_2CH_3$), 0.11 (q, J = 8.0 Hz, 2H, $ZnCH_2CH_3$), -0.07 (q, J = 8.0 Hz, 2H, $ZnCH_2CH_3$). ^{13}C NMR (75 MHz, $CDCl_3$-d) δ 159.22 (Ar), 139.97 (Ar), 138.93 (Ar), 125.32 (Ar), 124.76 (Ar), 124.47 (Ar), 68.66 (CH_2), 62.44 ($ArCH_2$), 59.41 ($NCH_2CH_2CH_3$), 35.39 ($C(CH_3)_3$), 34.21 ($C(CH_3)_3$), 31.94 ($C(CH_3)_3$), 30.39 ($C(CH_3)_3$), 25.66 (CH_2), 12.29 ($ZnCH_2CH_3$), 12.11 ($ZnCH_2CH_3$), 11.68 ($ZnCH_2CH_3$), -2.03 ($ZnCH_2CH_3$).

4.3.4 $Zn_3(O$*i*$-Pr)_2[L1]_2$, 2

A solution of *i*-PrOH (0.18 g, 2.92 mmol) in pentane was added to a pentane solution of complex **1a** (1.00 g, 1.45 mmol), which caused the formation of a colourless precipitate. The reaction mixture was stirred for 4 h at ambient temperature. The upper solution was removed using a pipet. The remaining solvent was removed under vacuum

to yield a colourless powder. The powder was then washed twice with pentane to yield a pure product (yield: 0.92 g, 97%). Anal. Cal. for $C_{72}H_{116}N_2O_6Zn_3$: C 62.21, H 8.25, N 2.34%; Found: C 62.50, H 8.30, N 2.50%. ^{1}H NMR (300 MHz, $CDCl_3$) δ 7.26 (d, *J* = 2.5 Hz, 2H, ArH), 7.15 (d, *J* = 2.6 Hz, 2H, ArH), 6.60 (d, *J* = 2.6 Hz, 2H, ArH), 6.54 (d, *J* = 2.5 Hz, 2H, ArH), 4.32 (sep, *J* = 6.0 Hz, 2H, C*H*(CH_3)$_2$), 4.13 (sep, *J* = 6.0 Hz, 2H, C*H*(CH_3)$_2$), 3.51 (d, *J* = 13.4 Hz, 2H, $ArCH_2$), 3.12 (d, *J* = 13.4 Hz, 2H, $ArCH_2$), 2.70 (d, *J* = 13.2 Hz, 2H, $ArCH_2$), 2.55 (d, *J* = 13.2 Hz, 2H, $ArCH_2$), 2.59 (m, 4H, NC*H*$_2$$CH_2CH_3$), 1.50 (s, 18H, C($CH_3$)$_3$), 1.42 (d, *J* = 6.0 Hz, 6H, CH(C*H*$_3$)$_2$), 1.39 (s, 18H, C(CH_3)$_3$), 1.30 (s, 18H, C(CH_3)$_3$), 1.29 –1.26 (m, 4H, NCH_2C*H*$_2$$CH_3$), 1.23 (d, *J* = 6.0 Hz, 6H, CH(C*H*$_3$)$_2$), 1.19 (s, 18H, C(CH_3)$_3$), 0.73 (t, *J* = 7.3 Hz, 6H, NCH_2CH_2C*H*$_3$). ^{13}C NMR (75 MHz, $CDCl_3$) δ 162.34 (Ar), 157.31 (Ar), 141.42 (Ar), 139.52 (Ar), 137.93 (Ar), 135.72 (Ar), 126.40 (Ar), 125.73 (Ar), 125.66 (Ar), 124.30 (Ar), 123.94 (Ar), 120.08 (Ar), 68.00 (CH), 58.15 (Ar*C*H_2), 56.28 (Ar*C*H_2), 54.86 (N*C*$H_2CH_2CH_3$), 35.39 (*C*(CH_3)$_3$), 35.37 (*C*(CH_3)$_3$), 34.28 (*C*(CH_3)$_3$), 33.92 (*C*(CH_3)$_3$), 31.91 (C(*C*H_3)$_3$), 31.12 (C(*C*H_3)$_3$), 29.84 (C(*C*H_3)$_3$), 28.63 (CH(*C*H_3)$_2$), 28.04 (CH(*C*H_3)$_2$), 14.75, 11.50 (NCH_2CH_2*C*H_3). Complex **3**: ^{1}H NMR (300 MHz, Pyridine-d_5) δ 7.60 (d, *J* = 2.7 Hz, 4H, ArH), 7.14 (d, *J* = 2.6 Hz, 3H, ArH), 4.06 (d, *J* = 12.4 Hz, 2H, $ArCH_2$), 3.74 (d, *J* = 12.4 Hz, 2H, $ArCH_2$), 2.70 – 2.60 (m, 2H, NC*H*$_2$$CH_2CH_3$), 1.68 (s, 18H, C($CH_3$)$_3$), 1.44 (s, 18H, C($CH_3$)$_3$), 1.32 (d, *J* = 6.1 Hz, CH(C*H*$_3$)$_2$ of Zn(OCH(CH_3)$_2$)$_2$), 0.47 (t, *J* = 7.3 Hz, 3H, NCH_2CH_2C*H*$_3$).

4.4 General Procedure of *rac*-Lactide Polymerization

4.4.1 General Procedure of Melt Phase *rac*-Lactide Polymerization

In the glove box, *rac*-lactide (0.5 g, 3.47 mmol) and the appropriate amount of zinc complex **1a** (according to the desired lactide to complex ratio) were added to a vial equipped with a magnetic stir bar. The vial was removed from the glove box and placed on a preheated hot plate where it was heated and stirred for the specified time. The vial was removed from the hot plate and cooled in an ice bath to terminate polymerization. A sample of the solidified material was analyzed by NMR. The polymer was dissolved in $CHCl_3/CH_2Cl_2$ and precipitated with MeOH. The upper solution was decanted off and the polymer was dried under vacuum.

4.4.2 General Procedure of *rac*-Lactide Polymerization in Toluene

In the glove box, *rac*-lactide (0.5 g, 3.47 mmol) was added to an ampule equipped with a magnetic stir bar, followed by 6 mL of toluene. Individual stock solutions for BnOH and complex **1a·THF** were prepared in toluene and the appropriate amounts of each were added to the ampule in sequence. The ampule was removed from the glove box and placed on a preheated oil bath where it was heated and stirred for the specified time. The ampule was removed from the oil bath and a sample of the reaction mixture was analyzed by NMR. The reaction mixture was transferred into a vial followed by adding 20 mL hexane to precipitate the polymer. The upper solution was decanted off and the polymer was dried under vacuum.

4.4.3 General Procedure of *rac*-Lactide Polymerization in NMR Scale

In the glove box, 75 mg (0.521 mmol) lactide was added to a J-Young NMR tube, followed by adding 700 μL toluene-d_8. Individual stock solutions for BnOH or *i*-PrOH and complex **1a·THF** or **2** were prepared in toluene-d_8 and the appropriate amounts of each were added to the NMR tube in sequence. The appropriate amount of toluene-d_8 was added to the NMR tube to make the total volume 790 μL ([LA] = 0.66 M). The NMR tube was sealed, removed from the glove box and loaded into the spectrometer. Before preparing the NMR sample, the spectrometer was preheated to desired temperature and the lock, tune and shimming were conducted and saved using a blank sample, which contained the same concentration of *rac*-lactide in toluene-d_8. The measurements were started upon the stabilization of spin with a time interval of 120 s and a sufficient relaxation delay time for completing the polymerization.

4.5 Crystallographic Experimental

Measurements were made on a Bruker APEXII CCD equipped diffractometer (30 mA, 50 kV) using monochromated Mo Kα radiation (λ = 0.71073 Å) at 125 K by Professor Jason Masuda (Chemistry Department, St. Mary's University, Halifax, Nova Scotia, Canada). Refinement of the data was performed by Professor Louise N. Dawe (Department of Chemistry and Biochemistry, Wilfrid Laurier University, Waterloo, Ontario, Canada). Structures were solved using Olex2[2] with ShelXT[3] structure solution program using Direct Methods and refined with the ShelXL[3] refinement package using Least Squares minimisation. H-atoms were introduced in calculated positions and refined

on a riding model, while all other atoms were introduced in difference map positions and refined anisotropically. For **1c**, two pendant ligand -$NCH_2CH_2CH_3$ groups were disordered. Distance (SADI) restraints and anisotropic constraints (EADP) were applied. Occupancy was allowed to refine to convergence, with C19-21 at 0.757(6) occupancy and C19A-21A at 0.243(6) occupancy; and C46-48 at 0.763(7) occupancy, and C46A-48A at 0.237(7) occupancy. For **2**, two disordered *t*-butyl groups are present. C56-C58:C56A-C58A at 0.581(8):0.419(8) occupancy and C60-C62:C60A-C62A at 0.731(8):0.269(8) occupancy. Both groups were refined anisotropically with SADI and RIGU restraints. All other non-hydrogen atoms were refined anisotropically, without restraints.

4.6 References

1. Qian, X.; Dawe, L. N.; Kozak, C. M. *Dalton Trans.* **2011,** *40*, 933-943.
2. Dolomanov, O. V.; Bourhis, L. J.; Gildea, R. J.; Howard, J. A.; Puschmann, H. *J. Appl. Crystallogr.* **2009,** *42*, 339-341.
3. Sheldrick, G. *Acta Cryst.* **2008,** *A64*, 112-122.

Appendix: NMR Spectra

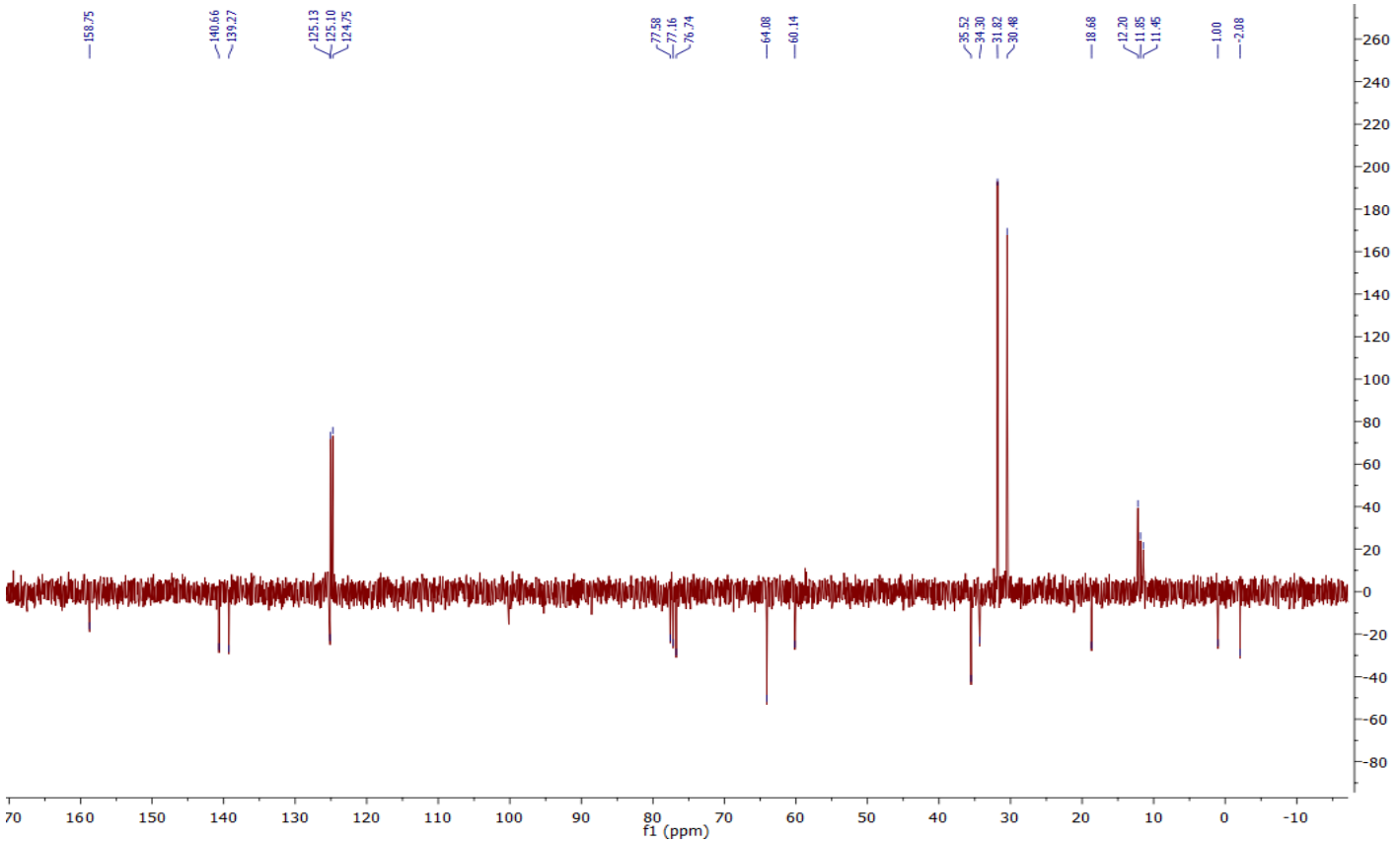

Figure A - 1 ATP spectrum of **1a** (75 Hz, $CDCl_3$, 298 K).

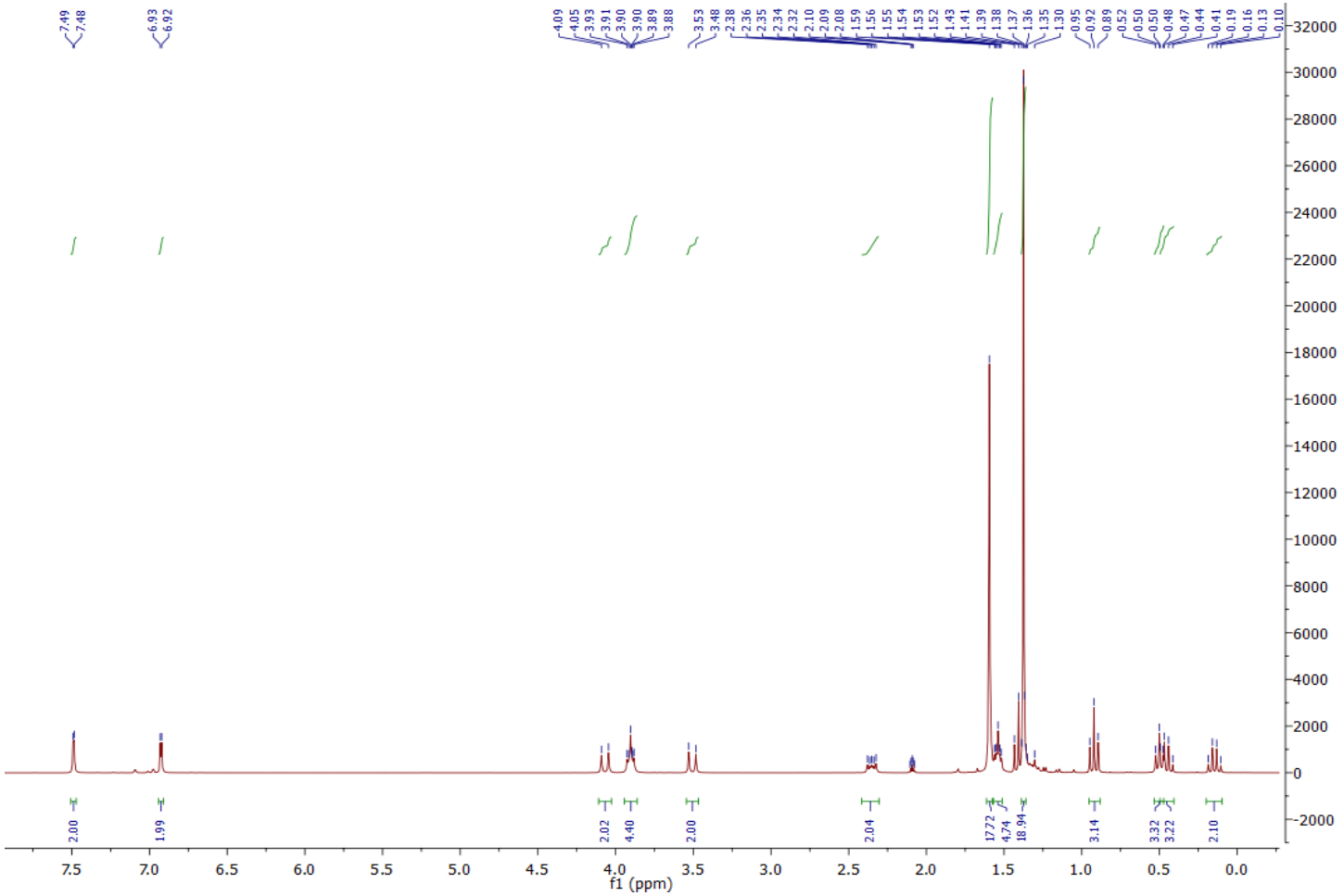

Figure A - 2 ^{1}H NMR spectrum of **1a·THF** (300 MHz, toluene-d_8, 298 K).

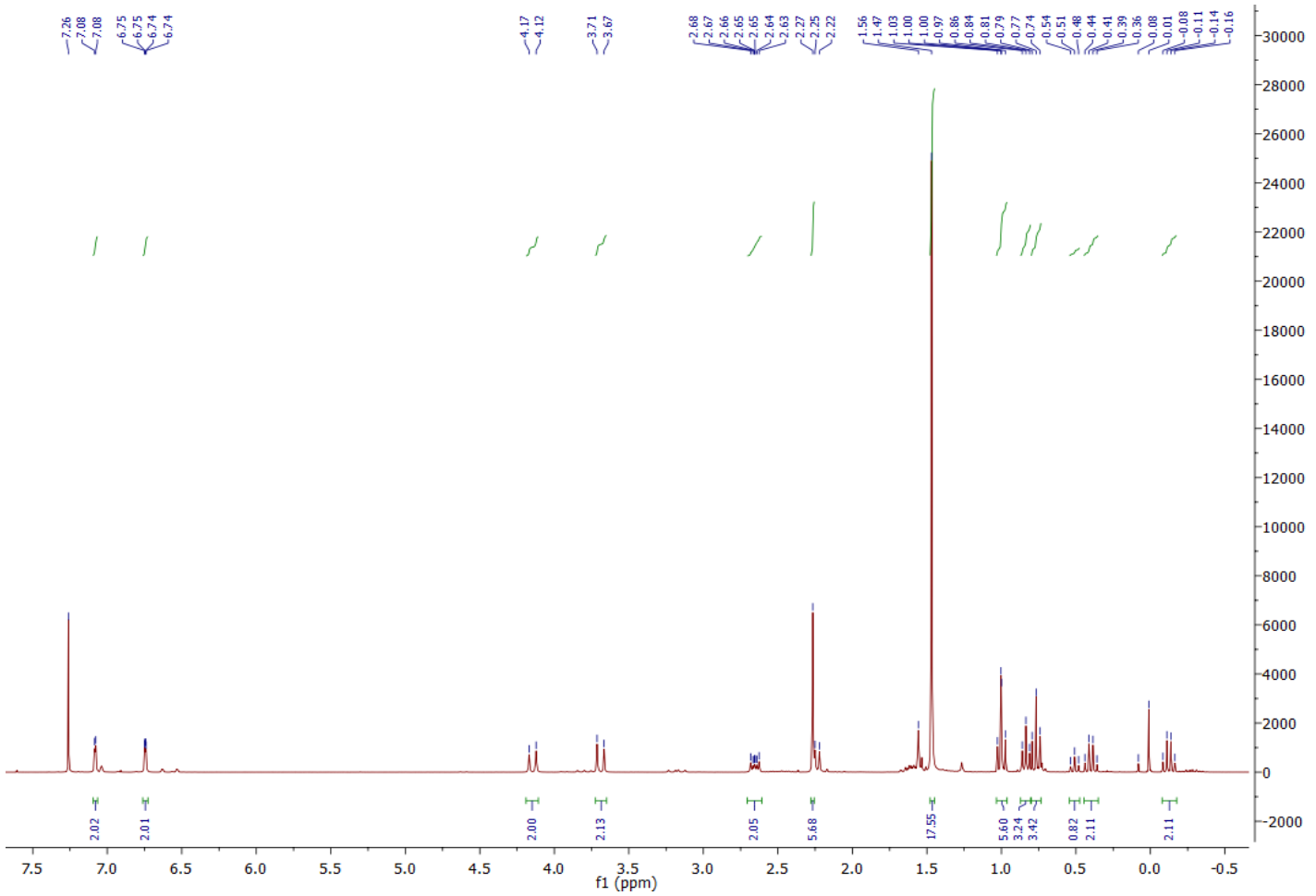

Figure A - 3 ^{1}H NMR spectrum of **1b** (300 MHz, $CDCl_3$, 298 K).

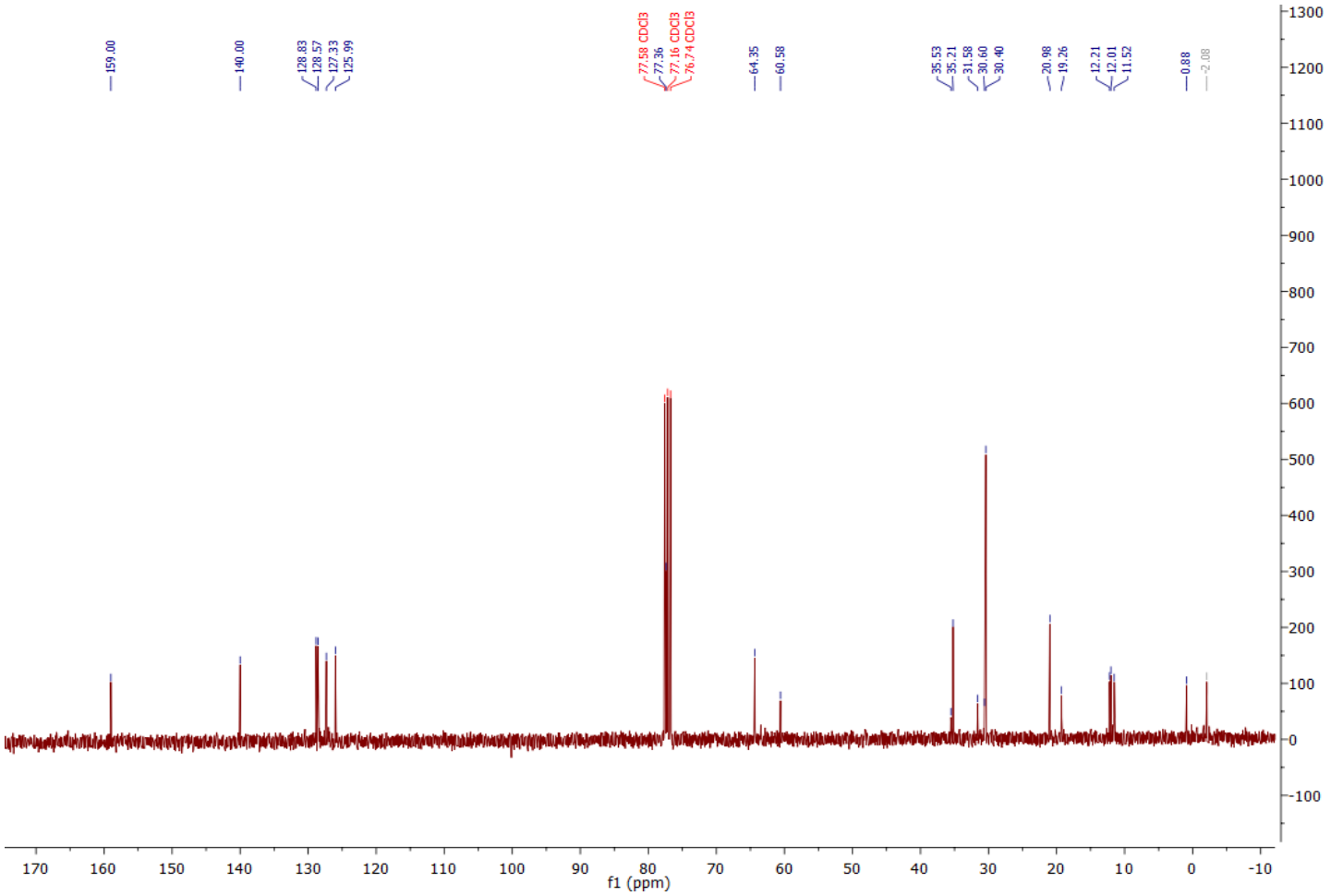

Figure A - 4 ^{13}C NMR spectrum of **1b** (75 MHz, $CDCl_3$, 298 K).

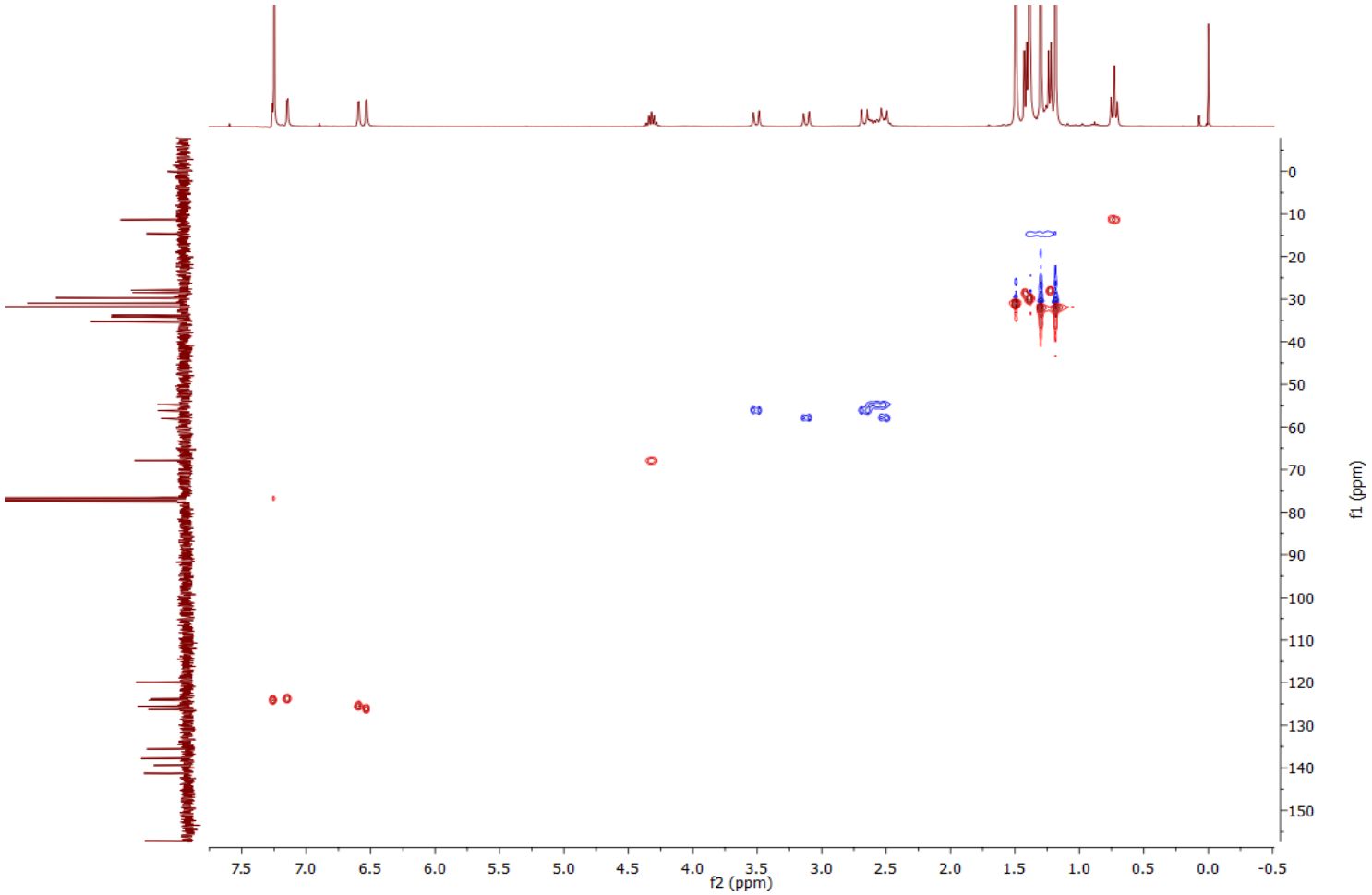

Figure A - 5 HQSC spectrum of **2** ($CDCl_3$, 298 K).

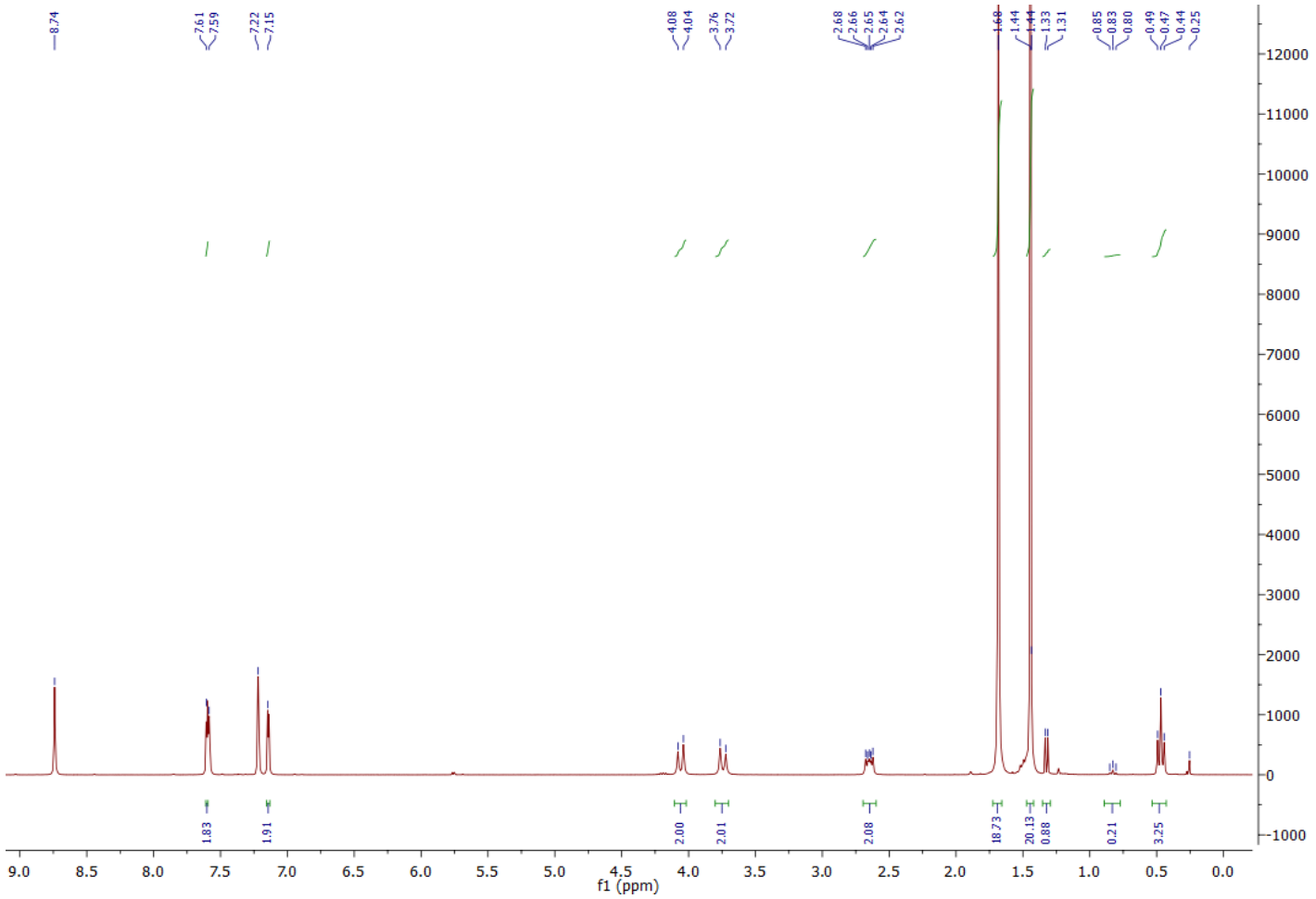

Figure A - 6 ^{1}H NMR spectrum of **2** (300 MHz, pydine-d_5, 298 K).

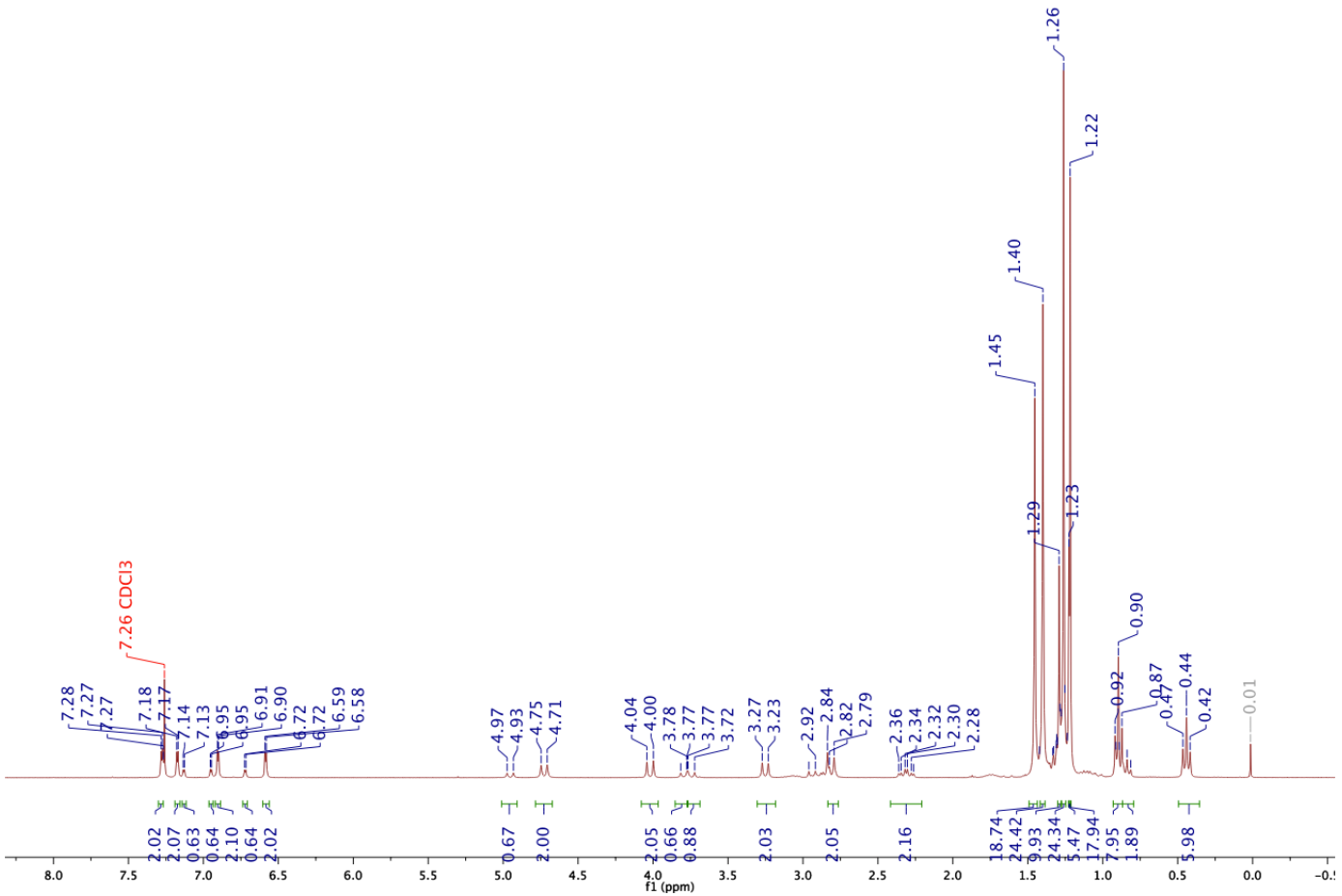

Figure A - 7 ^{1}H NMR spectrum of the reaction product of H_2[**L1**] and one equiv. of $ZnEt_2$ (300 MHz, $CDCl_3$, 298 K).

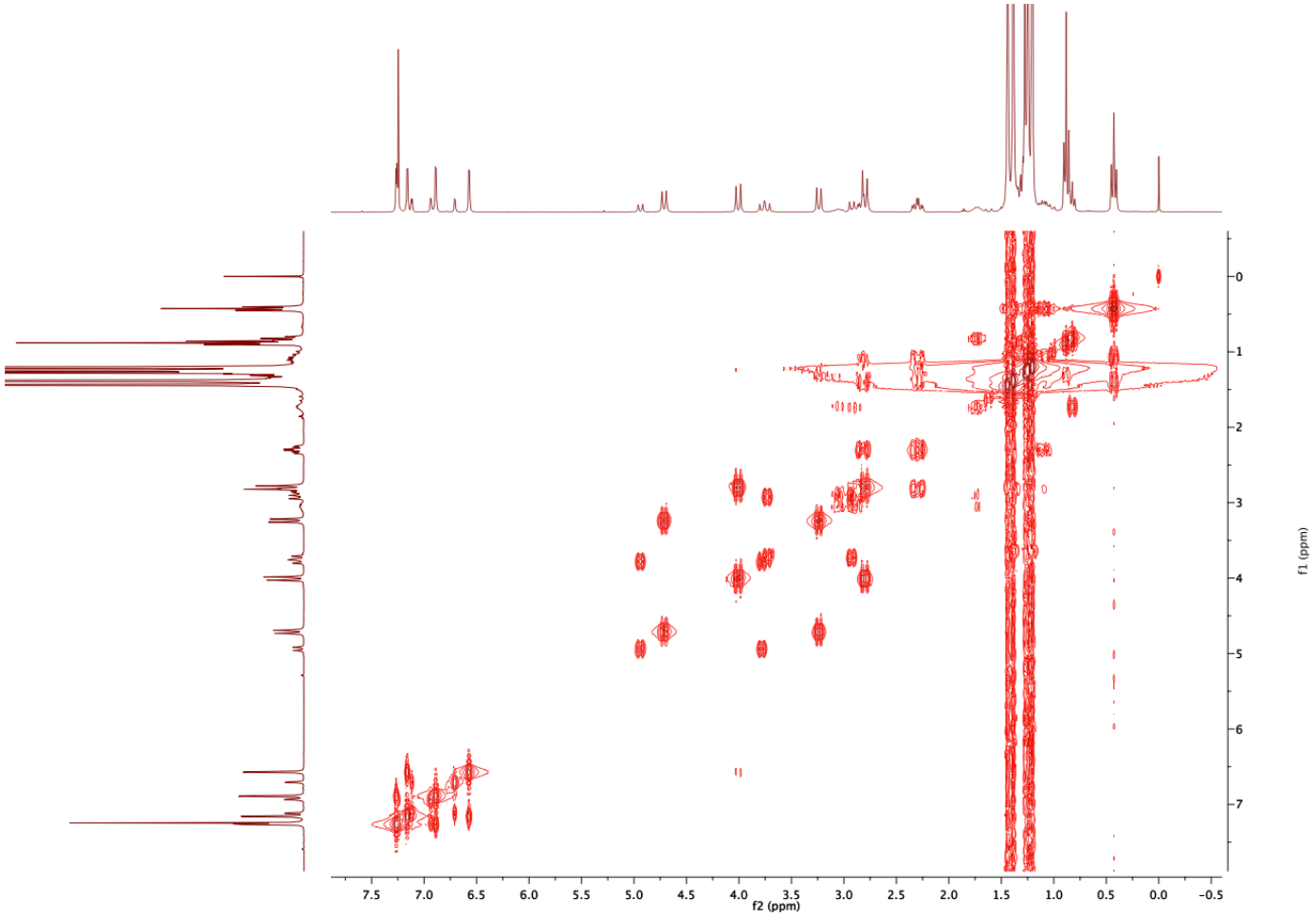

Figure A - 8 COSY spectrum of the reaction product of H_2[**L1**] and one equiv. of $ZnEt_2$ (300 MHz, $CDCl_3$, 298 K).

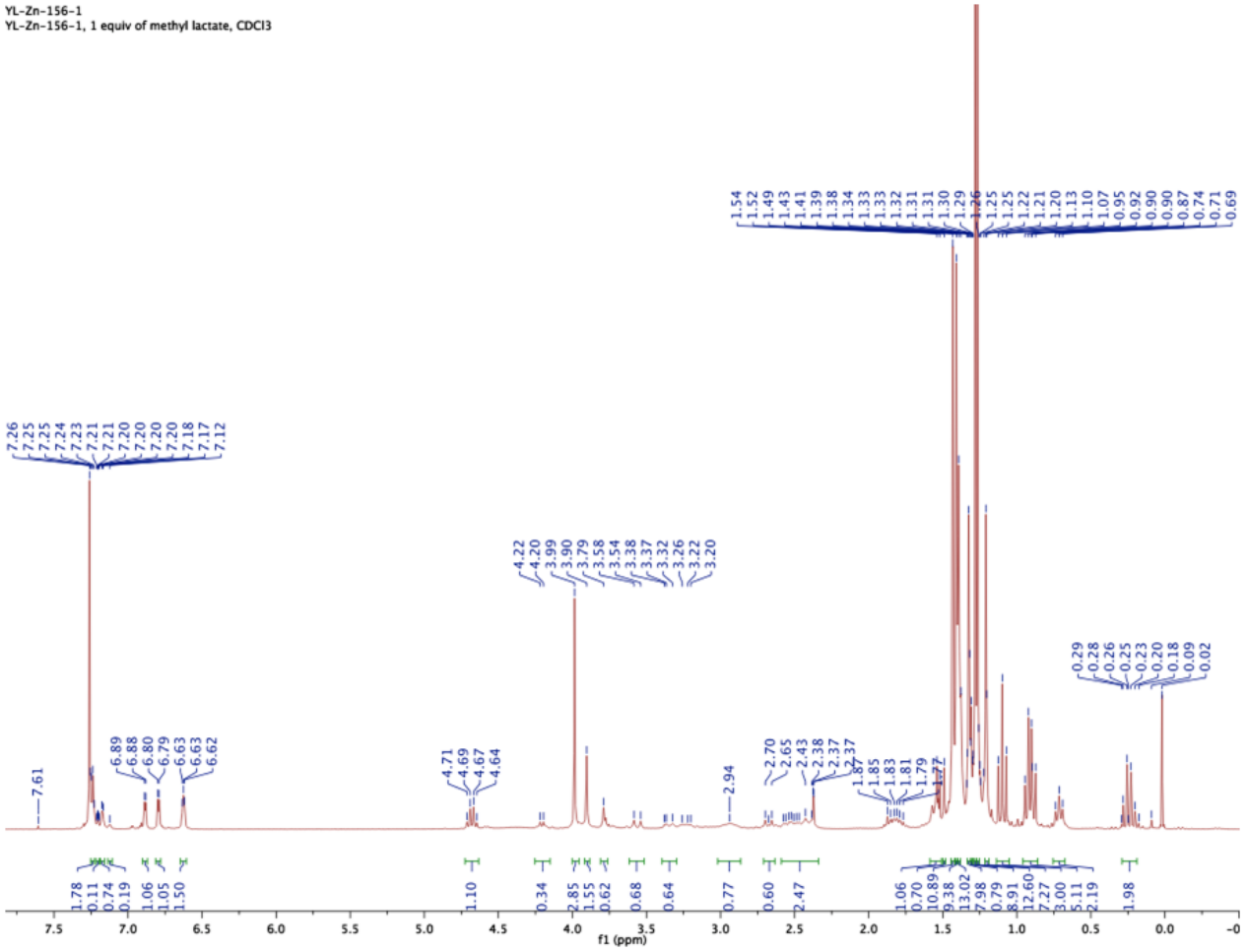

Figure A - 9 ^{1}H NMR spectrum of the reaction product of **1a** and one equiv. of methyl lactate (300 MHz, $CDCl_3$, 298 K).

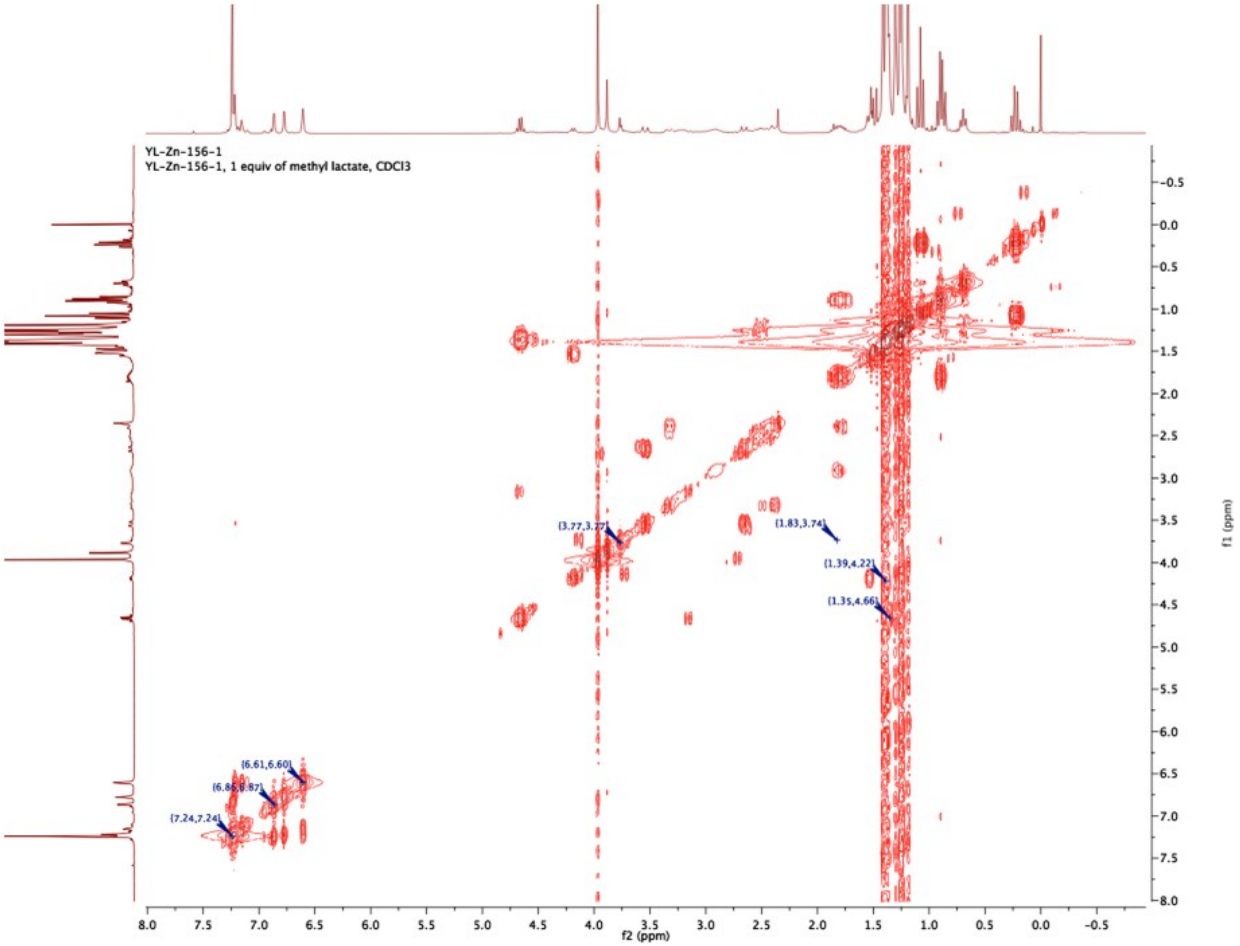

Figure A - 10 COSY spectrum of the reaction product of **1a** and one equiv. of methyl lactate (300 MHz, $CDCl_3$, 298 K).

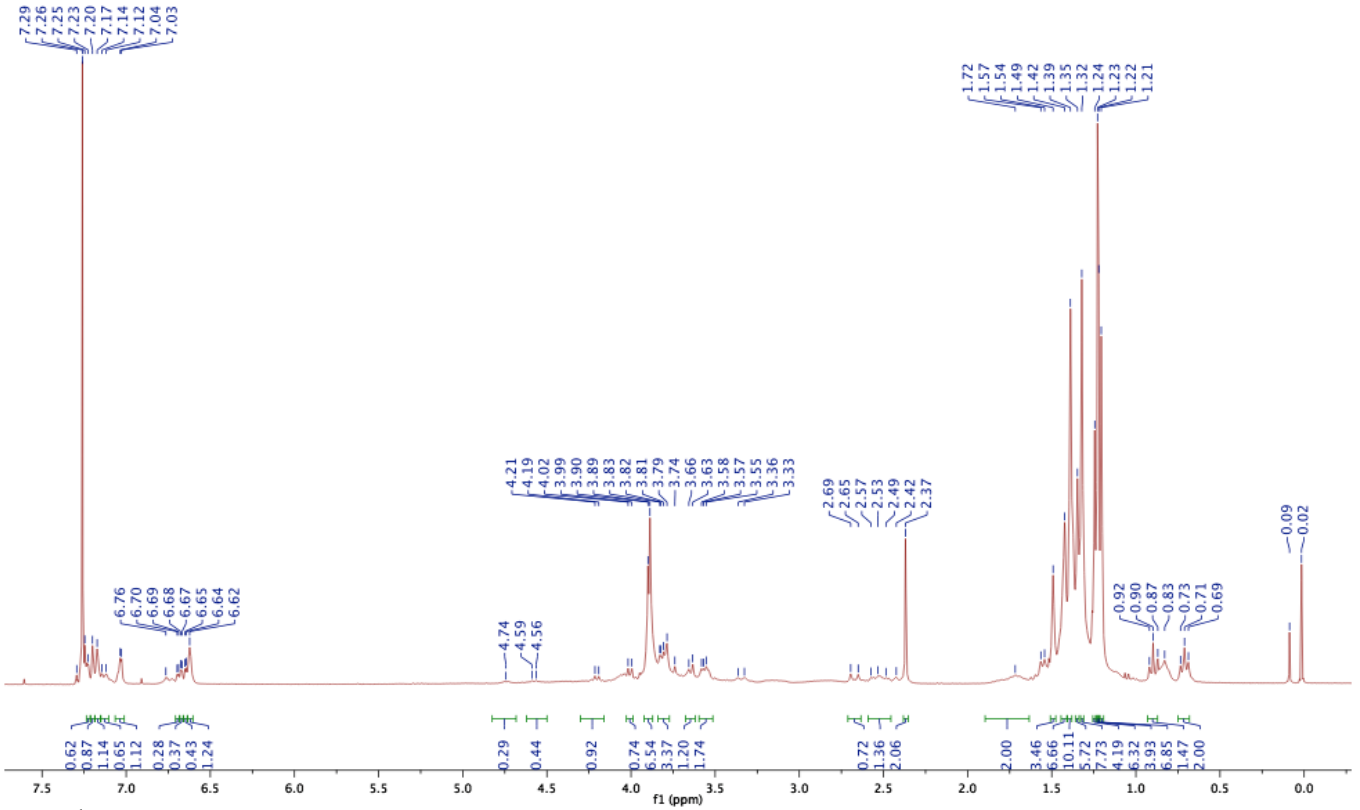

Figure A - 11 ^{1}H NMR spectrum of the reaction product of **1a** and two equiv. of methyl lactate (300 MHz, $CDCl_3$, 298 K).

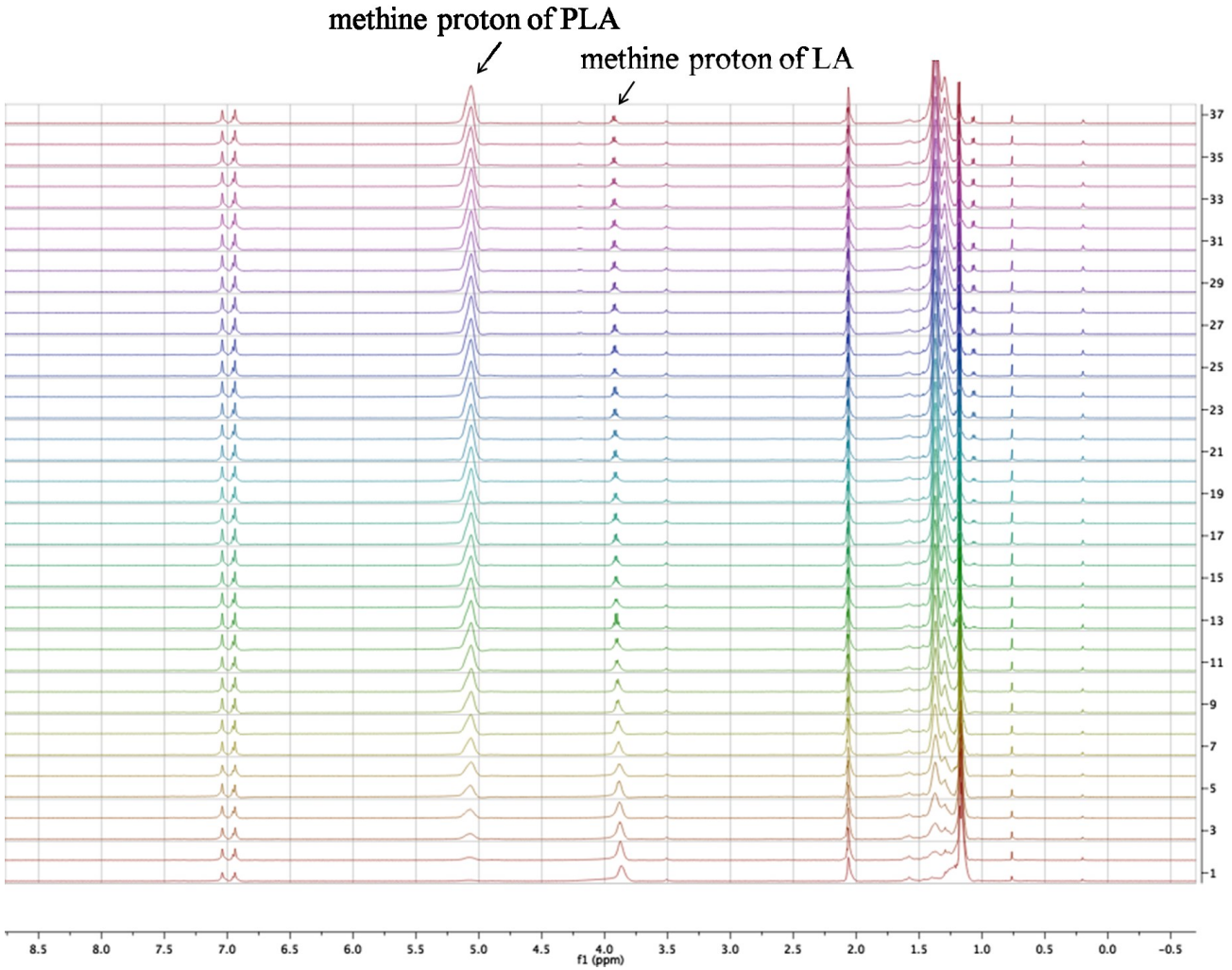

Figure A - 12 ^{1}H NMR spectra of a typical *rac*-lactide polymerization in NMR scale (500 MHz, [LA]:[**1a·THF**]:[BnOH] = 200:1:1, [LA] = 0.66 M in toluene-d_8 at 353 K, interval (D20) = 120 seconds, number of spectra (td) = 37).